Deciphering novel functions of Cyclin dependent kinase 8 using *Drosophila melanogaster*

by

Jenny Zhe Liao

B.Sc. (with Distinction), Simon Fraser University, 2019

Thesis Submitted in Partial Fulfillment of the
Requirements for the Degree of
Doctor of Philosophy

in the
Department of Molecular Biology and Biochemistry
Faculty of Science

SIMON FRASER UNIVERSITY
Fall 2024

Declaration of Committee

Name:	**Jenny Zhe Liao**
Degree:	**Doctor of Philosophy (Molecular Biology and Biochemistry)**
Title:	**Deciphering novel functions of Cyclin dependent kinase 8 using *Drosophila melanogaster***
Committee:	**Chair: Edgar Young** Associate Professor, Molecular Biology and Biochemistry
	Esther Verheyen Supervisor Professor, Molecular Biology and Biochemistry
	Sharon Gorski Committee Member Professor, Molecular Biology and Biochemistry
	Michel Leroux Committee Member Professor, Molecular Biology and Biochemistry
	Harald Hutter Examiner Professor, Biological Sciences
	Andrew Simmonds External Examiner Professor, Cell Biology University of Alberta

Abstract

Cyclin dependent kinase 8 (CDK8) is a serine/threonine protein kinase that forms a module with Cyclin C, Mediator 12 and Mediator 13. The kinase module reversibly interacts with the Mediator, a 26-subunit protein complex that regulates RNA Polymerase II-mediated gene expression. CDK8 is implicated in regulating multiple signaling pathways, and enhanced activity of CDK8 has been found in tumorigenesis. Functional analysis of CDK8 is limited across different model organisms. Using Drosophila as a genetic model organism, researchers previously found that *cdk8* mutations led to lethality and heterozygous *cdk8* mutants had increased fat contents during larval stages. We found a novel function of Cdk8 in regulating mitochondrial morphology when we analyzed the function of Cdk8 throughout development of Drosophila. Ubiquitous depletion of Cdk8 produced progeny with abnormal wing postures with significant reduced survival rates and climbing ability. Cdk8 plays a critical role in regulating the structure of mitochondria, with its loss causing elongated mitochondria in muscles throughout development. We used multiple approaches to demonstrate that Cdk8 promotes the phosphorylation of Dynamin-related protein 1, Drp1 at S616, a protein required for mitochondrial fission. Interestingly, PTEN-induced kinase 1 (Pink1), a mitochondrial kinase implicated in Parkinson's disease, also phosphorylates Drp1 at the same residue. Indeed, overexpression of Cdk8 significantly suppresses the phenotypes observed in flies with low levels of Pink1, including elevated levels of ROS, mitochondrial dysmorphology, and behavioral defects.

Drosophila *Cdk8* is the sole orthologue of vertebrate *CDK8* and *CDK19.* Expression of human CDK19 can significantly rescue defective phenotypes caused by Cdk8 depletion in fly muscles and neurons, indicating the conserved functions between fly Cdk8 and CDK19. Interestingly, CDK19 has both cytoplasmic and nuclear localization in muscles, which is consistent with the endogenous GFP-tagged fly Cdk8. This localization supports potential cytoplasmic functions. Expressing wildtype CDK19 or cytoplasmically targeted CDK19 can rescue behavioral defects in *pink1* mutant flies, which demonstrates that the rescuing ability between fly Cdk8 and CDK19 are likely to be non-nuclear.

Altogether, we found that Cdk8 can modulate *Pink1* mutant phenotypes by promoting Drp1-mediated fission to restore mitochondrial homeostasis. Furthermore, we found fly Cdk8 shares conserved functions with CDK19 in regulating mitochondrial morphologies.

Keywords: Cdk8; mitochondrial fission; Drp1, Pink1; Parkinson's Disease; non-nuclear function

Dedication

For the years that I spent in Simon Fraser University

Acknowledgements

First and foremost, I would like to express my deepest gratitude to my senior supervisor, **Dr. Esther Verheyen**, for her invaluable advice and continuous support over the years. The completion of my PhD studies would not have been possible without her guidance and encouragement. Deepest thanks to Esther for giving me the opportunities to explore, to learn, to fail, to lead, and to grow as an independent female scientist.

I would like to extend my appreciation to my supervisory committee, **Dr. Sharon Gorski, Dr. Michel Leroux** and my previous supervisory committee member, **Dr. Nicholas Harden**, for their constructive feedback and continuous support. Thanks to my thesis examiners, **Dr. Harald Hutter** and **Dr. Andrew Simmonds,** for evaluating my work. Thanks to **Dr. Edgar Young** for chairing my defence.

Thank you for all the members of the Verheyen lab, Kewei Yu, Gamze Akarsu, Karampal Grewal, Ece Yücel, Gurpreet Moroak and Chris Tam for all the great discussion, helps and fun outside of the lab. Thank to Dr. Gritta Tettweiler for chaperoning me when I first joined the lab. Thank you to all the past members who I have overlapped with in the lab, Katja MacCharles, Dr. Kenneth Wong, Claire Shih, Dr. Stephen Kinsey, Landiso Madonsela, Nivi Ramkumar, for all the helps and supports. Special thanks to Claire Shih and Katie Sew for the time we spent together during revision.

I would like to thank our collaborators, Dr. Hyunglok Chung for continuation of the project, Dr. Paul Marcogliese and Dr. Oguz Kanca for generating the fly lines, and the members of Hugo Bellen's Lab at the Baylor College of Medicine in Texas for sharing reagents and data. Thanks to the MBB department staff at Simon Fraser University, Jamie Chen, Christine Beauchamp, Deidre de Jong-Wong, Ziwei Ding and Tim Heslip.

Finally, I would like to thank my parents for their support and understanding. To my beloving husband, Mike Chen, thank you for always being there for me. To my lovely first-born pet, Stella, thank you for accompanying me in the middle of the night while I was working, you are my therapy. To my second-born pet, Stanley (Dundun), thank you for being such a sweet boy with your older sister. To my little one on the way, thank you for bearing with me during this stressful time. 感恩遇见，一路上有你们，真好！

Table of Contents

List of Tables

List of Figures

List of Acronyms

A-431	human epidermoid carcinoma cell line
Acc	acetyl-CoA carboxylase
ACOX 1	acyl-CoA oxidase 1
Acs	acetyl-CoA synthetase
AD	Alzheimer's Disease
ADHD	attention deficit hyperactivity disorder
Akt	Ak strain transforming, also known as Protein kinase B (PKB)
ALS	Amyotrophic lateral sclerosis
AML	acute myeloid leukemia
ASD	Autism specturm disorder
ATP	adenosine triphosphate
ATP5α	Mitochondrial membrane ATP synthase alpha subunit
AVG	Anterior guidepost neuron
CAK	CDK-activating kinase
CDK	Cycline dependent kinase
CDK19ΔNLS	human CDK19 with a deletion of the NLS
Cdk8::GFP	Endogenous GFP tagged Drosophila Cdk8
cDNA	complementary DNA
cic-1	*C. elegans* Cyclin C
CNS	central nervous system
CTD	carboxy-terminal domain of Polymerase II
Cyc C	Cyclin C
Da-Gal4	daughterless-Gal4
DAPI	4′,6-diamidino-2-phenylindole
DEE87	developmental and epileptic encephalopathy 87
dGstD	glutathione transferase D1
DHE	Dihydroethidium
DLM	dorso-longitudinal muscles

DNA	deoxyribonucleic acid
DNM1L	Dynamin 1-like (human Drp1)
Drp1	Dynamin-related protein 1
DUB	deubiquitinating enzymes
DVL	dorso-ventral muscles
ER	endoplasmic reticulum
ETC	electron transport chain
FAO	fatty acid oxidation
Fasn 1	Fatty acid synthase 1
Fis1	mitochondrial fission 1 protein
FM7	Multiply Inverted X Chromosome Balancer FM7
fwd	four-wheel drive
G1	Gap phase 1
G2	Gap phase 2
GBA	Glucocerebrosidase (GCase)
GDNF	Glial cell line-derived neurotrophic factor
GDP	Guanosine diphosphate
GFP	green fluorescent protein
GTP	Guanosine triphosphate
GWAS	genome wide associated studies
HA-tag	Human influenza hemagglutinin (HA) tag
HD	Huntington’s Disease
HEK293	Human embryonic kidney 293 cell line
HeLa	HeLa cervical cancer cell line
HepG2	hepatocellular carcinoma cell line
Hipk	Homeodomain interacting protein kinase
hPINK1	Human PTEN-induced protein kinase 1
HSC	hematopoietic stem cells
IFM	indirect flight muscles
IMM	inner mitochondrial membrane
IMS	inter-membrane space

IP-MS	immunoprecipitation followed by Mass Spectrometry
KD	kinase dead
kDa	kiloDalton
LAC	Library and Archives Canada
LAMP1	lysosome associated-membrane protein 1
LD	lipid droplet
M	Mitosis phase of cell cycle
Mad	Mother against dpp
Marf	Mitochondrial assembly regulatory factor
mdt-12	*C. elegans* Mediator 12
mdt-13	*C. elegans* Mediator 13
Med12	mediator complex subunit 12
Med13	mediator complex subunit 13
Mff	mitochondrial fission factor
MFN1	Mitofusin 1
MFN2	Mitofusin 2
MiD-49	mitochondrial dynamics proteins of 49 kDa
MiD-51	mitochondrial dynamics proteins of 51 kDa
MiNA	mitochondrial network analysis
mitoGFP	mitochondrially targeted GFP
MLB	multilamellar bodies
MRI	magnetic resonance imaging
mRNA	messenger RNA
Myc tag	polypeptide protein tag derived from the c-myc protein
NAC	N-acetylcysteine
NACA	N-acetylcysteine amide
NADH	reduced nicotinamide adenine dinucleotide
NIH-3T3	mouse embryonic fibroblast cell line
NLS	nuclear localization sequence
nSREBP	nuclear SREBP
nSREBP-1c	one of the three SREBP isoforms found in vertebrates

OCR	oxygen consumption rate
OMIM	Online Mendelian Inheritance in Man
OMM	outer mitochondrial membrane
Opa1	Optic atrophy 1
OXPHO	oxidative phosphorylation
P-TEFb	positive transcription elongation factor b
PCR	polymerase chain reaction
PD	Parkinson's Disease
PIC	preinitiation complex
PINK1	PTEN-induced protein kinase 1
pink1[B9]	B9 allele of Drosophila pink1 gene
PLA2G6/PARK14	calcium-independent phospholipase A2 β
Pol II	RNA Polymerase II
qRT-PCR	quantitative real-time reverse-transcription PCR
RET	Rearranged During Transfection
RFP	red fluorescent protein
RNAi	RNA interference
RNAseq	RNA sequencing
ROS	reactive oxygen species
S	Synthesis phase of cell cycle
S2-R+	Schneider 2 (S2) cell line expressing the Wingless receptor
S616	Serine 616 of Drp1
SD	standard deviation
sfGFP	superfold-GFP
SFU	Simon Fraser University
SH-SY5Y	Human neuroblastoma cell line
Sirt3	mitochondrial sirtuin 3
sod1	superoxide dismutase 1
SREBP	Sterol-regulatory element binding protein
SW620	Human colorectal Cancer Cell Line

TFIIB	Transcription factor II B
TFIID	Transcription factor II D
TFIIE	Transcription factor II E
TFIIF	Transcription factor II F
TFIIH	Transcription factor II H
THP-1	human monocytic cell line
TMRE	tetramethylrhodamine ethyl ester
TOPO cloning	Topoisomerase based cloning
TTD	Trichothiodystrophy
TUNEL	Terminal deoxynucleotidyl transferase dUTP nick end labeling
U-251MG	human malignant glioblastoma Cell Line
U2OS	Human Bone Osteosarcoma Epithelial Cells
UAS	Upstream activating sequence
Uch	ubiquitin carboxy-terminal hydrolase
UCHL1	human ubiquitin C-terminal Hydrolase L1
USP8	Ubiquitin carboxyl-terminal hydrolase 8
VNC	ventral nerve cord
WCL	whole cell lysate
XPB	Xeroderma pigmentosum group B gene
XPD	Xeroderma pigmentosum group D gene

Chapter 1. Introduction

1.1. *Drosophila melanogaster* as a model to study human diseases

In the early twentieth century, Thomas Hunt Morgan and his students at Columbia University discovered the sex-linked inheritance in mutant white male flies. This finding led to the first chromosome linkage maps[1]. In the 1980s, work done by E. Lewis and C. Nüsslein-Volhard and E. Wieschaus led to the discovery of dozens of genes involved directly in regulating embryonic development[2,3]. These pioneering works have made Drosophila a powerful genetic tool to study basic and translation research.

Drosophila has been used as a valuable genetic tool to study human diseases for decades. 60% of genes found in human can also be found in flies, and 75% of genes identified in human genetic disease, which makes the fly a suitable model organism to study human diseases [4]. The low genetic redundancy in flies can unmask phenotypes and underlying molecular mechanisms where it would be difficult to address using mammalian cell culture or in vertebrate models[5]. In particular, there are many conserved organ systems and tissue types relevant to human health. In my work, I focussed heavily on the larval and adult muscles to investigate Cdk8 function.

1.1.1. Conserved muscle structure between fly and human

Drosophila shares conserved striated muscle structure and function with those found in vertebrate models including humans. The simplest contractile unit in striated muscle is the sarcomere, which is well conserved throughout evolution[6,7]. A sarcomere is composed of myosin-containing thick filaments flanked and interlaced with bundles of actin-containing thin filaments. Regulatory proteins such as troponin and tropomyosin are distributed evenly across the thin filaments and form complexes with actin to regulate the contraction of the sarcomere upon Ca2+ stimulation (Fig. 1.1).

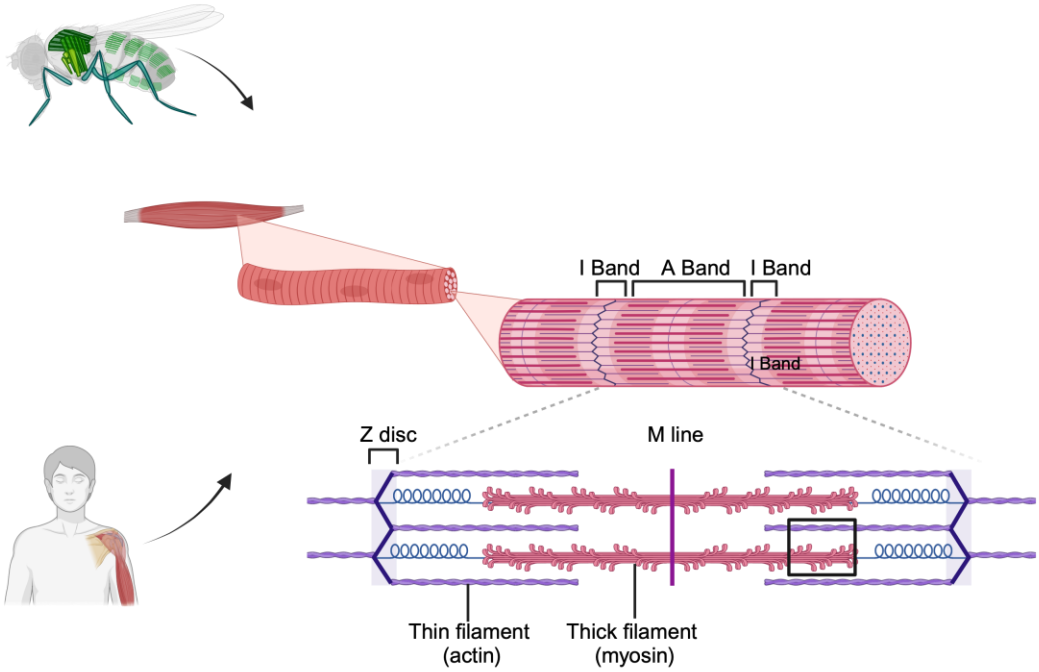

Figure 1.1. Conserved muscle structure between Drosophila and Human.

The striated muscle fibers are conserved between Drosophila and human. The single contractile unit is shown with indicated thin and thick filaments along with M line, and Z disc.

1.1.2. A conserved nervous system allows study of human neurodegenerative diseases using the fly

The fly central nervous system (CNS) contains neurons that are about a fraction of the billions found in the human brain[8]. Despite its simplicity, key features of neuronal development, structure, and function are similar to those in more complex organisms, such as humans[9,10]. The simple yet sophisticated brain and nerve system of Drosophila has made it an excellent model organism to study human neurodegenerative diseases. The conserved genomes and underlying molecular mechanisms between Drosophila and human led to the generation of reliable fly models to study Alzheimer's disease (AD)[11–13], Parkinson's disease (PD)[14–16], and Huntington's disease (HD)[17–19].

1.1.3. Advantages of using Drosophila as model organism for human diseases

It is advantageous to use fruit flies as a research organism as there are abundant tools for genetic analysis that are available to the fly research community. In addition, flies are easy to maintain and have a relatively short life cycle of about ten days. There are four developmental stages in a fly's life cycle including embryonic, larval, pupal and adult stages. For developmental related diseases, we can study phenotypes in flies when they are in embryonic or larval stage. For diseases that are associated with neurodegeneration that tend to occur in older humans, we can examine the eclosed adult flies and monitor their behaviors as they age[20–22].

To study genes responsible for human diseases in fruit flies, there are a number of possible approaches, including the following. First of all, we can delete the fly ortholog that corresponds to human disease-causing gene and study its loss of function effect in flies if the human disease is due to loss of function. Secondly, we can mutate the fly ortholog with an analogous mutation that is found in patients and characterize the mutated gene in flies. Thirdly, we can express the ortholog gene from humans in flies to study the overexpressed effects to gain insight into functions. Lastly, we can study the effect of a mutation that is found in humans by directly expressing the disease associated mutant human gene in flies to further characterize the pathogenicity of the mutation[20–22].

1.1.4. GAL4/UAS Binary system

To modulate gene expression we utilize a binary system that is adapted from yeast, the GAL4-UAS system[23]. GAL4 is a transcription factor from yeast, which can be expressed by inserting it into the genome downstream of any promotor or enhancer element. If GAL4 is inserted downstream of a ubiquitous promoter, such as Actin, then the expression of GAL4 will be present everywhere in the organism. However, if Gal4 is inserted downstream of a tissue-specific promoter, the expression of GAL4 will be restricted to that specific tissue type. UAS is the DNA upstream activating sequence that requires binding of GAL4; thus, expression of GAL4 is required to drive expression of the sequence downstream of UAS, in this case the sequence of our gene of interest or a sequence encoding a double stranded hairpin for mRNA silencing. Drosophila stock

centers have large collections of Gal4 strains that are readily available, which provide numerous temporal and spatial experimental conditions when we study our gene of interest. In addition, the activity of GAL4 is temperature sensitive. The experimental temperatures generally are 18°C, 25°C and 29°C. Higher temperature yields significantly higher activity of GAL4[24], which in turn results in higher efficiency in expressing our gene of interest. Researchers modulate the experimental temperatures accordingly. For instance, when depletion of our gene of interest causes lethality in embryonic stages at 25°C, we may revise the experimental condition to 18°C to reduce GAL4 activity. The developmental time also varies when experimental temperatures are altered. Flies raised at 29°C have a life cycle about eight to nine days, whereas flies raised at 18°C have a relatively longer life cycle about fifteen to sixteen days. We often study the loss of function of a gene using RNA interference (RNAi) to reveal its physiological function in the organism[25,26].

Researchers can also overexpress their gene of interest in genetic interaction analyses, where one can try to identify the hierarchy between two or more proteins within a common pathway. The Gal4-UAS system along with versatile genetic tools that are available to the fly community have made the fruit fly an excellent model organism to study fundamental developmental process and also gain insight into human disease mechanisms.

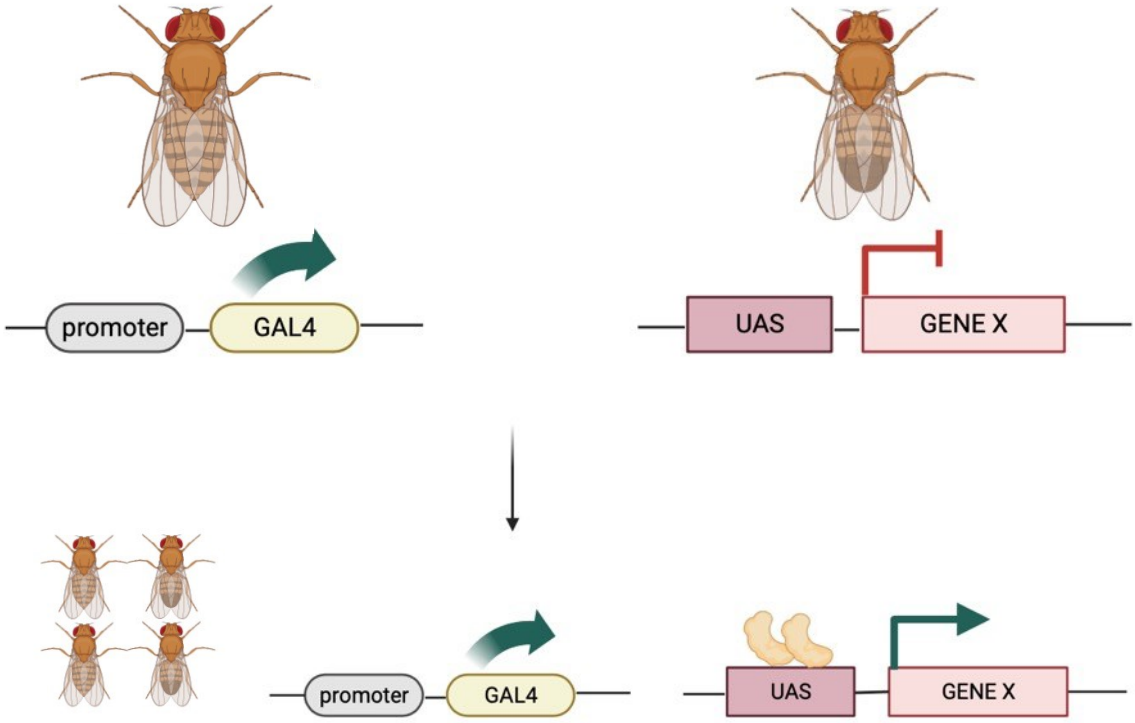

Figure 1.2. Binary GAL4-UAS system.

A cross scheme with GAL4-UAS is shown. Virgin females that carry GAL4 under specifically defined promoter are collected and crossed with males that carry the gene of interest (GENE X) that is downstream of the UAS. The progeny will contain both GAL4 and UAS, which leads to expression of the gene of interest, allowing for downstream applications including phenotypic analysis. Figure was generated using Biorender.

1.2. Cyclin-dependent kinases (CDKs)

Cyclin-dependent kinases (CDKs) are a family of serine-threonine protein kinases that are sub-grouped into subfamilies based on their functionalities[27,28]. CDKs have a generally conserved kinase domain and unique C-termini. The activity of CDKs is regulated by their association with partner subunits known as cyclins in the form of a heterodimer[29,30]. The kinase activity of CDKs can further regulated by other regulators beside cyclins by phosphorylation in the activation segment (also known as T-loop) of the kinase domain[31]. The most well-known CDKs are those involved in cell cycle regulation where they act together with their cyclin partner to control the stages of the cell cycle through a series of regulated degradation steps[32]. In contrast, the other major family of CDKs is involved in various aspects of transcriptional regulation (Fig.1.3).

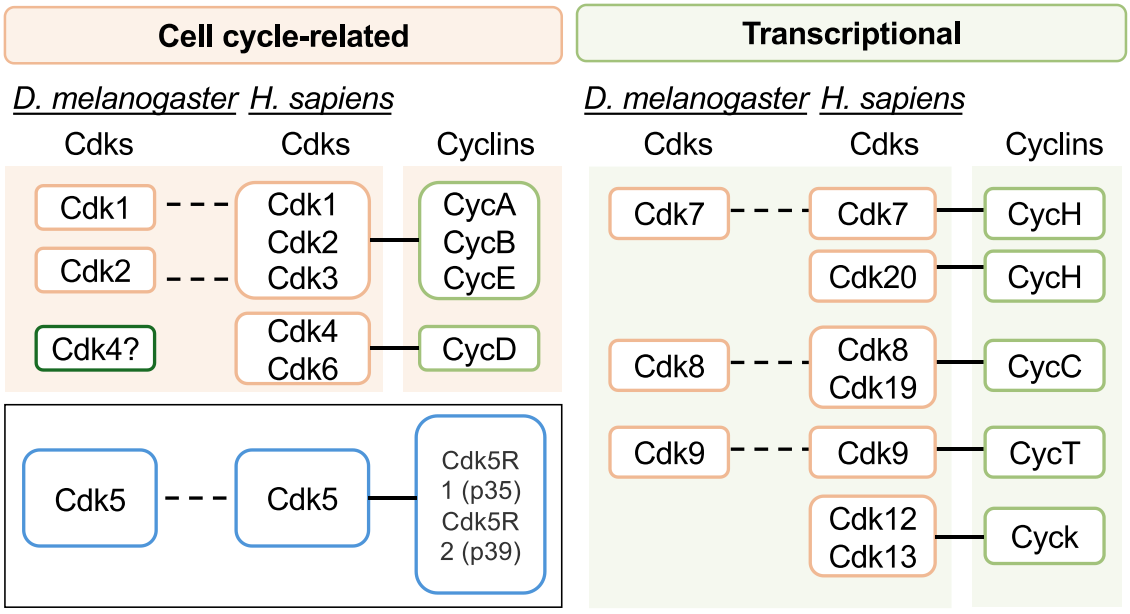

Figure 1.3. Cyclin-dependent kinases in Drosophila and Human.

CDKs are a family of serine-threonine protein kinases that are sub-grouped into two categories based broadly on their functions. CKDs share conserved function between Drosophila and Human. The two groups of CDKs are distinguished with their functions in regulating cell cycle, or transcription. CDK5 is considered as an outliner as it functions in a tissue-specific fashion. The figure is adapted from Malumbres's[27]. Licensed under CC BY https://creativecommons.org/licenses/by/4.0/

1.2.1. Cell-cycle related CDKs

The cell cycle is a series of events that takes place where a cell replicates its genetic material and usually divides; although, in Drosophila salivary glands, a process known as endoreplication occurs in cell cycle, where a cell increases its DNA content without cell division[33]. The cell cycle is composed with four phases, Gap phase 1 (G1 phase), DNA synthesis (S phase), Gap phase 2 (G2 phase) and mitosis (M phase). CDK1, CDK2, CDK4 and its paralog CDK6 (CDK4/6) and their corresponding cyclins regulate at different phases during the mitotic cell cycle (Fig. 1.4). When extracellular signals such as growth factors or mitogenic stimuli are present in early G1 phase, it results in release of cyclin D, which is the partner of CDK4/6[34]. Binding with cyclin D activates CDK4/6 kinase activity that subsequently phosphorylates the Retinoblastoma protein[31,35]. Retinoblastoma is a tumor suppressor that functions in regulating cell growth and prevent cells from dividing in an uncontrolled way[36]. Phosphorylated retinoblastoma results in release of E2F transcription factor, where its downstream responsive genes expression is required for cell-cycle progression[37,38]. The two early E2F responsive genes are Cyclin A and Cyclin E[39]. Newly synthesized Cyclin E binds to CDK2 in late G1 phase to further phosphorylate Rb, which results in completed Rb inactivation, allowing the cells to enter S phase[40–45]. During S phase, Cyclin E is replaced by Cyclin A and forms complex with CDK2 to phosphorylate proteins that are responsible for DNA replication[46,47]. Later during the G2/M transition phase, Cyclin A forms complexes with CDK1 to initiate mitosis[48], and Cyclin B later binds to CDK1 to participate in completing mitosis by the end of cycle[49]. Cell cycle exit starts with reduced transcription of Cyclin D[50], which inhibits the complex formation with CDK4/6, and prevents transcription of E2F responsive genes including Cyclin E; thus, inhibit the function of CDK2/Cyclin E complex. Since the activity of CDKs on phosphorylating retinoblastoma proteins are diminished by reduced cyclins level, retinoblastoma proteins return to hypo-phosphorylated active state, allowing cells to exit the cycle[51].

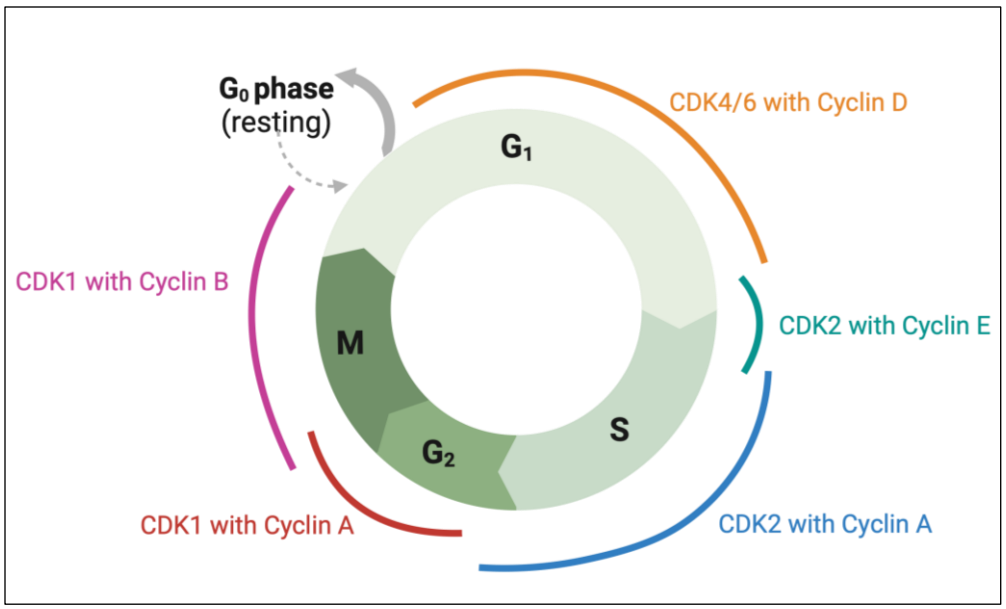

Figure 1.4. CDKs in cell cycle.

Four phases of cell cycle are regulated by different complexes of CDKs. CDK4/6 complex with Cyclin D regulates the G1. CDK2 with Cyclin E regulates the G1/S transition phase specifically, whereas later CDK2 binds with Cyclin A to regulate the S phase and S/G2 phase. CDK1 and Cyclin A complexes are formed to initiate mitosis during the G2/M phase, and later CDK1 binds to Cyclin B to ensure the completion of mitosis by the end of M phase. Figure adapted from Parua et al[38]. Licensed under CC BY https://creativecommons.org/licenses/by/4.0/

1.2.2. Function and localization of cell-cycle related CDKs

CDK1 and its binding partner Cyclin B participate in the G2 phase transition to mitosis. The complexes can be further regulated by checkpoint kinases such as Wee1-like protein kinase and Checkpoint kinase 1 to prevent damaged DNA from being distributed to daughter cells. It has been found that CDK1 in complex with Cyclin B is continually shuttling between the nucleus and cytoplasm before G2/M transition, which is observed in both fly and human[52–55]. Cdk1/Cyclin B accumulates in mitochondria during G2/M transition, phosphorylating mitochondrial proteins including complex I (CI) subunits to increase mitochondrial respiration, which in turn provides efficient bioenergy for a successful cell cycle progression in human breast epithelial MCF10A cells[56].

CDK2 is a major cell cycle component that controls the G1/S and S/G2 transition in dividing cells. It can form complexes with either Cyclin E or Cyclin A[40,41,46,47]. It has been shown that CDK2 is mainly located in the nucleoplasm[57,58]. However, expressing CDK2 in HeLa cells suggests that CDK2 localizes in both nucleoplasm and cytosol, suggesting potential functions in the cytosol[58] (From The Human Protein Atlas, an open access resource for human proteins, https://www.proteinatlas.org/ENSG00000123374-CDK2/subcellular).

CDK4 and CDK6 are paralogs which can each form a complex with cyclin D[30,31]. Direct inhibition of the cyclin D-CDK4/6 heterodimer activity prevents cell cycle progression from G1 to S phase of the cell cycle[59]. Immunolocalization assays revealed that CDK4/Cyclin D complexes are formed in the cytoplasm in HEK293, Hela and NIH-3T3 cells[60]. Complexes accumulate on nuclear membrane and enter the nucleus during G1/S transition phase.

1.2.3. Diseases associated with Cell-cycle related CDKs

Drosophila has homologs of the cell-cycle regulators that bind to the same type of cyclins as are found in vertebrates[61,62]. In humans, altered expression of cell-cycle related CDKs are commonly seen in different types of cancer. Dysregulated CDK1 is found in breast, lung and colorectal tumors[63]; whereas aberrant expression of CDK2 and Cyclin E have been associated with ovary and prostate carcinomas[64]. Identifying inhibitors of CDK4/6 have promising results as numerous cancers are found to be particularly sensitive to CDK4/6 inhibition[65]. The complex of CDK4/6 with Cyclin D can activate the Ras signaling pathway, which is one of most commonly altered pathways found in tumors[66]. While people with mutations in CDK4 have a very high lifetime risk of developing melanoma[67], analysis of homozygous *Cdk4* mutants in Drosophila has shown that Cdk4 is dispensable in regulating the cell cycle as flies are fertile and developed to the adult stage with no delay[68].

Mutations in CDK6 have been identified in a rare development disorder. Patients with autosomal recessive primary microcephaly have reduced head circumference and cerebral cortex size along with intellectual disability. A nucleotide mutation was identified in CDK6 exon 5 c.589G>A, where an alanine is substituted to a threonine at residue 197 within the kinase domain[69]. Cells with mutated CDK6 exhibited disorganized

microtubules and mitotic spindle during mitosis along with overall reduced cell proliferation in primary patient fibroblasts[69].

1.2.4. Transcriptional-related CDKs

The main function of transcription is to make an RNA copy from genomic DNA, where a subset of RNA known as messenger RNA (mRNA) is subsequently translated into proteins. Some RNA remains in the form of transfer RNA (tRNA) or ribosomal RNA (rRNA), which function in aiding translation and ribosomal assembly, respectively. As an analogy to the cell cycle, transcription can also be divided into four “phases” termed initiation, elongation, termination and recycling. Consistent with CDKs in cell cycle, different CDK substrates are phosphorylated at different times in transcription to drive events in proper sequence. CDKs that participate in transcriptional regulation are CDK7, 8/19, 9, 12/13. RNA polymerase II (Pol II) is the most studied type of RNA polymerase. The central hub of regulation in Pol II is the carboxy-terminal domain (CTD) of the largest subunit of Pol II, DNA-directed RNA polymerase II subunit (Rpb1), which comprises heptad repeats with the consensus sequence: Tyr1-Ser2-Pro3-Thr4-Ser5-Pro6-Ser7[70]. Multiple positions within the heptads are phosphorylated by CDKs and other kinases, which in turn regulates transcription[25, 38].

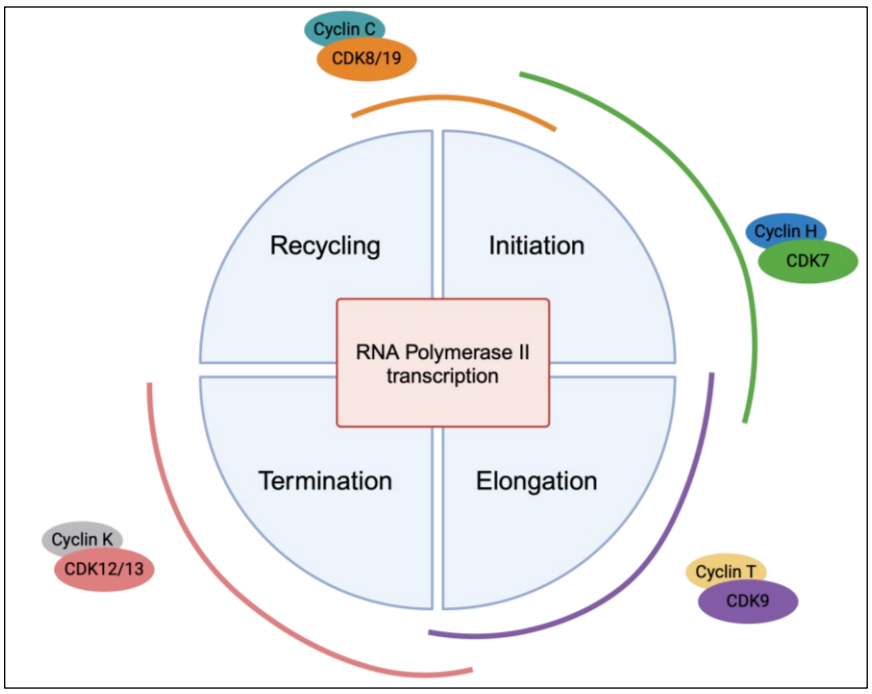

Figure 1.5. CDKs in transcription.

RNA polymerase II mediated transcription can be divided into four steps: initiation, elongation, termination and recycling. CDKs mostly participate in the first three steps. CDK8/19 complexes regulate the formation of pre-initiation complex (PIC), which determines the initiation of transcription. CDK7 and CDK9 complexes both regulate the elongation process. CDK12/13 complexes participate at the termination stage by regulating mRNA processes of the nascent mRNA. Recycling of unphosphorylated Pol II to re-initiate the cycle. Figure is adapted from Łukasik et al[65]. Licensed under CC BY https://creativecommons.org/licenses/by/4.0/

1.2.5. Function and localization of transcriptional-related CDKs

CDK8 or its vertebrate paralog CDK19 forms a kinase module (called the Cdk8 module) with Cyclin C together with Mediator 12 and Mediator 13 (MED12/13) that associates reversibility with the core mediator (Fig. 1.6). The core mediator is a multiprotein complex composed of 26-30 subunits that regulates transcription by serving as a bridge between the transcription factors that have bound DNA regulatory sequences and the Pol II machinery assembled near the promoter. Interestingly, most of the substrate activity is dictated by the partner cyclins, but in the case of CDK8/19, the substrate selectivity is regulated by MED12/13[72,73].

The CDK8/19 kinase module is involved in both transcriptional activation and repression by phosphorylating the CTD of free Pol II during preinitiation complex (PIC) formation[74]. The formation of PIC requires binding of general transcription factors including TFIID, TFIIB, TFIIE, TFIIF, TFIIH along with Pol II[75]. Once the PIC is formed, CDK8/19 promotes the recruitment of bromodomain protein 4, which functions in acetylating histone and remodeling chromatin to make DNA more accessible for transcription, and trigger transcription elongation[76]. CDK8 is found mostly present in the nucleoplasm, which is consistent with its nuclear function in regulating transcription[77]. However, the paralog CDK19 is shown to have both nucleoplasm and cytoplasmic localization across three different human cell lines (U2OS, SH-SY5Y and THP-1). (From The Human Protein Atlas, an open access resource for human proteins https://www.proteinatlas.org/ENSG00000136807-CDK19/subcellular).

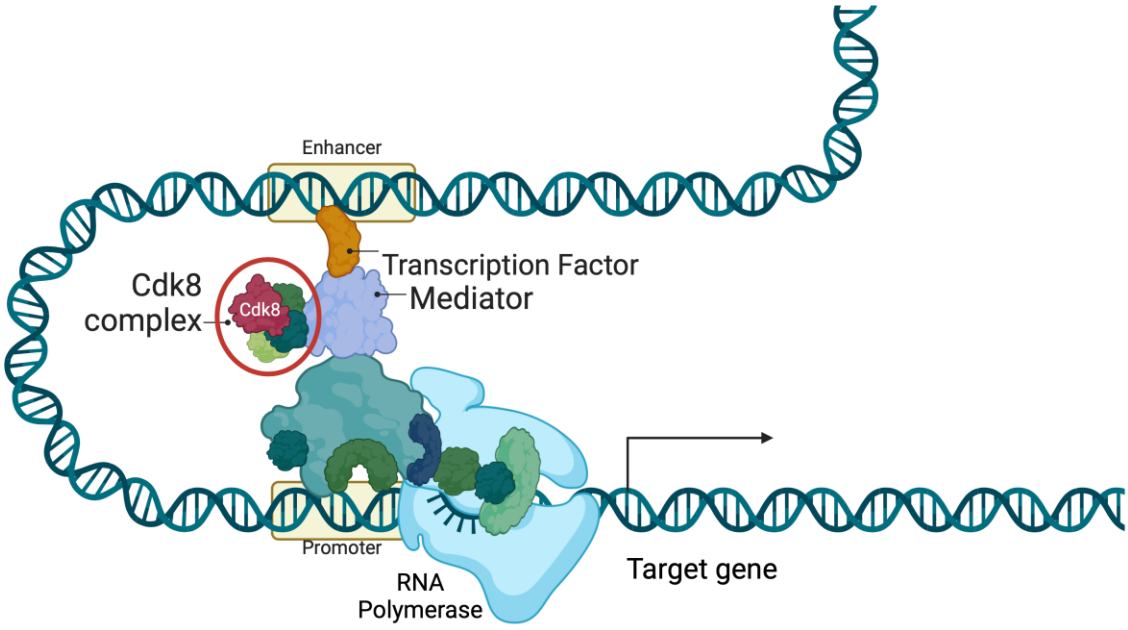

Figure 1.6. Cdk8 and its partners in the submodule known as Cdk8 complex.

Cdk8 forms the kinase module with its partners Cyclin C, Med12 and Med13 (Circled in red), which is known as Cdk8 complex. The complex interacts with the core mediator in turn to regulate RNA polymerase II mediated transcription. Figure was generated using Biorender.

CDK7 forms a complex with Cyclin H to act as CDK-activating kinase (CAK) in transcription[78–81]. CDK7 complex is part of initiation factor TFIIH to exert catalytic activity[82]. Early in transcription, CDK7 complexes phosphorylates Ser5 and Ser7 of Pol II CTD to facilitate promoter clearance and initiating transcription[83,84]. In addition, it is found that phosphorylation on Ser5 promotes co-transcriptional 5'-end capping of the nascent transcript[85,86]. CDK7 was also found to regulate the promoter-proximal pause during Pol II elongation which takes place -50-100 base pair downstream the transcription start site[87]. The pausing during Pol II elongation forces coupling between the transcript elongation and co-transcription processes[87]. To alleviate the pausing on elongation, CDK7 acts as CAK on CDK9 by phosphorylating to promote continuation of transcription elongation. CDK7 expression level in cells remain constantly low, and the CDK7 complex is found to locate in both nucleus and cytoplasm in A549 human lung carcinoma[88,89]. CDK20 is a paralog of CDK7 and can form a complex with Cyclin H as well[90]. The localization of CDK20 is primarily found in nucleoplasm. (From The Human Protein Atlas, an open access resource for human proteins https://www.proteinatlas.org/ENSG00000156345-CDK20/subcellular).

CDK9 is a driver of Pol II elongation, and forms a complex with cyclin T. CDK9 complex forms the core of positive transcription elongation factor b (P-TEFb), which functions in alleviating the promoter-proximal pause into rapid elongation[71]. Phosphorylation of Thr186 in the T-loop of CDK9 results in activation of the CDK9 complex[91,92]. The effect can be reversed by phosphatases or acetylation of cyclin T. Interestingly, despite its function in transcription elongation, CDK9 is found in nucleoplasm as well as in cytoplasmic bodies in different human cell lines (U2OS, A-431 and U-251MG). (From The Human Protein Atlas, an open access resource for human proteins https://www.proteinatlas.org/ENSG00000136807-CDK9/subcellular).

CDK12 and CDK13 are paralogs, and form a complex with cyclin K[93]. The CDK12/13 complex is implicated in Pol II CTD phosphorylation on Ser2 and Ser5[94]. CDK12/13 is highly expressed in embryonic stem cells and reduced upon differentiation[95]. Depletion of CDK12 results in significantly reduced Ser2 phosphorylation in human cells, whereas depletion of CDK13 resulted in no observable change in the level of phosphorylated Ser2. CDK12/13 shares arginine/serine-rich domains[95], which is a critical component of proteins involved in nuclear pre-mRNA processing. Depletion of CDK12/13 in cultured cells resulted in repression in genes

encoding RNA-processing factors and causing defects in transcription elongation. CDK12 is found predominantly in the nucleoplasm, whereas CDK13 is found in cytosol and Golgi apparatus when expressed in SiHa cells and HeLa cells, respectively. (From The Human Protein Atlas, an open access resource for human proteins https://www.proteinatlas.org/ENSG00000167258-CDK12/subcellular for CDK12 and https://www.proteinatlas.org/ENSG00000065883-CDK13/subcellular for CDK13).

1.2.6. Diseases associated with transcriptional-related CDKs

CDKs that are classified as being involved in transcriptional regulation are conserved between Drosophila and humans and the same binding partners are related to their functions in tissues[81,96,97]. Given their important roles, numerous diseases have been identified due to mutations in human *CDK* genes.

CDK7 has been implicated in trichothiodystrophy (TTD), known as Tay syndrome, which is a rare autosomal recessive multisystem disorder with clinical features including brittle hair, microcephaly, intellectual disability and growth retardation[98,99]. Mutations in *XPB* and *XPD* are also associated with this syndrome[100]. XPB and XPD are xeroderma pigentosum group B and D genes, which encode two ATP-dependent DNA helicases that function in unwinding the double helix of DNA. XPB and XPD are subunits of the early initial factor TFIIH that participates in RNA Polymerase II mediated transcription, which is tightly associated with the CDK7 complex[100]. In addition, TFIIH also functions in nucleotide excision repair to remove bulky DNA lesions. Mutations in either XBP or XPD resulted in compromised transcription as well as DNA damage response, ultimately resulting in development of TTD[99].

Heterozygous missense mutations have been found in both CDK8 and CDK19. All the missense mutations are located in the highly conserved kinase domain[101–106]. Patients with CDK8 or CDK19 mutations exhibit mild to moderate developmental delay, facial dysmorphism, muscle hypotonia, as well as emotional and psychological symptoms of behavioral disorders including autism spectrum disorder (ASD) and attention deficit hyperactivity disorder (ADHD)[105,107]. Some patients also exhibited additional clinical features including congenital heart defects and loss of hearing[101,105,107].

The effort has been put in to further characterization of these pathogenic variants using different model organisms including Drosophila[101–106] (see below).

A mutation c.673C>T; p.Arg225Cys in CDK9 was identified in five individuals using exome sequencing. It was first identified in a pair of cousins from a single consanguineous family using autozygosity mapping and exome sequencing. Patients with homozygous CDK9 mutation have multiple-malformation syndrome with clinical features include microcephaly, coloboma, which is a condition missing normal tissue around or in the eye at birth, congenital heart disease, and global developmental delay[108,109]. Recently, a patient with compound heterozygous pathogenic variants of CDK9 has been identified. The patient presented with multiple clinical features including facial asymmetry, bilateral hearing loss, cleft lip and palate, undescended testis and intellectual disability. After trio exome sequencing, the patient is identified to carry two rare missense variants in exon 7 of CDK9, c.862G>A, p.(A288T) (inherited from maternal) and c.907C>T, p.(R303C) (inherited from paternal)[110]. All the *de novo* mutations in CDK9 are located within the kinase domain and are found to be well conserved across several vertebrate species. The kinase activity from the variants is significantly reduced in comparison to wildtype CDK9 when Sachiko Nishina et al.[110] modeled the variants in zebrafish, which suggested the variants cause loss of function in CDK9[110].

Heterozygous missense mutations in CDK13 were first identified as a cause for congenital heart defects[111]. Today, CDK13 *de novo* mutations have been reported in 43 unrelated individuals[111–114]. Consistent with missense mutations found in CDK8/19 and CDK9, all the mutations are located within the kinase domaim[111–114]. Patients with CDK13 mutations exhibited developmental delay and intellectual disability, and most of the patients have congenital heart defects with facial dysmorphism including hypertelorism, short and broad columella, wide nasal bridge[111–114]. Nearly all individuals display impaired verbal language skills after one year old. Some patients have feeding difficulties in infancy[112,114]. Knockout mice of *cdk12*, the close paralogue of *cdk13*, demonstrated that CDK12/13 are essential for development, as *cdk12* knockout mice die after implantation[111].

1.2.7. The outlier CDK5

CDK5 is a divergent member of the CDK family as it does not belong to either cell-cycle related or transcriptional subgroup. Nucleocytoplasmic CDK5 is enriched in the brain and shares conserved functions in flies and vertebrates in post-mitotic neurons[115–117].

A homozygous point mutation in CDK5 is reported in human lissencephaly, which is characterized with brain malformations with absence of cerebral convolutions and smooth cortical surface[118]. The homozygous mutation is located within the intron-exon boundary near exon 8 of CDK5 c. 2634G>A, p.V162S, which results in a frameshift and exon skipping in exon 8. The resulting CDK5 has a truncated C-terminus when compared to cDNA from wildtype CDK5. The frameshift led to a premature stop codon at residue 19 downstream of the frameshift (V162SfsX19). The p.V162SfsX19 mutation causes lack of endogenous CDK5 expression in affected dermal fibroblasts and brain tissue at the mRNA and protein levels, likely due to activation of the nonsense-mediated mRNA decay[118].

CDK5 has also been implicated in neurological disorders including Alzheimer's disease (AD) and Parkinson's diseases (PD). Protein aggregates are one of the pathological features associated with neurodegeneration[119]. Activated CDK5 is found to promote Aβ generation and accumulation in neurons, which is one of key factors in AD progression[120]. In addition, dysregulated CDK5 is found to associated with loss of dopaminergic neurons and progression of PD[121]. Inhibiting aberrant CDK5 exerts neuroprotective effect in PD by prevent the dopaminergic neuron loss and alleviating behavioral changes in a PD mouse model[122]. These findings indicate CDK5 plays a critical role in development of nervous system. The findings that CDK5 functions mainly in the postmitotic neurons suggests CDK has tissue specific functions.

1.3. Cyclin-dependent kinase 8 and 19 (Cdk8/CDK19)

CDK8 and its paralog, CDK19, are cyclin-dependent kinases known to regulate transcription. Either CDK8 or CDK19 are components of a 4-protein complex called the Mediator kinase module[74] (Fig. 1.6). They are mutually exclusive in this complex to regulate RNA Polymerase II-mediated gene expression. In recent years, dysregulation of Mediator kinase module proteins, including CDK8/19, have been implicated in the development of different human diseases, in particular, cancer [123]. In vertebrates, CDK8 is expressed ubiquitously [124]. Enhanced CDK8 activity is implicated in tumorigenesis including in colorectal and breast cancer and melanoma[125–128].

In vertebrates, expression of CDK19 is highest in the brain[124]. CDK19 was thought to function similarly or redundantly to CDK8 given that they share 84% amino acid sequence similarity and 97% identity in the kinase domain (Fig. 1.7)[129]. However, significant functional differences have been uncovered in different model organisms.

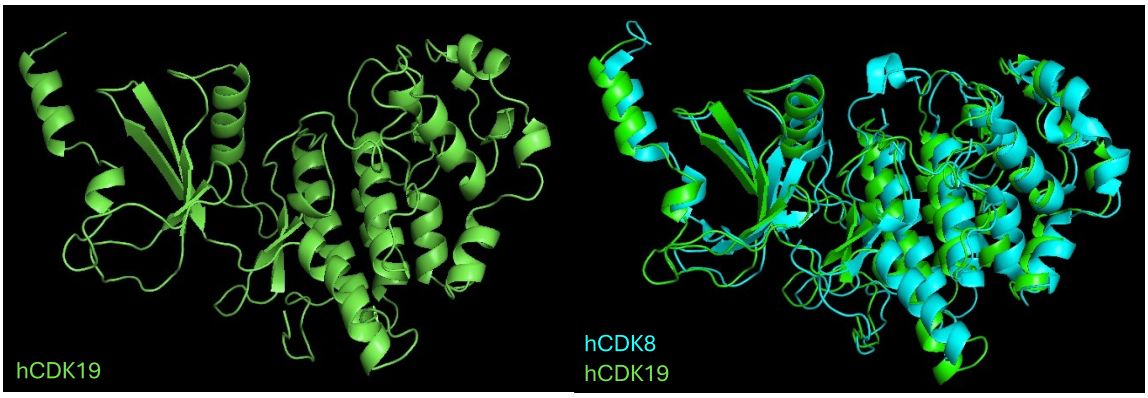

Figure 1.7. Protein folding structure of CDK19 and overlayed with CDK8.

The kinase domains of CDK8 and CDK19 are well conserved as the structures between the two paralogs are mostly overlapped. Modelled using FASTA sequence from Uniprot (CDK19:Q9BWU1-1) in Phyre 2.0 Molecular Modelling Software. Graphs generated using PyMOL.

1.3.1. Cdk8 function in mice

Heterozygous mutation of *Cdk8* in mice causes no observable phenotypes in appearance and breeding capacity in comparison to wildtype mice[130]. Homozygous

depletion of Cdk8 in mice is embryonic lethal. Blastomeres at the 4-cell or 8-cell stage of the developing mouse embryo have fragmented morphologies, and no embryo with *Cdk8* homozygous mutations was found beyond the 8-cell stage, suggesting a requirement of Cdk8 in preimplantation[130]. Conditional knockout of Cdk8 was established to compare the tissue homeostasis and tumour development in vivo upon Cdk8 reduction. Condition homozygous mutation of *Cdk8* in young adult mice has no observable phenotypes, suggesting Cdk8 may be dispensable for somatic cellular homeostasis[131]. However, depletion of Cdk8 in an intestinal tumour model significantly reduced animals' survival rate and enhanced the size and growth of tumour, which indicates Cdk8 acts as a tumour suppressor under context specific conditionsX[131].

1.3.2. Cdk8 function in *C. elegans*

In *C. elegans*, mutant *cdk-8* and *cic-1* (Cyc C in *C. elegans*) lead to defective phenotypes including embryonic and larval lethality, as well as egg-laying defects[132]. Mutant *mdt-12* (Mediator 12 in *C. elegans*) leads to similar defective phenotypes along with uncoordinated movement[132]. Mutant *mdt-13* (Mediator 13 in *C. elegans*) results in mild axonal defects in anterior guidepost neuron (AVG) in the ventral nerve cord (VNC). The ventral nerve cord is the main nerve bundle along the anterior-posterior body axis of *C. elegans* and consists of two axon tracts that direct the axon guidance towards to the right or left of VNC. AVG is the first axon pioneering the right VNC axon tract from anterior to posterior[132]. Axon navigation depends on guidance receptors. Proper transcriptional regulation of the guidance receptors is crucial as it can alter the guidance decision when expression is dysregulated. Interestingly, it has been shown that mutations in individual components in the Cdk8 module results in defects in axon guidance decisions in the VNC and during dorsal axon navigation. Mutations in the Cdk8 module cause irregular cross over of interneuron axons, as well as aberrant axon navigation of the motoneurons in VNC[132]. In addition, a subset of commissural neurons was severely disrupted in either *cdk-8* or *mdt-12* mutant animals[132], suggesting the transcriptional role of Cdk8 module is involved in proper axon navigation in certain subsets of neurons in *C. elegans*.

1.3.3. Cdk8 function in Drosophila

In Drosophila, Cdk8 is the sole homolog of human CDK8 and CDK19. *Cdk8* and its partner, *Cyclin C* are essential in *Drosophila* as homozygous *cdk8* or *cyc C* null allele flies die as late third instar larvae or early pupae[133]. Null alleles of *med12* and *med13* in flies are also recessive lethal, indicating the components of the kinase module are required for viability of the fly[134,135]. Somatic clones of *cdk8* null alleles in larval leg discs led to abnormalities in adult legs, especially in males as increased numbers of sex combs are found in flies with *cdk8* mutation[133]. Sex combs are a male-specific group of bristles located on the foreleg of Drosophila. Mitotic clones of cells that are of *cdk8 or cycC mutant* have no effect on the developing eye in flies, whereas clones of *med12* or *med13* fail to differentiate the developing eye disc to ommatidia. Loss of sensory bristles on the notum of adult flies is observed in clones of *cdk8* due to reduced expression of *senseless*, which is the transcription factor that is specifically expressed in sensory organ precursors[133].

To circumvent the lethality in homozygous *cdk8* mutants, researchers used RNAi instead to knockdown most of endogenous *cdk8*, where defective phenotypes can be investigated at different stages of fly development[136]. The difference between *cdk8* mutants and *cdk8* depleted flies is that in *cdk8* mutants, there was absolute absence of endogenous Cdk8, whereas in the case of Cdk8 depleted flies, there was still some remaining endogenous Cdk8 present, depending on the efficiency of the RNAi treatment. These approaches allowed characterization of cellular effects due to reduced though not completely absent Cdk8 function[136].

Overexpression of Cdk8 in the wing resulted in disrupted veins in the wing blades, whereas depletion of Cdk8 caused ectopic vein formation that has the same morphology as those seen after expressing a kinase dead version of Cdk8[136]. These findings suggest the observable phenotypes depend on the kinase activity of Cdk8, which needs to be tighly regulated for proper vein patterning in the fly wing. Genetic screening identified that Mothers against dpp (Mad), the downstream transcription factor of the Decapentaplegic (Dpp) signaling pathway, which is equivalent to transforming growth factor-β (TFGβ) in vertebrates, is positively regulated by Cdk8 and Cyclin C[136].

Expression of Cdk8 and Cyc C negatively regulates Sterol regulatory element-binding proteins (SREBP)-mediated lipogenesis. SREBP is the master transcription factor that regulates biosynthesis of cholesterol, fatty acids, and lipids[137]. Mutant *cdk8* or *cycC* larvae appeared to be more opaque in comparison to wildtype larvae due to having increased triaglycerol in their fat body, which is a tissue that preserves all the fat cells in flies[138]. Recent findings indicate that Cdk8 regulates the stability of SREBP by phosphorylation at threonine 390, a highly conserved threonine residue across species, to alter the SREBP-mediated lipogenic gene profile[138].

1.3.4. Cyclin C can translocate from the nucleus to the cytoplasm to promote mitochondria fission

Interestingly, the partner of Cdk8, Cyclin C, has been shown to exert a mediator independent function in promoting mitochondrial fission under oxidative stress conditions in both yeast and mouse embryonic fibroblasts[139,140]. The translocation takes place under stress conditions, and not under physiological conditions. It was found that the translocation from nucleus to cytoplasm allows Cyclin C to interact with the mitochondrial fission regulator, Dynamin-related protein 1[139–141]. This effect does not seem to require the presence of Cdk8. In addition, translocated Cyclin C not only promoted mitochondrial fragmentation via Drp1, but it also triggered intrinsic apoptosis by interacting with integral membrane protein B-cell lymphoma-2 associated X protein, Bax[78]. These findings suggest that all functions of the Cdk8 kinase module have not been fully elucidated[140–143].

1.3.5. CDK19 function in mice

Knockout of *Cdk19* results in mice that are asymptomatic, fertile and have a normal lifespan[144]. A recent publication has shown that Cdk19, but not the paralog Cdk8, is relatively enriched in mouse hematopoietic stem cells (HSCs)[145]. A significant increase in expression of Cdk19 is found when cells are treated with proliferative stressors[145]. In addition, overexpression of Cdk19 in the HSCs enhanced the repopulation ability of HSCs, which is not observed when Cdk8 is expressed. Treatment with SenexinB, which is an inhibitor of Cdk8/Cdk19, resulted in decreased proliferation in HSCs as well as in reducing the number and size of colonies in a colony-forming unit assay. Consistent phenotypes were observed in Cdk19 knockout HSCs in mice[145]. These findings suggest

that loss of Cdk19 compromises the proliferation and function of HSCs. Since acute myeloid leukemia (AML) cells are a type of malignant hematopoietic cell with aberrant cell cycle regulation, Zhang et al.[145] tested the efficiency in suppressing Cdk19 in attenuating proliferation in AML cells. Treatment with SenexinB in AML cells potently attenuated the proliferation of AML cells, indicating Cdk19 may be a potential therapeutic target for modulating the proliferation of AML cells[145].

1.4. Developmental syndromes due to mutations in CDK8 and CDK19

Mutations in *CDK8* and *CDK19* are associated with severe neurodevelopmental disorders in human[101–106]. While these two syndromes are considered distinct in the Online Mendelian Inheritance in Man database (OMIM), the similarities between the two suggest that the clinical differences are likely due to the variations in cells in which the genes are normally expressed.

1.4.1. Clinical features associated with de novo mutation in CDK8

Whole genome or exome sequencing was used to identify a total of 10 *de novo* heterozygous mutations in *CDK8* among 14 unrelated children between two independent research groups (Table 1.1)[104,105]. Patients with *CDK8* mutations are classified as Intellectual developmental disorder with hypotonia and behavioral abnormalities (IDDHBA) in OMIM, (IDDHBA, OMIM 618748). All the identified *de novo* mutations are located within the highly conserved kinase domain of CDK8 (aa21-335) (Fig. 1.8). Patients with *CDK8* mutations shared some common features including hypotonia, which is the reduced muscle tone, intellectual disabilities, and developmental delays in early infancy[105,107]. Seven out of twelve patients (two were not tested) show congenital heart defects[105,107].

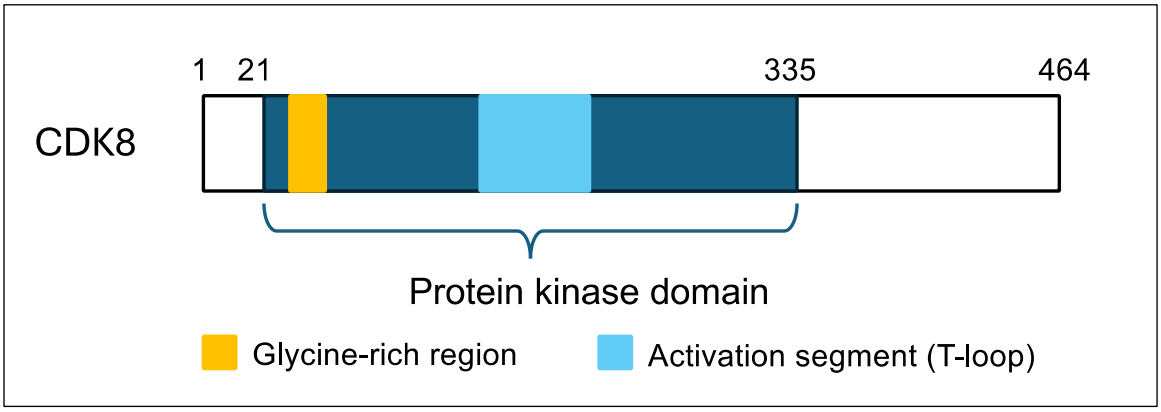

Figure 1.8. CDK8 protein structure.

CDK8 is comprised of 464 amino acids. It contains a N-terminus with a well conserved kinase domain between amino acid 21 to 335. The C-terminus of CDK8 is considered as a disordered domain. The kinase domain can be further distinguished by the glycine-rich region and activation segment, which is also known as the T-loop.

Table 1.1. De novo mutations found in CDK8.

Mutation	Substitution	Model organism / Cell line	Reference
c. 79G>C	p.Val27Leu	SW620* CDK8, CDK19 double KO	Calpena et al 2019 [104]
c.85C>G	p.Arg29Gly	SW620 CDK8, CDK19 double KO	Calpena et al 2019
c.88G>A	p.Gly30Ser	SW620 CDK8, CDK19 double KO	Calpena et al 2019
c.185C>T	p.Ser62Leu	SW620 CDK8, CDK19 double KO	Calpena et al 2019
c.291T>G	p.Phe97Leu	SW620 CDK8, CDK19 double KO	Calpena et al 2019
c.533G>A	p.Arg178Gln	SW620 CDK8, CDK19 double KO	Calpena et al 2019
c.578T>G	p.Val193Gly	SW620 CDK8, CDK19 double KO	Calpena et al 2019
c.669A>G	p.Ile223Met	SW620 CDK8, CDK19 double KO	Calpena et al 2019
c.83G>C	p.Gly28Ala	Zebrafish	Uehara et al 2020 [105]
c.467A>G	p.Asn156Ser	Zebrafish	Uehara et al 2020

Note: * SW620 human colorectal carcinoma cells were used to study mutations by generating double knockout of CDK8 and CDK19 using CRISPR technique

1.4.2. Clinical features associated with de novo mutation in CDK19

A female patient who had congenital bilateral falciform retinal fold associated microcephaly and intellectual disability, was found to have a pericentric inversion on Chromosome 6, where *CDK19* is disrupted due to the chromosomal rearrangement[146]. Congenital retinal fold is a rare eye condition which if left untreated can result in vision loss[146]. It was the first case that is associated with CDK19 in affecting the neurodevelopment in infancy.

In recent years, additional mutations affecting CDK19 have been identified, and patients with CDK19 mutations are classified with a syndrome that is newly defined: developmental and epileptic encephalopathy 87 in OMIM (DEE87, MIM: 618916). DEE87 often starts in infancy. Children have frequent and severe seizures which are often drug-resistant[147]. Children with DEE87 can exhibit significant developmental delay, known as encephalopathy[101–103,106]. Trio-exome sequencing (ES-Trio) in which DNA from patients and their parents is studied, was used to identify a total of 8 *de novo* mutations in *CDK19* among 15 unrelated children between multiple research groups (Table 1.2)[101–103,106]. All the patients have developmental delay and intellectual disabilities. Hypotonia was found in 12 out of 15 patients. Abnormal brain images using magnetic resonance imaging (MRI) were found in 9 patients. Features including brain atrophy with white matter abnormalities, delayed myelination, widening of part of the cerebral lobe were observed[101–103,106]. The common facial dysmorphic features shared among these patients is hypertelorism, a prominent nose with a bulbous tip, low nasal bridge, a large mouth with widely spaced teeth and an arched upper lip, which highly resembled patients with *CDK8* mutations[101–103,106].

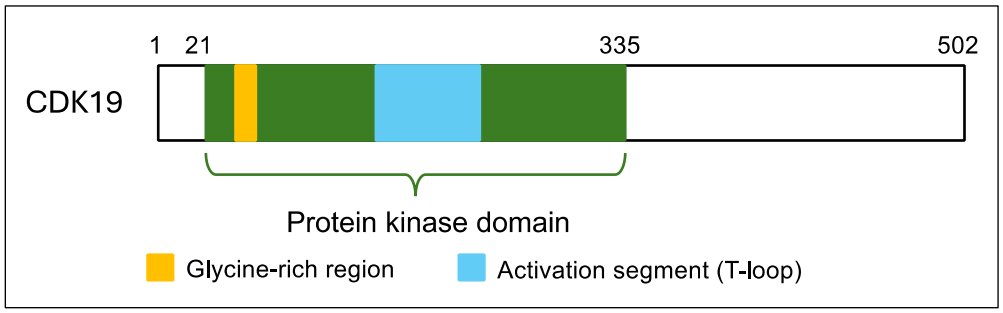

Figure 1.9. CDK19 protein structure.

CDK19 has a similar protein structure as CDK8, especially within the kinase domain, which is between amino acid 21 to 335. The C-terminus of CDK19 is extended to amino acid 502. The kinase domain can be further distinguished by the glycine-rich region and activation segment, which is also known as the T-loop.

Table 1.2. De novo mutation found in CDK19 and models for their study

Mutation	Substitution	Model organism / Cell line / other	Reference
c.586A>G	p.Thr196Ala	Drosophila	Chung et al 2020 [102]
c.94T>C	p.Try32His	Drosophila Proband MRI Zebrafish; HEK293	Chung et al 2020 Sugawara et al 2020 [106] Zarate et al 2021 [101]
c.92C >A	p.Thr31Asn	Proband brain MRI*	Yang et al. 2021 [103]
c.82G>C	p.Gly28Ala	Zebrafish; HEK293	Zarate et al 2021
c.82G>A	p.Gly28Ala	Zebrafish; HEK293	Zarate et al 2021
c.83G>C	p.Gly28Ala	Zebrafish; HEK293	Zarate et al 2021
c.95A>G	p.Try32Cys	Proband ES-trio	Zarate et al 2021
c.589T>C	p.Phe197Leu	Proband ES-trio	Zarate et al 2021
c.594G>C	p.Trp198Cys	Proband ES-trio	Zarate et al 2021
c.598C>T	p.Arg200Trp	Proband ES-trio	Zarate et al 2021

Note: * magnetic resonance image

1.5. Models for CDK8/19 Syndromes

Since all the mutations that have been identified are located within the well conserved kinase domain in CDK8 and CDK19 (Fig. 1.10), researchers further characterized the effect of these variants on kinase activity in CDK8 and CDK19. Model organisms such as fruit flies and zebrafish, along with cell culture, have been used to characterize and to understand the underlying pathology of these variants in more depth.

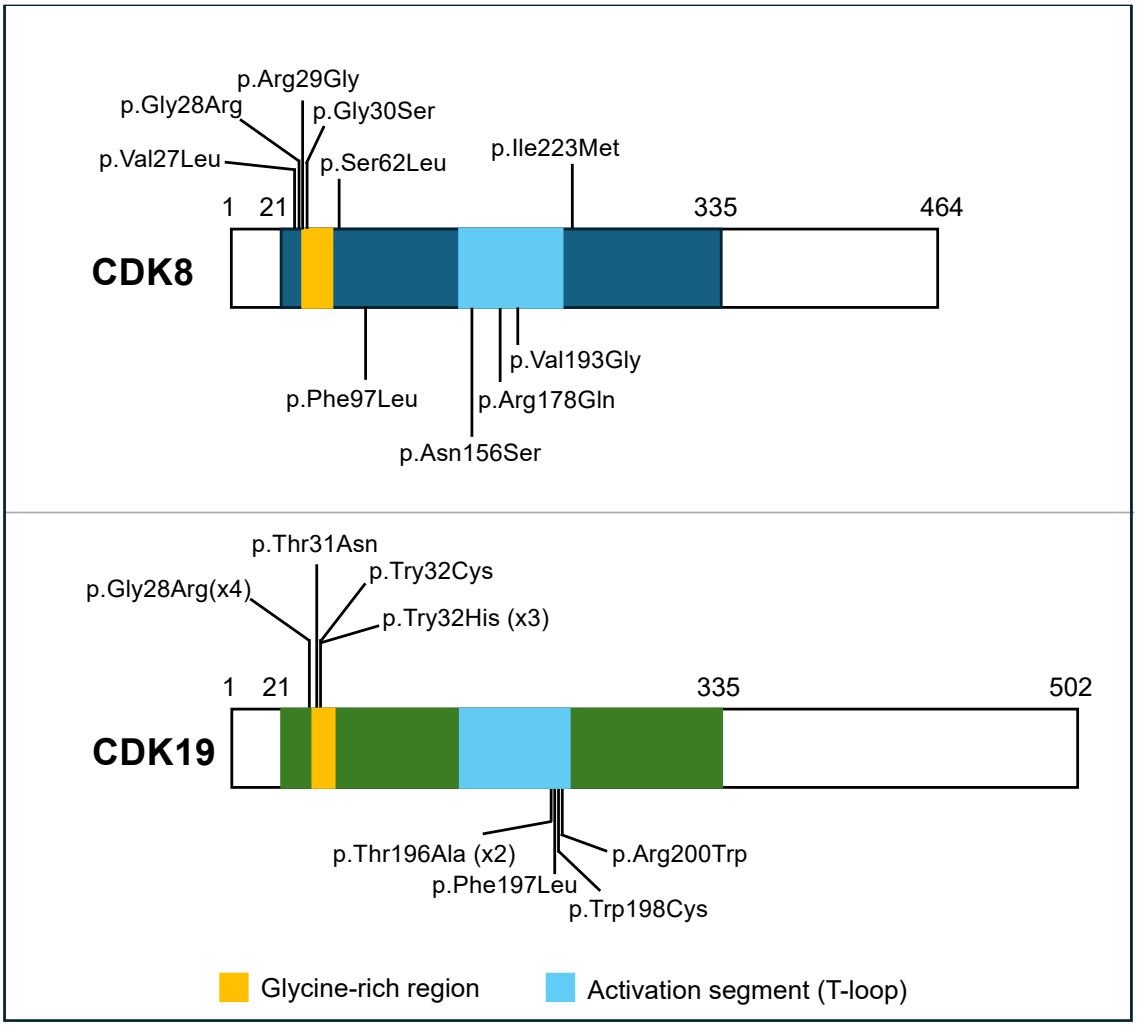

Figure 1.10. De novo mutations identified in CDK8 and CDK19.

Missense mutations found in CDK8 and CDK19 are all located in the well-conserved kinase domain and mostly distributed in two distinct regions, the ATP binding region in glycine-rich region and activation segment where kinase gets activated by phosphorylation from other regulators.

1.5.1. Modeling *CDK8* de novo mutations using human cell lines

The human cell line SW620, which is a colorectal carcinoma cell line and human embryonic kidney cells 293 (HEK293) were used to assess the kinase activity of *de novo* variants in CDK8 *in vitro*.

In the case of SW620, a double knockout of CDK8 and CDK19 was first generated[104]. Calpena et al.[104] reintroduced wildtype CDK8 into the double knockout background and tested the phospho-status of STAT1 at S727, which is one of the well-validated targets for CDK8 kinase activity[148–150]. Site-direct mutagenesis on the CDK8 cDNA was used to generate plasmids that encode individual mutations. Decreases in the phospho-level of STAT1 was observed when each variant plasmid was transfected into the double knockout background to a same extent as transfecting catalytically inactive CDK8 kinase-dead (Asp173Ala), suggesting all the mutations in CDK8 affect its kinase activity[104].

In the case of HEK293, Uehara et al.[105] examined the kinase activity of p.G28A or p.N156S mutations in comparison to CDK8 wildtype. The amount of ADP generated was used as a readout for kinase activity. Reduced kinase activity was found in both variants in comparison to wildtype, which suggests these variants interfere with the kinase activity of CDK8.

1.5.2. Modeling CDK8 de novo mutations using zebrafish

To characterize the pathogenicity of p.G28A or p.N156S further, Uehara et al.[105] examined the effect of injecting wildtype, *CDK8-G28A* or *CDK8-N156S* mRNA into the zebrafish embryo. Overexpression of wildtype or the two variants caused defective phenotypes including short body axis, hypoplastic anterior structure with aberrant tail. The variants were found to induce these effects at a lower frequency than wildtype, which suggested that the two variants are hypomorphic alleles of CDK8. Drug inhibition of the kinase activity of CDK8 using Senexin A resulted in structural anomalies in the heart and craniofacial cartilage in zebrafish that are reminiscent of phenotypes seen in the patients. These findings further indicate that the kinase function of CDK8 is essential throughout development of zebrafish and likely in humans as well.

1.5.3. Modeling CDK19 de novo mutations using human cell lines

Two *de novo* mutations in CDK19 have been observed recurrently, p.Gly28Arg and p.Tyr32His, where each was identified in four unrelated individuals. Gly28 and Tyr32 residues are located within the glycine-rich loop ATP binding pocket (aa 27-35)[101]. Mutations within the region may affect the binding affinity for ATP, which is essential for kinase function. To further characterize the kinase activity of these two recurrent variants, Zarate et al.[101] performed in vitro kinase assay using HEK293 cells.

Kinase activity of CDK19 can be examined by monitoring its role in transcription to phosphorylate the C-terminal domain (CTD) of RNA polymerase II. Expression of Gly28Arg resulted in significant reduction of the phosphor-status of CTD in comparison to effects seen with wildtype CDK19. In contrast, expression of the Tyr32His mutation resulted in enhanced phosphorylated level of CTD relative to wildtype CDK19, suggesting it might be a gain of function. Thus far, this is the only published result to suggest such an effect, and it would need further characterization to confirm. Further analysis on the kinase activity of these two *de novo* variants was performed by measuring the intake of ATP and production of ADP in HEK293 cells in the CDK19 wildtype background[101]. Consistent results suggesting that the kinase function was impaired were observed.

1.5.4. Modeling CDK19 de novo mutations using zebrafish

Zarate et al.[101] utilized the model organism zebrafish to further characterize the pathogenic mechanism of the two recurrent variants. They introduced an extra copy of wildtype human CDK19 or the variants by injecting mRNA into zebrafish embryos with endogenous Cdk19 present in the background and characterized the abnormal phenotypes. Introducing an extra copy of CDK19 in variant or wildtype form caused abnormalities such as a shortened body axis, hypoplastic anterior structures, and an aberrant tail. The percent of abnormalities in zebrafish embryo increased when either Gly28Arg or Tyr32His were expressed, along with increased lethality. These findings suggest that the two recurrent variants are pathogenic and likely interfering with the wildtype Cdk19 in zebrafish.

1.5.5. Modeling CDK19 de novo mutations using Drosophila

The identification that a disrupted *CDK19* gene was associated with congenital bilateral falciform retinal fold led Mukhopadhyay et al.[146] to further examine the physiological roles of CDK19 in the developing nervous system using the model organism *Drosophila melanogaster*. Fly Cdk8 is the sole ortholog of human CDK19, and it shares 66% identity with human CDK19 at the protein level[102]. Their goal was to learn about roles for Cdk8/19 family members in the nervous system by knocking down *Cdk8* in flies and inferring roles for CDK19 from their observations. To further examine the effect of depleting *Cdk8* in dendritic development in flies, they examined the type 4 multiple dendritic sensory neurons that are located in the peripheral nervous system in larval flies and were shown previously to be relevant in other fly models with intellectual disability[151,152]. Depletion of *Cdk8* in the Drosophila type 4 multiple dendritic neurons resulted in reduced dendritic branching and altered morphology in dendrite arborization in comparison to control[146]. It was found that 90% of dendrites in *Cdk8* depleted background showed restricted extension, indicating that CDK19, the ortholog of fly Cdk8 may also play a role in complex development nervous system[146].

In Chung et al.[102], they identified two *de novo* mutation in *CDK19* in three unrelated families through whole-genome sequencing between probands and their parents. The two variants are Tyr32His and Thr196Ala. The authors performed sequence alignments between four species, human, mouse, zebrafish and Drosophila, and found that the sites that are mutated in probands are well conserved across species. They found expressing $CDK19^{WT}$ in flies with endogenous *Cdk8* in the background had no effect on viability; however, when they introduced either variant to flies, there is more than 50% lethality, indicating these variants are behaving in a dominant fashion, likely interfering with the cellular processes in flies. They found expressing $CDK19^{WT}$ or fly Cdk8 in a *Cdk8* mutant background can rescue the lethality caused by the mutant background, but expressing CDK19 variants failed to rescue the lethality, suggesting that these two variants are acting as loss of function. Furthermore, they found depletion of fly *Cdk8* in neurons caused significantly enhanced susceptibility towards impairment in a banging assay. The banging assay is a method to measure the recovery rate for flies which have seizures due to external stimuli, such as vigorously banging of the vials[153]. In negative control flies, the recovery time takes less than 10 seconds; however, depletion of *Cdk8* in the neurons results in flies with a recovery time of more than 60

seconds. Expressing CDK19^{WT} in the *Cdk8* depleted background completely restored the recovery time; however, introducing either variant had similar results as depletion of *Cdk8* alone, further suggesting the mutations are pathogenic as they fail to rescue the susceptibility towards banging. Chung et al. examined the localization of the variants and CDK19^{WT} in adult fly brains and found that CDK19^{WT} is found predominantly in the cytoplasm with some protein localized in nuclei. However, the two variants were solely localized in the cytoplasm, suggesting that CDK19^{WT} has potential cytoplasmic localization and function, and mutations in CDK19 interferes with its potential function.

1.6. Pink1/Parkin and familial form of Parkinsonism

Mutation in PTEN-induced protein kinase (PINK1) and *parkin* are two of the most common causes of autosomal recessive Parkinsonism[154,155]. Since the initial discovery of *pink1* and *parkin* in familial form of Parkinsonism, the fly research communities have generated reliable models to study *pink1/parkin* mediated Parkinsonism[156–159]. PINK1 is a serine/threonine kinase that functions with Parkin in mitochondrial quantity and quality control[160]. In healthy mitochondria where the membrane potential is well-established, mitochondrially bound PINK1 get rapidly cleaved, and subsequently degraded in a proteasome-dependent manner in the inner mitochondrial membrane[161]. However, when the mitochondria are damaged, PINK1 accumulates on the mitochondrial outer membrane, and subsequently recruits its downstream partner Parkin, an E3 ubiquitin ligase, to ubiquitinate the dysfunctional mitochondria[162,163]. Ultimately, the ubiquitin-coded mitochondria separate from the healthy pool of mitochondria and are subjected to degradation via autophagy. This process is known as mitophagy[156–159].

1.6.1. Clinical features and molecular mechanisms associated with Parkinson's disease

Parkinson's disease (PD) is the second most common neurodegenerative disease worldwide[164]. The degeneration mainly targets the nervous system and progresses over time. The primary pathogenic characteristic of PD is degradation of neurons in brain, including dopaminergic neuron degradation[164]. Clinical features associated with patients of PD are characterized as motor symptoms and non-motor symptoms. Motor symptoms include bradykinesia, muscle stiffness, tremor, postural and gait difficulties, whereas cognitive decline, depression, sleep problems, exhaustion are considered as non-motor symptoms[165]. The underlying molecular pathogenesis associated with PD includes aggregation of α-synuclein, increased oxidative stress, dysfunctional mitochondria, and elevated neuroinflammation[165].

1.6.2. Phenotypes found in fly models of PD

In *Drosophila*, *pink1* or *parkin* mutant flies exhibited numerous phenotypes that resemble many of the symptoms of Parkinson's disease (PD) patients. Reduced life span was found in mutants with either *pink1* or *parkin*. Flies with mutated *pink1* or *parkin*

exhibited significantly reduced lifespan with less than 20 days in comparison to control flies with lifespan of more than a month[166]. Defects in locomotor activity are observed in *pink1* mutant flies, where researchers examine the climbing ability within a certain time frame between *pink1* mutant flies and wildtype flies. The climbing assay indicates *pink1* mutant flies have severely impaired climbing ability as flies are predominantly found to stay at the bottom of vials[157,167]. Another phenotype that resembles patient with PD is the degeneration of dopaminergic neurons. Depletion of *Pink1* in fly brains resulted in reduced numbers of tyrosine hydroxylase staining, which is a marker for dopaminergic neurons[157,166].

Mitochondrial homeostasis defects were also found in *pink1* or *parkin* mutant flies. In *pink1* mutant flies, the fly indirect flight muscles had enlarged and swollen mitochondria with undefined cristae structure when under transmission electron microscope. MitoTracker red was used to visualize the integrity of mitochondria in fly muscles[156,157,168]. Muscle degeneration was one of the most prominent phenotypes seen in PD flies with apoptotic cell death in thoracic muscle ultimately leading to thorax indentation and flight and mobility defects[157,166]. Terminal deoxynucleotidyl transferase dUTP nick end labeling (TUNEL) staining was used to determine the prevalence of cell death in fly muscles between *pink1* mutant and control flies. Increased cell death in thorax muscle is found to associated with mutation in *pink1* in flies[156,157,166,168–170].

These findings are all applicable to PD patients, and researchers have continued to study the underlying molecular mechanisms associate with *pink1/parkin*, and hopefully will shed some lights on potential therapeutic treatments for patients suffering from PD.

1.7. Mitochondria in health and diseases

Mitochondria are cytoplasmic organelles that are enclosed with double membranes consisting of the outer mitochondrial membrane (OMM), inner mitochondrial membrane (IMM), inter-membrane space (IMS) and matrix[171]. Historically they were viewed as bean shaped organelles based on the microscopy techniques, but it is now appreciated that they are highly dynamic and often tubular and interconnected structures in the cytoplasm[171].

1.7.1. Mitochondrial functions

The electron transport chain (ETC) refers to a series of redox reactions that transfer electrons in turn to generate an electrochemical gradient of protons, which generates cellular energy in the form of ATP in a process known as oxidative phosphorylation. The ETC is composed of transmembrane protein complexes along with freely mobile electron transfer carriers, ubiquinone and cytochrome c. All the transmembrane protein complexes are in the inner membrane of mitochondria. The ETC can initiate at Complex I or Complex II depending on where the electrons originate from[172].

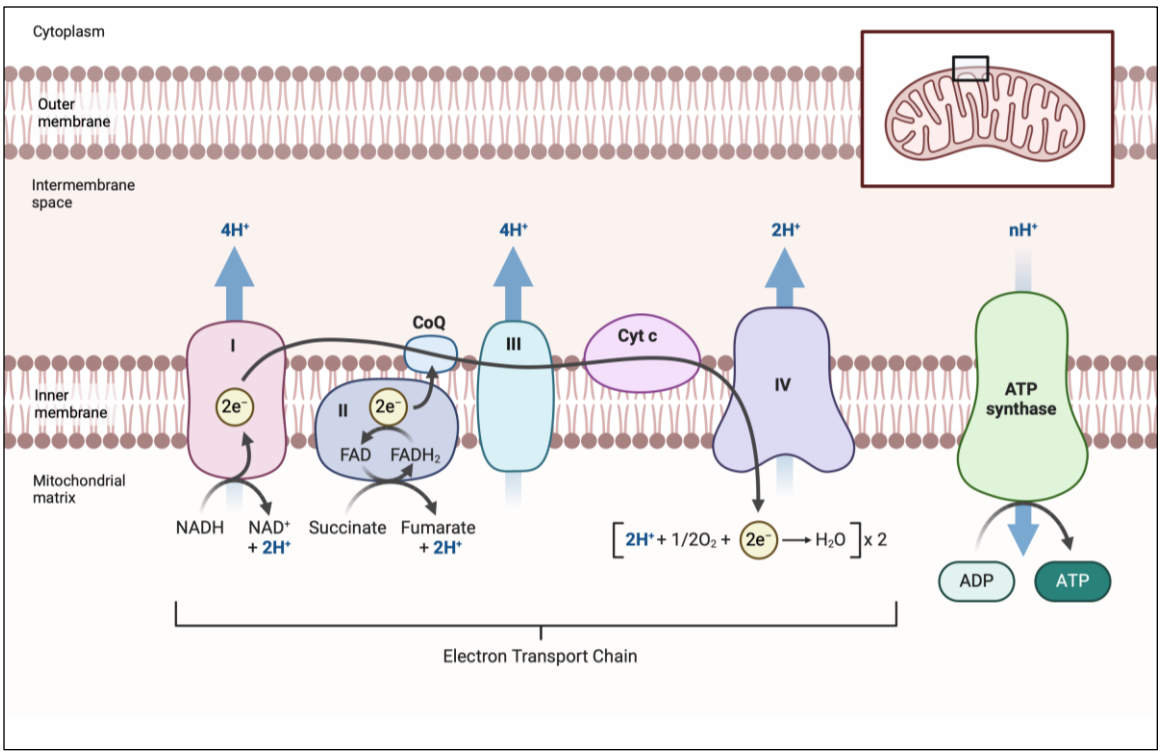

Figure 1.11. Complexes participating in mitochondrial electron transport chain.

The electron transport chain is comprised of five complexes. Electrons are transported from either Complex I or Complex II and picked up by quinone, and then transferred to cytochrome c to final acceptor O2 to generate 2 molecules of H2O. During the process, the protons located in the mitochondria matrix are pumped out to counteract the energy required for electron transfer. At the end, the electrochemical gradient generated by the protons drive them pass back to matrix via ATP synthase, which in turn to generate ATP. Figure was generated using Biorender.

Complex I, known as NADH-ubiquinone oxidoreductase, is the largest multisubunit enzyme complex in the ETC with an L-shape protein structure. It functions in transferring electrons from NADH in the matrix to ubiquinone in turn to pump out four protons from the matrix to the intermembrane space. During the process of electron transfer, generation of oxygen radicals can occur[173,174].

Complex II is known as the succinate dehydrogenase, which catalyzes the oxidation from succinate to fumarate in turn to transfer electrons to quinone. Once quinone uptakes two electrons, it becomes the reduced form known as ubiquinol[175].

Reduced ubiquinol transfers electrons to Complex III, which is known as Q-cytochrome c reductase, where electrons are subsequently transferred from ubiquinol to cytochrome c. In this process, reactive oxygen species can be generated during the electron transferring from ubiquinol[172].

Reduced cytochrome c carries electrons to complex IV, which is the cytochrome c oxidase. Electrons are transferred to terminal electron acceptor O_2 to generate H_2O from cytochrome c. A total of four electrons are transferred to generate two molecules of H_2O with a total of 8 protons removed from the matrix[176,177].

Lastly, the electrochemical gradient generated by protons between the matrix and the intermembrane space drives protons back into the matrix through F_o from F_1F_0 ATP synthase (Complex V). In turn, the stored energy created by the proton electrochemical gradient through F_1F_0 ATP synthase to generate adenosine triphosphate (ATP)[178].

Reactive oxygen species (ROS) are byproducts generated during the ETC. Complex I and Complex III are main sources for generating oxygen radicals. Elevated level of ROS are associated with neurodegeneration along with dysfunctional mitochondria, suggesting the level of ROS needs to be tightly regulated to avoid oxidation of the lipid, proteins and eventually the cell[179].

Another function of mitochondria is their role in intrinsic apoptosis, which can be trigged by elevated ROS level or extensive DNA damage. The intrinsic apoptosis is mediated by pro-apoptotic BCL-2 family proteins Bax/Bak. Binding of Bax/Bak on the OMM initiates permeabilization of mitochondrial membranes, which results in release of cytochrome c to the cytosol. Released cytochrome c binds to adaptor proteins to recruit and activate procaspase 9. Activated caspase 9 subsequently activates the downstream effector caspase 3 and caspase 7 to initiate the apoptosis[180].

1.7.2. Mitochondria in disease

A spectrum of diseases and pathologies have been broadly characterized with impaired mitochondrial function including neurodegenerative diseases, cancers and metabolic diseases. For instance, deficiency in Complex I is found to contribute to the development of Parkinson's Disease[181–183] and elevated ROS levels have been

observed in Alzheimer's Disease[184,185]. In addition, an improper balance between the fused and fragmented mitochondrial morphology has been detected in cancerous cells including human colon, lung and gastric cancer cells[186,187]. Furthermore, disturbance between mitochondrial morphologies have been implicated to cause heart failure in both mice and Drosophila[188,189].

1.8. Mitochondrial dynamics

Mitochondria are highly plastic and dynamic organelles as they are constantly changing their morphologies in response to various cellular conditions[190,191]. Under low glucose conditions, mitochondria in cells tend to interconnect with one another in a fused morphology, to enhance the generation of ATP through oxidative phosphorylation[192]. When cells are grown in the nutrient-rich media, mitochondria become fragmented with reduced ATP production[193]. Furthermore, fragmentation of mitochondria contributes to mitochondrial quality control by elimination of impaired or dysfunctional mitochondria and promotes apoptosis under severe cellular stress[194]. The change in mitochondrial morphologies is known as mitochondrial dynamics.

1.8.1. Mitochondrial fusion regulators

The currently known mitochondrial regulators that participate in mitochondrial fusion are Optic atrophy 1 (Opa1), Mitofusins 1 and 2 (human MFN1 and MFN2), which participate in inner membrane and outer membrane fusion processes of mitochondria, respectively. In Drosophila, mitochondrial assembly regulatory factor (Marf) is responsible for the OMM fusion[195,196].

1.8.2. Mitochondrial fission regulators

Dynamin-related protein 1 (Drp1), is the fission regulator that regulates mitochondrial fragmentation (Fig. 1.12). Drp1 is a GTPase enzyme that localizes predominantly in the cytosol and is recruited onto mitochondria via interactions with Drp1 receptors anchored to the OMM. Recruited Drp1 localizes to the OMM where it oligomerizes into a ring structure around the mitochondria, constricting and severing the mitochondrion in a GTP hydrolysis-dependent manner[197,198]. The adaptor proteins for Drp1 include mitochondrial fission 1 (Fis1), mitochondrial fission factor (Mff), mitochondrial dynamics protein (MiD)-49, and MiD51[199,200]. Drosophila only have Fis1 and Mff as adaptors for Drp1[201–203].

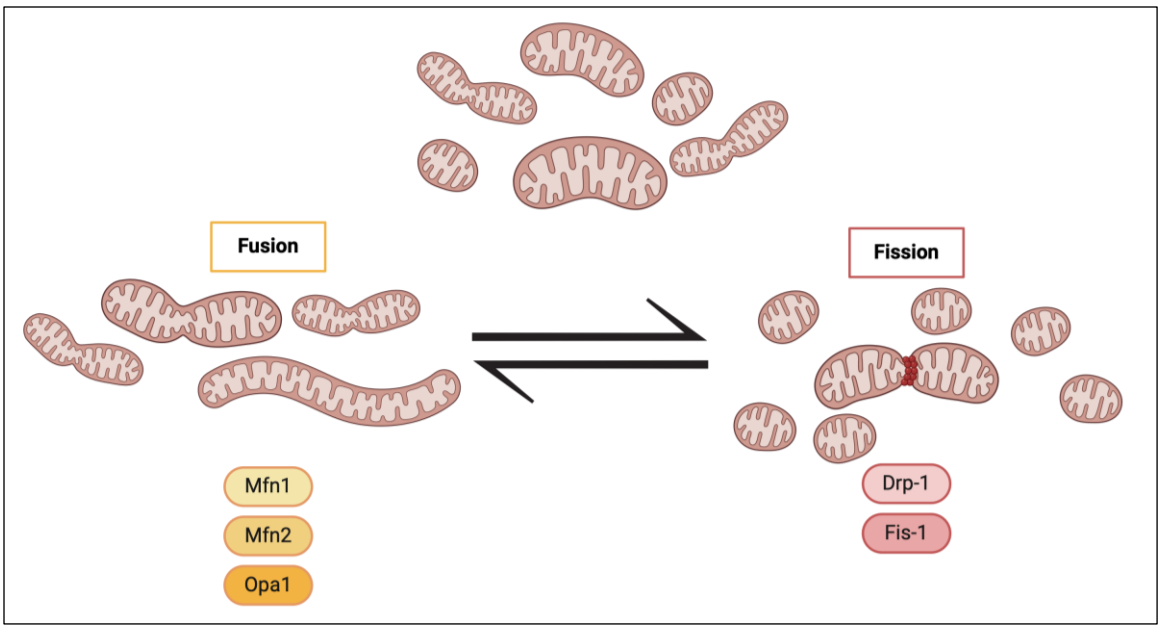

Figure 1.12. Mitochondrial dynamics.

The morphology of mitochondria is constantly altered in response to changes in cellular environment. Fusion is achieved by Mfn1/2 and Opa1 for outer and inner membrane, in respectively. The fission is achieved by Drp1 with its adaptor Fis-1. The dynamic of mitochondria is required in turn to maintain the homeostasis of mitochondria. Figure is generated from Biorender.

1.8.3. Post-translational modification of fusion regulators

Post-translational modification of fusion regulators can modulate their ability to affect mitochondrial dynamics. Deacetylation of OPA1 by mitochondria sirtuin 3 (Sirt3), a redox sensor to sustain genome integrity, can promote the elongation of mitochondria[204]. Akt (Protein Kinase B) is a serine/threonine kinase that mediates cytoprotective effect against various proapoptotic stimuli. It has been found that Akt promotes mitochondrial fused networks by increasing the expression of OPA1; thus enhancing the activity of mitochondrial fusion[205,206]. Mitochondrial ROS production can reflect on the functional status of mitochondria, as elevated ROS production is often associated with dysfunctional mitochondria. Redox stress can promote hyperfusion of mitochondria, which is considered as protective, as elongated mitochondria are prevented from being targeted for degradation by mitophagy[207–209].

1.8.4. Post-translational modification of fission regulators

Post-translational modification of Drp1 has been highly investigated[210,211]. The activities of Drp1 can be regulated by phosphorylation, acetylation and SUMOylation in turn to alter the structure of mitochondria[212]. Phosphorylation of Drp1 at S616 often promotes fission. For instance, CDK1 and CDK5 were found to phosphorylate Drp1 at S616 in turn to facilitate fragmentation of mitochondria[210,213,214]. In addition, Pink1 was found to phosphorylate Drp1 at the same S616 site in both fly tissues and patient samples[215,216]. Furthermore, SUMOylation of Drp1 has been shown to stabilize Drp1 in promoting mitochondrial fragmentation. Bax/Bak are two identified regulators that SUMOylate Drp1 to promote its stabilization during apoptotic cell death[217].

1.8.5. Mitochondrial dynamics and mitophagy

Mitochondrial dynamics play a role in mitophagy, the quality control of mitochondria[187]. Genetic studies in Drosophila have shown that impaired mitophagy is often associated with elevated levels of fusion regulators, MFN1/2, or reduced expression of fission regulator, Drp1[169,170]. Dysfunctional mitophagy can be restored either by suppressing MFN1/2 or supplementing Drp1[169,170]. It has been shown that supplementing Drp1 in a *pink1* mutant background can significantly restore the muscle and mitochondrial morphology in fly thoraxes as well as in patient samples[215,216]. Consistent results were observed when Marf or Opa1 were depleted in the same mutant background[169,170]. Furthermore, Pink1 can activate Drp1 by phosphorylating S616 site; thus, bypassing the need for recruitment of Parkin, the E3 ubiquitin ligase, to initiate mitophagy[215,216]. Mitochondrial fission plays a crucial role in mitophagy as it participates in priming the damaged mitochondria prior before mitophagy by segregating the damaged mitochondria away from the rest of healthy pool[215,216].

Chapter 2. Cdk8 regulates mitochondrial dynamics under physiological conditions.

2.1. Contributions to the Chapter

This chapter reflects the work performed in collaboration with several labs, primarily that of Dr. Hugo Bellen and his postdoctoral fellow Dr. Hyung-lok Chung. The work was published in April 2024[167]. In this collaboration our lab focussed primarily on phenotypes in muscles, while the Bellen lab carried out most of the studies in neuronal tissues. In this thesis I include for the most part only the work performed by me and Claire Shih, a research technician in the Verheyen lab. Thus, all figures, except Figure 2.8, 2.9 and 2.13a, were generated by me, with help from Claire Shih.

2.2. Introduction

In the Verheyen lab, we study the roles of several protein kinases during development and disease. One of the protein kinases is the homeodomain-interacting protein kinase (Hipk). In numerous studies our lab and others have shown that Hipk can modulate signal transduction cascades during normal development[218–221]. Furthermore, we found that Hipk has tumorigenic-like activity in Drosophila epithelial tissues[222], which indicates that Hipk can promote metastatic cell behavior and abnormal cell growth that could ultimately result in cancer. A previous unpublished genetic screen performed by lab members Jessica Blaquiere and Rubia Chung aimed to find potential regulators of Hipk by using double stranded RNA (RNAi) to knock down a set of kinases individually in a Hipk overexpression background, as we had done previously to dissect regulators of Wnt signaling[223]. By knocking down each kinase, we could detect if the phenotype caused by overexpressed Hipk was modified, either enhanced or suppressed. Such an observation might indicate that the kinase interacts with or regulates Hipk. In this screen, they found a number of genes whose knockdown could modify the Hipk overexpression phenotype, including *Cdk8.*

Cdk8 is a cyclin-dependent kinase that acts as part of the Mediator complex, which regulates RNA polymerase II mediated transcription[74]. It forms a Cdk8 module with Cyclin C (CycC), mediator complex subunit 12 (Med12), and mediator complex subunit 13 (Med13)[74]. In Drosophila, Cdk8 and Cyclin C physically and genetically interact with Med12 and Med13.[133] Only a few studies have studied the roles of Cdk8 in the development of Drosophila. While *cdk8* mutations are pupal lethal, mitotic clones showed phenotypic effects in distal leg and external sensory organ development[133]. It has also been shown that Cdk8-CycC positively regulates Mother against dpp (Mad)-dependent transcription of target genes, including *spalt* (*sal*), a well-known target gene of Mad that participates in vein patterning[136]. While investigating the potential interaction between Hipk and Cdk8, we found compelling phenotypes when *Cdk8* was knocked down ubiquitously which had not been previously described (see below). These findings diverted our focus to further investigate the consequences of reduced Cdk8 levels in flies, and its function in the Drosophila development.

2.3. Results

2.3.1. Depletion of Cdk8 causes altered wing posture, reduced lifespan, and defects in locomotion

We examined the effects of ubiquitous knockdown of *Cdk8* using the *Act5c-Gal4* strain (*Act5c>Cdk8 RNAi). Cdk8* mRNA expression was reduced by approximately 80% (Fig. 2.1a), and only about 50% of the flies eclosed at 25ºC (Fig. 2.1b). We found that depletion of Cdk8 ubiquitously in flies lead to significantly shorter life span, as control flies continued to thrive after a month whereas flies with *Cdk8* depletion were dead within three weeks (Fig. 2.1c). Furthermore, sterility was found in both male and females of *Cdk8* depleted flies in comparison to w^{1118} control flies (Fig. 2.1d). We noticed that the flies that eclosed exhibited abnormal wing postures with either held-up or droopy wings shortly after eclosion (Fig. 2.1e). This kind of phenotype is often associated with impaired muscle function as the adult indirect flight muscles (IFMs) ensure that wings are held at the correct angle for flight[224].

We also observed that *Act5c>Cdk8 RNAi* tend to stay at the bottom of vials in comparison to *Act5c>RFP* negative control flies. Thus, we performed climbing assays to quantify this effect (Fig. 2.2). Flies of different genotypes were transferred to transparent empty tubes and flies were tapped down to the bottom of the vials. We examined the number of flies that can climb up to the target line of 5 centimeter within 15 seconds. Videos were used to accurately document and quantify the results. We found that *Act5c>Cdk8 RNAi* flies have impaired climbing abilities (Fig. 2.2a, b). Climbing defects are often associated with either neuronal or muscular defects[225].

To investigate this further, we used Gal4 lines that limited the knockdown to selected tissues. Knocking down *Cdk8* using either a muscle-specific (*Mef2-Gal4*) or a neuron-specific (*Appl-Gal4*) driver caused similar, though slightly less severe, climbing defects (Fig. 2.2a, b) when compared to ubiquitous knockdown. When a kinase-dead version of Cdk8 ($Cdk8^{KD}$), which carries a single amino acid mutation within the well-conserved kinase domain[199], was expressed in muscles using *Mef2-Gal4* it caused severe lethality in comparison to control (Fig. 2.1f) and we found severe climbing defects in escaper adults (Fig. 2.2a, b). These data suggest that the kinase function of Cdk8 is essential throughout the development cycle of flies and that the kinase dead form can

interfere with normal functions of Cdk8 and cause dominant effects in a Cdk8 wildtype background.

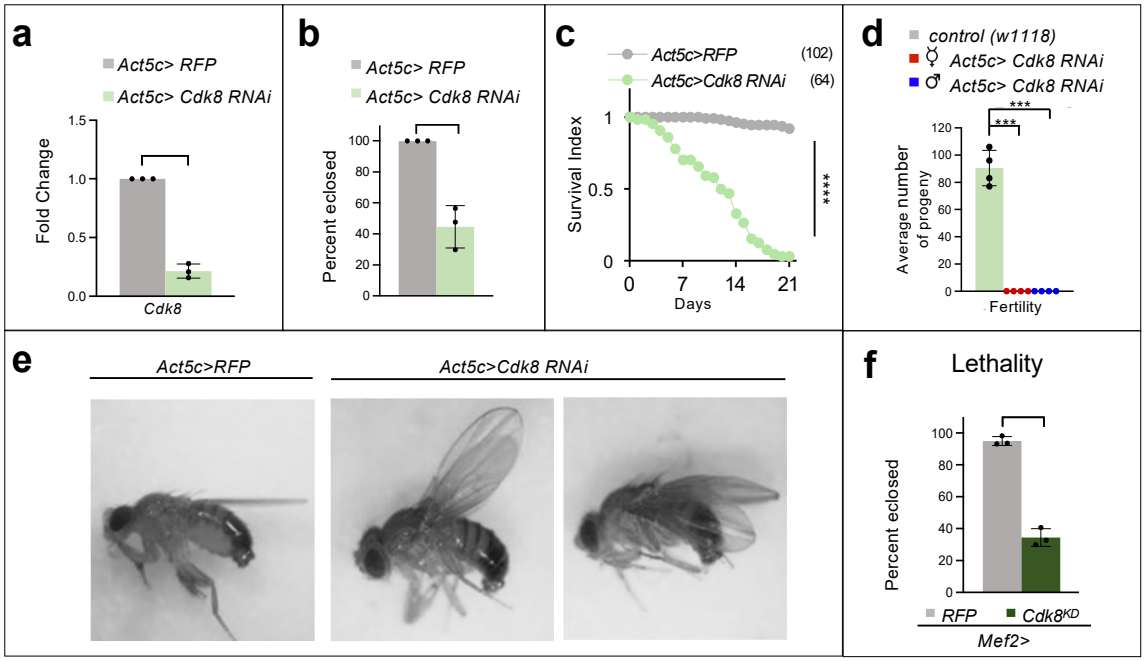

Figure 2.1. Depletion of Cdk8 causes multiple phenotypes

(a) qRT-PCR analysis of Cdk8 gene expression in Act5c>Cdk8 RNAi relative to control sample (Act5c>RFP). Data are mean ± SD. n = 3 independent experiments. (b) Semi-lethality is found in Act5c>Cdk8 RNAi pupae in comparison to Act5c>RFP (n=104 per genotype). Data are mean ± SD. (c) Life span assay between Act5c>RFP and Act5c>Cdk8 RNAi. (d) Infertility is found in both female and male Act5c> Cdk8 RNAi flies when crossed to w1118 in comparison to control (*w1118*). Data are mean ± SD. n = 4 independent experiments. (e) Wing postures of flies expressing Act5c>RFP and Act5c>Cdk8 RNAi. (f) Lethality is found in Mef2>Cdk8KD pupae in comparison to Mef2>RFP. Total examined 222 pupae in Mef2>RFP and 327 pupae in Mef2>Cdk8^{KD}. Data are mean ± SD with three biological replicates. All raised at 25°C. All statistics are generated using unpaired two-tailed t-test. ** p<0.01, *** p<0.001, **** p<0.0001, ns: no significance.

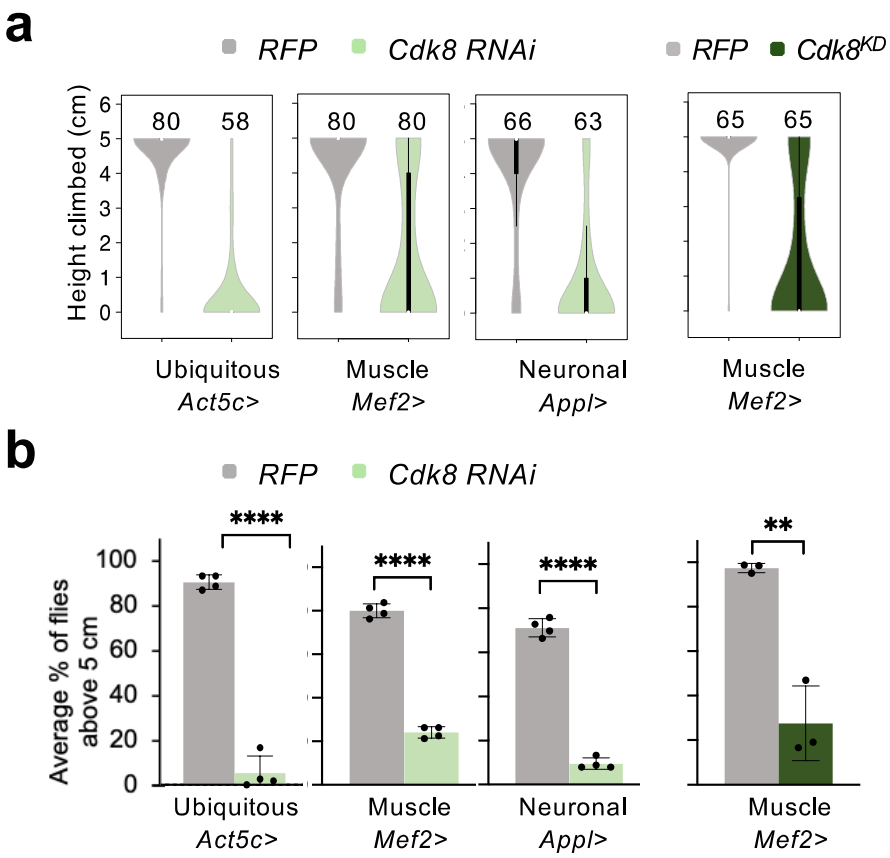

Figure 2.2. Depletion of Cdk8 causes locomotion defects

(a) Violin plots showing distributions of climbing ability in control (RFP) and Cdk8 knock-down flies using either ubiquitous (Act5c), muscle (Mef2), or neuronal-specific (Appl) Gal4 drivers. (b) Average percent of flies that reached the target line of indicated genotypes in a climbing assay. Each experiment is individually repeated four times. The total number of progeny are assessed between white RNAi and Cdk8 RNAi with different drivers: n = 165, 144 in Act5>, 180, 189 in Mef2>, and 160, 160 in App>, respectively. Violin plot showing distributions of climbing ability between control (RFP) and escapers of $Cdk8^{KD}$ with the Mef2Gal4 (b) Average percent of flies that reached the target line of indicated genotypes in a climbing assay. Each experiment is individually repeated three times. Results are mean ± SD. An unpaired two-tailed t-test is used to generate the statistics. All raised at 25 °C.

2.3.2. Expression of Cdk8 affects mitochondrial morphology

Climbing defects and altered wing posture are often associated with impaired muscular or neuronal processes that could involve in ATP generation[226,227]. Furthermore, in fly models of Parkinsonism with impaired mitochondrial quality control such phenotypes are also observed. Mitochondria are known as the hubs for generating cellular energy in the form of ATP through oxidative phosphorylation; thus, we decided to examine the mitochondrial phenotypes in muscles. We examined mitochondrial morphology in larval body wall muscles using a muscle-specific driver and labeled mitochondria with UAS-mitoGFP[125]. In control larval body wall muscles (*Mef2>mitoGFP*/+), we observed a balance between punctate and filamentous structures (Fig. 2.4a-a'). However, when *Cdk8* levels were reduced using RNAi, we observed filamentous mitochondrial morphology (Fig. 2.4b-b'). Quantification using mitochondrial network analysis (MiNA)[228,229] indicated that there was an increase in branching length, mitochondrial length, and total mitochondrial area when *Cdk8* was depleted in muscle (Fig. 2.4e-g). In contrast, overexpression of the wild-type *Cdk8* cDNA caused the mitochondrial morphology to take on a punctate-like structure (Fig. 2.4c-c'). Quantification suggested there was no significant difference in branch number or total mitochondrial area in comparison to control; however, overexpression of Cdk8 caused a decrease in length relative to control (Fig. 2.4e-g). Moreover, overexpression of kinase-dead Cdk8 ($Cdk8^{KD}$) lead to extensively elongated mitochondria (Fig. 2.4d-d') with significantly increased numbers of branches, mitochondrial length as well as total mitochondrial area (Fig. 2.4e-g). In summary, we found expression of Cdk8 can modulate the mitochondrial morphology in larval body wall muscles. Loss of *Cdk8* or expression of kinase dead Cdk8 affected mitochondrial morphology to become predominately elongated whereas overexpression of Cdk8 promoted fragmentated, round-shaped mitochondrial morphology in developing larval muscles. These data suggest the defective phenotypes that we observed when Cdk8 is depleted may be associated with the underlying alternated mitochondrial morphology.

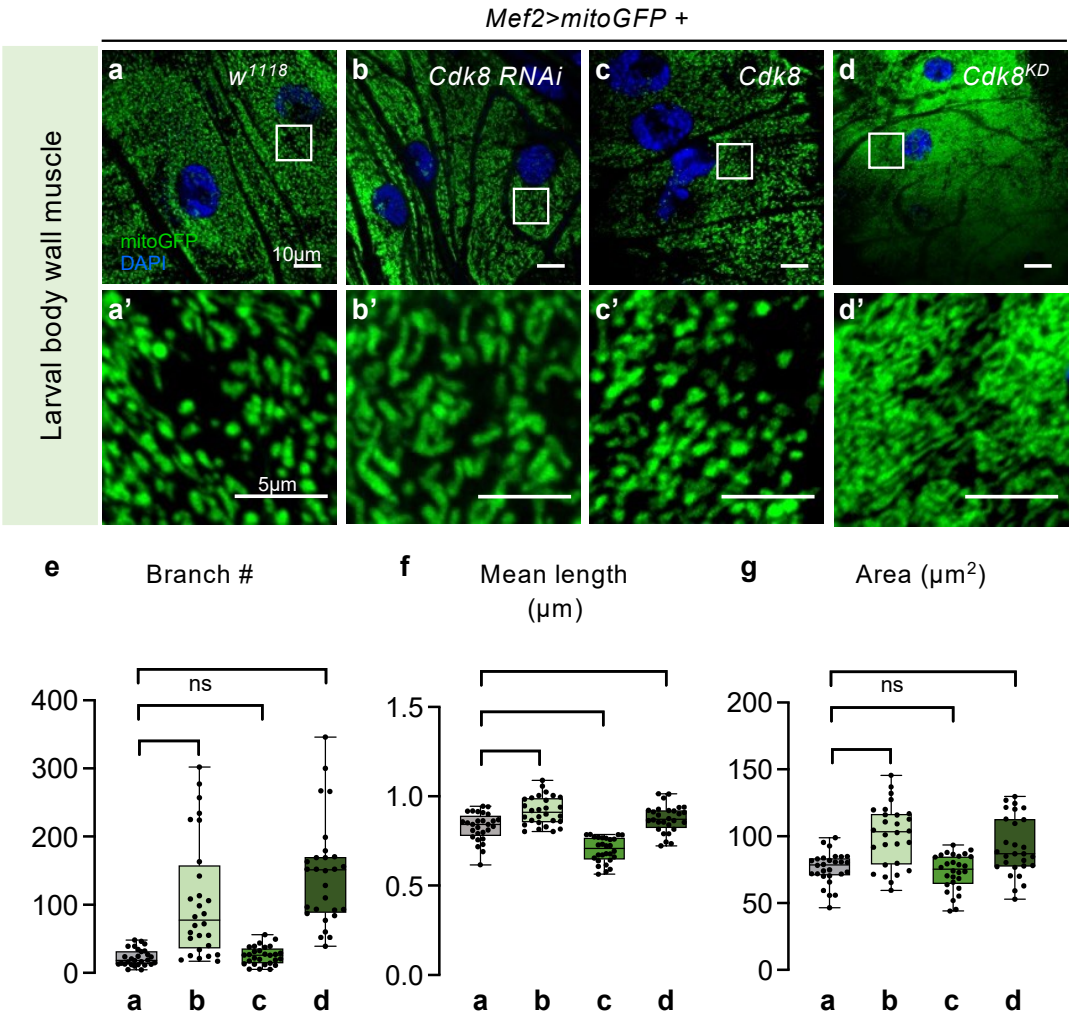

Figure 2.3. Cdk8 regulates mitochondrial morphology in larval body wall muscle under physiological conditions.

(a–d) Mitochondrial morphology of larval body wall muscles in (a) w1118 control or expressing (b) Cdk8 RNAi, (c) Cdk8WT, (d) Cdk8^{KD} with Mef2-Gal4>mitoGFP, raised at 29 °C. Scale bar: 1 µm. (a'–d') Representative magnified sections from (a–d). Scale bar: 5 µm. (e–g) Quantification of mitochondrial morphology showing the (e) number of branches. P value is 0.0003 for Cdk8 RNAi, 0.4533 for Cdk8, and 6.97e-10 for Cdk8KD (f) the mean mitochondrial length. P value is 0.0023, 6.29e-8, and 0.0178, respectively, in order. (g) The mitochondrial area. P value is 0.0002, 0.5512, and 0.0167, respectively, in order, in larval body wall muscles of the indicated genotypes. All in comparison to w1118. Letters (a–d) refer to the genotypes shown in panels (a–d). Quantifications were calculated by the MiNA toolset. n = 6 per genotype. Data were presented as box plots (center line at the median, upper bound at 75th percentile, lower bound at 25th percentile) with whiskers at minimum and maximum values. An unpaired two-tailed t-test is used to generate the statistics. $*p < 0.05$, $**p < 0.01$, $***p < 0.001$, $****p < 0.0001$, ns no significance.

The changes in larval muscle mitochondrial morphologies in response to modulation of Cdk8 suggest that Cdk8 activity might regulate mitochondrial dynamics, where mitochondria constantly change their shape in response to changes in cellular environment. We hypothesized that Cdk8 depletion promotes the fusion morphology with elongation of mitochondria, whereas Cdk8 overexpression promotes the punctate-like morphology of fragmentated mitochondria. To further examine the mitochondrial morphology in depth, we next examined mitochondrial morphology in adult indirect flight muscles (IFMs). In these muscles, the mitochondria are found between the long muscle fibers and thus appear to be in columns or rows (Fig. 2.4).

In control animals, we observe both elongated and fragmented mitochondria (Fig. 2.4a-a'). *Cdk8* depletion caused elongated mitochondria (Fig. 2.4b-b') whereas overexpression of Cdk8 lead to small and round mitochondria, indicative of increased fission (Fig. 2.4c-c'). Since expression of $Cdk8^{KD}$ caused pupal lethality at 29ºC (Fig. 2.1f), we examined the mitochondrial morphology of escapers raised at 25ºC (Fig. 2.4d-d') and again observed elongated mitochondria. These mitochondrial morphologies were consistent with observations of mitochondrial morphologies in larval muscles. We further quantified the number of mitochondria and length of mitochondria in adult IFM (Fig. 2.4e, f, respectively), and found that reduced number of mitochondria within a selected region is associated with extended length of mitochondria in both Cdk8 depleted condition or overexpression of $Cdk8^{KD}$. In contrast, we found a significant increase in the number of mitochondria associated with reduced length when Cdk8 is overexpressed. These data further suggest that expression of Cdk8 plays a critical role in regulating morphology of mitochondria throughout development.

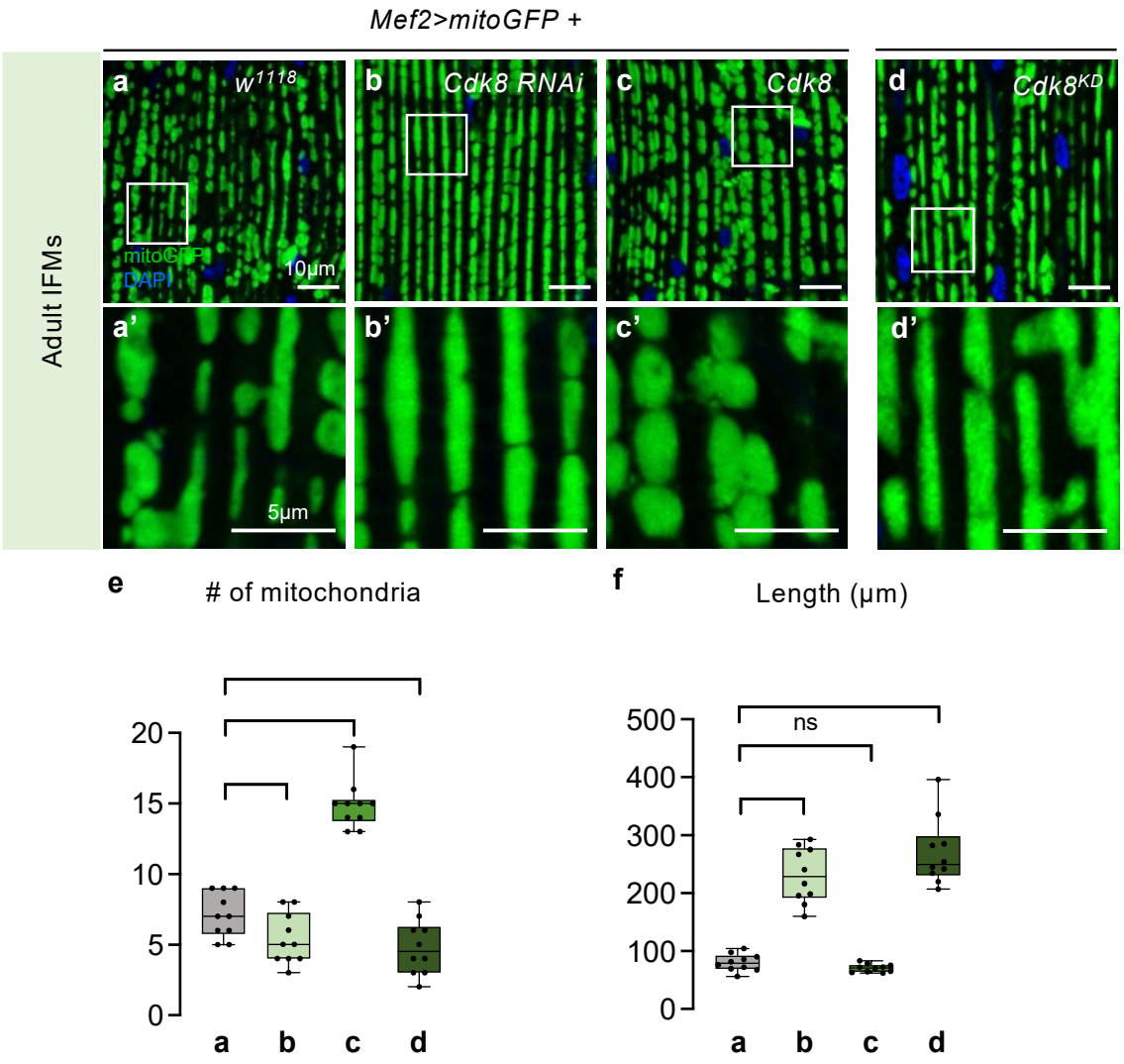

Figure 2.4 Cdk8 regulates mitochondrial morphology in adult indirect flight muscle under physiological conditions

Mitochondrial morphology of adult IFM in (a) w1118 control or expressing (b) Cdk8 RNAi, (c) Cdk8WT, (d) Cdk8KD with Mef2-Gal4>- mitoGFP. Flies were grown at 29 °C, except escapers expressing Cdk8KD were raised at 25 °C. Scale bar: 10 μm. k'–n' Representative magnified sections from (a–d). Scale bar: 5 μm. o–p Quantification of mitochondrial morphology showing the (e) number of mitochondria, p value is 0.0371 for Cdk8 RNAi, 4.25e-9 for Cdk8, and 0.0095 for Cdk8KD. f The mean mitochondrial length of the indicated genotypes. P value is 1.56e-8, 0.l0809, and 7.89e-9, respectively in order. All in comparison to w1118. n = 5 per genotype. Data were presented as box plots (center line at the median, upper bound at 75th percentile, lower bound at 25th percentile) with whiskers at minimum and maximum values. An unpaired two-tailed t-test is used to generate the statistics. ∗p < 0.05, ∗∗p < 0.01, ∗∗∗p < 0.001, ∗∗∗∗p < 0.0001, ns no significance.

To further validate our findings and to avoid any off-target effect of the transgene lines that we used, we compared mitochondrial morphologies in larval body wall muscles using different RNAi lines for Cdk8 (Fig. 2.5b-c), as well as different overexpression lines of *UAS-Cdk8* (Fig. 2.5d-e). We included the expression of $Cdk8^{KD}$ in larval muscles as a positive control since this line has been previously validated by Li et al[136]. We found consistent elongated morphology among two Cdk8 RNAi lines (denoted as Cdk8 RNAi 1 and 2), which exhibited the similar morphology as $Cdk8^{KD}$ (Fig. 2.5f-f'). Furthermore, we found expression of either UAS-Cdk8 (Cdk8) or UAS-$Cdk8^{3xHA}$ (an HA-tagged version of UAS-Cdk8) transgenes changes the mitochondrial morphology to be predominantly punctate-like. These data are in line with our previous findings when animals were raised at 29ºC. Furthermore, examination of mitochondrial morphology from adult indirect flight muscle expressing the second RNAi line and $Cdk8^{3xHA}$ have similar phenotypes as expressing Cdk8 RNAi or UAS-Cdk8, since depletion of Cdk8 promotes fusion morphology, whereas ectopic expression of Cdk8 promotes fission morphology in Figure 2.5 g and h, respectively.

We next quantified the expression of each Cdk8 line at the mRNA level using RT-qPCR (Fig. 2.5i). We used a weaker ubiquitous driver, *daughterless (Da-Gal4),* to express each line because expression of either UAS-Cdk8 or UAS-$Cdk8^{3xHA}$ using Act5c-Gal4 causes toxicity, where no larvae with the corresponding genotype can be detected. We found that both Cdk8 RNAi lines have a knockdown efficiency of depleting endogenous *Cdk8* approximately 80-90%. We found expression of UAS-Cdk8 enhanced the expression of Cdk8 by three-fold in comparison to the endogenous level of Cdk8 in control, and that expression of UAS-$Cdk8^{3xHA}$ increased the expression of Cdk8 by approximately six-fold.

Since the Cdk8 protein complex can regulate gene expression at the transcriptional level, we tested the effect of Cdk8 on transcription of genes known to be regulators of mitochondrial dynamics. Ubiquitous knockdown of *Cdk8* led to a modest increase in expression of both a regulator of mitochondrial fusion (mitochondrial assembly regulatory factor, *marf*) and fission (*Drp1*), suggesting the mitochondrial morphology defects are not likely due to reduced mRNA levels of these genes (Fig. 2.5j).

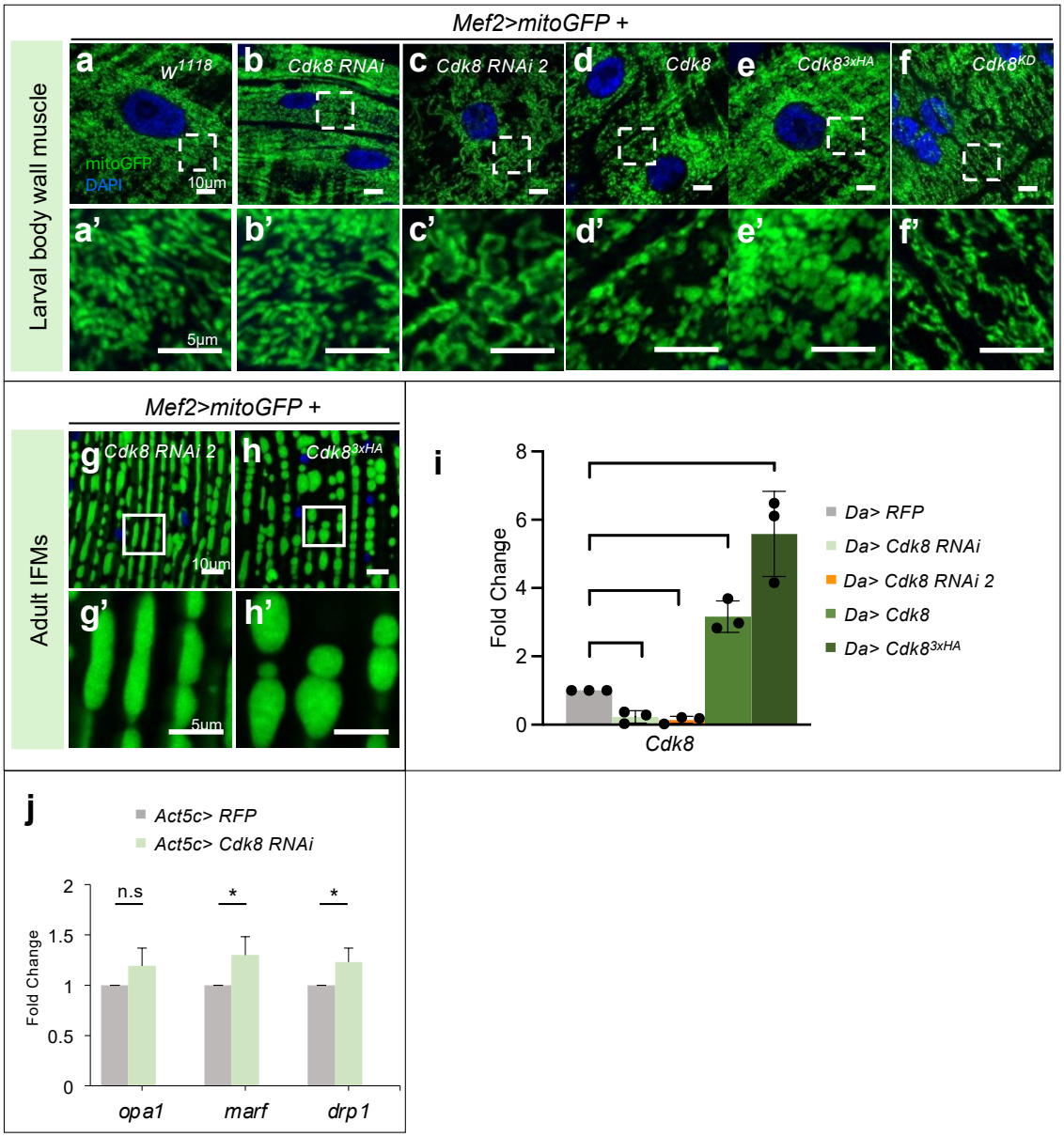

Figure 2.5. Consistent mitochondrial morphologies between different transgenic lines of Cdk8 RNAi or overexpression lines.

Mitochondrial morphology with larval body wall muscles in (a) control or expressing (b) Cdk8 RNAi, (c) Cdk8 RNAi 2, (d)Cdk8, (e) Cdk8HA, (f) Cdk8KD. Scale bar: 10 μm. (a'-f') Representative magnified sections from a-f (indicated with dashed boxes). Scale bar: 5 μm. a-f raised at 25°C. (g-h) Mitochondrial morphology of adult IFM expressing (g) Cdk8 RNAi 2, (h) $Cdk8^{3xHA}$. Scale bar: 10 μm. (g'-h') A representative magnified section from (i-j) with corresponding genotypes listed above. Scale bar: 5 μm. Raised at 29°C. (i) qPCR analysis of *Cdk8* gene expression in Daughterless Gal4 (*Da>*) expressing either Cdk8 RNAi, Cdk8 RNAi 2, Cdk8, or $Cdk8^{3xHA}$ relative to control (*Da>RFF*) at 25°C. (j) qPCR analysis of *opa1, marf, and drp1* in *Act5c> Cdk8 RNAi* relative to control (*Act5c> RFP*) at 25°C. All qPCR data is present as mean ± SD. n = 3 independent experiments. Unpaired two-tailed t-test is used to generate the statistics.

2.3.3. Altered myofibril morphology is found in Cdk8 depleted muscles

Correct wing postures are critical aspects of controlling the ability to fly, since wing blades constantly flap upward and downward in cycle with high frequency to exert flight ability[224]. There are two antagonistic sets of indirect flight muscles that are responsible for controlling the upward (held up) or downward (droopy) wing postures, namely the dorso-longitudinal muscles (DLM) and the dorso-ventral muscles (DVL). When the DLM are contracted, it causes relaxation of the DVM, which results in the held-up wing posture. In contrast, contraction in DVM leads to relaxation in the DLM, which results in the droopy wing postures (Fig. 2.6)[224]. We observed both wing postures in Cdk8 depleted flies, suggesting that flies have failed to contract their IFMs properly. To investigate the underlying muscle integrity in IFM, we examined the effect of Cdk8 expression on muscle morphology in adult IFM (Fig. 2.7).

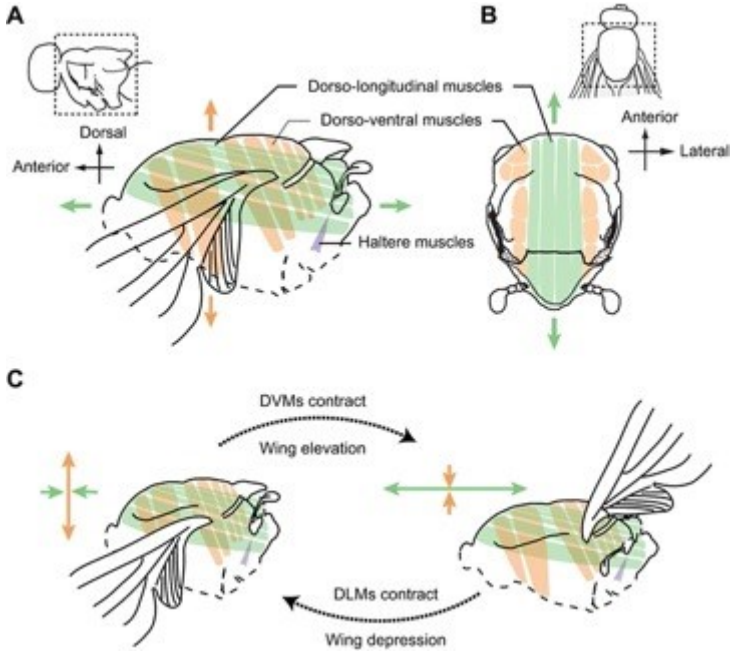

Figure 2.6. Schematic illustration of flapping wing movements in Drosophila.

Two antagonistic sets of indirect flight muscles are responsible for controlling the upward (held up) or downward (droopy) wing postures, namely the dorso-longitudinal muscles (DLM) and the dorso-ventral muscles (DVL). The orange color highlights the dorso-ventral muscle, whereas the green highlights the dorso-longitudinal muscle. Figure is from Tanvi Deora et al[224].

We found depletion of Cdk8 leads to broadening of the myofibril width along with elongated mitochondria in comparison to control (Fig. 2.7b to a). Overexpression of $Cdk8^{3xHA}$ under the same conditions had no effect on the myofibril width phenotype (Fig. 2.7c'-c''). Furthermore, we found expression of $Cdk8^{KD}$ also caused an increase in myofibril width (Fig. 2.7 d-d''''). The quantification further validated our findings where depletion of Cdk8 or overexpression of $Cdk8^{KD}$ lead to increased muscle fiber width in comparison to control, whereas overexpression of Cdk8 had no significant difference in altering the muscle morphology (Fig. 2.7e).These data along with mitochondrial morphology alterations indicate that expression of Cdk8 plays a role in both regulating mitochondrial and muscle morphology under physiological condition, and that Cdk8 expression needs to be tightly regulated in turn to maintain the structure of IFM.

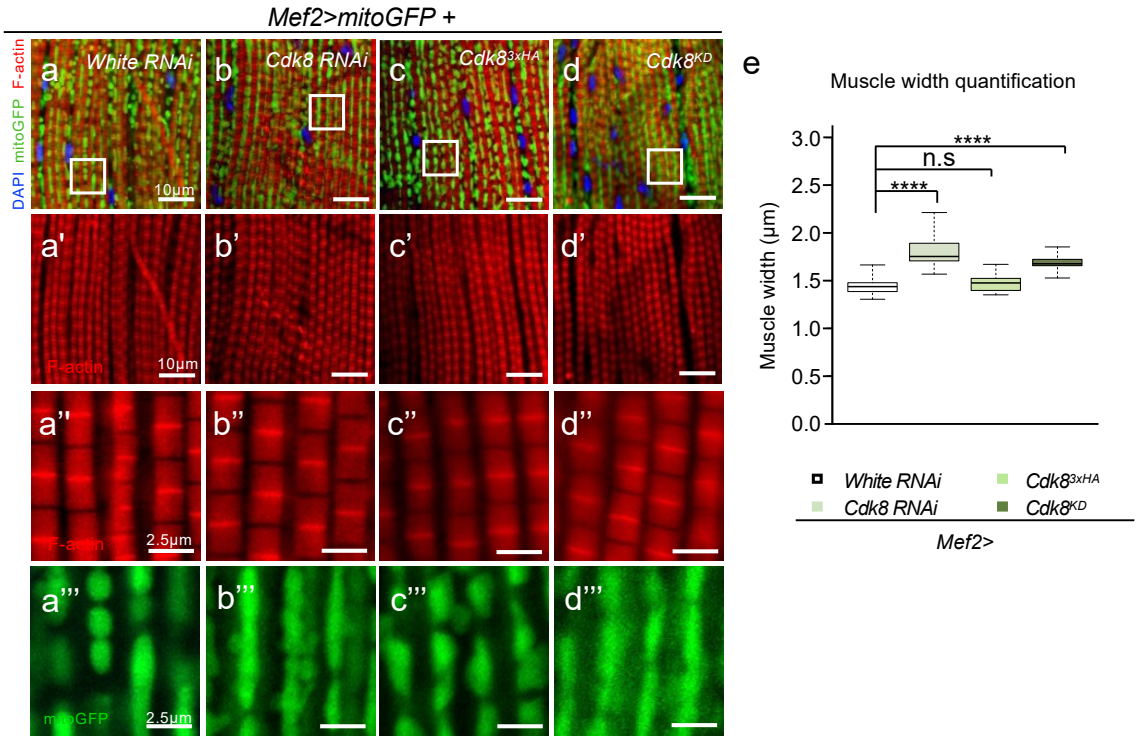

Figure 2.7. Expression of Cdk8 alters muscle fiber width in adult indirect flight muscles.

Adult indirect flight muscle in (a) control or expressing (b) Cdk8 RNAi, (c) $Cdk8^{3xHA}$ or (d) $Cdk8^{KD}$. Merged images including DAPI (stains for nucleus) and mitoGFP (stains for mitochondria) of corresponded genotype in a-d. Rhodamine phalloidin is used to show muscle morphology of corresponded genotype in a'-d'. Scale bar: 10 μm. (a''-d'') Representative magnified sections from a-d (indicated with white boxes) for muscle morphology. (a'''-d''') Representative magnified sections from a-d (indicated with white boxes) for mitochondrial morphology. Scale bar: 2.5 μm. All raised at 25°C. n = 5 per genotype with three biological replicates. (e) Quantification of adult indirect flight muscle fiber width in 3-day old flies. n = 5 per genotype. Data are presented as box plots (centre line at the median, upper bound at 75th percentile, lower bound at 25th percentile) with whiskers at minimum and maximum values. Unpaired two tailed t-test is used to generate the statistics. $*p < 0.05$, $**p < 0.01$, $***p < 0.001$, $****p < 0.0001$, ns no significance.

2.3.4. Loss of Cdk8 alters mitochondrial distribution in the central nervous system neuropil

High expression of Cdk8 is found in both larval central nervous system (CNS) as well as in adult brain[230]. To further examine the depletion effect of Cdk8 in CNS, we next assessed the effects of depletion of Cdk8 in the nervous system. To assess mitochondrial distribution in the adult CNS, we expressed Cdk8 RNAi in neurons using a pan-neuronal driver, *elav-Gal4*, and probed the mitochondria with an anti-ATP5 antibody. As shown in Fig. 2.8a, mitochondria are indeed more clustered in cell bodies, and less abundant in the neuropil when compared to control animals (*elav>control RNAi*) (Fig. 2.8a). We further quantified the length of mitochondrial area and branches to assess the morphological changes. As shown in Fig. 2.8b, the area of mitochondria is significantly increased, but branch length is not altered (Fig. 2.8c). Taken together, our data indicate that loss of Cdk8 affects mitochondrial dynamics, which results in a mitochondrial transport defect into the neuropil as well as a dysfunction of the mitochondria.

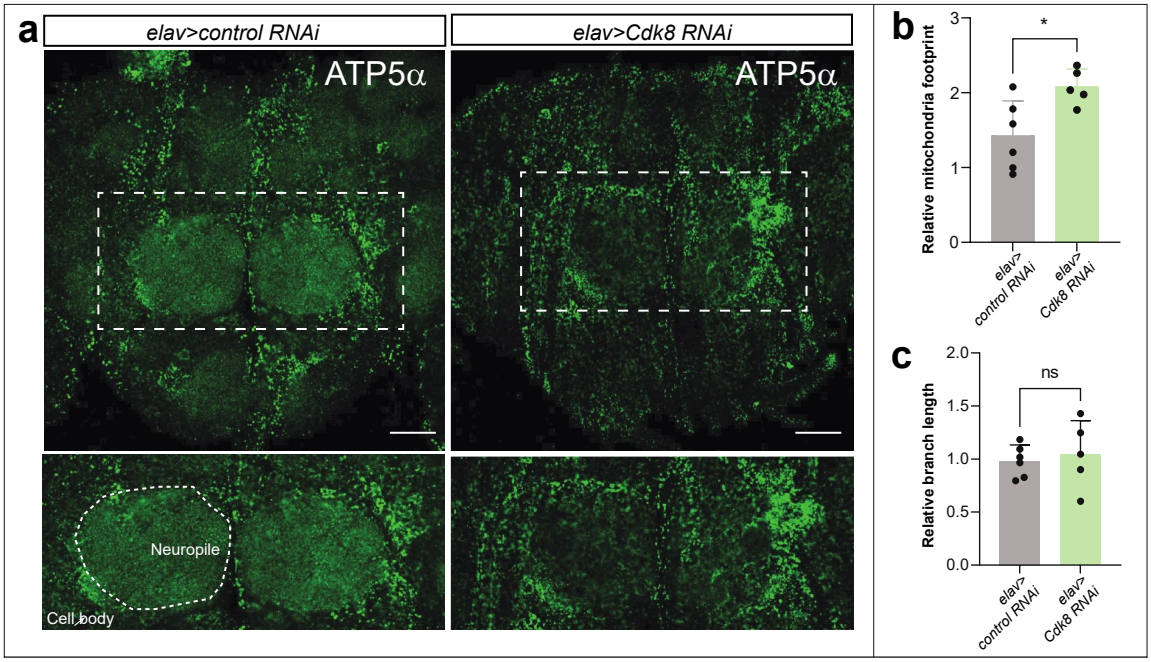

Figure 2.8. Loss of Cdk8 alters mitochondrial distribution in the central nervous system neuropil.

(a) Mitochondrial distribution in the CNS neuropil. ATP5a marks mitochondria in the brain of control (*elav>control RNAi*) and flies that express *Cdk8 RNAi* (*elav>Cdk8 RNAi*). Scale bar: 10 μm. (b) Quantification of relative mitochondrial footprint ($n = 6$ for control, $n = 5$ for *elav>Cdk8 RNAi*). (c) Quantification of relative mitochondrial branch length ($n = 6$ for control, $n = 5$ for *elav>Cdk8 RNAi*). $*p < 0.05$, $**p < 0.01$, $***p < 0.001$, $****p < 0.0001$, ns no significance.

2.3.5. Loss of Cdk8 affects mitochondrial size and distribution in photoreceptor terminals

To determine mitochondrial size and distribution in photoreceptors (PR) and their synapses, we performed TEM in the retina and lamina upon reduction of *Cdk8* levels using RNAi driven by Rhodopsin1-Gal4 (*Rh1> Cdk8 RNAi*). We found that the size of mitochondria is significantly reduced, and the number of mitochondria is significantly increased in the PR cell body, compared to control (*Rh1 > UAS-Luciferase RNAi*) (Fig.2.9a, c) In addition, the number of mitochondria is reduced in photoreceptor terminals in *Rh1>Cdk8 RNAi* flies when compared to control flies (Fig. 2.9b). Loss of Drp1 in photoreceptors leads to an increase in small mitochondria in the cell body of PR that are highly clustered as well as a loss of mitochondria at synapses[231]. The data suggested that loss of Drp1 leads mitochondria to be clustered like beads on a string and hence interconnected, and that they form a network that is poorly transported to synapses. These data clearly indicate that Cdk8 loss partially phenocopies the Drp1 loss phenotypes in photoreceptors. Given that there is a depletion of mitochondria at synapses, we surmised that there may be a defect in synaptic transmission. Indeed, Verstreken et al.[231] argued that the recycling of synaptic vesicles at synapses requires the presence of functional mitochondria and proper ATP levels to drive the recycling process[232]. We therefore performed Electroretinograms (ERGs) in flies in which *Cdk8* levels are reduced (*elav>Cdk8 RNAi)* and observed a dramatic reduction of on-and-off transients, indicating that the PR fails to communicate with the postsynaptic cells and that synaptic transmission is nearly abolished (Fig. 2.9d). In contrast, the ERG amplitudes are not altered, suggesting that the phototransduction cascade is not affected (Fig. 2.9e). Altogether, these data indicate that loss of Cdk8 affects mitochondrial size and distribution in photoreceptor terminals, and the phenotypes are strikingly similar to the loss of *Drp1* in photoreceptors[231].

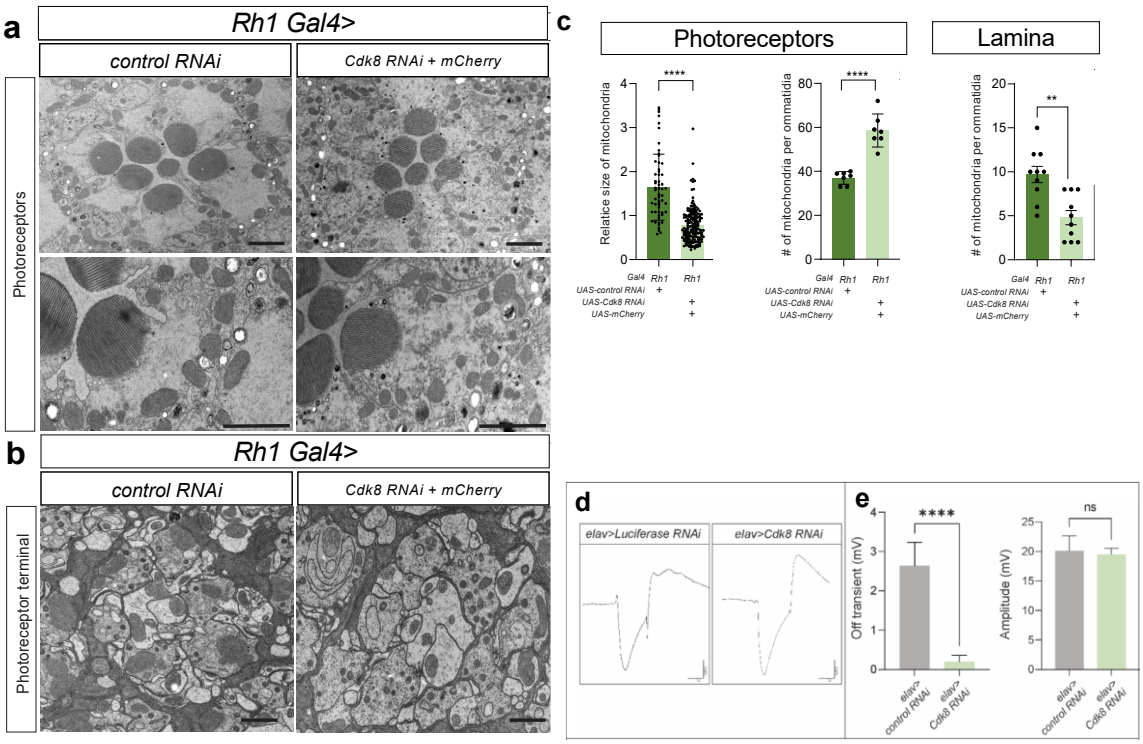

Figure 2.9. Loss of *Cdk8* in photoreceptors affects mitochondrial size and distribution in photoreceptor terminals.

(a) Mitochondrial distribution in the cell bodies of the photoreceptors of the indicated genotypes. Scale bars: 2 μm. (b) TEM images of photoreceptor terminals. The size of mitochondria is smaller than in the control but observed more mitochondria in clusters in photoreceptors of flies that express Cdk8 RNAi (*Rh1>Cdk8 RNAi; UAS-mCherry*) when compared to the control (*Rh1>control RNAi*). Scale bars: 2 μm. (c) Quantification of mitochondrial size and number in photoreceptors ($n > 50$ per genotype for the quantification of mitochondria size, $n = 7$ per genotype for the quantification of mitochondrial number). Quantification of mitochondrial number per photoreceptor terminal (Right) ($n = 10$ per genotype). Statistical analyses are one-way ANOVA followed by a Tukey post hoc test. Results are mean ± SEM. (d) ERG traces of control (*elav>luciferase RNAi*) and the flies that reduce the level of Cdk8 (*elav>Cdk8 RNAi*). (e) Quantification of off transient (left) and depolarization amplitude (right).
$*p < 0.05$, $**p < 0.01$, $****p < 0.0001$, ns no significance

2.3.6. Elevated Reactive Oxygen Species (ROS) levels are found in Cdk8 depleted muscles

Abnormal mitochondrial morphology can result in an increase in the generation of reactive oxygen species (ROS)[156]. To test if it is the case with Cdk8 modulation, we performed dihydroethidium (DHE) staining to assess ROS in adult IFM where expression of Cdk8 is modulated using the muscle specific driver, Mef2-Gal4 (Fig. 2.10). DHE is a dye that is oxidized by ROS to yield red fluorescent 2-hydroxyethidium that can be detected and quantified to determine the levels of ROS in cells. We found depletion of Cdk8 resulted in increased DHE intensity (Fig. 2.10b-b') in comparison to the negative control which established basal level of ROS (Fig. 2.10a-a'). In contrast, elevated Cdk8 showed no significant difference in DHE intensity when compared to negative control (Fig. 2.10c-c'), and expression of the $Cdk8^{3xHA}$ transgene led to a slight decrease in ROS production (Fig. 2.10d-d'). The difference between two UAS-Cdk8 lines is likely due to the Cdk8 expression levels, where UAS-$Cdk8^{3xHA}$ had higher expression relative to the UAS-Cdk8 (Fig. 2.5i). These data suggest that modulating expression of Cdk8 alters mitochondrial morphology, and subsequently results in altered redox homeostasis as the production of ROS is elevated when Cdk8 is depleted in fly muscle.

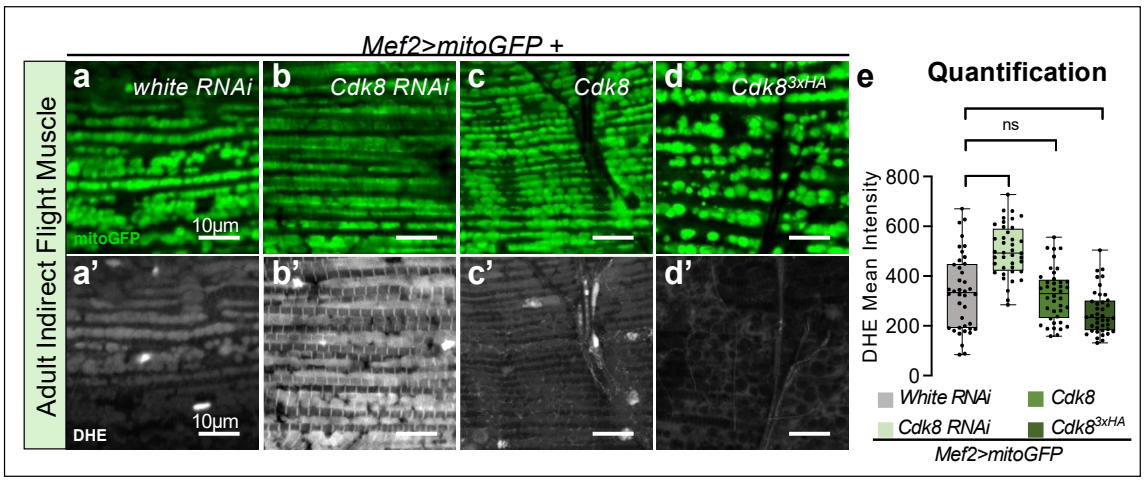

Figure 2.10. Depletion of Cdk8 causes elevated Reactive Oxygen Species (ROS) level.

(a-d) Mitochondrial morphology of adult IFM of the indicated genotypes where transgenes are expressed in muscles using Mef2-Gal4 and mitochondria are detected using UAS-mitoGFP. Scale bar: 10 μm. (a'-d') DHE staining of the indicated genotypes. (e) Quantification of DHE mean intensity for panels c'-f'. n = 8 per genotype. Data are presented as box plots (centre line at the median, upper bound at 75th percentile, lower bound at 25th percentile) with whiskers at minimum and maximum values. Unpaired two tailed t-test is used to generate the statistics. **p < 0.01, ****p < 0.0001, ns: no significance.

2.3.7. Cdk8 interacts with the fission regulator, Dynamin-related protein 1 (Drp1)

The mitochondrial changes we observed when expression of Cdk8 is modulated suggested that the morphology can be altered by either promoting fragmentation process via Drp1 or suppressing the elongation of mitochondria via inhibiting Marf and Opa1, which are responsible for the outer and inner membrane fusion of mitochondria, respectively (Fig. 2.11).

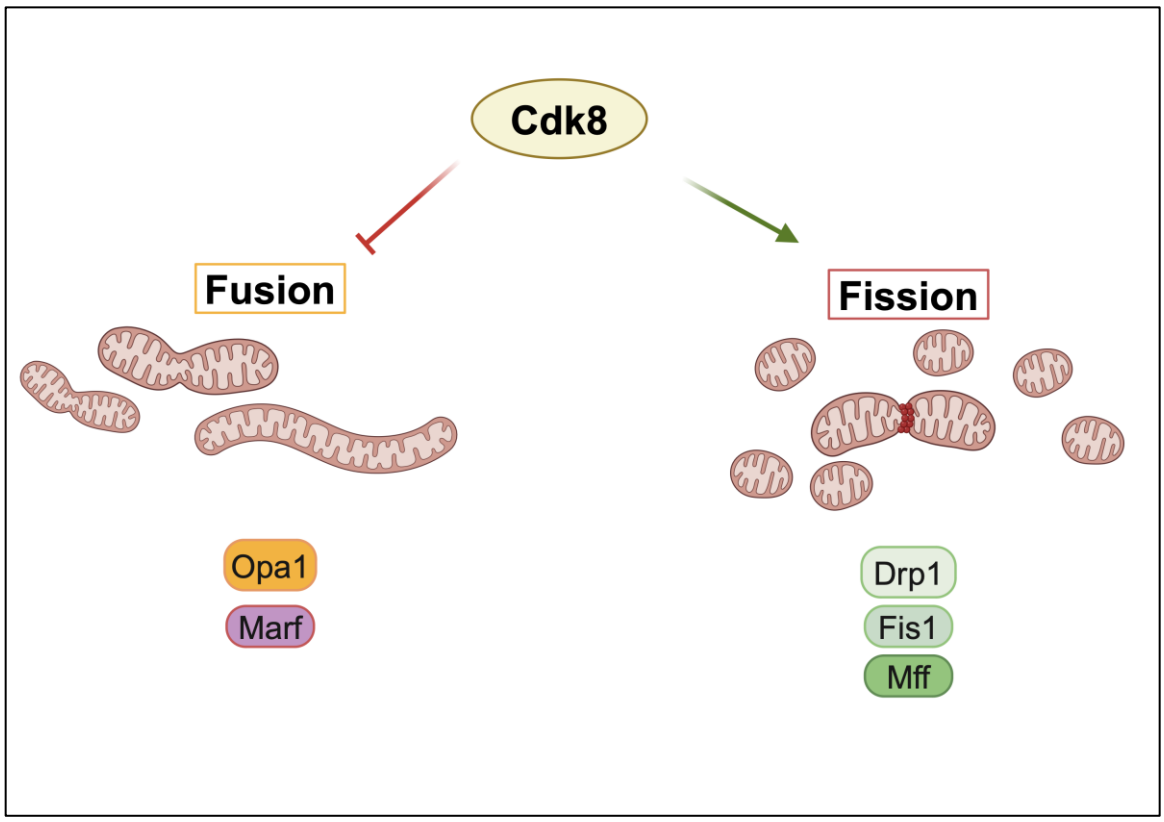

Figure 2.11. Hypothetical model on how Cdk8 can regulate mitochondrial morphology via regulators of mitochondrial dynamics.

The mitochondrial morphologies when expression of Cdk8 is modulated suggest that Cdk8 can either achieve the corresponded mitochondrial phenotypes by either promoting fission via Drp1 or inhibiting fusion via Marf or Opa1.

Since the elongation of mitochondria is enhanced in flies expressing $Cdk8^{KD}$, it suggests that $Cdk8^{KD}$ is acting in dominant negative way. Thus, we suspected that the kinase function of Cdk8 may be important in regulating mitochondrial dynamics. We

performed protein sequence alignments using the CDK consensus phosphorylation motif S/T-P-X-R/K[233–235] and searched among regulators of mitochondrial dynamics, including Opa1, Marf, and Drp1[210,236–238]. We did not find the motif in the fusion proteins (Opa1and Marf) but the fission regulator Drp1 carries the motif at serine 616 (Fig. 2.12a), a site that is known to be regulated by phosphorylation, acetylation and SUMOylation[187]. These findings suggest that the effects of mitochondrial dynamics of Cdk8 may be mediated by the fission regulator, Drp1.

We next asked if Cdk8 expression affects the abundance of Drp1 or S616-phosphorylated Drp1 endogenously. We examined the levels of both total Drp1 and phospho-S616-Drp1 (using an antibody that detects only the Serine 616-phosphorylated form of Drp1[215,216]) in lysates from fly tissues in which Cdk8 was either knocked down or overexpressed in larval body wall muscles. We found no significant difference in the levels of total Drp1 protein between control and either Cdk8-RNAi or Cdk8 overexpression (Fig. 2.12b). However, an antibody that recognizes pDrp1^{S616}, shows a significant decrease following Cdk8 depletion and an increase in pDrp1^{S616} when Cdk8 is expressed (Fig. 2.12b).

To determine if loss of Cdk8 also affects the phosphorylation of Drp1 in other tissues such as the nervous system, we assessed the protein levels of phospho-Drp1 S616 and normal Drp1 by performing western blot using the extracts of heads of *elav>Cdk8 RNAi* flies. We had previously shown that nervous system depletion of Cdk8 caused climbing defects, thus we suspected it played a role in these cell types. In these tissues we used a neuronal driver to deplete Cdk8 and compared this to control head extracts that are heavily enriched for neuronal tissue. We found that the phospho-Drp1 S616 level is decreased by about 25% (Fig. 2.12c). In summary, the data show that expression of Cdk8 can affect the endogenous level of phospho-Drp1 by promoting phosphorylation of Drp1 at S616 to activate the mitochondrial fragmentation process.

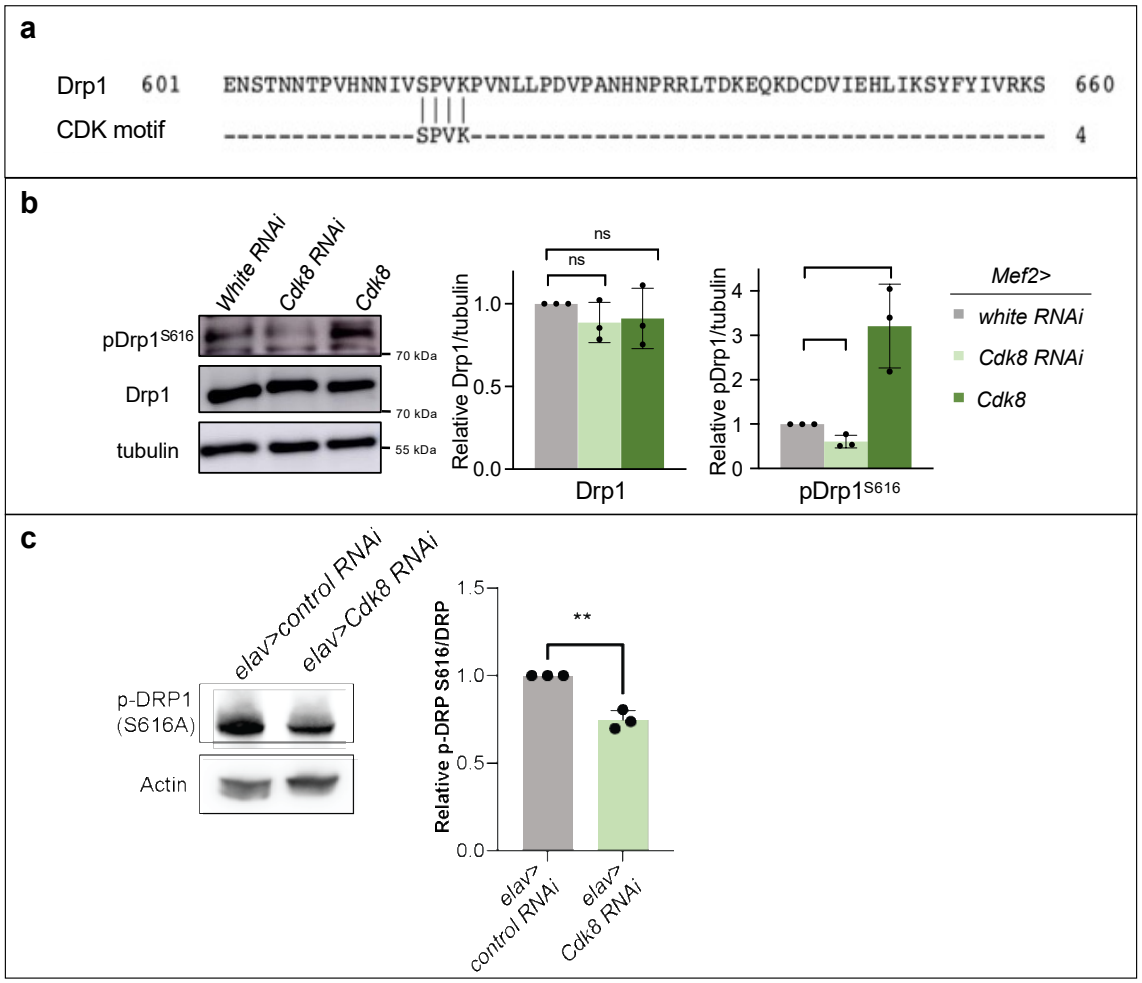

Figure 2.12. Cdk8 regulates the phospho-status of Drp1 at S616 site

(a) Protein sequence alignment between the fission regulator Drp1 and the consensus CDK phosphorylation motif. (b) Western blot showing the level of total Drp1 or S616 phospho-Drp1 in control (Mef2>white RNAi), Mef2>Cdk8-RNAi and Mef2>Cdk8HAflies. Quantifications of blots normalized to actin levels (n=3 per genotype). Results are mean ± SD. Unpaired two tailed t-test is used to generate the statistics. P value is 0.1850 for Cdk8 RNAi, and 0.4490 for Cdk8 in comparison to white RNAi. Flies were raised at 25 °C. (c) Western blot results showing the level of phosphor Drp1 S616 and its quantification versus total DRP1 level in the heads of control (elav>control RNAi), and flies that express Cdk8 RNAi (elav>Cdk8 RNAi) (n=3 per genotype). $*p < 0.05$, $**p < 0.01$, $***p < 0.001$, $****p < 0.0001$, ns no significance.

To learn more about Cdk8 function, we next sought to determine its subcellular localization since our findings about Drp1 suggested it could have a role in the cytoplasm (Fig.2.13). Since there are no commercially available or reliable researcher-generated antibodies for detecting Cdk8 in flies, we first utilized the Drosophila embryonic cell culture, S2-R+ cells, to determine the subcellular localization of tagged Cdk8 and Drp1. We used the TOPO cloning technique and generated plasmids that contain either C-terminally Myc-tagged Cdk8 (pAWM-Cdk8) or HA-tagged Drp1 (pAWH-Drp1) under a ubiquitous Actin promoter. These plasmids were validated by Sanger sequencing before being transfected into S2-R+ cells.

We relied on the immunolabelling of Myc-tag to determine the localization of exogenous Cdk8 and found it is primarily located in the cytoplasm. Interesting, we found regions of staining where the mitochondrial marker ATP5a overlapped with the Myc staining, which suggests that exogenous Cdk8 can be found associated with mitochondria (Fig. 2.13a). Consistent with our immunolabelling findings, the subcellular fractionation of Myc-tagged Cdk8 indicates that exogenous Cdk8 was predominantly present in the cytoplasmic fraction, with only a trace of Cdk8 present in the nuclear fraction. We next examined the localization of pAWH-Drp1 in S2-R+ cells using the same approach. We found HA-tagged Drp1 is only present in the cytoplasm, and the subcellular fractionation blot further validated this finding (Fig. 2.13b). In conclusion, we found exogenous Cdk8 and Drp1 both have a cytoplasmic localization in Drosophila S2-R+ cells.

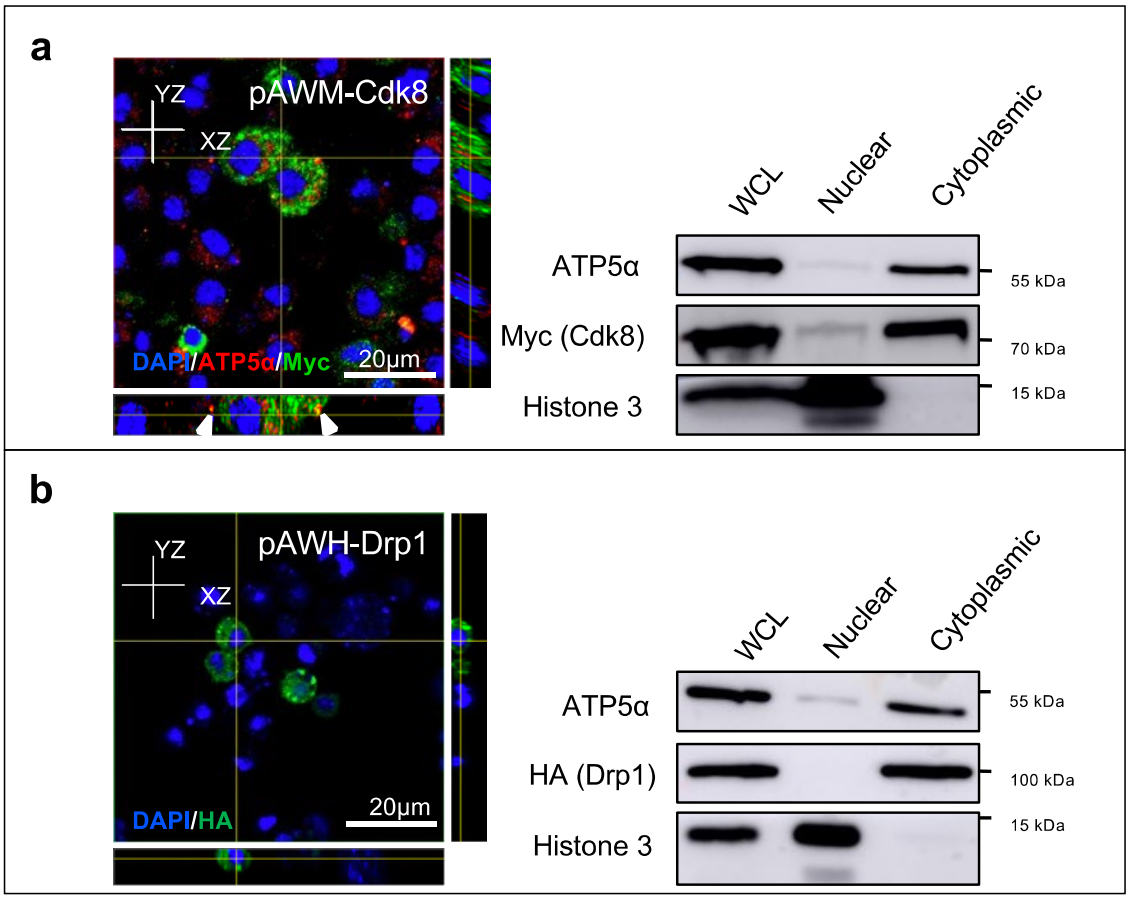

Figure 2.13. Localization of Myc-tagged Cdk8 and HA-tagged Drp1 in S2-R+ insect cells

(a) Single plane image of Myc-tagged Cdk8 (green) localization in S2-R+ cells. Co-staining with DAPI (blue) and ATP5a (red) highlights cytoplasmic localization. Whole cell lysate (WCL), nuclear and cytoplasmic fractions were blotted to detect Cdk8. Experiments are repeated three times. (b) Single plane image of HA-tagged Drp1 (green) localization in S2-R+ cells, co-stained with DAPI (blue). Whole cell lysate (WCL), nuclear and cytoplasmic fractions were blotted to detect Drp1. n = 3 independent experiments.

Based on the Drp1 western blot data from fly tissues in which we modulated Cdk8 levels (Fig. 2.12), along with the localization of exogenous Cdk8 and Drp1 in S2-R+ cells, we decided to perform reciprocal co-immunoprecipitation by using either HA-agarose or Myc-agarose to see if Drp1 and Cdk8 have potential interaction within a protein complex. Given that we hypothesize that Cdk8 phosphorylates Drp1, we anticipated detecting a small fraction of Myc-tagged Cdk8 when Drp1 gets pulled down by the HA-agarose. Indeed, it was the case as shown in Figure 2.13a. A faint band was detected at approximately 70 kDa, which is the anticipated molecular weight for Myc-tagged Cdk8. In addition, we found HA-tagged Drp1 was immunoprecipitated by Myc-Cdk8 with a molecular weight approximately around 100 kDa. Together, these findings suggest that Drp1 and Cdk8 can interact within a protein complex in Drosophila S2-R+ cell.

Previously we showed that expression of a kinase dead version of Cdk8, where a single amino acid is altered from aspartic acid (D) to an alanine (A) in the well-conserved kinase domain of Cdk8, denoted as D173A[136], further enhances the elongation morphology of mitochondria in both larval wall muscle and adult indirect flight muscle in comparison to depletion of Cdk8 (Figs. 2.3, 2.4). We next asked if the Cdk8 kinase function was required to see increased the phospho-Drp1 level. To address this question, we performed a kinase assay. The overall protocol is outlined in Figure 2.13b. We immunoprecipitated Myc-Cdk8 from the cytoplasmic fractions of S2-R+ cells transfected with both Myc-Cdk8 and HA-Drp1 constructs. The immunoprecipitated proteins were then subjected to *in vitro* kinase assays in the absence or presence of ATP (Fig. 2.14c) since ATP is required for phosphorylation. We quantified the total amount of Cdk8 pulled down using anti-Myc antibodies, which was equivalent between experimental conditions. We next determined relative amounts of total Drp1 and pS616-Drp1. The two bands indicate the endogenous Drp1 and larger exogenous Drp1 with the HA-tag which are both detected by the anti-Drp1 antibody. We found that phosphorylation of co-immunoprecipitated cytoplasmic Drp1 is significantly elevated in the presence of ATP (Fig. 2.14c).

Altogether, these data from the S2-R+ cell experiment indicates that cytoplasmic Cdk8 can pull down both endogenous and exogenous Drp1, and the level of phosphorylation of Drp1 depends on the kinase activity of Cdk8 in the presence of ATP.

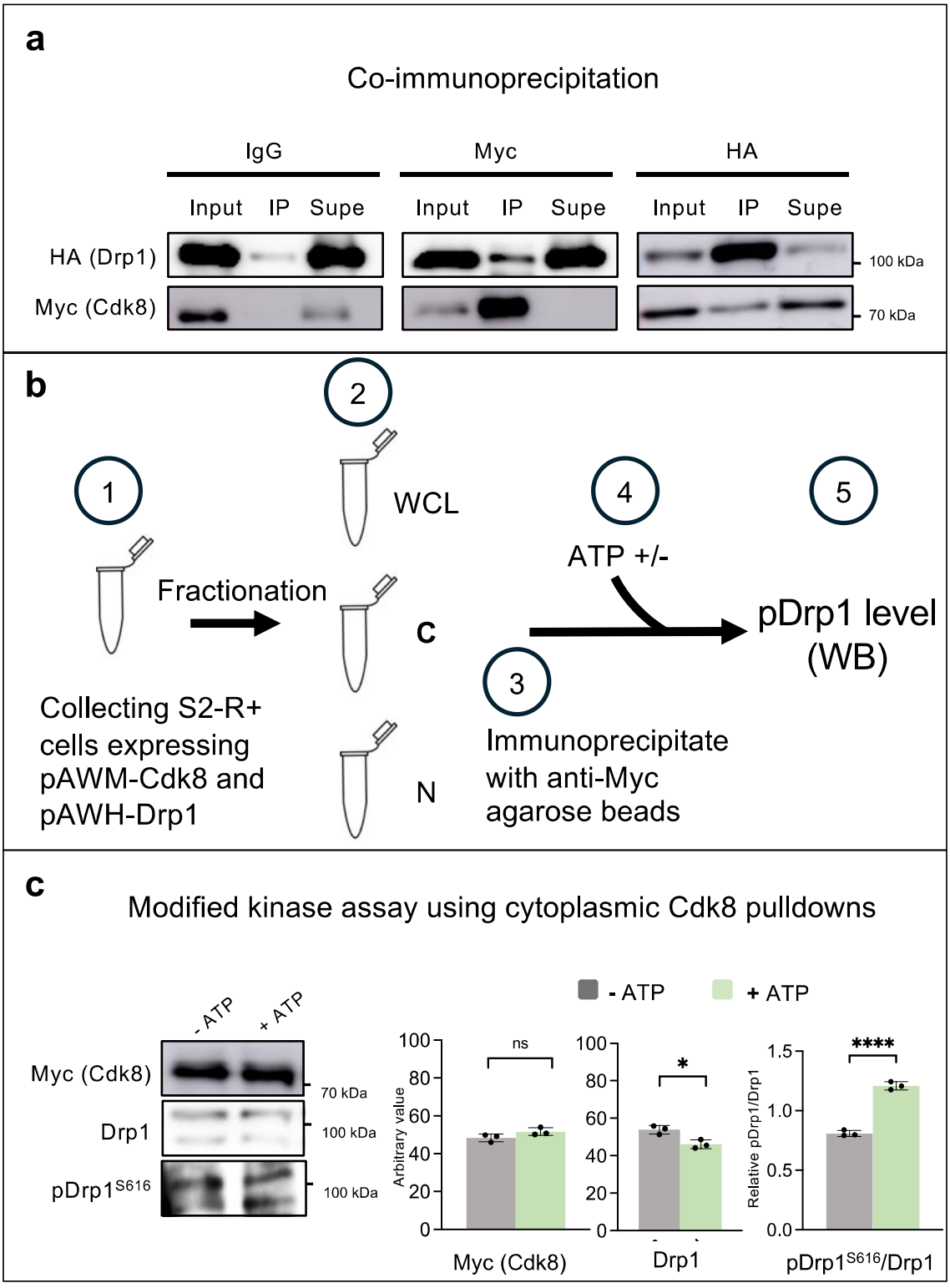

Figure 2.14. Exogenous Cdk8 interacts with Drp1 in S2-R+ cells by phosphorylation.

(a) Co-immunoprecipitation using S2R+ cells co-transfected with HA-tagged Drp1 and Myc-tagged Cdk8 plasmids. IgG agarose beads were used as negative control. IPs used HA-agarose beads, or the reciprocal pulldown with Myc-agarose beads. (b) Schematic demonstration of the kinase assay. Numbers in circles indicate the order. (c) Myc-Cdk8 and HA-Drp1 from S2R+cytoplasmic fractions were immunoprecipitated with Myc-agarose and subjected to in vitro kinase assays in the presence or absence of ATP. Experiments are repeated three times. Results were mean ± SD. Unpaired two tailed t-test is used to generate the statistics. P-value is 0.0149 for Drp1, and 8.54e-05 for pDrp1/Drp1. Samples were probed with antibodies to Myc to quantify Myc-Cdk8 levels (which were equivalent between conditions), Drp1 to detect degree of Drp1 binding to Cdk8, and with anti-pDrp1S616 to quantify the degree of phosphorylation relative to total Drp1. $*$ $p<0.05$, $**$ $p<0.01$, $****$ $p<0.0001$, ns: no significance.

2.3.8. Endogenous GFP-tagged Cdk8 interacts with Drp1

Until this point, most of the biochemistry experiments we performed relied on the ectopic expression of Cdk8 or Drp1 or both. We were keen to ask if the findings hold true with endogenous Cdk8. As mentioned previously, there is a lack of commercially or academically available antibodies for fly Cdk8. To circumvent this problem, our collaborator Dr. Oguz Kanca generated an endogenously GFP-tagged Cdk8 line using a CRISPR approach, denoted as *Cdk8::GFP*[239]. The schematic illustration is included in Figure 2.15a. This approach resulted in the inclusion of a superfold-GFP (sfGFP) in frame in the C-terminus of Cdk8. The construct also encodes a scarless DsRed in the untranslated region of *Cdk8* which aids in the selection of transformed flies. *Cdk8::GFP* homozygous flies are viable and do not exhibit any overt phenotypes, indicating that insertion of sfGFP does not affect Cdk8 function. To test if endogenous GFP-tagged Cdk8 can physically interact with Drp1, we performed co-immunoprecipitation using fly muscles expressing HA-tagged Drp1 in the *Cdk8::GFP* fly strain (Fig. 2.15b). Drp1 was pulled down using anti-HA beads and *Cdk8::GFP* was detected using an anti-GFP antibody in co-immunoprecipitations of Drp1 but not with anti-IgG agarose. This finding shows that Drp1, which is cytoplasmic, interacted with endogenous GFP-tagged Cdk8. In addition, this finding is in line with the co-immunoprecipitation data where Cdk8 was pulled down with Drp1 in the HA-tagged Drp1 immunoprecipitation (IP), while Cdk8 was absent from the control IgG IP in S2-R^{+} insect cells where Myc-tagged Cdk8 and HA-tagged Drp1 plasmids are co-transfected (Fig. 2.14a).

Altogether, the S2-R+ cell culture experiments along with endogenous tagged Cdk8 coimmunoprecipitation data show that Cdk8 physically interacts with Drp1, and Cdk8 is likely to have potential function outside of the nucleus. Our data strongly suggest that the effect of Cdk8 on Drp1 is direct, although we cannot rule out entirely that it is indirect via an associated kinase.

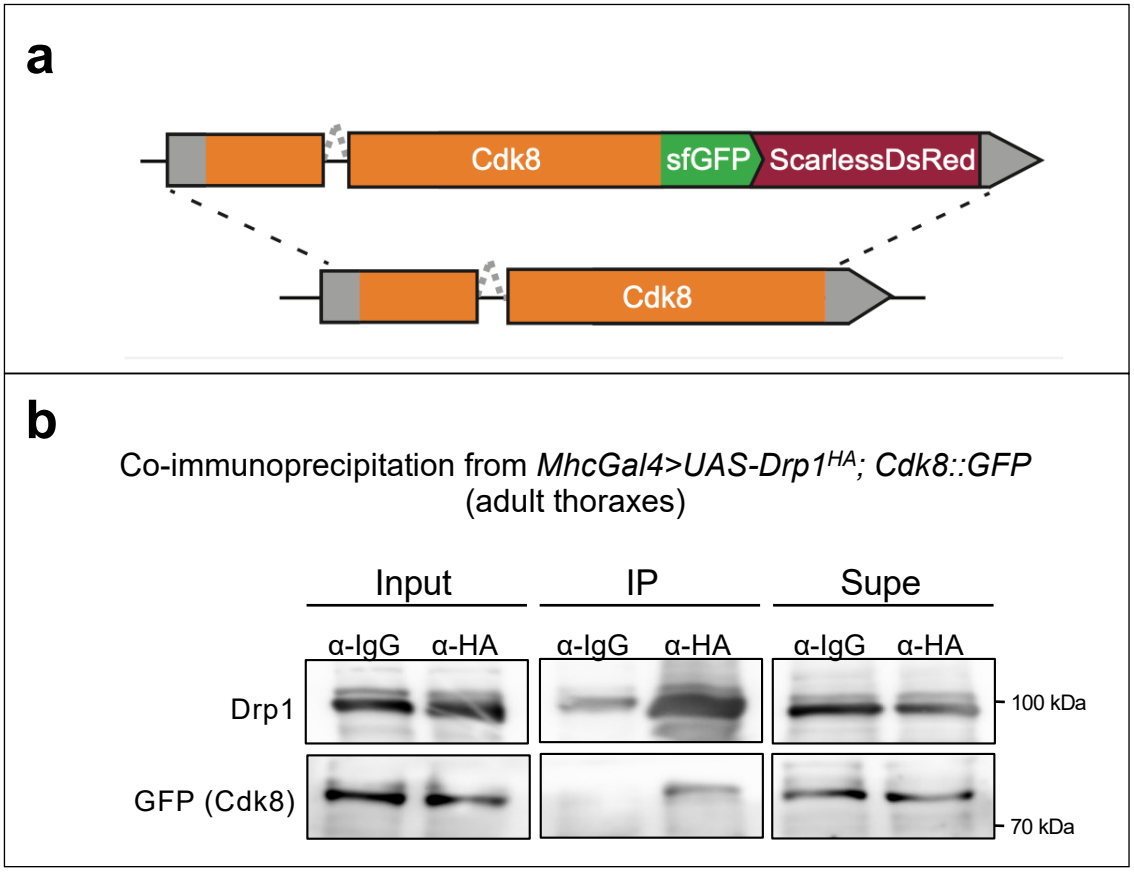

Figure 2.15. Endogenous GFP-tagged Cdk8 interacts with Drp1

(a) Schematic illustration for generation of endogenously tagged *Cdk8::GFP* flies. (b) Co-immunoprecipitation using adult thoraxes expressing *MhcGal4> UAS-Drp1^{HA}+Cdk8::GFP* at 25 °C. IgG agarose beads were used as negative control. IPs used HA-agarose beads and detected endogenous Cdk8::GFP using rabbit anti-GFP antibody. n = 3 independent experiments.

2.3.9. Depletion of Cyclin C causes pupal semi-lethality, abnormal wing posture and impaired climbing

It was previously shown that Cyc C can translocate from the nucleus to the cytoplasm to promote mitochondrial fission in yeast and mouse embryonic fibroblasts [139,140]. We therefore wanted to know if this function of Cyc C is conserved in flies as it might also act together with Cdk8 in regulating mitochondrial morphology. To address this question, we examined the effects of Cyc C in the assays we used to characterize Cdk8 function. We first knocked down Cyc C and assayed climbing ability. Due to larval lethality caused by *Act5c>Cyc C RNAi* we instead used the ubiquitous daughterless *Da-Gal4* driver to knock down approximately 70% of endogenous Cyc C (Fig. 2.16a). Cyc C depletion also caused abnormal wing postures after flies eclosed and pupal semi-lethality (Fig. 2.16b), which is consistent with studies showing that Cyc C was essential[240]. We next examined locomotor activity in *Cyc C* depleted flies. Climbing ability was significantly reduced following ubiquitous knockdown (Fig. 2.16c). Climbing defects were seen in two-week-old flies when Cyc C is depleted in muscle. In contrast to climbing defects seen after ubiquitous depletion of Cdk8 and Cyc C, neuronal knockdown of Cyc C did not show any altered climbing phenotypes (Fig. 2.16c), which suggests that Cyc C is not essential in neuronal function in this context, whereas Cdk8 is. This finding further indicates that even though Cdk8 and Cyc C are known to function as part of Mediator complex in transcriptional regulation, they do have distinct functions that are specific in the tissue type where the depletion has occurred.

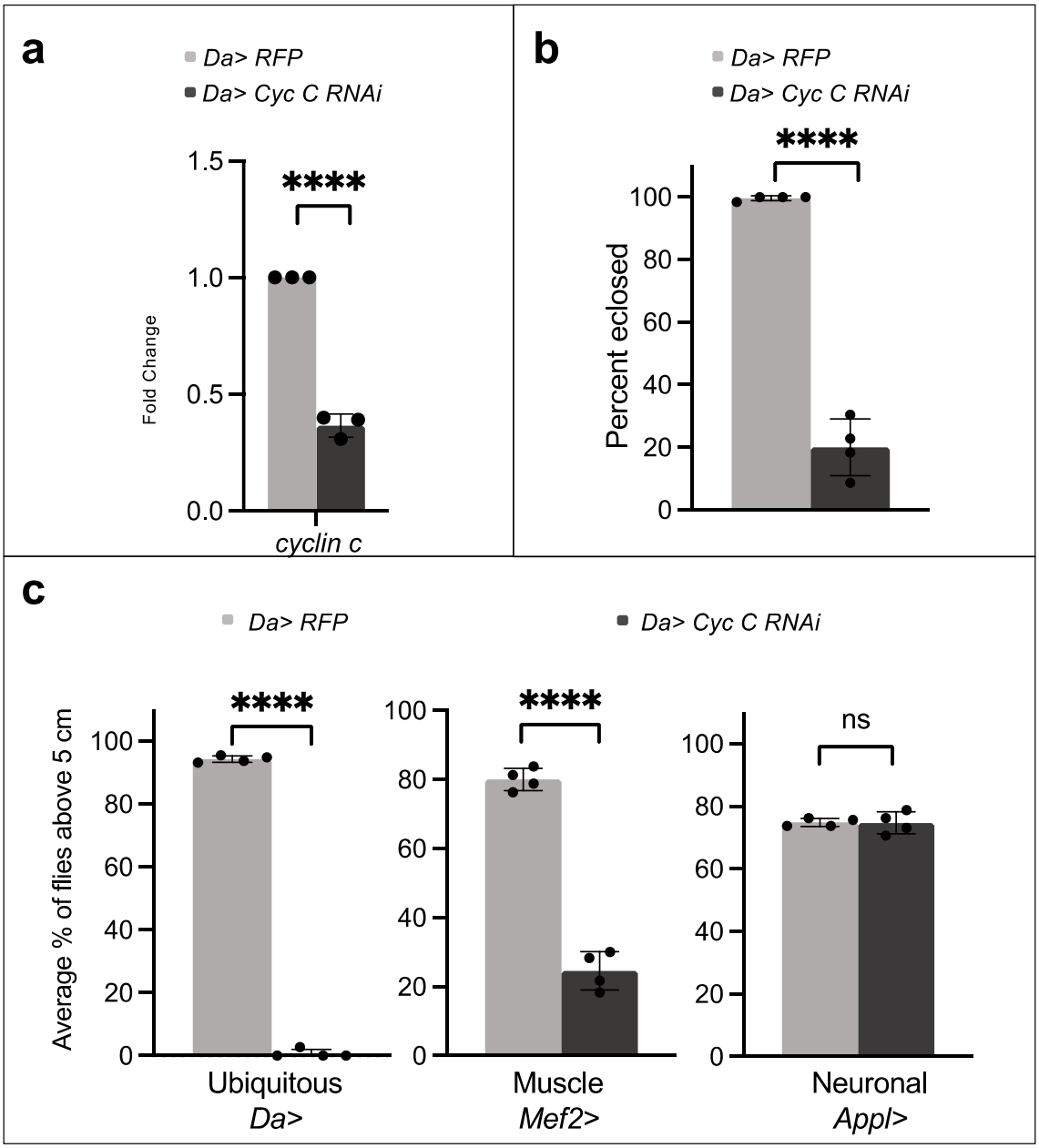

Figure 2.16. Depletion of Cyclin C causes lethality and climbing defects

(a) qPCR analysis of CycC gene expression following *CycC RNAi* expression relative to control (*da>RFP*). Data are mean ± SD. n = 3 independent experiments. (b) Semi-lethality is found in Da>Cyc C RNAi pupae in comparison to Da>RFP (n=4 per genotype). Data are mean ± SD. (c) Average percent of flies that reached the target line of indicated genotypes in a climbing assay. Each experiment is individually repeated four times. The total number of progeny are assessed between white RNAi and Cyc C RNAi with different drivers: n = 118, 120 in Da>, 159, 160 in Mef2>, and 115, 119 in App>, respectively. n = 4 independent experiments. Results are mean ± SD. An unpaired two-tailed t-test is used to generate the statistics.

2.3.10. Expression of Cyclin C modulates mitochondrial morphologies

Cyc C has previously been shown to exit the nucleus under oxidative stress conditions to regulate mitochondrial morphology in yeast and mouse embryonic fibroblast[139,140]. To better characterize the mitochondrial morphology when expression of Cyclin C is modulated under physiological conditions, we assessed the mitochondrial morphology in adult IFMs. We found that depletion of *Cyc C* in muscles led to elongation of mitochondria in comparison to control cells (Fig. 2.17b-b'), and overexpression of Cyc C promotes fragmentation of mitochondria (Fig. 2.17c-c'). Since the mitochondrial morphologies mimicked the fusion and fission like what we observed when Cdk8 expression is modulated, we next asked if Cyc C, as part of the Cdk8 module has any transcriptional effects on regulators of mitochondrial dynamics (Fig. 2.17d). Ubiquitous knockdown of *Cyc C* led to a modest increase in expression of both a regulator of mitochondrial fusion (mitochondrial assembly regulatory factor, *marf*) and fission (*Drp1*), suggesting the mitochondrial morphology defects are not likely due to reduced mRNA levels of these genes (Fig. 2.17d).

In summary, both Cdk8 and Cyc C modulate mitochondrial morphology, and proper expression of Cdk8 and Cyc C are needed to maintain the balance in mitochondrial dynamics.

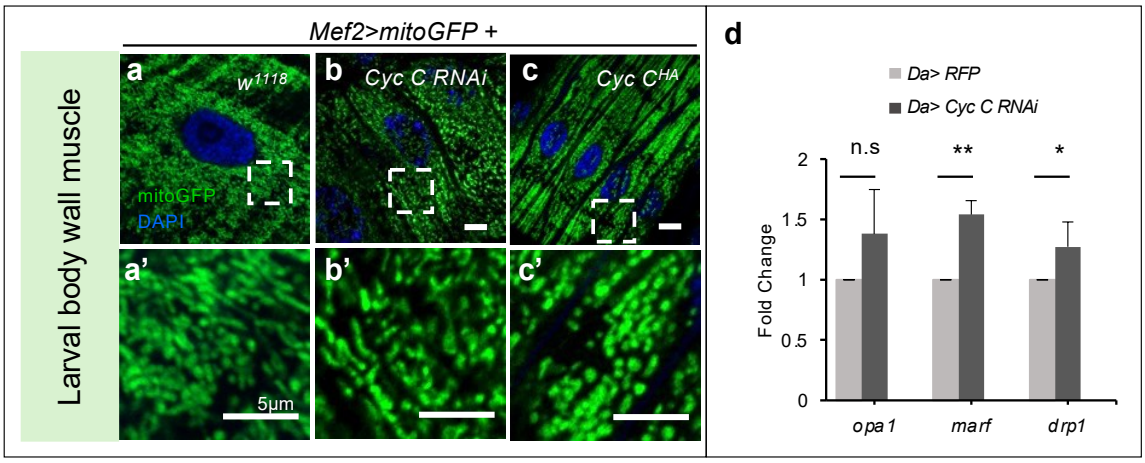

Figure 2.17. Cyclin C regulates mitochondrial morphology in larval body wall muscle under physiological conditions.

Mitochondrial morphology of larval body wall muscles in (a) control or expressing (b) CycC RNAi or (c) Cyc CHA. Scale bar: 10 µm. (a'-c') Representative magnified sections from b-d (indicated with dashed boxes). Scale bar: 5 µm. b-d raised at 25°C. (d) qPCR analysis of *opa1, marf, and drp1* in *Da> Cyc C RNAi* relative to control (*Da> RFP*) at 25°C. Data are mean ± SD. n = 3 independent experiments. Unpaired two-tailed t-test is used to generate the statistics. $*p < 0.05$, $**p < 0.01$, $***p < 0.001$, $****p < 0.0001$, ns no significance.

2.3.11. Cdk8 and Cyclin C likely use distinct mechanisms to regulate mitochondrial morphologies

The resemblance in mitochondrial morphologies between *Cdk8* depleted and *Cyc C* depleted flies prompted us ask if Cdk8 functions to promote the activity of Cyc C in turn to regulate mitochondria. To address our question, we tested whether elevated Cyc C expression could rescue Cdk8 depletion phenotypes using the muscle specific driver, myosin heavy chain-Gal4, Mhc-Gal4 (Fig. 2.18). We could not use Mef2-Gal4 as it caused lethality with depletion of Cyc C. Depletion of Cdk8 caused elongated mitochondrial morphology (Fig. 2.18a-a''), and ectopic expression of Cdk8 rescued the mitochondrial phenotypes caused by an expression of *Cdk8-RNAi* (Fig. 2.18b-b''). However, Cyc C expression failed to rescue the elongated mitochondrial phenotype as we observed further enhanced filamentous mitochondrial morphology (Fig. 2.18c-c''). We also performed the reciprocal experiment in which we tested whether Cdk8 could rescue the effects of *Cyc C* knockdown (Fig. 2.18d-f). Cdk8 expression alters the mitochondrial abnormalities caused by an expression of *Cyc C-RNAi* but does not rescue (Fig. 2.18e-e''). However, expression of Cyc C did rescue the mitochondrial fusion caused by depletion of Cyc C (Fig. 2.18f-f'', d-d''), suggesting that our assay could in principal work to restore mitochondrial homeostasis. Hence, these results suggest that Cdk8 and Cyc C likely use distinct mechanisms to modulate mitochondrial dynamics in this context, although further research would be needed to confirm this hypothesis.

In summary, we found the Cdk8 plays a novel role in regulating mitochondrial morphology. Our immunoprecipitation data from S2-R+, as well as fly muscles, demonstrated that Cdk8 interacts with Drp1. The difference in mitochondrial morphology when Cdk8 is modulated is achieved by directly phosphorylating the fission regulator, Drp1 at S616. In addition, we found depleting Cyc C, the partner of Cdk8 shares some phenotypic resemblances as Cdk8 depleted flies in abnormal wing posture and lethality, which demonstrate the essentialness of Cdk8 and Cyc C in development of flies. Furthermore, we found Cyc C expression plays a role in regulating mitochondrial morphology as well, which validated other's findings where Cyc C is known to promote fission in different models. Despite the observation that Cdk8 and Cyc C result in similar mitochondrial phenotypes in muscles, our reciprocal genetic experiments indicate that Cdk8 and Cyc C likely using different underlying mechanisms to regulate mitochondrial morphology.

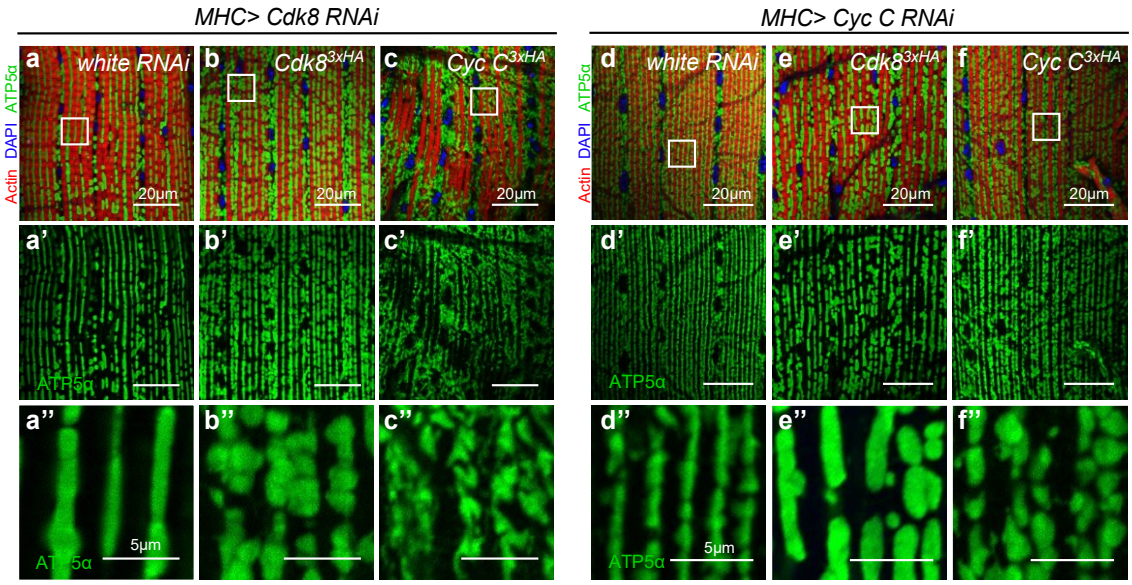

Figure 2.18. Cdk8 and Cyclin C do not interact to regulate mitochondrial dynamics

Mitochondrial morphology of adult IFM expressing either (a) *white RNAi,* **(b)** *Cdk8*^{HA} or (c) *Cyc C*^{HA} in a *Cdk8* depleted background. Scale bar: 20 μm. **(a'-c')** are single channel images incubated with mouse-α-ATP5α from a-c. **(a''-c'')** Representative magnified sections from a-c (indicated with white boxes). Scale bar: 5 μm. Raised at 25°C. (n = 6 per genotype). Mitochondrial morphology of adult IFM expressing either (d)*white RNAi* , **(e)** *Cdk8*^{HA} or (f) *Cyc C*^{HA} in a *Cyc C* depleted background. Scale bar: 20 μm. **(d'-f')** are single channel images incubated with mouse-α-ATP5α from d-f. **(d''-f'')** A representative magnified section from d-f (indicated with white boxes). Scale bar: 5 μm. Raised at 25°C. (n = 7 per genotype)

2.4. Discussion

In this chapter, we showed that Cdk8 plays an essential role in organismal survival and function as depleting endogenous *Cdk8* led to semi-lethality, shorter survival rate, abnormal wing postures as well as locomotion defects (Figs. 2.1, 2.2). Since loss of the ability to fly and climb are associated with muscle defects within thoraxes and legs, we examined the muscle and mitochondrial morphologies in indirect flight muscles (IFM) due to their accessibility as well as their role in regulating wing postures. We found expression of Cdk8 can significantly alter the mitochondrial morphologies in a kinase-dependent fashion in both larval body wall muscles and adult IFM (Figs. 2.3, 2.4). We observed elongated mitochondrial morphology in depletion of *Cdk8*, whereas fragmentation of mitochondria following ectopic expression of Cdk8. In addition, we found loss of Cdk8 altered mitochondrial distribution in both neuropil and photoreceptor terminals, which indicated its function in central nervous system development (Figs. 2.8, 2.9, respectively). Furthermore, we found depletion of Cdk8 causes increased muscle fiber width in IFM along with elevated ROS (Fig. 2.8), suggesting expression of Cdk8 needs to be tightly regulated to maintain the homeostasis of cells, especially their mitochondria.

Previous studies of Cdk8 in yeast showed contradictory effects on stress-induced mitochondrial dynamics[140–143]. Cdk8's obligate partner Cyc C, but not Cdk8, was shown to promote mitochondrial fission in both stressed and unstressed conditions[140–143]. We found that both Cdk8 and Cyc C regulate mitochondrial morphology in the physiological context of a multicellular tissue. However, Cyc C failed to rescue Cdk8 depleted phenotype in mitochondria, and vice versa (Fig. 2.18c-c'', e-e''). These findings suggest that Cdk8 and Cyc C do not compensate for each other in regulating mitochondria. The possibility remains that Cyc C requires abundant Cdk8 for its activation, and in our experiments, we were unable to activate the excess Cyc C. Future studies could address this by expressing an activated Cyc C[140–143].

Lastly, we identified that Cdk8 interacts with the fission regulator of mitochondrial dynamics, Dynamin-related protein 1 (Drp1). The reduced mitochondrial size in photoreceptors when Cdk8 is depleted was strikingly resembled the phenotype seen with loss of *Drp1*[231], which provided the first clue to further investigate the connection between Cdk8 with mitochondrial dynamics. We utilized multiple approaches including

western blotting, insect cell cultures and kinase assay to demonstrate that indeed Cdk8 interacts with Drp1 (Figs. 2.12-2.15), which further explains the phenotypic resemblance in synaptic transmission when either Drp1 or Cdk8 is depleted (Fig. 2.9). Our findings strongly support the model that Cdk8 interacts and phosphorylates Drp1 to promote mitochondrial fission. Previous studies showed that both Cdk1 and Cdk5 can phosphorylate Drp1 on this same residue[210,213,214]. However, we cannot rule out the possibility that another kinase is being co-immunoprecipitated from cell lysates and acting on Drp1.

Altogether, this chapter demonstrates that Cdk8 plays a novel function in regulating mitochondrial homeostasis by phosphorylating the fission regulator, Drp1.

2.4.1. Mitochondrial dynamics and its role in myofibril development

We found that depletion of Cdk8 leads to both elongated mitochondrial morphologies along with enhanced myofibril width in DLMs (Fig. 2.7). It has previously been showed that mitochondrial dynamics impact myofibril development in DLMs[241,242]. Depletion of either Opa1 or Marf in muscle alters the muscle organization and size, where the area of each fibre was reduced along with greater space between muscle fibres[241]. In addition, it has been shown that overexpression of Drp1 in the muscle causes mitochondria to become small and fragmented but leaves the diameter of myofibrils unchanged, which is consistent with what we observed when Cdk8 is overexpressed in Fig. 2.7. It has been proposed that intercalating hyperfused mitochondria between muscle fibres can affect the overall organization of muscle fibers[242]. This may explain the increased myofibril width that we observed only when *Cdk8* is depleted (Fig. 2.7b-b'''). In the future, one can test if depleting either Opa1 or Marf in a *Cdk8* depleted background can suppress the enhanced myofibril width in DLMs. In addition, contractions between the two sets of antagonistic IFM are the key to exert flight ability. Since we observed either held-up or droopy wing postures when Cdk8 is depleted, it would be interesting to further examine the components of the sarcomere to determine the missing link for activating the contractions between IFMs.

2.4.2. Abnormal mitochondria or mitochondrial fusion can both lead to elevated ROS

Depleted *Cdk8* results in elongated mitochondrial morphology with elevated ROS and defective phenotypes including climbing defects, abnormal wing postures, and semi-lethality. It has been documented that under oxidative stress condition, mitochondria tend to form hyperfused structures[243]. ROS is considered one oxidative stress condition which can act as a second messenger for maintaining the redox homeostasis of a cell when the concentration of it remains low. However, when levels of ROS build up within the cell, they can be detrimental by damaging proteins, lipids, DNA and even mitochondria where they were originally generated[179]. By western blotting and co-immunoprecipitation, our experiments clearly indicate that Cdk8 interacts with Drp1, the fission regulator (Figs. 2.12b-c, 2.14, 2.15), but we did not differentiate whether the mitochondrial morphology that we observed when Cdk8 was depleted is functional fused mitochondria or dysfunctional impaired mitochondria. Either scenario can lead to elevated ROS that can ultimately result in abnormal phenotypes such as lethality, sterility, and reduced survival index. One way to distinguish dysfunctional mitochondria is to perform mitochondrial membrane potential staining by utilizing tetramethylrhodamine ethyl ester (TMRE)[244], which is a positively charged red fluorophore that can bind to healthy mitochondria with well-establish membrane potential. Staining using TMRE in indirect flight muscle where Cdk8 is depleted could indicate whether the defective phenotypes are caused by dysfunctional mitochondria, or accumulation of ROS from hyperfusion.

2.4.3. Mitochondrial dynamics under physiological conditions associated with the translocation of Cyc C and Cdk8

Cyc C is a binding partner of CDK8/CDK19. Under normal conditions, CDK8-Cyc C regulates transcription through association with the Mediator complex of RNA polymerase II[133]. However, in contrast to other cyclins, the expression level of Cyc C does not fluctuate during cell cycle progression[245]. Instead, previous work has shown that oxidative stress can induce a nuclear release of Cyc C to the mitochondria, where it facilitates fission through Drp1 and mitochondrial fission factor (Mff) in mouse embryonic fibroblasts[246–248]. Here we show that expression of Cdk8 can modulate mitochondrial morphology under physiological conditions likely through regulating Drp1, in a similar

fashion as Cyc C. However, we found that the effects of Cdk8 depletion could not be rescued by ectopic Cyc C, suggesting that under our experimental conditions the two proteins may act on Drp1 through distinct mechanisms.

Chapter 3. Cdk8 and CDK19 rescue abnormal phenotypes in a familial form of Parkinsonism caused by *pink1*^{B9} mutation

Chapter 3 is based off the following published work with modification.

3.1. Contributions to the Chapter

This chapter reflects the work performed in collaboration with several labs, primarily that of Dr. Hugo Bellen and his postdoctoral fellow Dr. Hyung-lok Chung. The work was published in April 2024[167]. In this collaboration our lab focussed primarily on phenotypes in muscles, while the Bellen lab carried out most of the studies in neuronal tissues. In this thesis I include for the most part only the work performed by me and Claire Shih, a research technician in the Verheyen lab. Thus, all figures, except Figs. 3.8, 3.9a,b, 3.11, were generated by me, with help from Claire Shih.

3.2. Introduction

In the previous chapter, we demonstrated that depletion of *Cdk8* in flies led to abnormal wing postures, reduced survival rate, climbing defects, altered mitochondrial morphology with elevated ROS. Surprisingly, we found these phenotypes closely resembled *pink1* and *parkin* mutant phenotypes in Drosophila. Mutations in PTEN-induced kinase 1 (*PINK1)* and *PARKIN* have been identified in patients with the familial form of the neurodegenerative disorder Parkinson's Disease (PD)[140]. PD is the second most common neurodegenerative disorder that mainly targets the central nervous system and motor movement and shows increasing severity over time[154,155,249,250]. The currently known underlying molecular pathogenesis of PD includes α-synuclein aggregation[251] and mitochondrial dysfunction[252–254].

Pink1 is a serine/threonine kinase that functions with Parkin (an E3 ubiquitin ligase) in mitochondrial quality control, leading to mitophagy of defective mitochondria[156–159]. In *Drosophila*, *pink1* or *parkin* mutant flies exhibit numerous phenotypes that resemble the symptoms of PD patients including defects in locomotor activity, reduced life span, degeneration of dopaminergic neurons and mitochondrial homeostasis defects[156,157,166,168–170]. Muscle degeneration is one of the most prominent phenotypes seen in PD flies with apoptotic cell death in thoracic muscle ultimately leads to thorax indentation and flight and mobility defects[88,93]. PD flies have impaired mitophagy and accumulation of dysfunctional mitochondria, impeding processes that require high energy demands such as muscle movement. Based on the resemblance between *Cdk8* depleted flies and *pink1* mutant flies, as well as the novel function of Cdk8 in regulating mitochondria, we hypothesized that Cdk8 has therapeutic function in a *pink1/parkin* mutation mediated Parkinsonism model.

As described in Chapter 2, we initiated a collaboration with the Bellen lab to further characterize Cdk8 function since they had previously described that human CDK19 could rescue loss of fly Cdk8[102]. Therefore, we started to investigate the conserved function between fly Cdk8 and human CDK19 in Drosophila. Chung et al.[102] found that expressing the $CDK19^{WT}$ in the *Cdk8* depleted background in fly adult brains can reduce susceptibility toward seizures. In addition, they found that when they expressed tagged human CDK19 in flies, it showed a cytoplasmic localization in the adult brain. This led to the hypothesis that cytoplasmic CDK19 could carry out and

restore functions lost when Cdk8 is depleted. To further investigate the potential cytoplasmic function of CDK19, they generated a line where the predicted nuclear localization sequence (NLS) has removed, denoted as $CDK19^{\Delta NLS}$. Based on Chung et al. publication[102], we hypothesized that human $CDK19^{WT}$ shares conserved function of fly Cdk8 in regulating mitochondria. Introducing $CDK19^{WT}$ could suppress the Cdk8 depleted mitochondrial phenotypes. Furthermore, we hypothesize that if introducing $CDK19^{\Delta NLS}$ into the *Cdk8* depleted background exerted a similar effect as introducing $CDK19^{WT}$, indicating a cytoplasmic function is shared between fly Cdk8 and human CDK19.

3.3. Results

3.3.1. Cdk8 and Cyc C do not affect *pink1* or *parkin transcription*

The defects observed in *Cdk8* or *Cyc C* knockdown flies phenocopy many of the effects of depletion of either *pink1* or *parkin*, which are both well-established Drosophila models for the familial form of Parkinsonism[156,157,166,255]. Mutations in *PINK1* cause a familial form of Parkinson's Disease[143,146,150] and loss of *pink1* disrupts mitochondrial homeostasis and impairs mitophagy[255,259,260]. Since the Cdk8 module is a well-known transcriptional regulator, we asked using qRT-PCR if the phenotypes were due to its role in down regulating the transcription of *pink1* and *parkin*. We found no significant differences in mRNA levels of *pink1* or *parkin* when either *Cdk8* or Cyc C were knocked down ubiquitously (Fig. 3.1a, b respectively). These findings suggest that the phenotypic resemblance between Cdk8 or Cyc C depleted flies and *pink1* mutant flies is not achieved by transcriptional regulation by the Cdk8 module on either *pink1* or *parkin*.

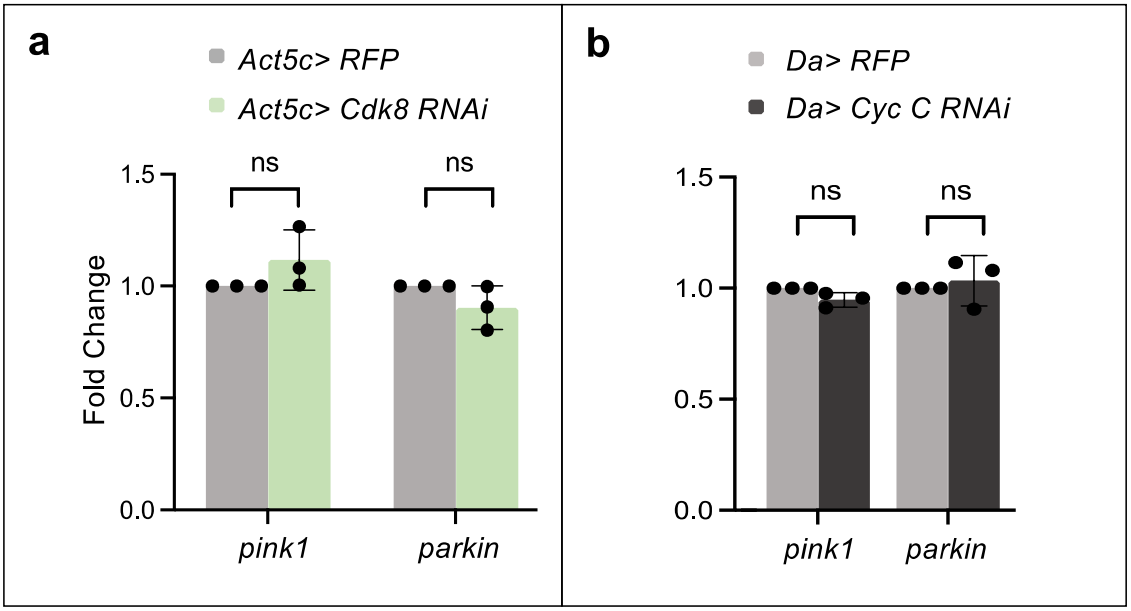

Figure 3.1. Cdk8 and Cyc C do not affect *pink1* or *parkin* transcription

(a) qRT-PCR analysis of *pink1* and *parkin* gene expression in Act5c>Cdk8 RNAi relative to control sample (Act5c>RFP). (b) qPCR analysis of *pink1* and *parkin* gene expression following *CycC RNAi* expression relative to control (*da>RFP*). Data are mean ± SD. n = 3 independent experiments. A unpaired two-tailed t-test is used to generate the statistics.

3.3.2. Expression of Cdk8 can rescue *pink1* mutant phenotypes

Given the phenotypic parallels between knockdown of *Cdk8* and loss of *pink1* along with the qRT-PCR data from Fig. 3.1, we examined the effects of Cdk8 in a *pink1* null mutant (*pink1*^{B9}) PD model[170]. Since *pink1* is on the X chromosome, we selected males that were hemizygous for *pink1*^{B9} for subsequent experiments. Experiments were first performed when flies were three days old, and we performed the same set of experiments on flies that were three weeks old to further examine the phenotypes associated with aged flies.

First, we analyzed the percent of flies with a thorax indentation (Fig. 3.2a), which is a well-known indicator for underlying muscle degeneration in *pink1* mutant flies[157]. Approximately 70% of *pink1*^{B9} flies had thorax indentations. Expression of human PINK1 (hPINK1) using the muscle specific driver, *Mef2-Gal4*, completely rescued the phenotype. Overexpression of Cdk8 significantly rescued this phenotype with only 40% of flies showing thorax indentation (Fig. 3.2a). Defective locomotion in *pink1*^{B9} mutants has been well-characterized[157,261,262]; therefore, we next asked if the locomotor defects found in *pink1*^{B9} flies can be rescued by expression of Cdk8 (Fig. 3.2b). We found *pink1*^{B9} mutant flies had impaired climbing activity as the quantification shows that less than 20% of the flies can reach the target in time (Fig.3.2b). Ectopic expression of hPINK1 in the same mutant background can almost completely restore the climbing defects, proving that under our experimental conditions we can achieve rescue (Fig. 3.2b). Most importantly, ectopic expression of Cdk8 in the same *pink1* mutant background can also significantly rescue the climbing defects, as the distribution violin plot shares a similar trend as the one seen when expressing hPINK1 (Fig. 3.2b).

These findings indicate that ectopic expression of Cdk8 in the *pink1* mutant background can significantly rescue thorax indentation and the underlying muscle degeneration phenotype, as well as the locomotion defect that is well-characterized in the *pink1* mutant.

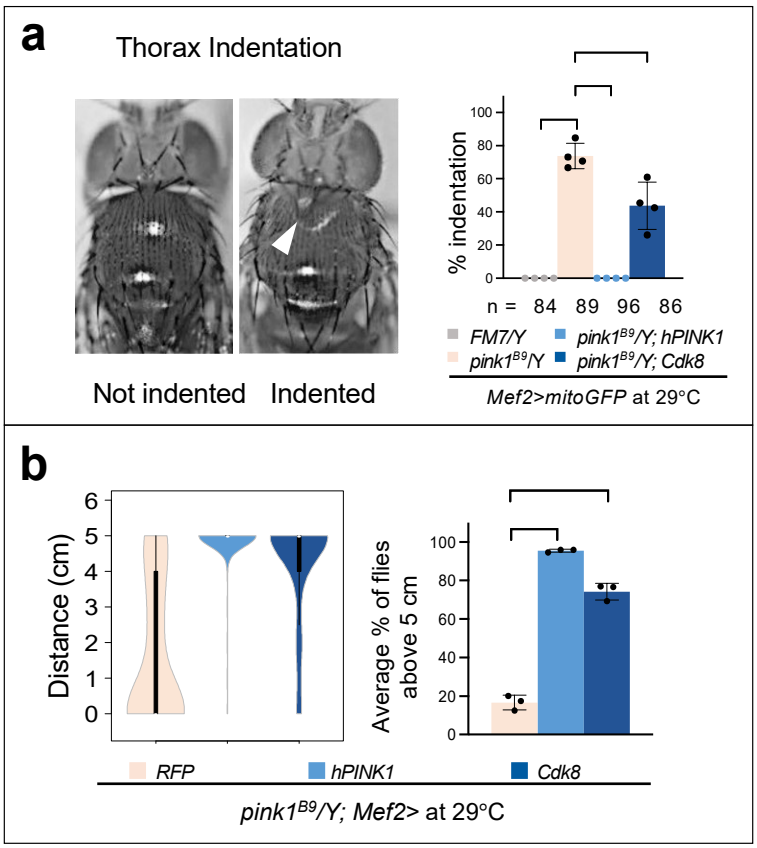

Figure 3.2 Elevated Cdk8 can rescue the defects in thorax integrity and climbing ability in *pink1*^{B9} mutant flies

(a) Thorax indentation (white arrowhead indicates indentation) with quantification of percent indentation in 3-day-old flies expressing either RFP, hPink1, or Cdk8 with Mef2Gal4 in the *pink1*^{B9} mutant background compared to FM7/Y control flies. Experiments are repeated four times. The total number of progeny are assessed, n = 120, 130, 137, 119, respectively, in order. Results are mean ± SD. An unpaired two-tailed t-test is used to generate the statistics. P value is 1.30e-6 for both FM7/Y and hPINK1 and 0.01 for Cdk8 in comparison to the *pink1*^{B9} mutant. (b) Violin plots showing the distribution of climbing activity of RFP, hPink1, or Cdk8 with Mef2-Gal4 in the pink1B9 mutants. The average percent of flies that reach the target line in indicated genotypes. Experiments are repeated three times. The total number of progeny are assessed, n = 80, 74, 65, respectively, in order. Results are mean ± SD. An unpaired two- tailed t-test is used to generate the statistics. P value is 3.96e-6 for hPINK1 and 6.62e-5 for Cdk8 in comparison to the pink1B9 mutant. Raised at 29 °C. *p < 0.05, ** p<0.01, *** p<0.001, **** p<0.0001, ns: no significance.

3.3.3. Cdk8 expression can rescue mitochondrial defects and muscle degeneration in *pink1^{B9}* flies

Pink1 is known to function in the quality control of mitochondria. If mitochondria are sensed to be defective, they are selectively destroyed through a process known as mitophagy. To further analyze the ability of Cdk8 to rescue *pink1^{B9}* phenotypes, we examined the muscle and mitochondrial morphology in dissected adult IFMs. We used UAS-mitoGFP to visualize mitochondrial morphology (Fig. 3.3a-d) and rhodamine phalloidin to visualize F-actin and overall muscle integrity (Fig. 3.3a'-d'). In control flies (FM7/Y), elongated and tubular mitochondria (Fig. 3.3a) were found evenly distributed and intercalated between well-defined F-actin bundles (Fig. 3.2a') along with nuclei stained with DAPI (Fig. 3.3a''). Mitochondrial morphology was severely disrupted in *pink1* mutants as reduced mitochondria with irregular shapes were found scattered between the myofibril, which were significantly narrowed in width (Fig. 3.3b')[156,157,166]. Aggregates of mitochondria (white arrowheads) were also seen (Fig. 3.3b), as has been shown previously[151,152]. Expression of hPINK1 rescued the defects in both mitochondria and muscle (Fig. 3.3c-c'')[263,264]. Expression of Cdk8 rescued the mitochondrial and muscle morphology as robustly as hPINK1 expression (Fig. 3.3d-d''). We quantified the myofibril width of each genotype (Fig. 3.3e) and found that expression of either hPINK1 or Cdk8 in *pink1* mutants significantly suppressed muscle degeneration (Fig. 3.3e), which is in line with our quantification on thorax indentation (Fig. 3.2a).

Together, these findings show that elevated expression of Cdk8 can restore numerous mitochondrial and muscle defects seen in the *pink1^{B9}* PD model.

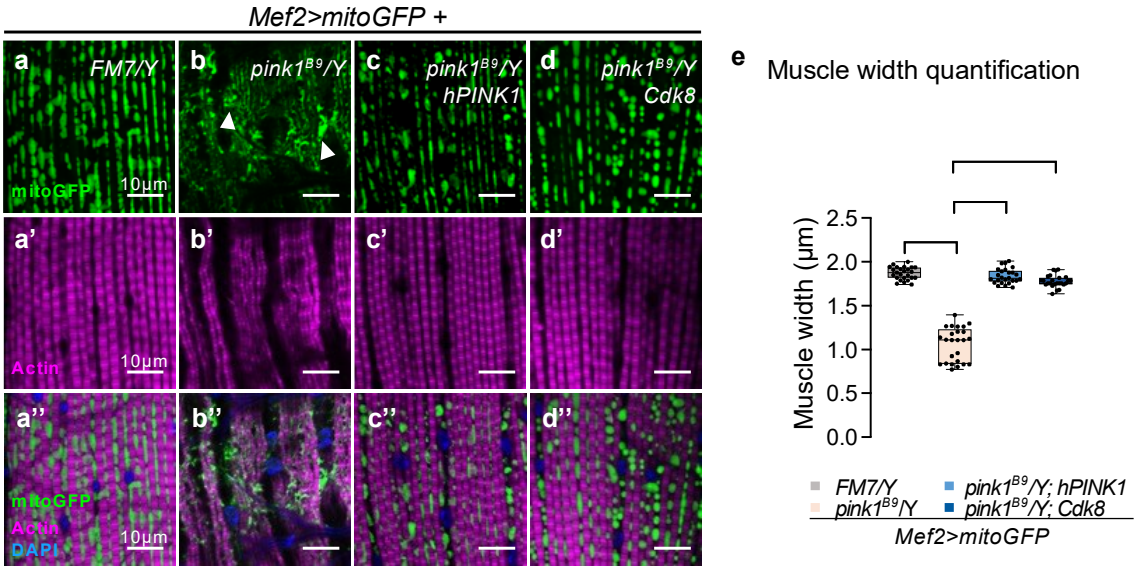

Figure 3.3 Cdk8 can rescue *pink1^{B9}* mitochondrial and muscle defects

(a–d) Mitochondrial morphology in indirect flight muscle (IFM) in (a) FM7/Y, (b) pink1B9/Y, and either (c) hPINK1, or (d) Cdk8 expressed in the pink1B9 mutant background with Mef2>mitoGFP. (a′–d′) Rhodamine-phalloidin staining (magenta) stains actin filaments to visualize the muscle morphology. (a″–d″) Merged images, including DAPI staining for DNA (blue). Scale bars: 10 μm. (e) Quantification of adult indirect flight muscle width in 3-day-old flies (n = 5 per genotype). Data were presented as box plots (center line at the median, upper bound at 75th percentile, lower bound at 25th percentile) with whiskers at minimum and maximum values. An unpaired two-tailed t-test is used to generate the statistics. *p < 0.05, ** p<0.01, *** p<0.001, **** p<0.0001, ns: no significance.

3.3.4. Cdk8 suppresses ROS production in *pink1^{B9}* mutants without activating transcription of antioxidant genes

Loss of Pink1 causes accumulation of dysfunctional mitochondria, leading to generation of ROS[166]. Dihydroethidium (DHE) staining was used to analyze the ROS in adult indirect flight muscles in the *pink1^{B9}* background. The FM7/Y control shows redox homeostasis under physiological conditions (Fig. 3.4a-a'''). Disrupted mitochondrial morphology in *pink1^{B9}* flies causes enhanced DHE intensity, indicative of elevated ROS production (Fig. 3.4b-b'), and elevated DHE staining is found near aggregated mitochondria (Fig. 3.4b''-b''' yellow arrowhead). hPINK1 significantly restored the mitochondrial integrity as less mitochondrial aggregation was seen and DHE stain showed no ROS elevation (Fig. 3.4c-c'). ROS production in Cdk8-expressing *pink1^{B9}* flies was reduced and mitochondrial integrity was restored (Fig. 3.3d-d'). Quantification of DHE mean intensity demonstrated that hPINK1 and Cdk8 can significantly suppress the elevated ROS production caused by *pink1^{B9}* mutants (Fig. 3.3e). To validate the finding using an alternative approach, we used a spectrophotometer to measure emitted DHE fluorescence from adult thoraxes (Fig. 3.3f). We confirmed that elevated ROS found in *pink1^{B9}* flies is significantly suppressed by expression of either hPINK1 or Cdk8. Enhanced ROS production was also found in patient derived cells with a *hPINK1* mutation[265], which is consistent with our findings.

Since Cdk8 is a part of the Mediator complex and plays a significant role in regulating transcription, we next asked if Cdk8 elevates transcription of genes encoding antioxidant enzymes. We chose several genes that encode scavengers that maintain the redox homeostasis in mitochondria, namely *catalase*, glutathione transferase D1 (*dGstD)*[266,267] and superoxide dismutase 1 (*sod1)*[268,269] and which are elevated in *pink1^{B9}* flies (Fig. 3.3g); likely in response to the accumulation of damaged mitochondria. This transcriptional upregulation was suppressed by expression of either *hPINK1* or *Cdk8* in *pink1^{B9}* flies, consistent with reduced ROS production in those genotypes.

In summary, these findings indicate that ectopic expression of Cdk8 can restore the defective mitochondrial morphology caused by *pink1* mutant and in turn to restore the redox homeostasis.

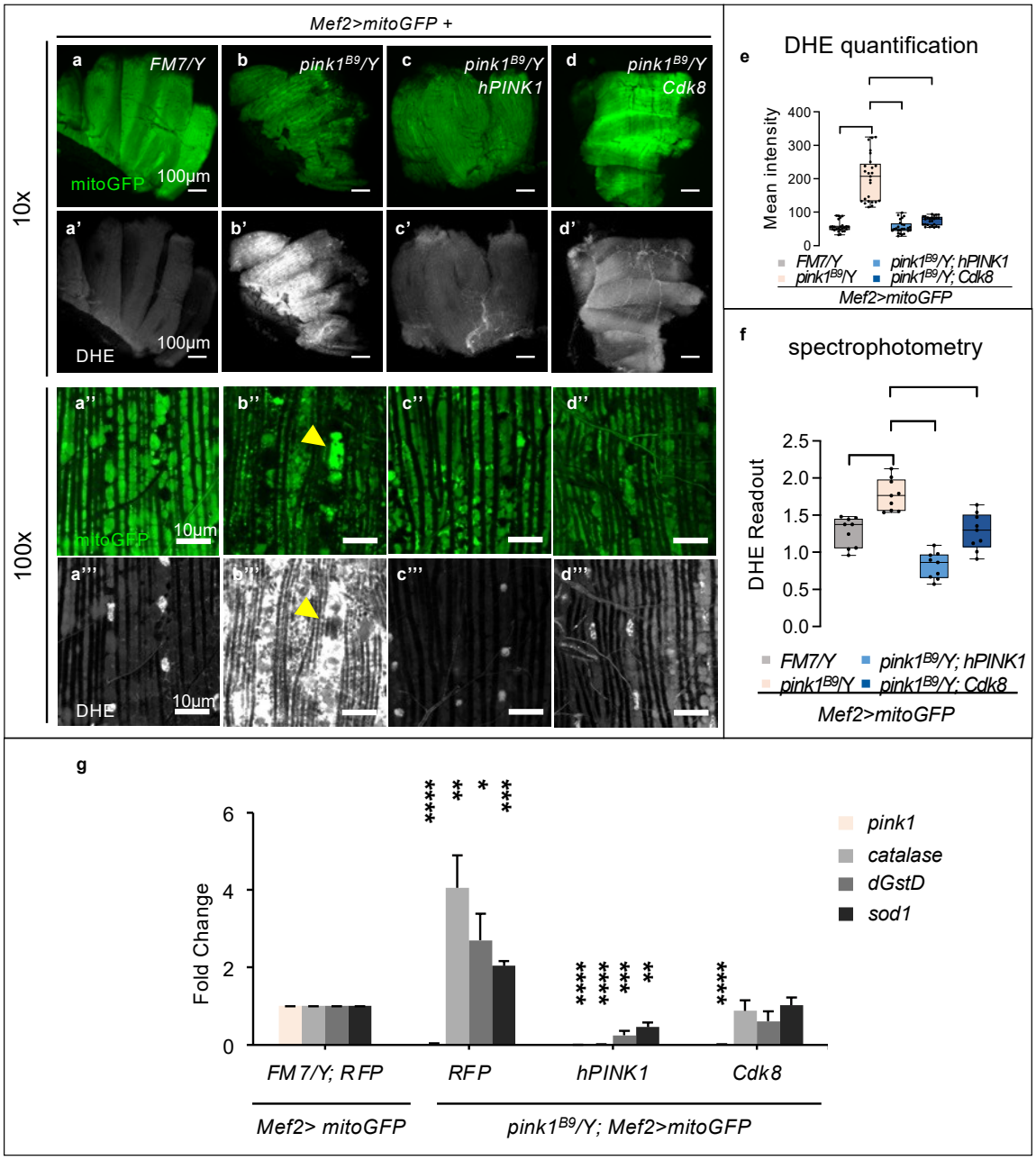

Figure 3.4. Cdk8 suppresses ROS production in *pink1*^{B9} mutants without activating transcription of antioxidant genes

(a–d) Indirect flight muscle in (a) FM7/Y, (b) pink1B9, and (c) hPink1 or (d) Cdk8 expressed in the *pink1*^{B9} mutant background with *Mef2>mitoGFP* raised at 29°C. (a′–d′) DHE staining of corresponding genotypes in (a–d). Scale bars: 100 μm. (a′'-d′') Representative magnified sections of mitochondrial morphology from (a–d). (a′''-d′'') Representative magnified sections of DHE staining from (a–d). Scale bar: 10 μm. (e) Quantification of mean DHE fluorescence intensity in live adult IFM of the indicated genotypes (n = 8 per genotype). Data were presented as box plots (center line at the median, upper bound at 75th percentile, lower bound at 25th percentile) with whiskers at minimum and maximum values. (f) Quantification of the DHE fluorescent intensity using spectrophotometry. Data are presented as box plots (centre line at the median, upper bound at 75th percentile, lower bound at 25th percentile) with whiskers at minimum and maximum values. (g) qPCR analysis of *pink1*, *catalase, dGstD, sod1* gene expression between RFP, hPink1 or Cdk8 expressed in the *pink1*^{B9} mutant background with Mef2>mitoGFP relative to control FM7/Y. Data are mean ± SD. *n* = 3 independent experiments. An unpaired two-tailed t-test is used to generate the statistics. *p < 0.05, ** p<0.01, *** p<0.001, **** p<0.0001, ns: no significance.

To test how well the expression of Cdk8 can exert its rescuing ability in the *pink1* mutant background in a long term, we performed the same phenotypic analyses on aged flies that were three weeks old. First, we analyzed the thorax indentation (Fig. 3.5a) and climbing ability (Fig. 3.5b). We found ectopic expression of Ckd8 in the *pink1* mutant background can still significantly rescue thorax indentation as well as the climbing defects, but with less effectiveness. Only 40% of progeny that expressed Cdk8 in the *pink1* mutant background have normal thorax structures, and about 50% of the progeny can reach the target line in our climbing assays. However, ectopic expression of hPINK1 in aged flies can completed rescue the muscle degeneration as before with almost intact climbing ability.

Next, we examined the mitochondrial and muscle morphology of those aged flies (Fig. 3.5c-g). Consistent with what we found in flies that were three days old, FM7/Y control flies have well-organized mitochondria that are intercalated between myofibrils (Fig. 3.5 c'-c'''). The mitochondrial morphology is mostly diminished with some aggregates of dysfunctional mitochondria in $pink1^{B9}$ mutant flies (Fig. 3.5d'). The muscle fibers are loosely packed in comparison to control with narrower myofibril width (Fig. 3.5d''), which is consistent with the data in three days old flies. These findings indicate that in *pink1* mutant flies, severe phenotypes in both mitochondrial and muscle morphologies arise as the flies age. The structure of mitochondria and muscle in hPINK1-expressing aged *pink1* mutant flies mimicked the phenotypes that we observed in control (Fig. 3.5e'-e'''), suggesting that expression of hPINK1 can completely restore severely damaged mitochondria and degenerated muscles in the *pink1* mutant background over time. Lastly, when we examined the morphologies in Cdk8-expressing three-week aged flies we found two distinct phenotypic groups. One group resembled the *pink1* mutant flies (Fig. 3.5f'-f''') with loosely packed muscle fibers along with reduced mitochondria, and with narrowed myofibril width. These findings suggest that the accumulated damage due to the loss of Pink1 could exceed the rescuing ability of Cdk8. On the other hand, we observed well-organized mitochondria intercalated with healthy muscle fibers in IFM in some aged flies expressing Cdk8 in the *pink1* mutant background (Fig. 3.5g'-g'''). This suggests that the rescuing ability of Cdk8 in the mutant background is not completely abolished. We next quantified the myofibril width using rhodamine-phalloidin to detect actin fibers across these four genotypes, and found a difference in Cdk8 expressing aged flies, as we observed two groups of myofibril width, one with a similar width as the *pink1* mutant flies while the other is similar in width to

both the control or hPINK1 expressing flies (Fig. 3.5e) like we had seen when we examined mitochondrial morphology.

These findings indicate that expression of Cdk8 can partially restore the defective phenotypes caused by the *pink1* mutant background, but that the ability of Cdk8 to rescue mutant phenotypes gradually declined with age, likely due to age-related accumulation of defects in $pink1^{B9}$ flies. In summary, Cdk8 expression can significantly rescue the thorax indentation and climbing defects in $pink1^{B9}$ mutants.

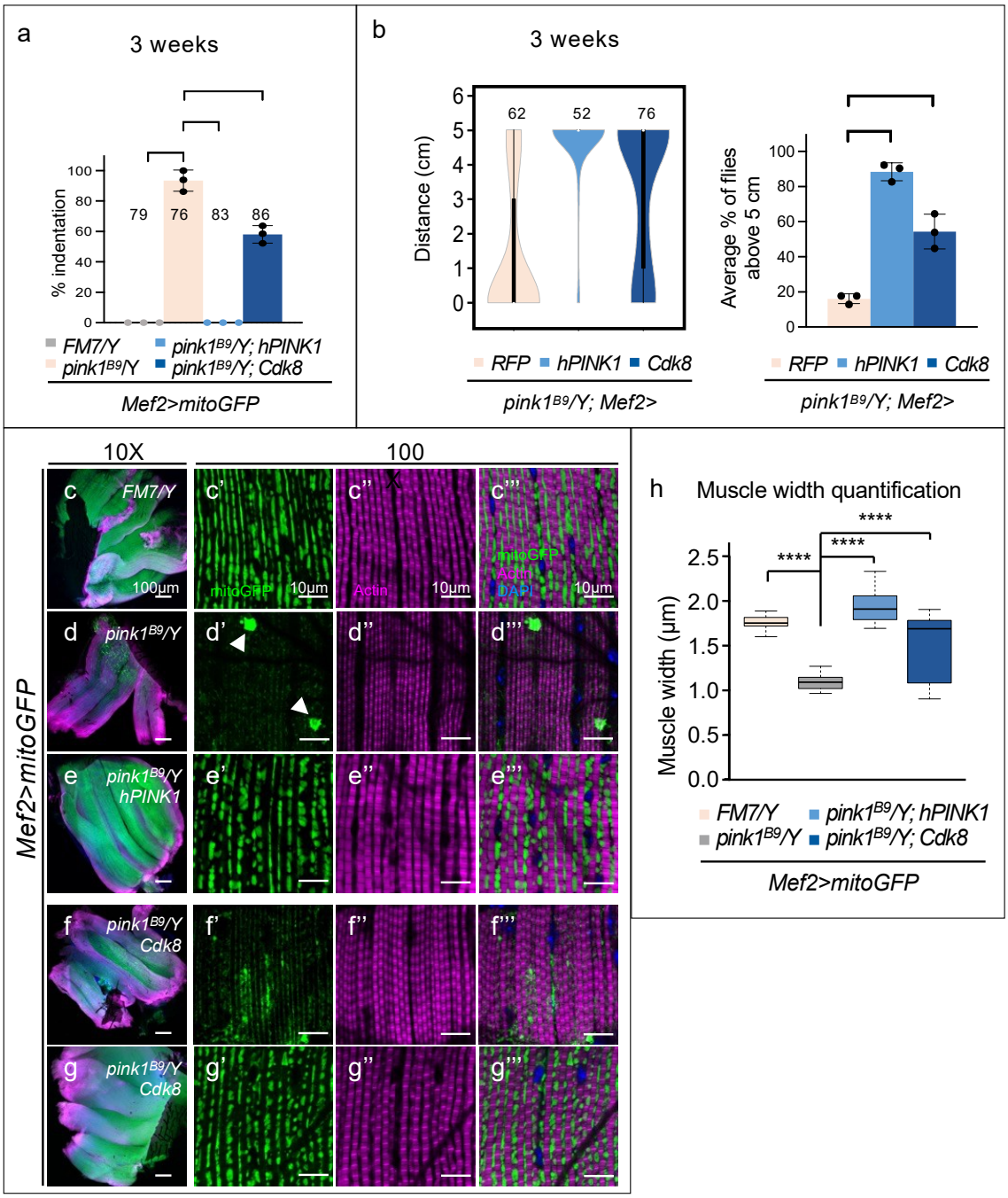

Figure 3.5. **Ectopic Cdk8 expression can rescue defects found in aged *pink1^{B9}* mutants, and rescuing ability gradually declines.**

(a) Quantification of the thorax indentation in three weeks old flies expressing either RFP, hPink1 or Cdk8 in a d*pink1*^{B9} mutant background. Total number of progeny are assessed, n = 79, 76, 83, 86 respectively in order. Results are mean ± SD. Unpaired two tailed t-test is used to generate the statistics. (b) Violin plots showing distribution of climbing activity of three weeks old flies expressing RFP, hPink1 or Cdk8 in a *pink1*^{B9} mutant background. (b') Average percent of flies that reached the target line. Results are mean ± SD. Unpaired two tailed t-test is used to generate the statistics. (c-g) IFM in (c) *FM7/Y*, (d) *pink1*^{B9}/Y, and (e) *hPink1* or (f, g) *Cdk8* both expressed in the aged *pink1*^{B9} mutant background with *Mef2>mitoGFP.* Scale bar: 100µm. (c'-g') Section of magnified images of mitochondrial morphology of genotypes indicated in (c-g). (c''-g'') Section of magnified images of muscle morphology of genotypes indicated in (c-g). (c'''-g''') Section of magnified images of merged morphologies including DAPI (for nucleus) of genotypes indicated in (c-g). Scale bar: 10 µm. n = 10/genotype with three biological replicates. All raised at 29°C. (h) Quantification of adult indirect flight muscle width in 3-weeks-old males (n = 5 per genotype). Data were presented as box plots (center line at the median, upper bound at 75th percentile, lower bound at 25th percentile) with whiskers at minimum and maximum values. An unpaired two-tailed t-test is used to generate the statistics. *p < 0.05, ** p<0.01, *** p<0.001, **** p<0.0001, ns: no significance.

Previously, we found the expression of Cdk8 in the *pink1* mutant background can suppress elevated ROS found in three days old flies. Since we observed divergent results in mitochondrial and muscle morphologies in Cdk8 expressing flies, we next examined the levels of ROS that are associated with these distinct phenotypes in adult indirect flight muscle (Fig. 3.6a-e).

We performed DHE staining to detect the ROS levels across four genotypes. The FM7/Y control shows redox homeostasis of three weeks old flies under physiological conditions (Fig. 3.6a-a'''). Aggregates of mitochondria appear as speckles observed in $pink1^{B9}$ flies along with enhanced DHE intensity (Fig. 3.6b-b'). Accumulation of impaired mitochondria is seen throughout the IFM with elevated DHE staining that is found near the aggregated mitochondria (Fig. 3.6b''-b''' yellow arrowhead). Expression of hPINK1 suppresses the elevated ROS level in the mutant background to a similar extent as what we observed in control (Fig. 3.6c-c'''). Consistent with our findings in aged flies when we examined their mitochondrial and muscle morphologies (Fig. 3.5), we found two distinct phenotypic classes associated with aged flies expressing Cdk8 in the $pink1^{B9}$ background (Fig 3.6d, e). DHE staining from the Cdk8 expressing flies showed similar mitochondria aggregates in speckles with increased ROS production as we observed in mutant flies (Fig. 3.6d-d'''). On the contrary, others that express Cdk8 have organized bundle of muscle fibers (Fig. 3.6e-e') along with well-defined mitochondria in normal patterns (Fig. 3.6e''). The DHE staining showing a baseline level of ROS indicates that the redox homeostasis is well-maintained like we saw in the control (Fig. 3.6e'''). We quantified the mean intensity of DHE staining (Fig. 3.6f) and performed the alternative approach using spectrophotometry (Fig. 3.6e), and we found that expression of either hPINK1 or Cdk8 can still significantly suppress the ROS level in the *pink1* mutant background.

In summary, we found ectopic expression of Cdk8 can rescue the ROS level in *pink1* mutant background in three weeks old flies, but to a lesser extent. It is likely due to damage due to the *pink1* mutation along with effects of aging, which exacerbates the defective phenotypes; thus, the effectiveness of ectopic Cdk8 gradually decreases over time.

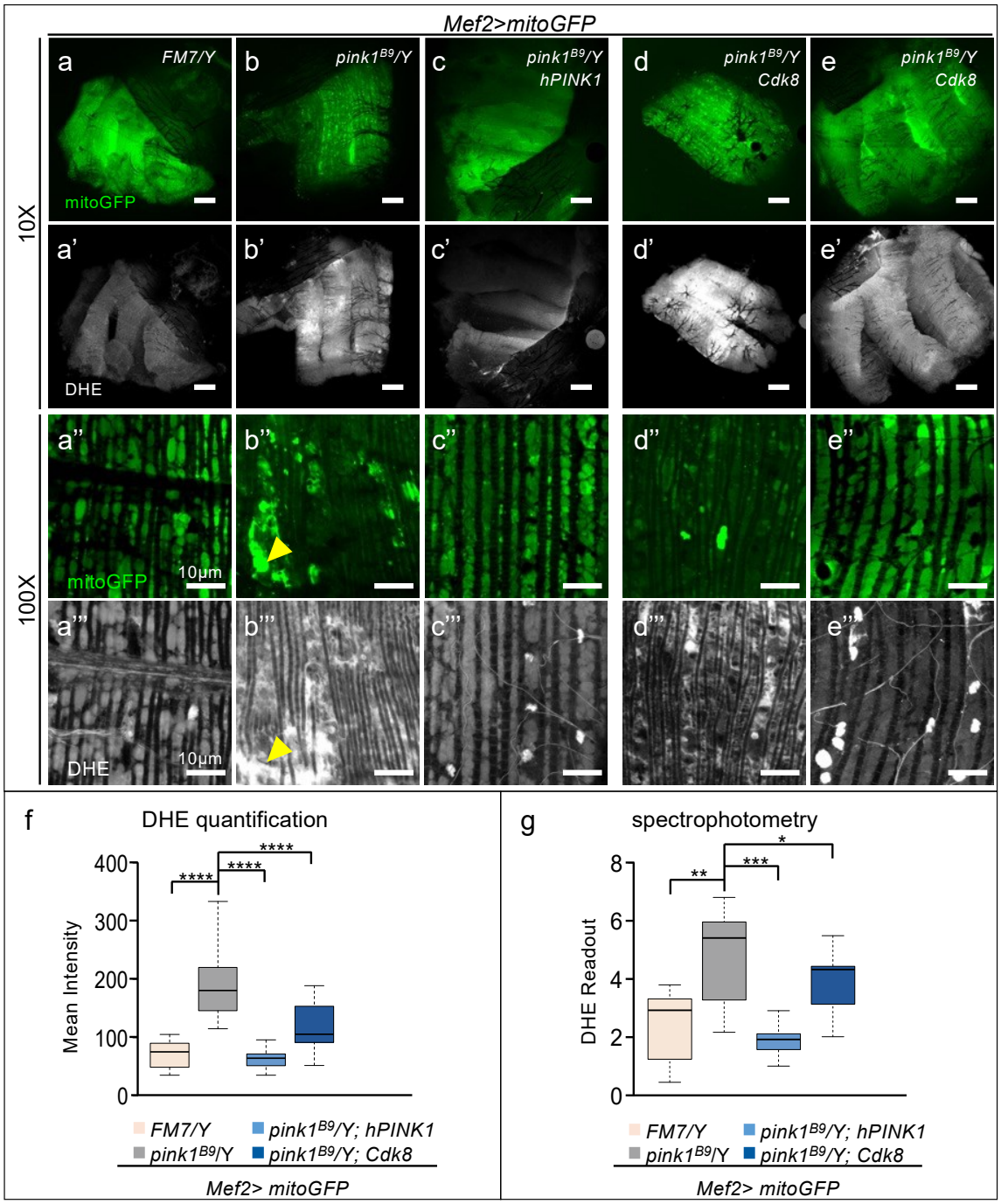

Figure 3.6. Cdk8 suppresses ROS production in aged *pink1^{B9}* mutants with rescuing ability gradually declined

(a–d) Indirect flight muscle in (a) FM7/Y, (b) *pink1*^{B9}, and (c) hPink1 or (d, e) Cdk8 expressed in the aged *pink1*^{B9} mutant background with *Mef2>mitoGFP*. (a′–d′) DHE staining of corresponding genotypes in (a–e). Scale bars: 100 μm. (a′'-e′') Representative magnified sections of mitochondrial morphology from (a–e). (a′''-e′'') Representative magnified sections of DHE staining from (a–e). Scale bar: 10 μm. (f) Quantification of mean DHE fluorescence intensity in live adult IFM of the indicated genotypes (n = 10 per genotype). Data were presented as box plots (center line at the median, upper bound at 75th percentile, lower bound at 25th percentile) with whiskers at minimum and maximum values. (f) Quantification of the DHE fluorescent intensity using spectrophotometry. Data are presented as box plots (centre line at the median, upper bound at 75th percentile, lower bound at 25th percentile) with whiskers at minimum and maximum values. Data are mean ± SD. *n* = 3 independent experiments. An unpaired two-tailed t-test is used to generate the statistics. *p < 0.05, ** p<0.01, *** p<0.001, **** p<0.0001, ns: no significance.

3.3.5. Cdk8 rescues *pink1*-induced decreases in phospho-Drp1

In chapter 2, we showed that modulating the expression of Cdk8 affects the phospho S616-level of endogenous Drp1 (Fig. 2.10b, c). This finding could explain how Cdk8 can promote mitochondrial fission in adult indirect flight muscle. Since Pink1 was shown to regulate Drp1 directly on the same residue, S616, independent of PINK1/Parkin mediated mitophagy[215,216], we next asked whether, in the absence of functional Pink1, elevated expression of Cdk8 could restore Drp1 phosphorylation. Using fly lysates from control, *pink1* mutants and *pink1* flies expressing wildtype Cdk8, we found that the overall levels of endogenous total Drp1 protein were similar in all three samples (Fig. 3.7). In contrast, *pink1* mutants showed significant decreases in pDrp1 S616 levels, relative to control, and these decreased levels were significantly rescued by expression of Cdk8 (Fig. 3.7). These data suggest the rescuing ability that we observed in *pink1* expressing wildtype Cdk8 flies is likely by partially restoring the phospho-level of Drp1 at S616, which in turn to restore the homeostasis of mitochondria.

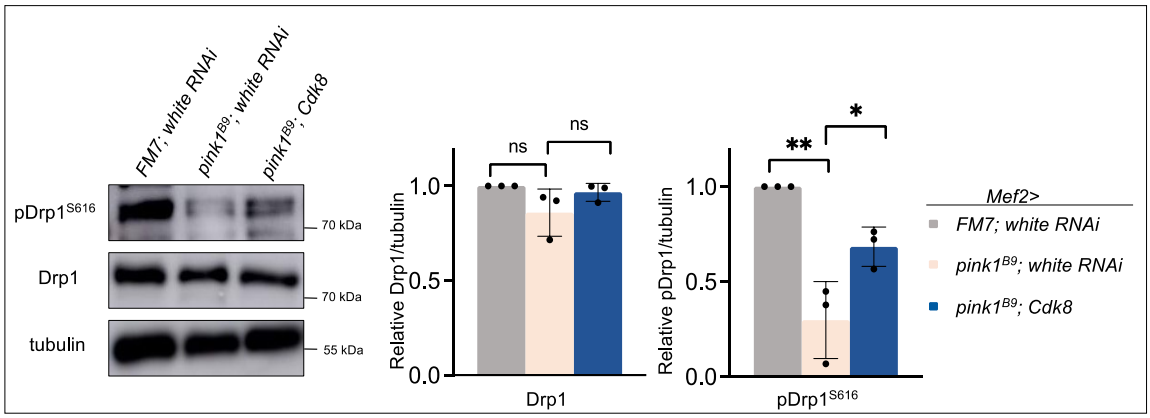

Figure 3.7. Expression of Cdk8 partially restore the endogenous pDrp1 level in the *pink1^{B9}* mutant background

(a) Western blots showing the level of total Drp1 or S616 phospho-Drp1 in control (*Mef2>white RNAi*), *pink1* mutant flies (*pink1^{B9}*; *Mef2>white RNAi)* and *pink1* expressing Cdk8 (*pink1^{B9}*; *Mef2>Cdk8$^{3xHA)}$*. (b) Quantifications of blots normalized to actin levels. (n=3 per genotype). Results are mean ± SD. Unpaired two tailed t-test is used to generate the statistics. P value is 0.0039 for FM7, and 0.0424 for Cdk8 in comparison to *pink1^{B9}* mutant for detecting level of pDrp1^{S616}. ∗ p<0.05, ∗∗ p<0.01, ∗∗∗∗ p<0.0001, ns: no significance.

3.3.6. CDK19 has context dependent subcellular localizations

We investigated the role of Cdk8 in the *pink1* mutant background and wondered whether the mammalian ortholog, CDK19, behaves similarly in the same context. Our collaborators have previously shown that human $CDK19^{WT}$ was primarily localized to cytoplasm in neurons under physiological conditions[102]. The finding suggests that CDK19 may play cytoplasmic roles.

To test the potential cytoplasmic function of CDK19, our collaboration relied on the predict classic nuclear localization sequence (NLS) predicted by software called cNLS Mapper (Fig. 3.8). NLS is a short peptide sequence that dictates the translocation of a protein from cytoplasm to nucleus. The sequence is enriched with basic amino acids including arginine (R), lysine (K), histidine (H) and asparagine (N). There are two classic NLS categories, monopartite and bipartite[270,271]. A monopartite NLS is a single cluster of short peptide sequence composed of 4 and more basic amino acids[271,272]; whereas, the bipartite category of NLS is two clusters of enriched basic amino acids separated by a linker region of 9 to 12 amino acids[270,271]. Our collaborators found a predicted monopartite NLS in both human CDK19 and in fly Cdk8 using the online software cNLS Mapper (Fig. 3.8). To assess the importance of the predicted nuclear localization sequence, our collaborators generated *UAS-CDK19ΔNLS* transgenic flies in which that predicted sequence was deleted, along with a 3XHA tag to allow detection in fly tissues, denoted as $CDK19^{\Delta NLS}$.

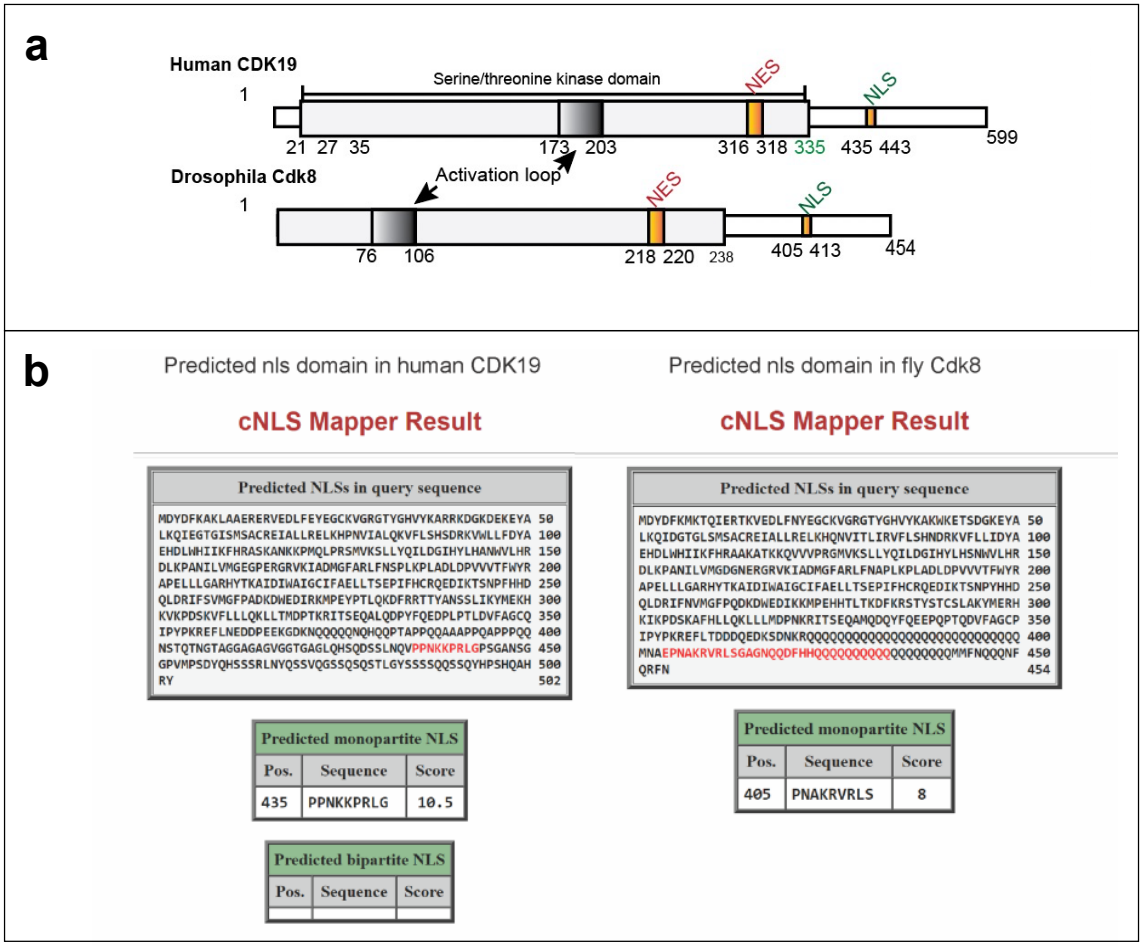

Figure 3.8. Sequence alignment between fly Cdk8 and human CDK19 with predicted location for nuclear localization sequence.

(a) Schematic image showing the key domains of human CDK19 and fly Cdk8, including NES and NLS. (b) NLS domain prediction of human CDK19 (435-443) and fly Cdk8 (405-413) using cNLS Mapper (mhttps://nls-mapper.iab.keio.ac.jp/cgi-bin/NLS_Mapper_form.cgi). This program is based on Kosugi et al., (2009) PNAS 106, 10171-10176.

We sought to further characterize the localization of CDK19^{WT} and CDK19$^{\Delta NLS}$ in several Drosophila tissues, before examining their role in the *pink1* mediated Parkinsonism model. Using an antibody to detect human CDK19 we confirmed the cytoplasmic localization of CDK19^{WT} in the adult central nervous system (Fig. 3.9a). We observed nuclear localization in larval wing imaginal discs and salivary glands when CDK19^{WT} was expressed using a ubiquitous driver, *Da-Gal4* (Fig. 3.9b). Expression of the CDK19$^{\Delta NLS}$ construct in wing discs and salivary glands using the same ubiquitous driver showed that deletion of the NLS lead to a cytoplasmic localization (Fig. 3.9b). Expression of CDK19^{WT} in indirect flight muscles showed it has both nuclear and cytoplasmic localization, as the staining to detect the HA-tagged CDK19^{WT} proteins is present in the nucleus as well as outside the nucleus in the same plane (Fig. 3.9c). In indirect flight muscles, CDK19$^{\Delta NLS}$ showed only cytoplasmic localization. Co-staining with DAPI to detect nuclear DNA and immunofluorescent detection of lamins in the nuclear membrane, highlights the exclusion of CDK19$^{\Delta NLS}$ from the nucleus (Fig. 3.9c). These findings validate that the predicted NLS sequences can target CDK19 to the nucleus, and further suggests that CDK19 has dynamic subcellular localizations depending on in which tissue type it is expressed.

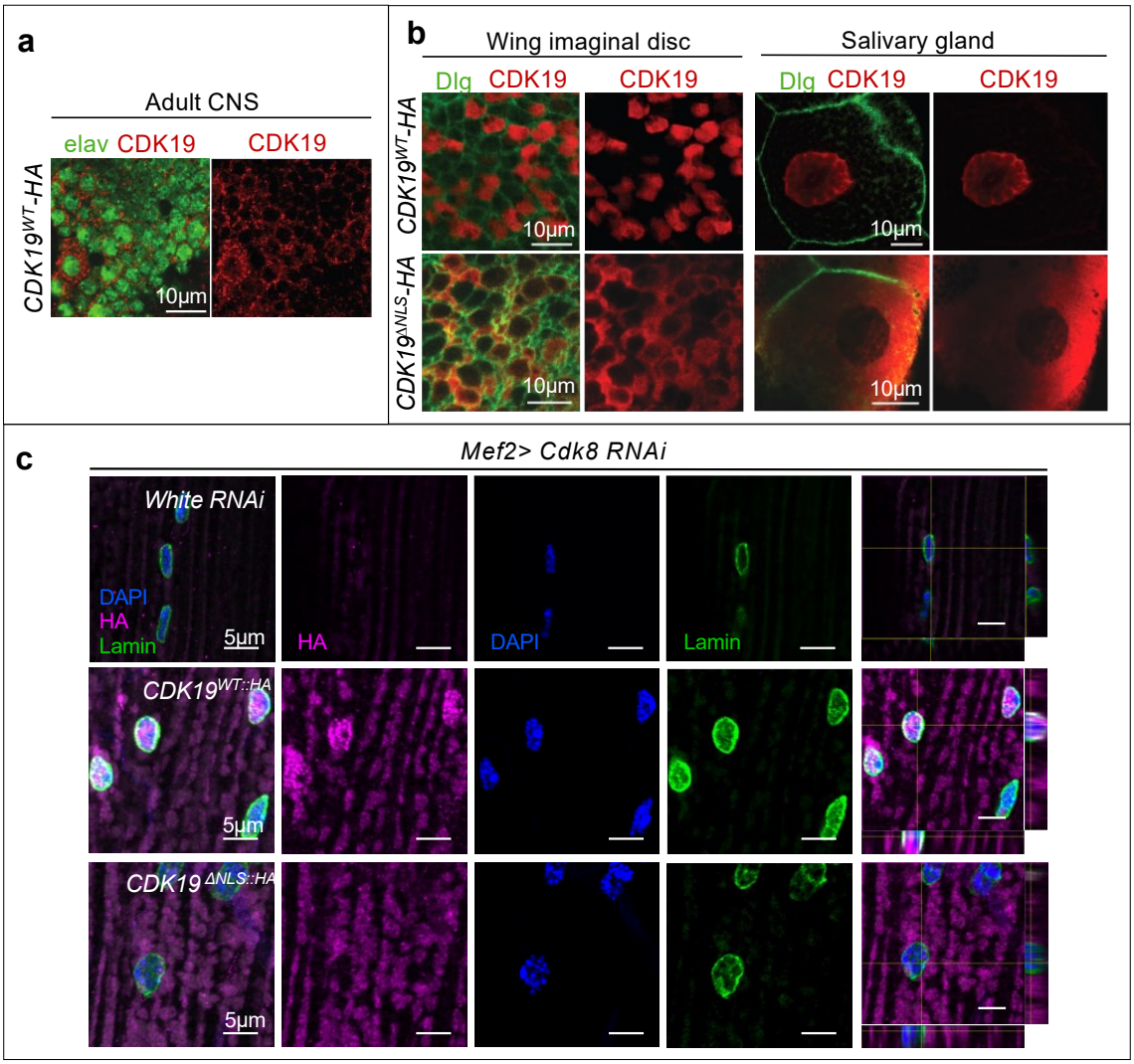

Figure 3.9. CDK19 has context dependent subcellular localizations

(a) Subcellular localization of *UAS-CDK19$^{WT\text{-}3xHA}$* in adult CNS. (b) Subcellular localization of *UAS-CDK19$^{WT\text{-}3xHA}$*and *UAS-CDK19$^{\Delta NLS\text{-}3xHA}$* in wing imaginal discs and salivary glands. Green indicates Dlg staining, which marks the cell membrane, and red indicates HA-tagged proteins. The stainings were independently repeated three times. (c) Subcellular localization of *UAS-CDK19$^{WT\text{-}3xHA}$*and *UAS-CDK19$^{\Delta NLS\text{-}3xHA}$* in adult indirect flight muscles. Anti-HA is used to visualize CDK19 localization. DAPI was used to detect nuclear DNA and anti-lamin antibody highlights the nuclear membrane. Cross sections of confocal Z-stacks are shown in the right most column.

3.3.7. Cdk8 has context dependent subcellular localizations

The findings that CDK19 has tissue specific localization led us to want to gain more insight into endogenous fly Cdk8 localization; thus, we examined the larval muscle and adult brains of *Cdk8::GFP* flies. Through this GFP insertion, detection of GFP in cells reflects the endogenous Cdk8 protein expression and localization. In these experiments, we detected the GFP fluorescence without the use of anti-GFP antibodies, to eliminate any chance of non-specific staining. We tested numerous anti-GFP antibodies and found a high level of non-specific signal, so we avoided using it for tissue staining. The *Cdk8::GFP* flies are healthy and fertile, demonstrating that the addition of the GFP protein does not disrupt endogenous functions of Cdk8. In larval body wall muscles Cdk8::GFP is primarily nuclear, though low level cytoplasmic staining was seen throughout the tissue when compared to control (Fig. 3.10a). In adult brains Cdk8 shows a dynamic distribution (Fig. 3.10b) characterized by nuclear and cytoplasmic staining (Fig. 3.10c). Some cells show primarily nuclear while others show primarily cytoplasmic localization (Fig. 3.10d), highlighting the diverse Cdk8 protein localizations and demonstrating *in vivo* that endogenous Cdk8 is present in the cytoplasm. We used fractionation of adult brain protein lysates to further validate the cytoplasmic localization of Cdk8::GFP (Fig. 3.10e). These findings indicate that endogenously GFP-tagged Cdk8 has dynamic tissue specific subcellular localizations.

The expression of Cdk8::GFP in larval body wall muscles is relative low in comparison to adult brain. The GFP signal cannot be detected when we performed subcellular fractionation using larval body wall muscles. To circumvent this issue, we could only rely on the HA tags encoded in the Cdk8 transgene to track the localization in subcellular fractions from fly extracts. This work extends the localization studies we carried out with tagged transgenes in S2-R+ cells. *Mhc>Cdk8*^{3xHA} flies were crossed to either UAS-*white* RNAi or UAS-Cdk8^{3xHA} to produce flies expressing one or two copies of exogenous Cdk8. Nuclear and cytoplasmic fractions were isolated from whole cell lysates and the presence of exogenous Cdk8 was detected with anti-HA antibodies (Fig. 3.10f). Antibodies to ATP5a were used to highlight the cytoplasmic fraction, while Histone 3 marked nuclear fractions. Exogenous Cdk8 was found in both nuclear and cytoplasmic fractions, and the relative distribution was unchanged when Cdk8 was elevated.

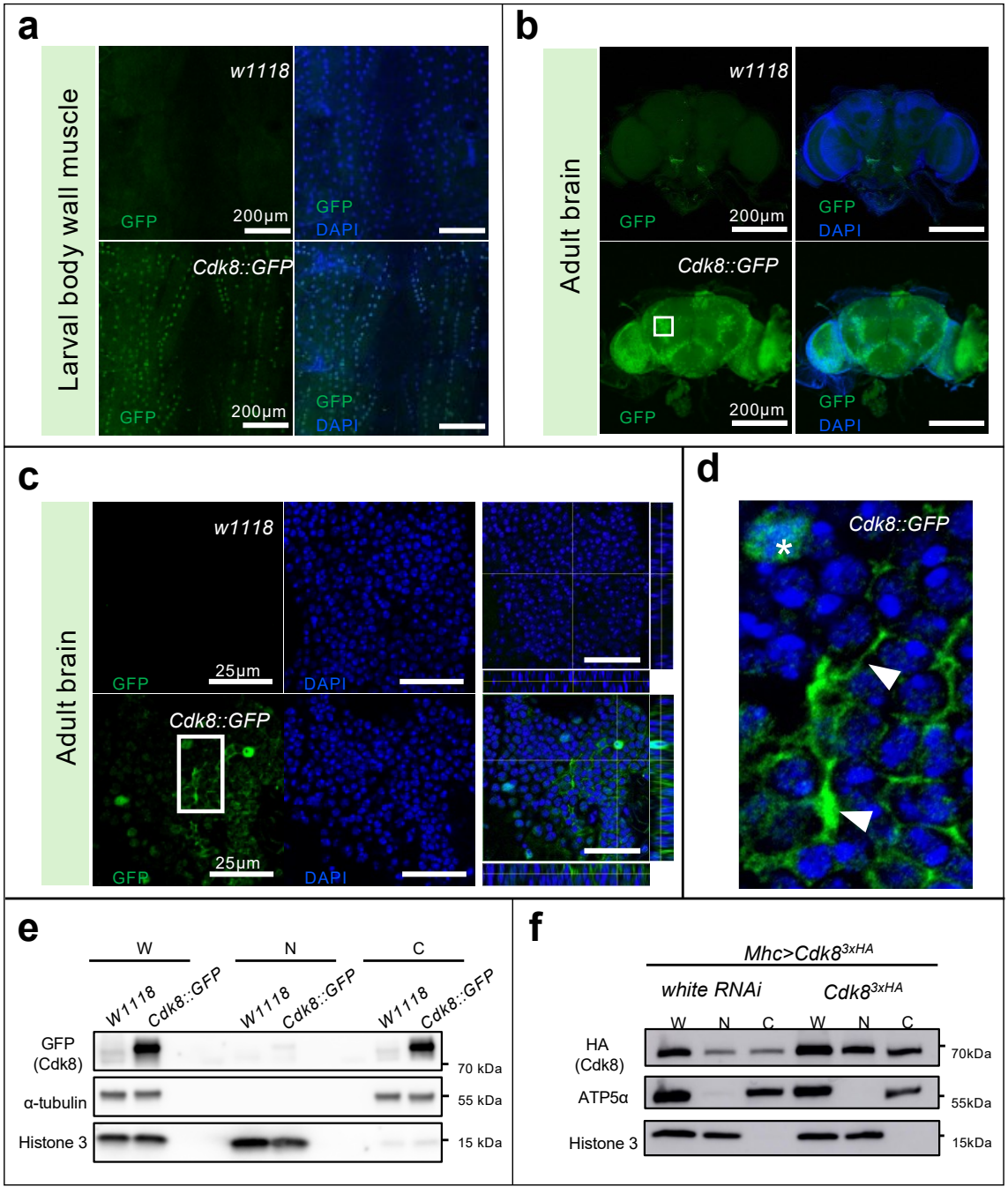

Figure 3.10. Endogenous GFP-tagged Cdk8 has dynamic subcellular localizations and ectopic expression of Cdk8 is primarily localized in cytoplasm in muscle

(a) subcellular localization of *Cdk8::GFP* in larval body wall muscles in comparison to w^{1118}, as well as in adult brain (b). Positive signals rely on the endogenously expressed GFP. n = 10 per genotype. (c) Single plane, zoom-in images with orthogonal views of adult brains comparing w^{1118} and *Cdk8::GFP*. n = 10 per genotype. Selected region is shown in (d) to further demonstrate the cytoplasmic localization of endogenous Cdk8. (e) Fractionation from adult brains from *w1118* or *Cdk8::GFP* flies. Whole cell lysate (W), nuclear (N) and cytoplasmic (C) fractions were prepared, and antibodies to a-tubulin and Histone 3 were used to detect the cytoplasmic and nuclear fractions, respectively. (f) Myosin heavy chain (Mhc)-Gal4 was used to express Cdk83xHA in muscles with either control white RNAi or an additional copy of Cdk83xHA. Whole cell lysate (W), nuclear (N) and cytoplasmic (C) fractions were prepared, and antibodies to ATP5a and Histone 3 were used to detect the cytoplasmic and nuclear fractions, respectively. Experiments were repeated three times.

3.3.8. CDK19 shares conserved functions with fly Cdk8

The data presented so far in muscles and neurons argue that both Cdk8 and CDK19 have functions in the cytoplasm. To test if human CDK19 function the same as fly Cdk8, we expressed *Cdk8 RNAi* in neurons (*elav>Cdk8 RNAi*) and examined the effects of expressing either the reference $CDK19^{WT}$ or $CDK19^{\Delta NLS}$. The expression of $CDK19^{\Delta NLS}$ let us further examine the potential cytoplasmic function of CDK19 that was previously suggested by localization in the nervous system[102]. As shown in Fig. 3.11a, expression of $CDK19^{\Delta NLS}$ is sufficient to rescue the lifespan defects observed in flies expressing *Cdk8 RNAi* in neurons (*elav>Cdk8 RNAi)* similar to what is found with $CDK19^{WT}$ expression (Fig. 3.11a).

Flies with neuronal depletion of Cdk8 failed to thrive as they survive only two weeks at most (Fig. 3.11a). We hypothesized that there may be an increase cell death associated with accumulated ROS production, as we previously showed in Chapter 2 that depletion of *Cdk8* led to elevated ROS production. Thus, we assessed cell death induced by *elav>Cdk8 RNAi* in the brains of ten-day old flies kept at 25ºC by staining with acridine orange (AO) and quantifying fluorescence intensity. We observed increased cell death when Cdk8 was depleted in the adult brain (Fig. 3.11b). However, elevated levels of AO can be significantly reduced by expression of either $CDK19^{WT}$ or $CDK19^{\Delta NLS}$ (Fig. 3.11b). We next examined the level of ROS within the adult brain. Previously we showed that depletion of Cdk8 in fly indirect flight muscles led to significantly elevated ROS production (Fig. 2.8). Consistently, we found fly adult brains expressing *elav>cdk8 RNAi* show a 40% higher level of ROS when compared to control animals (*elav>Luciferase RNAi*) (Fig. 3.11c). Flies expressing human CDK19 in a *Cdk8*-depleted background decrease the level of ROS by 20% (Fig. 3.11c, d), showing that CDK19 can partially rescue the elevated ROS due to depletion of *Cdk8*.

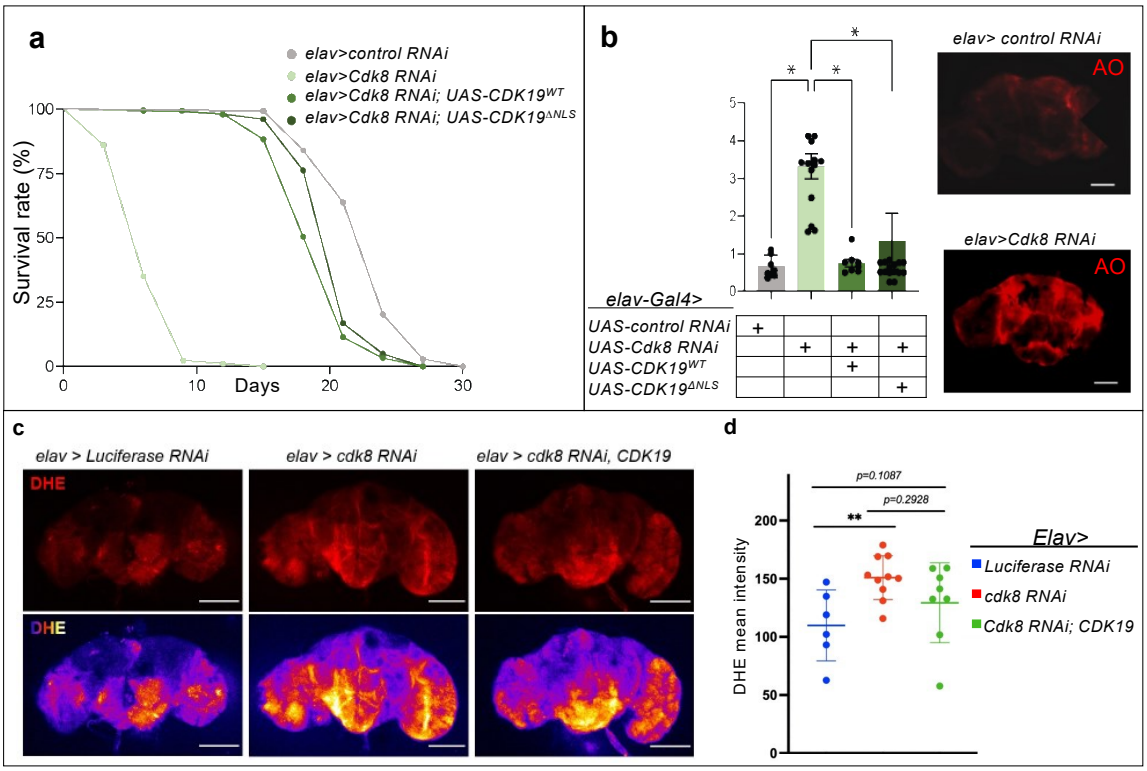

Figure 3.11. CDK19 restores survival rate, cell death and ROS production in Cdk8 depleted flies.

(a) CDK19 ΔNLS can suppress the life-span decrease caused by an expression of Cdk8 RNAi in the neuron to a similar extent to CDK19WT expression (n>100 per genotype). (b) Quantification of acridine orange staining (AO) which assesses neuronal death. when Cdk8 is decreased in adult brain neurons. Red indicates the dying neurons. (n=7, n=14, n=8 and n=16 respectively in order). Scale bar: 10 μm. Statistical analyses are one-way ANOVA followed by a Tukey posthoc test. Results are mean ± SEM (∗ p<0.05, ∗∗ p<0.01, ∗∗∗∗ p<0.0001, ns: no significance). (c) DHE staining in adult brains of the indicated genotypes. (d) Quantification of DHE mean intensity in brains shown in (i)∗ p<0.05, ∗∗ p<0.01, ∗∗∗∗ p<0.0001, ns: no significance.

Previously, we found neuronal depletion of Cdk8 using *Appl-Gal4* leads to impaired climbing ability (Fig. 2.2). To compare our results to those of our collaborators, we repeated the climbing assay using *Elav-Gal4* and found consistent results (Fig. 3.12a). Furthermore, we found defective climbing in Cdk8 depleted flies can be rescued by expression of either $CDK19^{WT}$ or $CDK19^{\Delta NLS}$ (Fig. 3.12a). These findings argue strongly that the function of Cdk8 in these assays is cytoplasmic since expression of a cytoplasmically targeted CDK19 can rescue phenotypes due to loss of Cdk8.

We next examined the effects of wildtype and cytoplasmic CDK19 in muscles. To visualize mitochondrial morphology, we used either mitoGFP or an antibody against ATP5α (Fig. 3.12b'-e'). Muscle fibers were visualized using rhodamine-phalloidin to detect filamentous actin (Fig. 3.12b-e). As shown before, *Cdk8* knockdown leads to a widening of myofibril compared to control (Fig. 3.12b-e, f). Expression of either $CDK19^{WT}$ or $CDK19^{\Delta NLS}$ restored myofibril morphology equally well (Fig. 3.12d-e). We next examined mitochondrial morphology. A mixture of elongated and fragmented mitochondria was found in control (Fig. 3.12b), and depletion of *Cdk8* caused a highly elongated mitochondrial morphology (Fig. 3.12c). We observed predominantly fragmented mitochondria when either $CDK19^{WT}$ or $CDK19^{\Delta NLS}$ was co-expressed in *Mef2>Cdk8 RNAi* background (Fig. 3.12d', e'). These results suggest that cytoplasmic CDK19 was sufficient to regulate mitochondrial morphology.

In summary, expression of either $CDK19^{WT}$ or $CDK19^{\Delta NLS}$ can significantly rescue defective phenotypes caused by Cdk8 depletion including survival rate, climbing ability, neuronal death, elevated ROS, and most importantly the mitochondrial morphology. These findings indicate that CDK19 shares conserved function with fly Cdk8 in regulating mitochondria, and since $CDK19^{\Delta NLS}$ can rescue the phenotypes to the same extent as $CDK19^{WT}$, which further suggests conserved functions between Cdk8 and CDK19 in the cytoplasm.

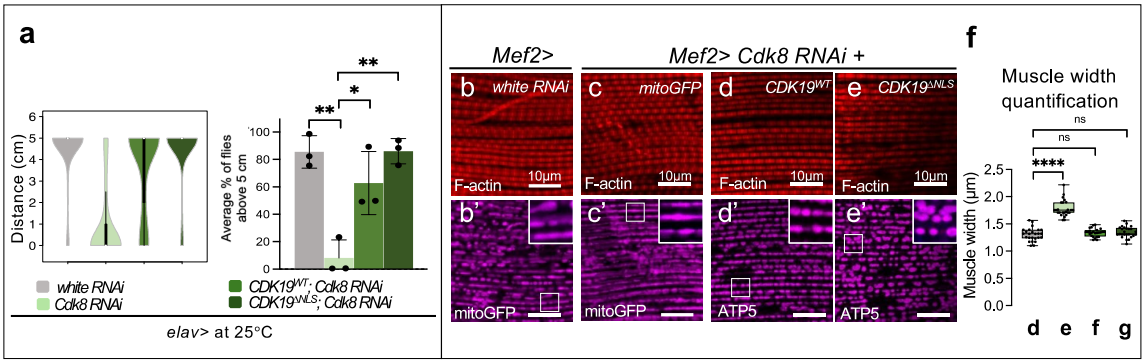

Figure 3.12. CDK19 rescues the climbing defect, muscle and mitochondrial morphology in Cdk8 depleted flies.

(a) Both CDK19^{WT} and CDK19$^{\Delta NLS}$ can significantly suppress the climbing defects due to neuronal depletion of cdk8 (elav>Cdk8 RNAi). Experiments are repeated four times. Results are mean ± SD. Unpaired two tailed t-test is used to generate the statistics. P value is 4.56e-05 for white RNAi, 2,38e-05 for CDK19^{WT}, and 0.0036 for CDK19$^{\Delta NLS}$ in comparison to *Cdk8 RNAi*. Total number of progeny are assessed, n = 160, 153, 140, 159 respectively in order. (b-e) Rhodamine phalloidin staining (F-actin, red) to visualize indirect flight muscles in (b) control *white RNAi* or (c) *Cdk8 RNAi* flies. (d) CDK19^{WT} and (e) CDK19$^{\Delta NLS}$ were expressed in the Cdk8 depleted background. (b'-e') Either mitoGFP or ATP5α staining (magenta) were used to visualize mitochondrial morphology in the indicated genotypes. Scale bars: 10 µm. (f) Quantification of adult indirect flight muscle width in 3-day old flies. n = 5 per genotype. Data are presented as box plots (centre line at the median, upper bound at 75th percentile, lower bound at 25th percentile) with whiskers at minimum and maximum values. Unpaired two tailed t-test is used to generate the statistics. P value is 1.78e-16 for white RNAi, 0.2295 for CDK19^{WT}, and 0.1816 for CDK19$^{\Delta NLS}$ in comparison to *Cdk8 RNAi*. All raised at 25°C.

3.3.9. Supplementing of CDK19 rescues a familial form of Parkinsonism caused by *pink1^{B9}*

We observed that either overexpression of CDK19^{WT} or CDK19$^{\Delta NLS}$ in the *Cdk8* depleted background can sufficiently induce mitochondrial fragmentation, as observed with overexpression of Cdk8 (Fig. 2.3, 2.4). Next, we hypothesized that introducing CDK19^{WT} or CDK19$^{\Delta NLS}$ could carry out the same function in regulating mitochondria as overexpressing fly Cdk8 in a wildtype background, which promotes mitochondrial fragmentation in muscle. We found that introducing either *CDK19^{WT}* or *CDK19$^{\Delta NLS}$* in a wildtype background led to rounded and fragmented mitochondria (Fig. 3.13b-b', c-c' respectively) in comparison to control (Fig. 3.13a-a'), indicating that elevated levels of CDK19 can promote fission.

These results led us to wonder if expression of CDK19^{WT} or CDK19$^{\Delta NLS}$ could rescue the *pink1^{B9}* mutant phenotypes, like what we found with expression of Cdk8. We assayed climbing activity (Fig. 3.13d) and thorax indentation (Fig. 3.13e) phenotypes when either CDK19^{WT} or CDK19$^{\Delta NLS}$ was expressed in a *pink1^{B9}* mutant background. Strikingly, both wildtype and cytoplasmic CDK19$^{\Delta NLS}$ can significantly rescue the climbing defect to the same extent (Fig. 3.13d), whereas expression of CDK19^{WT} is more effective in suppressing the muscle degeneration in comparison to CDK19$^{\Delta NLS}$ in the *pink1* mutant background. However, expression of either CDK19^{WT} or CDK19$^{\Delta NLS}$ can significantly restore the percent of thoracic indentation in flies under the mutant background (Fig. 3.13e).

Altogether, these findings indicate that Cdk8 and CDK19 share conserved functions in regulating mitochondria, and ectopic expression of Cdk8 or CDK19 rescues defective phenotypes in a familial form of Parkinsonism mediated by *pink1^{B9}*. Furthermore, our data suggests that CDK19$^{\Delta NLS}$, despite its cytoplasmic localization, can function the same as CDK19^{WT} in regulating mitochondria as well as in rescuing the climbing defect and thorax indentation phenotypes caused by *pink1^{B9}*, indicating potential cytoplasmic function that is shared between Cdk8 and CDK19 across species.

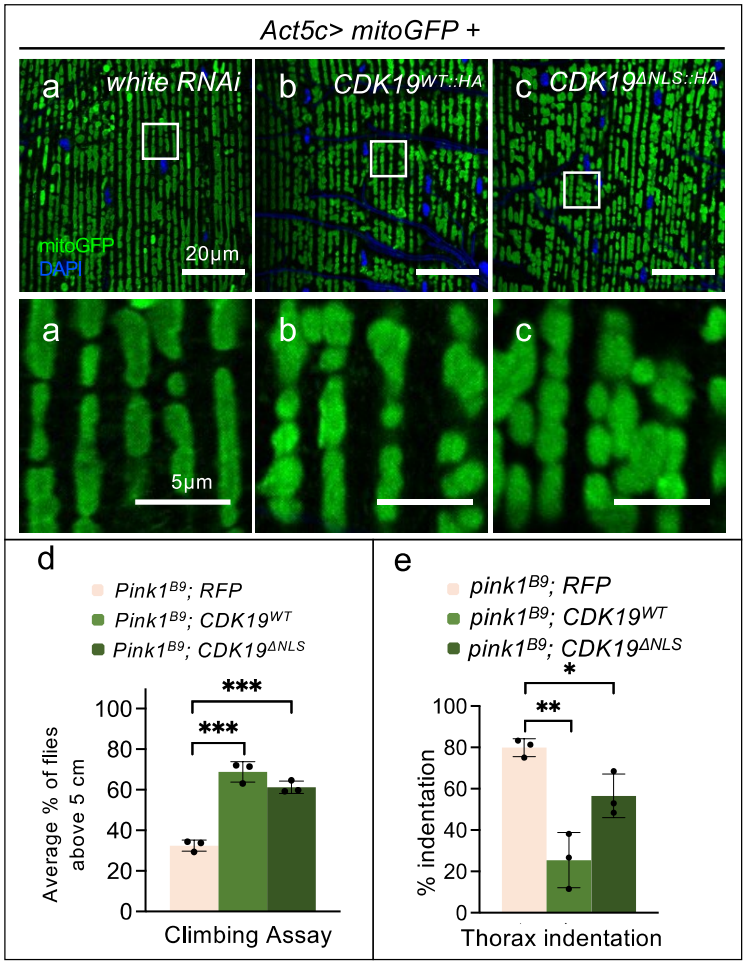

Figure 3.13. Expression of CDK19 promotes mitochondrial fission under physiological condition, and rescue the defects in thorax integrity and climbing ability in *pink1^{B9}*mutant flies

Mitochondria in Indirect flight muscle expressing either (a) white RNAi, (b) CDK19$^{WT::HA}$ or (c) CDK19$^{\Delta NLS::HA}$ under the ubiquitous driver, *Actin5cGal4* co-expressing *UAS-mitoGFP*. Scale bar: 20 µm (a'-c') Representative magnified sections of mitochondrial morphology from a-c. Scale bar: 5 µm. All raised at 25°C. n = 5 per genotype. (d) Climbing assay testing the ability of RFP, CDK19^{WT} or CDK19$^{\Delta NLS}$ expressed in the *pink1^{B9}* background to reach target line. Experiments are repeated three times. Total number of progeny are assessed, n = 56, 77, 98 respectively in order. Results are mean ± SD. Unpaired two tailed t-test is used to generate the statistics. P value is 0.0004 for *CDK19^{WT}* and 0.0002 for *CDK19$^{\Delta NLS}$* in comparison to *pink1^{B9}* mutant. (e) Quantification of thorax indentation in flies when RFP, CDK19^{WT} or CDK19$^{\Delta NLS}$ are expressed in the *pink1^{B9}* background, raised at 25°C. Experiments are repeated three times. Total number of progeny are assessed, n = 56, 71, 84. Results are mean ± SD. Unpaired two tailed t-test is used to generate the statistics. P value is 0.0025 for CDK19^{WT} and 0.0238 for CDK19$^{\Delta NLS}$ in comparison to *pink1^{B9}* mutant. * p<0.05, ** p<0.01, *** p<0.001, **** p<0.0001

3.4. Discussion

In this chapter, we investigated the role of Cdk8 and its ortholog CDK19 in modulating *pink1*-mediated PD-like phenotypes in muscles. Based on our initial results, we hypothesized that both Cdk8 and CDK19 could suppress *pink1* mutant phenotypes. We show that Cdk8 likely functions downstream of Pink1 as ectopic expression of Cdk8 can significantly rescue numerous *pink1* phenotypes, including locomotor impairment and defects in mitochondrial morphology and muscle integrity. The rescuing ability of Cdk8 is likely by partially restoring the phospho-level of Drp1 under the mutant condition as Pink1 is known to directly regulate Drp1 on S616. Furthermore, expressing the human ortholog $CDK19^{WT}$, or the cytoplasmic only $CDK19^{\Delta NLS}$, in the same mutant background can rescue the defective phenotypes caused by $pink1^{B9}$ mutant to the same extent. We demonstrated that human CDK19 shares conserved function with fly Cdk8, as expression of either wildtype $CDK19^{WT}$ or $CDK19^{\Delta NLS}$ can significantly rescue the climbing defects caused by Cdk8 depletion, as well as reverting the elongated mitochondria to fragmented, round-shaped mitochondria under the same Cdk8 depleted background. Lastly, we found tissue specific localization of CDK19 and Cdk8 suggesting they may have potential conserved cytoplasmic function.

In summary, our data reveal a new cytosolic function for Cdk8/CDK19 in mitochondrial fission by mediating the phosphorylation of Drp1 and this function parallels the function of *pink1.*

3.4.1. Functional conservation of Cdk8 and CDK19 localization

Our collaborators previously observed that human CDK19 is localized to the cytoplasm in adult fly neurons[102]. In our assays, we further examined the localization of $CDK19^{WT}$ in muscle and found it have both nuclear and cytoplasmic localizations (Fig. 3.9). Strikingly, when we examined the endogenously-GFP tagged Cdk8 in flies, we found consistent localizations in both muscles and brains (Fig.3.10). Furthermore, our data showed that expressing $CDK19^{WT}$ can significantly rescue defective phenotypes that caused by Cdk8 depletion including reduced survival rate, impaired climbing ability, elevated cell death, and hyper tubular mitochondrial morphologies (Figs. 3.11, 3.12).

Most importantly, expressing CDK19$^{\Delta NLS}$ can rescue Cdk8 depleted phenotypes in flies to similar extent as expressing CDK19^{WT}, further suggesting the potential cytoplasmic function of CDK19 that is likely to be conserved between human CDK19 and fly Cdk8. From cNLS Mappers (Fig. 3.8), there is a predicted NLS sequence in fly Cdk8. It would be interesting to generate a line where the predicted NLS sequence is deleted from fly Cdk8, denoted as Cdk8$^{\Delta NLS}$, and to perform functional assays by expressing Cdk8$^{\Delta NLS}$ in a Cdk8 depleted background to further tease apart the nuclear functions and cytoplasmic function of Cdk8.

3.4.2. Regulation of Drp1 by Cdk8/CDK19 and PINK1

Perturbations in mitochondrial morphology have been associated with several human disorders[102,273–277]. Some of the genes are involved in regulating fission and fusion[278]. Mitofusins (Mfn1 and Mfn2) regulate mitochondrial outer membrane fusion and are required to maintain a mitochondrial network in cells, while mitochondrial inner membrane protein Opa1 regulates mitochondrial inner membrane fusion[279]. Drp1, a cytosolic dynamin GTPase, is the key player in mitochondrial fission and Drp1 phosphorylation plays a critical role in controlling mitochondrial fission[280]. Phosphorylation of Drp1 at the S616, S579, and S600 sites promotes fission during mitosis and oxidative stress[281].

In Chapter 2, we found fly Cdk8 interacts with Drp1 as Drp1 shares a conserved CDK phosphorylation motif at S616. First, we found loss of Cdk8 abolished synaptic transmission in photoreceptors in a similar fashion as loss of Drp1. In addition, we found modulating expression of Cdk8 had significant effects on the phospho-status of Drp1 at S616 endogenously, while the overall abundance of Drp1 stayed the same. Most importantly, we found that muscle specific expression of Drp1^{HA} with Cdk8::GFP using anti-HA-agarose beads is able to co-immunoprecipitate down Cdk8::GFP, suggesting that Cdk8 interacts with Drp1. We found that flies that have reduced Cdk8 protein in most cells displayed phenotypes that were strikingly similar to the ones observed in *pink1* null mutants[213,282–284]. Importantly, overexpression of Cdk8 significantly suppresses the behavioral and mitochondrial defects associated with the loss of *pink1*, which encodes a putative serine/threonine kinase with a mitochondrial targeting sequence. Pink1 promotes mitochondrial clearance, and has been shown to phosphorylates Drp1 at site S616 in mice, Drosophila, and human fibroblasts[157,285]. The novel finding of Cdk8

in regulating phospho-level of Drp1 is further supported by the finding that ectopic expression of Cdk8 in the *pink1* mutant background can partially rescue the level of phosphorylation of Drp1 at S616. This finding combined with the fact that overexpression of Cdk8 or its ortholog CDK19 nearly fully suppresses climbing and muscle degeneration associated with loss of *pink1* strongly argues that Cdk8/CDK19 plays a critical and similar role in mitochondrial dynamics as Pink1 (Figs. 3.2, 3.13). Altogether, these findings suggest that supplementing Cdk8/CDK19 in the *pink1* mutant background partially restore the mitophagy pathway in clearance of damaged mitochondria by separating the damages ones from the rest of healthy pool. Subsequently, the isolated impaired mitochondria are targeted to degradation by autophagy (Fig. 3.14). Hence, these data implicate CDK19/Cdk8 in a critical mitochondrial function.

The promising effect of Cdk8 in the *pink1* mutant background by restoring the phospho-level of Drp1 gradually declines as the flies aged. It is likely due to the severity of accumulated defects in *pink1* mutant. The homeostasis of mitochondria needs to be well balanced. Over time, accumulated dysfunctional mitochondria caused by *pink1* along with general effects of ageing reduces the rescuing capability of Cdk8. Thus, we observed two distinct results in ROS suppression, muscle myofibril width, and mitochondrial morphology when Cdk8 is ectopically expressed under *pink1* mutant background when flies were three weeks old (Figs. 3.5, 3.6). It would be interesting to test the level of phospho-Drp1 in these aged flies to see if the reduced rescue effect of Cdk8 is solely due to insufficient activation of Drp1 at S616. In conclusion, these findings suggest that Cdk8 has a rescuing threshold in restoring the mitophagy pathway. Additional factors that act downstream of Pink1 and Parkin along with Cdk8 are needed to further enhance the clearance of impaired mitochondria and restore mitophagy when the mutant condition is worse over time.

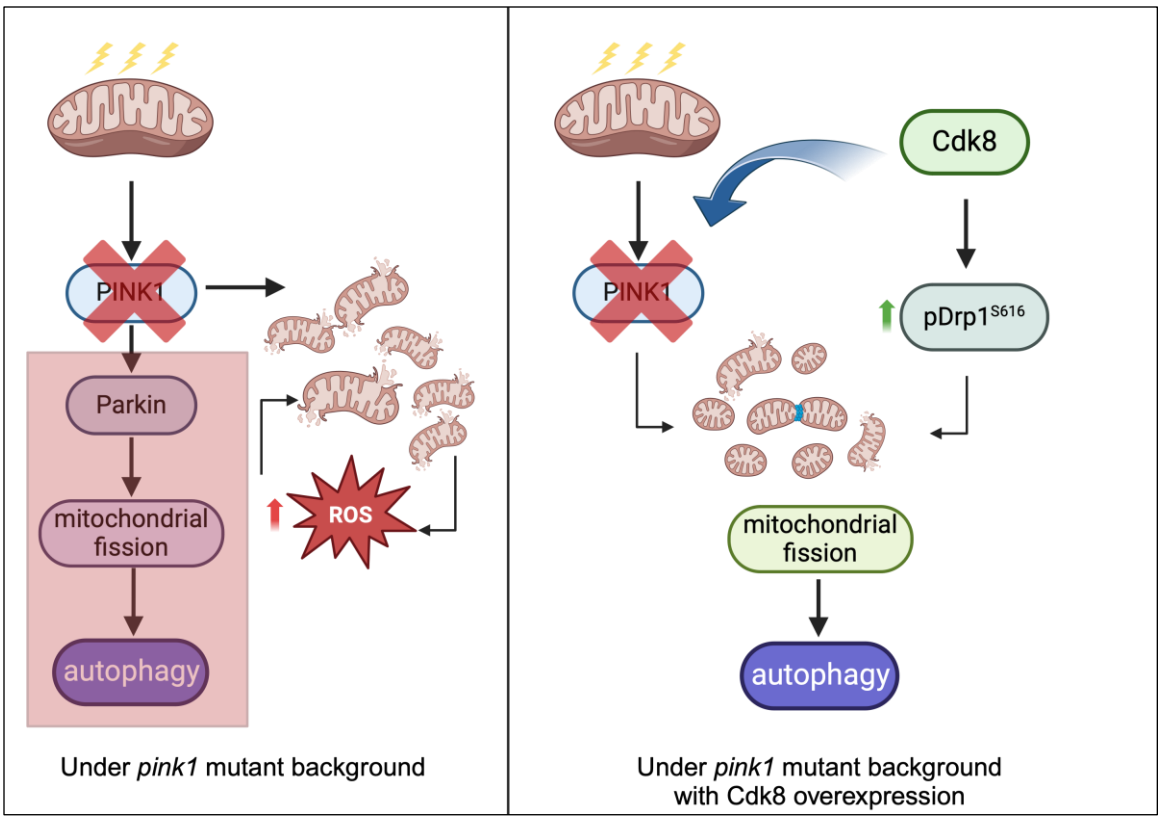

Figure 3.14. Current hypothetical model on ectopic expression of Cdk8 in rescuing impaired mitophagy in *pink1* mutant background.

In the *pink1* mutant background, damaged mitochondria are accumulated, which in turn enhances ROS production. The vicious cycles continue to cause buildup of damage and eventually flies in the *pink1* mutants fail to survive (Left). In the same *pink1* mutant background, expression of Cdk8 promotes the phospho-status of Drp1, which in turn to activate the fission process of mitochondria. Separating the damaged mitochondria away from the healthy pool reinitiates the downstream autophagy to clean up the damaged mitochondria for recycling. The impaired process of mitophagy is restored (Right). Figure generated by Biorender.

3.4.3. Regulators downstream of Pink1/Parkin mediated mitophagy

There are a number of positive and negative regulators that act downstream of *pink1* or *parkin* mutants to restore the impaired mitophagy. Overexpression or suppression of these regulators has been shown to be beneficial in ameliorating impaired mitochondrial morphology, climbing deficits, thorax indentation in fly indirect flight muscles[258,286–291]. Some have been shown to restore mitochondrial function, as well

as maintaining the number of dopaminergic neurons in fly brains in *pink1* or *parkin* mutant backgrounds.

One of the positive regulators is the mitochondrial outer membrane protein, Clueless (Clu). In fly oogenesis, mitochondria in germ cells are found evenly dispersed throughout the cytoplasm; however, double heterozygous mutant of *clu* and *pink1* in ovaries led to enhanced clumping and abnormally fused mitochondria that are centered near the nuclei[258,286]. Genetic interaction assays by overexpressing either Pink1 or Parkin in S2 cells with *clu* RNAi construct indicated that hyperfused mitochondrial morphology in *clu* mutant can be ameliorated by Parkin overexpression but not Pink1, suggesting Clu functions between Pink1 and Parkin.

Another positive regulator that acts downstream of Pink1 is Rearranged During Transfection (RET)[287], a receptor tyrosine kinase that is bound by Glial cell line-derived neurotrophic factor (GDNF) to promote the survival or dopamine neurons. The kinase activity of RET is essential in rescuing the mitochondrial morphologies in both fly muscles and dopaminergic neurons in *pink1* mutants but not in *parkin* mutants, as expression of the wildtype RET failed to rescue the defective phenotypes associated with *parkin* mutants. Consistent results were found in a human dopaminergic neuroblastoma cell line SH-SY5Y, where endogenous RET expression restores the mitochondrial morphology when *PINK1* is knocked out in the cell line[289].

Enhanced expression of Marf or reduced expression of Drp1 are found in *pink1* or *parkin* mutants; thus, downregulating the expression of Marf or elevating Drp1 can rescue the mutant phenotypes[156,157,166,169,170]. Ubiquitin carboxyl-terminal hydrolase 8 (USP8) is one of the deubiquitinating enzymes (DUBs) that is found to affect steady state levels of Marf in Drosophila and downregulation of USP8 reduces the protein level of Marf. Furthermore, genetic suppression of USP8 or pharmacologically supplementing flies with inhibitor of USP8 corrects phenotypes associated with *pink1* mutant [288]. Interestingly, knock out of ubiquitin carboxy-terminal hydrolase (UCH), the ortholog to human ubiquitin C-terminal Hydrolase L1 (UCHL1), is found to completely revert the indented thoraces and abnormal wing postures observed in the null mutant *pink1* and *parkin* flies. UCH is identified as another DUB that has deubiquitinase activity[290].

One of the negative regulators that participates in Pink1/Parkin mediated mitophagy is four-wheel drive (*fwd*), the phosphatidylinositol 4-kinase IIIβ ortholog in Drosophila. Depletion of *fwd* shares defective phenotypes that mimic both *pink1* or *parkin* mutants including climbing deficits, reduced longevity and increased length and connectivity (numbers of branching) of mitochondria in fly brain[291]. Overexpression of Fwd in a mutant background reverted the hyperfused mitochondria to fragmented, suggesting its role in mitochondrial dynamics. Further genetic interaction assays demonstrated that heterozygous loss of either Marf or Opa1, fusion regulators of mitochondrial dynamics, was sufficient to suppress the climbing deficit and revert branching in mitochondrial morphology caused by depletion of *fwd*; however, overexpression of Drp1 failed to ameliorate the climbing defect and branching phenotypes in the same depleted background, suggesting that Drp1 may require Fwd to execute mitochondrial fission[291]. The findings with overexpression of Fwd in a *pink1* mutant background are consistent with results we found upon ectopic expression of Cdk8 in the same mutant background. Furthermore, the role of Fwd in promoting mitochondrial fission through Drp1 made us question how Fwd and Cdk8 fit into the Pink1/Parkin mediated mitophagy pathway. It would be interesting to perform genetic interaction assays between Cdk8 and Fwd to see if both are needed to fully suppress the defective phenotypes found in *pink1* mutant background, especially in aged flies.

In summary, Pink1 and Parkin mediated mitophagy is crucial to regulate the homeostasis of mitochondria, as the list of potential positive or negative regulators of the pathway continues to grow. Our finding that overexpressing Cdk8 reverts defective phenotypes in the *pink1* mutant background makes Cdk8 a positive regulator of the pathway. It would be interesting to test the effect of Cdk8 in the *parkin* mutant background, as some research papers have demonstrated that the rescuing effects may be limited to only rescue *pink1* mutant phenotypes but fail to ameliorate defects in *parkin* mutants. Furthermore, performing genetic interaction assays between Cdk8 and currently known regulators in the *pink1/parkin* mutant background could provide additional insight in the molecular mechanism of Cdk8 in rescuing *pink1* mutant phenotypes, and shed light on understanding the underlying mechanism associated with *pink1/parkin* mediated Parkinsonism.

3.4.4. Function of Cdk8 in PINK1/Parkin independent mitophagy

We focused on the mitophagy that is mediated by PINK1 and Parkin, which is initiated mostly by having reduced mitochondrial membrane potential, as we previously described. Mitophagy can also be trigged in a PINK1/Parkin-independent pathway, where membrane potential is not the cue. Instead, it can be achieved by direct interactions between receptors that are anchored on the cytosolic face of the outer mitochondrial membrane (OMM) such as members of pro-apoptotic B-cell lyphoma-2 (Bcl-2) protein family [292–295], or FUN14 domain-containing protein 1 (FUNDC1) an integral mitochondrial outer-membrane protein[296,297] with ATG8 family proteins[160]. Here, we found that expression of Cdk8 can promote the fragmentation process in damaged mitochondria in a *pink1* mutant background, and in turn partially restore the homeostasis of mitochondria. The purpose of mitophagy is to recognize the damaged mitochondria and subsequently target them for degradation. Thus, it will be interesting to see if Cdk8 play any roles in PINK1/Parkin-independent mitophagy.

3.4.5. Drp1 and human diseases

DNM1L (Dynamin 1-like, synonyms Drp1) is a human homolog of Drp1, which is a member of the dynamin superfamily of GTPases. DNM1L mediates mitochondrial as well as peroxisomal fission[215], and a patient with loss of *DNM1L* presented with a lethal encephalopathy due to defective mitochondrial and peroxisomal fission (MIM #614388)[298]. This individual had poor feeding, poor growth, lactic acidosis, seizures, hypotonia, nystagmus, and an abnormal gyral pattern on magnetic resonance imaging and passed away at 37 days of life[299]. Mice lacking Dlp1, the homolog of DNM1L, die at embryonic day E12.5, indicating a crucial role for this gene in mammalian development. These mice display abnormal mitochondrial and peroxisomal morphology[298], indicating that Drp1 is critical in development across the species. Since we found that Cdk8 can promote Drp1 activity, it is notable that syndromes due to deletion of CDK8/CDK19 share some clinical features with loss of DNM1L. It would be interesting to detect the activity of Drp1 in flies expressing either $CDK19^{WT}$ or $CDK19^{\Delta NLS}$. Ultimately, to detect if the activity of Drp1 is reduced in CDK8/CDK19 patient samples. It may provide additional information to clinicians and physicians on how patients with CDK8/CDK19 mutations show similar but milder phenotypes, including developmental delay, seizure, and hypotonia.

In studying phosphorylated Drp1, we noted an inconsistency between phospho-Drp1^{S616} and total Drp1, where phospho-Drp1^{S616} appeared as doublets whereas total Drp1 generally appeared as a single band (Figs. 2.10, 3.7). The antibodies that we used against total Drp1 and phosphor-Drp1^{S616} were both validated in a fly model where Han et al.[215] expressed human Drp1 in the same *pink1^{B9}* mutant background. Since Drp1 is known to be modulated at multiple sites[300], we suspect the single band present in total Drp1 represents the overall modified status of Drp1 in our fly lysates. To circumvent this issue, ones can cast a gradient gel that targets the region between 70 kDa and 100 kDa specifically, and probe for total Drp1. We anticipate observing multiple bands as Drp1 is known to be highly post translational modified by phosphorylation, acetylation and SUMOylation[187]. Thus, in the phospho-Drp1^{S616} blots it is possible that the proteins we see as a doublet both represent pDrp1 at S616 but in one case it carries a second modification that alters its mobility. In the lanes where we detect total Drp1 these differences may be masked by additional modifications not detected with the pDrp1 antibody.

3.4.6. Roles of CDK8/19 in rare diseases and implications for common disorders like Parkinson's Disease

Patients harboring missense mutations in either CDK8 or CDK19 present with a range of clinical features, including neurodevelopmental defects, variable intellectual disability, hypotonia and facial dysmorphology[301]. Thus far, the features of these rare syndromes have been attributed to dysfunction of these kinases as part of the Mediator kinase module. We propose that aspects of these syndromes may also be due to altered function in the cytoplasm in regulation of mitochondrial morphology and function through effects on Drp1, independent of their role in mediating transcription. In my thesis I found that loss of *Cdk8* causes defects that show some similarity to Parkinsonism and both Cdk8 and CDK19 can suppress the phenotypes associated with fly *pink1* mutants. These findings suggest defects in CDK8/19 may also contribute to aspects of the development of Parkinson's Disease.

Chapter 4. Pathogenic CDK19 variants behave in a dominant negative fashion

4.1. Contribution to the chapter

The work shown in **Chapter 4** is unpublished and is part of an on-going collaboration with Dr. Hyung-lok Chung. All data presented in the thesis figures was generated by me, and in some cases together with Claire Shih.

4.2. Introduction

Single heterozygous *de novo* missense mutations of CDK19 have recently been identified in unrelated individuals[101–103,106]. They all experienced developmental and epileptic encephalopathy (DEE87), as well as infantile spasms, which are seizures in infants[302]. It is difficult to provide treatments for patients with such young age who suffer from refractory seizures as clinicians lack functional information about these newly identified *de novo* mutations in CDK19. Furthermore, it is difficult to understand the underlying biology of these mutations when the cohort has a sample size less than twenty unrelated individuals among different organizations across the world. To address this problem, clinicians and researchers are working as a team, where clinicians provide diagnosis results from patients, and researchers provide newly discovered information on these pathogenic CDK19 variants using different model organisms. Two of the CDK19 variants have previously been characterized using *Drosophila melanogaster*, CDK19-Y32H and CDK19-T196A[102]. CDK19-Y32H was identified in four unrelated individuals and is described in several unrelated publications[101,102,106], whereas CDK19-T196A mutations were identified in two unrelated individuals and described in the same study[102]. All the mutations are identified through either whole genome or exome sequencing, where the genome or exome of the patient is compared to the genome or exome of their parents.

Since the identified CDK19 mutations are known to cause DEE87, the Bellen group generated transgenic fly strains expressing the CDK19 variants Y32H and T196A and performed functional assays that mainly addressed the neuronal functions of these variants[102]. They found that expression of these two missense variants reduced the viability of wildtype flies, and they also failed to rescue the lethality caused by trans-heterozygous *Cdk8* mutations in flies. Furthermore, expression of variants made flies susceptible to bang sensitivity, where flies expressing the variant exerted seizure-like phenotypes and had a longer recovery time from the banging assay than control flies. They also found that when they express the wildtype and variants of CDK19 in fly adult brains, they found cytoplasmic localization of CDK19, which suggests potential cytoplasmic function of CDK19. Altogether, these data suggest that the variants are pathogenic, and they are likely behaving in a dominant negative fashion.

Given that we found expression of Cdk8 can affect mitochondrial morphology as well as muscle morphology in flies (in Chapter 2), we hypothesized that these pathogenic CDK19 variants causes phenotypic changes in mitochondrial and muscle morphology when these variants are expressed in adult IFM. By observing their effects, we could determine whether they behaved as dominant negative mutations leading to more severe effects than would be found with depleting of the homologous Cdk8 alone. In addition, we also want to examine the effect of these variants in other organelles beside mitochondria, as our collaborators found interesting features in CDK19 patient skin fibroblasts that are not related to elongated mitochondria. Lastly, to identify the potential therapeutic treatment that can be applicable to patients with CDK19 de novo variants in the long run, we performed drug testing between wildtype flies and Cdk8 depleted flies and used climbing ability as well as mitochondrial morphology as readout to demonstrate if the drug is a suitable treatment or not.

4.3. Results

4.3.1. Patient variants enhance the defective phenotypes caused by *Cdk8* depletion

All patients identified thus far with DEE87 are heterozygous for *CDK19* missense mutations. This indicates that the *de novo* variants are likely acting in a dominant fashion as phenotypes were observed in the presence of a single wildtype copy of *CDK19*. To further study patient-specific mutations, we expressed the CDK19 lines in a *Cdk8* depleted background to roughly mimic the genetic condition of patients with lower levels of wildtype protein. Previously, we found depletion of Cdk8 or expression of a kinase-dead version of Cdk8 in fly muscle leads to mitochondrial fusion morphology (Fig. 2.5) along with significant broadening of the myofibril width (Fig. 2.7). To test if expression of CDK19 variants would have a similar effect, we expressed $CDK19^{WT}$ and patient CDK19 lines using the muscle *Mef2-Gal4* driver in a *Cdk8* knocked down background and examined both the muscle fiber and mitochondrial morphology using adult indirect flight muscle (Fig. 4.1). We found ectopic expression of $CDK19^{WT}$ was able to suppress the widened myofibril width caused by *Cdk8* RNAi along with the fragmented mitochondria (Fig. 4.1b-b', c-c'), which indicates that $CDK19^{WT}$ also promote mitochondrial fission as we saw previously with ectopic expression of Cdk8. Interestingly, we found mixed localization of $CDK19^{WT}$ in muscle (Fig. 4.1c''-c'''), which is consistent with what we found previously in Fig. 3.9c. On the other hand, expression of either variant enhanced the broadening of myofibrils (Fig. 4.1f), enhancing the effects seen with depletion of *Cdk8* alone, suggesting that they may act in a dominant negative manner, potentially interfering with any residual Cdk8 protein (Fig. 4.1d, e). Furthermore, in line with the finding that Cdk8 depletion causes mitochondrial fusion, elongated mitochondria are observed when either variant is expressed (Fig. 4.1d', e'). Surprisingly, when we examined the localization of CDK19 in these lines using tagged HA at C-terminal, we found the two variants have different localizations as $CDK19^{Y32H}$ is localized in both nuclei and cytoplasm, whereas $CDK19^{T196A}$ is localized solely in cytoplasm (Fig. 4.1d''', e'''). This finding suggests that these variants may have tissue specific localizations, and different mechanisms may be involved, although this requires further investigation.

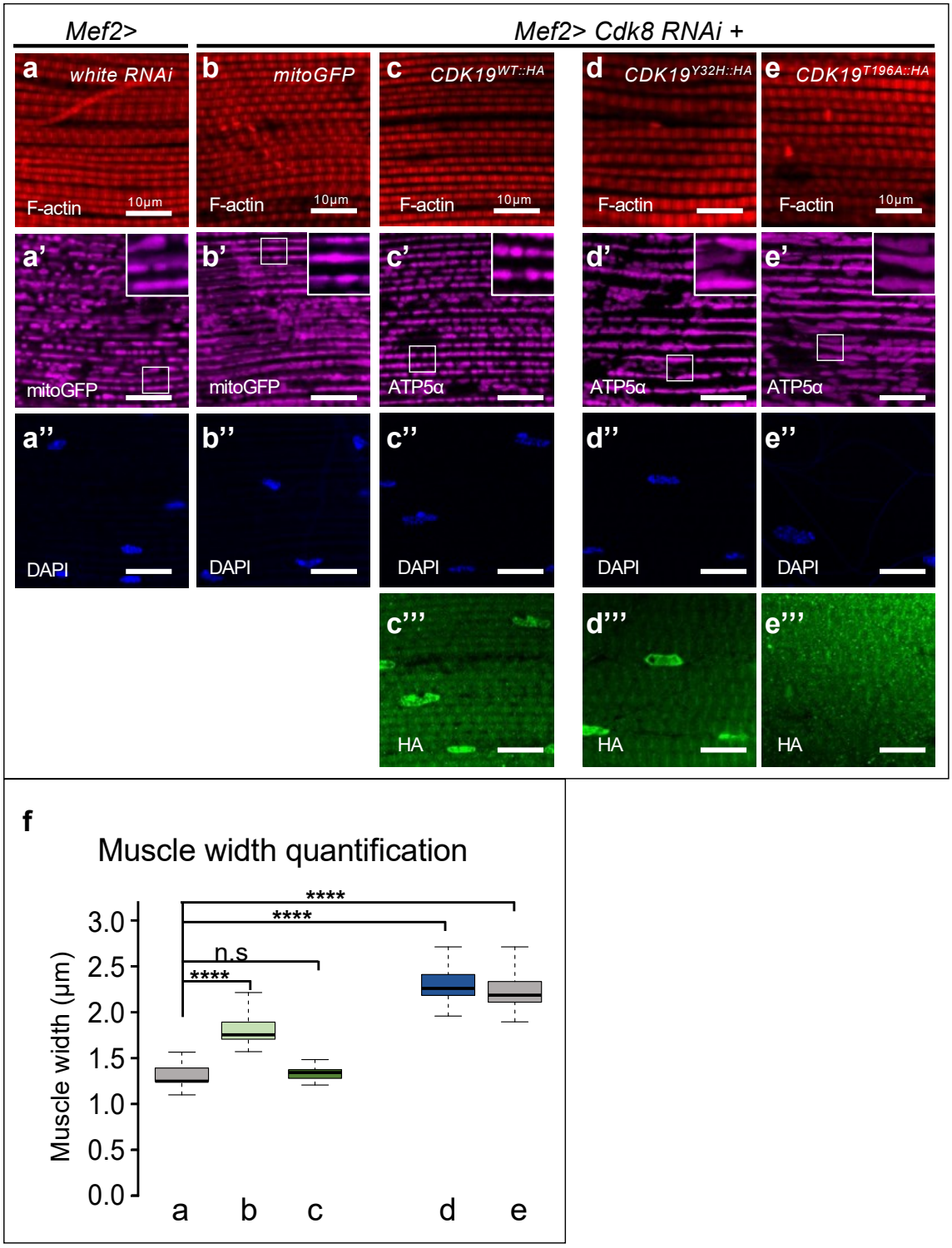

Figure 4.1. Expression of CDK19^{WT} rescues defects caused by Cdk8 depletion, while patient variants enhance these phenotypes.

Indirect flight muscle expressing (a) *white* RNAi, (b) *Cdk8* RNAi, (c) $CDK19^{WT}$ (d) $CDK19^{Y32H}$ (e) $CDK19^{T196A}$ with the Mef2Gal4 driver are stained with Rhodamine phalloidin. Dilution control mitoGFP is used in the (a) and (b), while all the CDK19 lines are expressed in the Cdk8 depleted background. (a'-e') mitoGFP or mouse-α-ATP5α is used for mitochondrial morphology (in magenta). (a''-e'') DAPI is used for DNA (in blue). (c'''-e''') mouse-α-HA is used to detect the localization of CDK19 in indirect flight muscles. All raised at 25 °C. Scale bar: 10 μm. (f) Quantification of adult indirect flight muscle width in 3-day old flies. n = 5 per genotype with three biological repeats. Data are presented as box plots (centre line at the median, upper bound at 75th percentile, lower bound at 25th percentile) with whiskers at minimum and maximum values. Unpaired two tailed t-test was used to generate the statistics.

4.3.2. Conserved mitochondrial morphology is found in patient skin fibroblast with T196A mutation

Fortunately, our collaborators shared their unpublished data from skin fibroblasts that they obtained from one of the patients that carries a *de novo* CDK19 T196A mutation. They performed transmission electron microscopy (TEM) using blind testing between the patient and patient's parent and relied on the structure of mitochondria to tell the differences between samples. They were thrilled to report that in their preliminary data, the patient skin fibroblasts exert similar mitochondrial morphology as what we found in the fly model that expressed the same mutation, where tubular structures of mitochondria were observed. In addition, in the patient sample they saw non-uniform cristae structures in mitochondria, whereas the patient parents have uniform cristae mitochondrial structures. Beside the difference in mitochondrial morphology, they also observed the presence of multilamellar bodies (MLBs) that are only present in the patient skin fibroblasts and not in the parents. The conserved mitochondrial morphology between CDK19^{T196A} expressed in flies and patient skin fibroblast further demonstrates the power of using Drosophila to model human diseases. Unfortunately, we are unable to share the images of their preliminary data in this thesis.

4.3.3. Effects of CDK19 lines in lysosome morphology when expressed in fly adult brain

The preliminary TEM images from our collaborators indicated that the patient skin fibroblast have extensive elongated mitochondria along with increase in numbers of multilamellar bodies (MLBs). MLBs are membrane-bound organelles which are specialized in lipid storage or are secretory organelles from lysosomal origins[101,102,105,107]. Enhanced or enlarged MLB formations are often associated with defects in lysosomes. Therefore, we wondered if depletion of *Cdk8* would result in any abnormal lysosomal morphologies in fly tissues (Fig. 4.3).

For these experiments we shifted to using a different neuronal driver (*nSybGal4)* which was combined in a single stock with a GFP reporter to detect lysosomes (*UAS-LAMP1-GFP*, Bloomington stock #42714). LAMP1 is the lysosome associated-membrane protein 1, which we used here as the marker for lysosomes. In these crosses, we first noticed that the number of surviving adult progeny was reduced after

expressing one of the CDK19 variants, CDK19^{T196A} (Table 4.1), which is consistent with a dominant effect as was seen by Chung et al[102] after ubiquitous expression. However, we did not observe any reduction in progeny with CDK19^{Y32H} (Table 4.1).

Our preliminary data on immunolabelling suggested that when *Cdk8* is depleted in the fly adult brain, there was an increased signal of the LAMP1-based GFP reporter (Fig. 4.2b'')[303]. While these phenotypes have not been quantified yet, it suggests that depletion of Cdk8 causes a disruption of lysosome levels. We found that expression of the CDK19 variants also caused a similar apparent increase of the number or size of lysosomes as what we had seen in a *Cdk8* depleted background (Fig. 4.2 d'', e''). Expressing CDK19^{WT} in the same *Cdk8* depleted background suppressed the elevated LAMP1-GFP intensity (Fig. 4.2c'') seen in *Cdk8* depleted neurons, as it mimics the signal intensity that we observed in the negative control (Fig. 4.2a''). In addition, we found that within the selected regions of the adult brain in antennal lobes and surrounding periesophageal neuropils, there appear to be fewer neurons within a given area of a fixed size in either *Cdk8* depleted or when CDK19 variants are expressed in the Cdk8 depleted condition, in comparison to the negative control (Fig. 4.2a''-e''). This suggests that when Cdk8 is depleted, neuronal cell size appears to increase and is accompanied by higher levels of LAMP1-GFP signal compared to controls.

Table 4.1. Number of progeny of indicated genotypes in triplicate crosses.

nSybGal4> UAS-LAMP1-GFP +	Number of progeny		
White RNAi	30+	30+	30+
Cdk8 RNAi	30+	30+	30+
CDK19$^{WT::HA}$; Cdk8 RNAi	30+	30+	30+
CDK19$^{Y32H::HA}$; Cdk8 RNAi	30+	30+	30+
CDK19$^{T196A::HA}$; Cdk8 RNAi	11	10	14

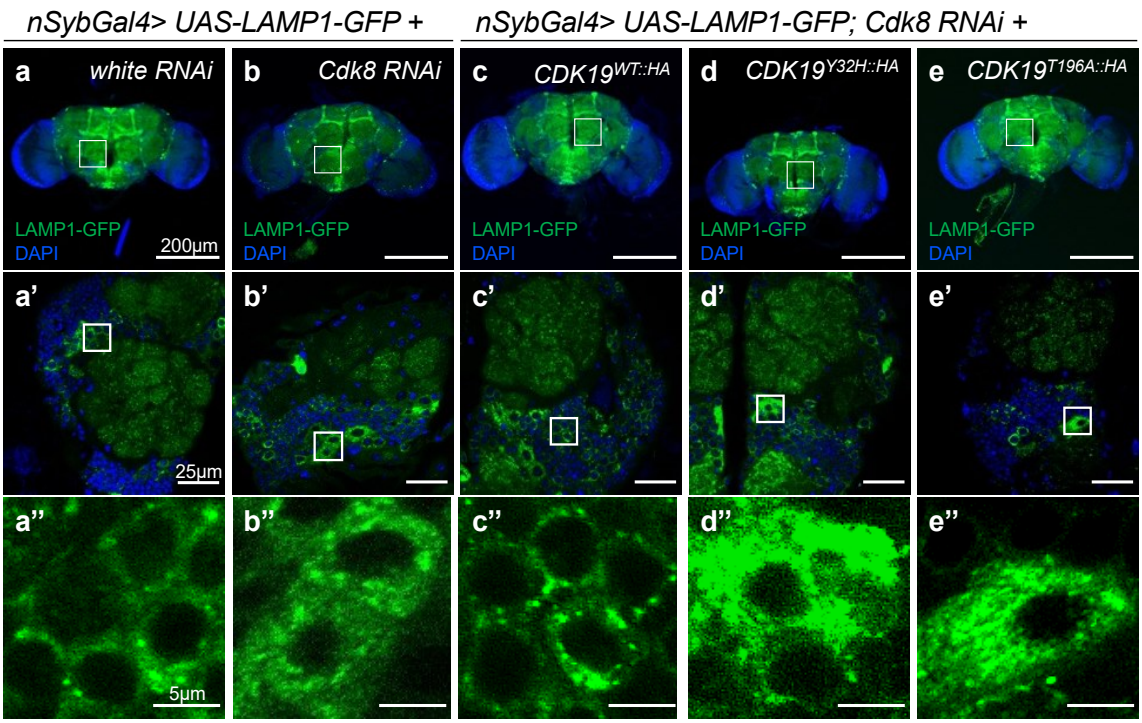

Figure 4.2. Lysosomal morphology in fly adult brain when CDK19 is expressed in a Cdk8 depleted background.

Adult brain expressing (a) white RNAi, (b) Cdk8 RNAi, (c) $CDK19^{WT::HA}$, (d)) $CDK19^{Y32H::HA}$, and (e)) $CDK19^{T196A::HA}$ with the *nSybGal4> UAS-LAMP1-GFP*. All the CDK19 lines are expressed in a Cdk8 depleted background. UAS-LAMP1-GFP is used for detecting lysosomal morphology with DAPI marking the nucleus. Maximum projection images are shown in a-e. (a'-e') single plane image from stacks that focuses on region that are selected from a-e. (a''-e'') single plane image of lysosomal morphology selected from a'-e' with corresponded genotypes. All raised at 25 °C. n = 5 per genotype with two biological repeats.

4.3.4. Testing N-acetylcysteine amide (NACA) as a potential therapeutic treatment for patients with CDK19/CDK8 mutations

We found that the expression of either of the CDK19 patient variants in fly muscles can lead to broadening of the myofibril width along with extensive elongated mitochondria (Fig. 4.1). Furthermore, our collaborators' TEM images indicated that skin fibroblasts from a patient with a heterozygous *CDK19 T196A* mutation contained extended mitochondria.

The next step we wanted to ask is whether we could find a potential treatment that can help patients with such mutations. Previously, we found depletion of *Cdk8* not only led to elongated mitochondrial morphology, but also a significantly elevated ROS level in both fly muscles and brains (Fig. 2.7, Fig. 3.6i, respectively). This was not a phenotype previously associated with mutations in CDK8 family members. Elevated ROS levels are an indication of increased oxidative stress, which is associated with progression of neurodegeneration as elevated ROS promotes lipid peroxidation, and mitochondrial dysfunctions which ultimately lead to further free radical generation. To test if administrating an antioxidant can break the chain of events of enhanced ROS production in *Cdk8* depleted flies, we performed drug testing using N-acetylcysteine amide (NACA). It is derived from N-acetylcysteine (NAC) with a substitution of a carboxyl group to an amide group (Fig. 4.3). NACA has previously been shown to replenish the reduced form of glutathione[304], which acts as an antioxidant to convert hydrogen peroxide to water, in turn to restore the redox balance within the cells. Furthermore, NACA was also shown to reverse lipid peroxidation[304], which is often found to be elevated prior to neurodegeneration[305]. In addition, NACA was previously proven to be protective in restoring mitochondrial dysfunction, reducing increased ROS in fly model of mitochondrial diseases, as well as in acyl-CoA oxidase 1 (ACOX 1) deficiency, which causes a rapid and severe loss of nervous system function in humans[306].

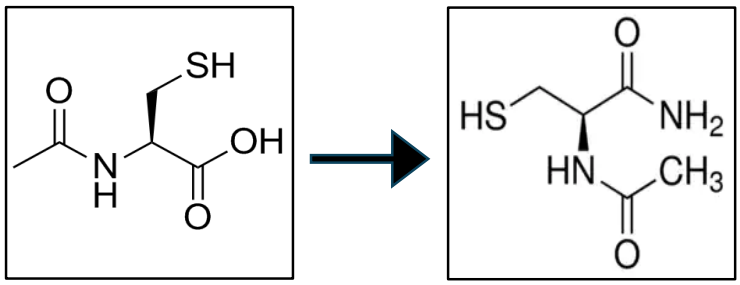

NAC NACA

Figure 4.3. Structure of N-acetylcysteine (NAC) and N-acetylcysteine amide.

N-acetylcysteine-amide (NACA) is a modified form of NAC containing an amide group instead of a carboxyl group of NAC.

We used a dosage of 80 microgram per milliliter as our initial starting point to test if NACA can revert the defective phenotypes caused by Cdk8 depletion. This dosage was informed by published data where researchers tested a variety of NACA concentrations ranging from 20 to 320 microgram per milliliter to treat another fly model of disease associated with elevated ROS[307]. We examined the climbing ability and mitochondrial morphology in *Cdk8* depleted flies when they were raised on normal food or on NACA-containing food. To take in account that Cdk8 plays essential roles throughout development of flies, we started to supplement the drug when crosses were initially set up so that larvae and adults ate the drug containing food for their whole lives.

We found flies raised on NACA food have significantly better climbing ability in comparison to flies that are raised on normal food in both females and males (Fig. 4.4). Females expressing *Mef2>Cdk8 RNAi* showed significant climbing defects when they are two weeks old, and the severity of defects progresses as they age on normal food. However, when flies with the same genotype are raised on NACA food, they have similar climbing ability as the negative control expressing *Mef2>white RNAi.* The rescuing effect is sustained when they were four weeks old and showed a significantly difference in comparison to the groups raised on the normal food (Fig. 4.4a). We observed similar effect in males expressing *Mef2>Cdk8 RNAi* on NACA food, and the rescuing effect is even earlier in comparison to females as we observed a significant rescue of climbing defect when they were three weeks old (Fig.4.4b). These data suggests that

supplementing NACA in fly food can restore the climbing defects caused by Cdk8 depletion in both sexes.

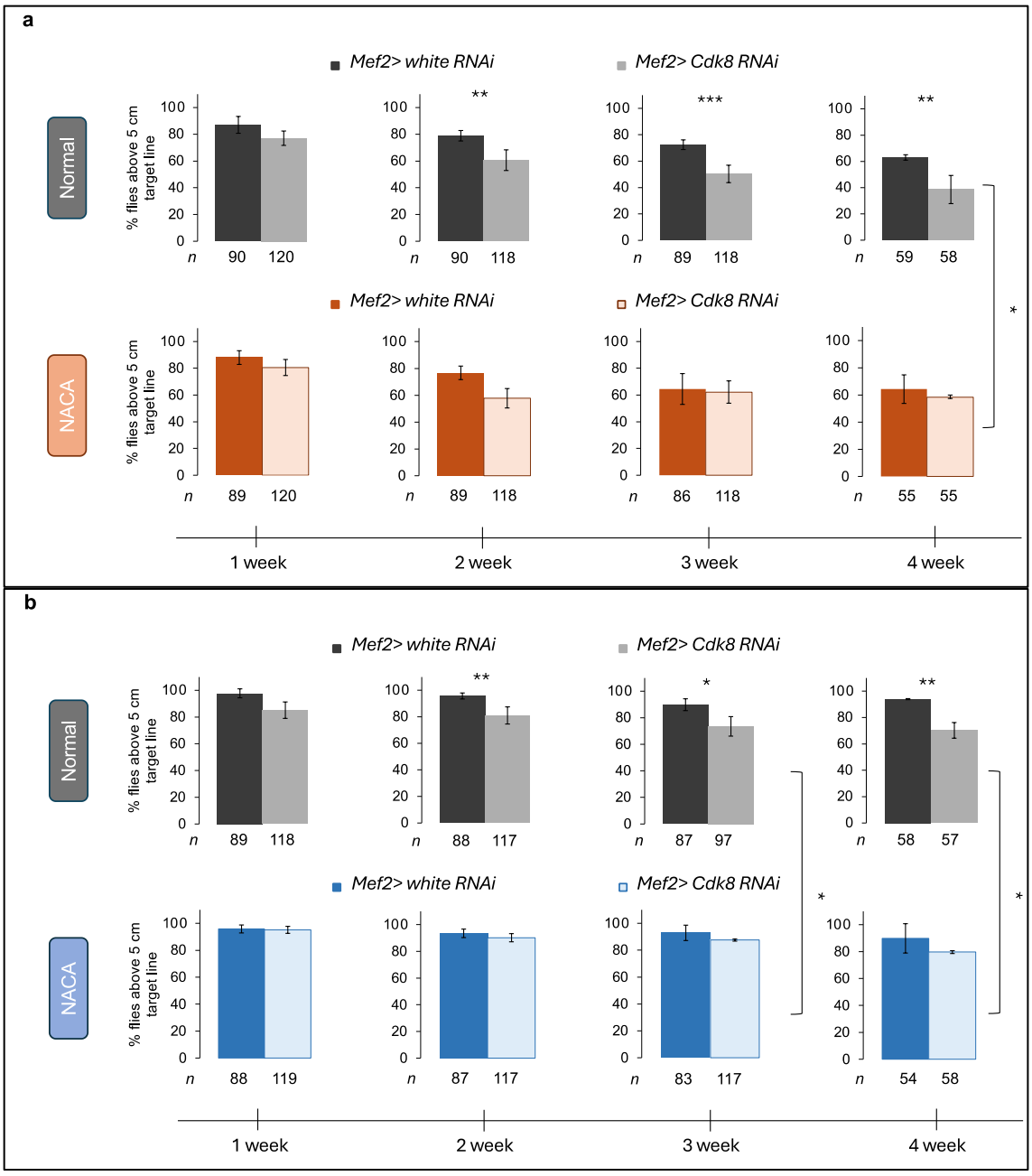

Figure 4.4. Cdk8 depleted flies on long exposure with NACA have better climbing ability in comparison to flies that are raised on normal food diet.

Climbing ability between progeny expressing either *Mef2> white RNAi* and *Mef2> Cdk8 RNAi* at four different time points in females (a) and in males (b) and compared them between on normal food or NACA food condition. Numbers of progeny are indicated. All raised at 25 °C. Experiments were individually repeated three times.

We next examined the mitochondrial morphology of flies raised on either normal food or NACA food when they were one week old. Although we did not observe any significant rescuing effect of NACA in climbing ability when flies were one or two weeks old, we did observe rescuing of mitochondrial morphology in adult indirect flight muscles (Fig. 4.5). We found elongated mitochondrial morphology when *Cdk8* is depleted in muscles in flies that were raised on normal food, whereas the negative control had a mixture of fragmented and elongated mitochondrial morphologies (Fig. 4.5a). Interestingly, we found no changes in mitochondrial morphology in control flies expressing *Mef2>white RNAi* when they were raised on NACA food, suggesting that treatment with NACA alone did not alter mitochondrial morphology. In contrast, mitochondrial morphology in muscles with *Cdk8* depletion were reverted to predominantly fragmented and rounded shapes instead of extensive elongated structures in flies that were raised on NACA food (Fig. 4.5b). These data suggest that NACA can revert the mitochondrial defects caused by *Cdk8* depletion, and that NACA is specifically targeting the elevated ROS that is found in *Cdk8* depleted flies, which further makes it a potential candidate for therapeutic treatment. Given that the patient variants induce very similar phenotypes in a broad range of assays, it suggests that NACA supplementation could also revert those phenotypes.

Altogether, our preliminary data suggest that Cdk8 depleted flies that are raised on NACA have promising rescuing effect in revert the climbing defects and elongated mitochondrial morphology in comparison to their counterparts that are raised on normal food.

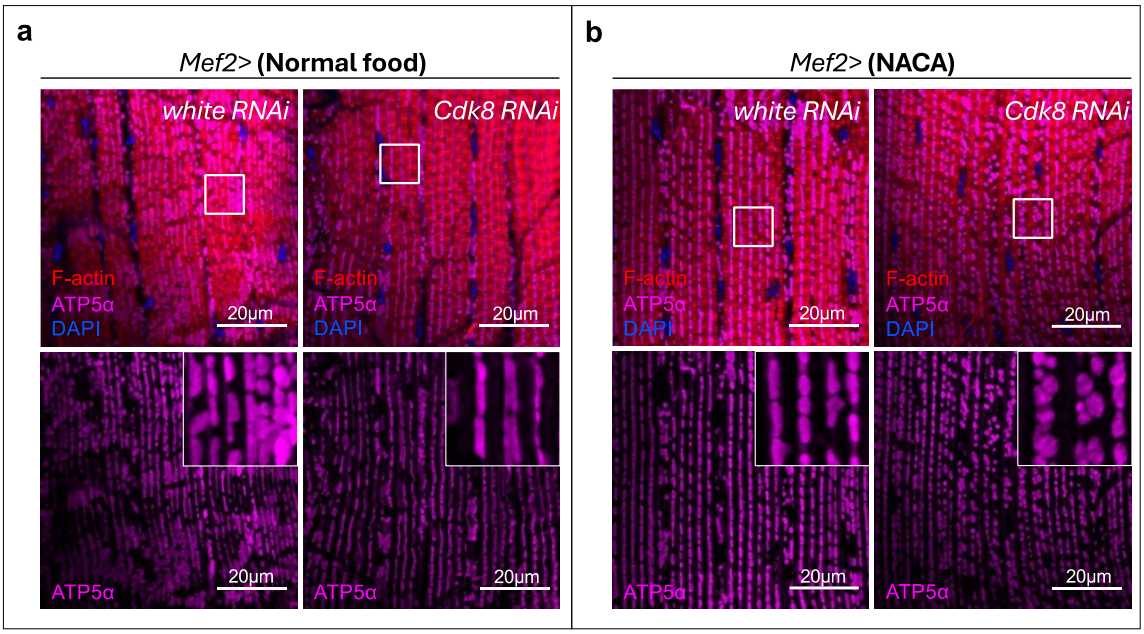

Figure 4.5. Cdk8 depleted flies on NACA food restores the mitochondrial morphology in comparison to flies that are raised on normal food diet

(a) Indirect flight muscle expressing either white RNAi or Cdk8 RNAi with the Mef2Gal4 driver raised on normal food or (b) NACA food. Rhodamine phalloidin is used for labeling myofibril (in red), mitochondrial morphology is labeled with mouse-α-ATP5α (in magenta) and DAPI is used to label nucleus (in blue). Mitochondrial morphology is shown a single channel image with inset included at the right corner. Examined one week old males. n = 5 per genotype with two biological repeats.

4.4. Discussion

In this chapter, we sought to investigate the cellular effect of two CDK19 patient variants to gain deeper insight into their pathogenic activities. We found that in fly IFM, expression of either variant in a Cdk8 depleted background enhances the elongated mitochondrial morphology, as well as the myofibril width in comparison to the depletion of Cdk8 alone. These findings illustrate the dominant negative effect of the variants. Furthermore, preliminary data from our collaborator on patient variant skin fibroblast further verified our initial findings in flies, indicating fly Cdk8 and its human ortholog CDK19 play a role in regulating mitochondrial structure under physiological condition. Depletion or mutation in Cdk8 or CDK19, respectively, results in hyperfused mitochondrial morphology that can subsequently lead to pathogenic phenotypes. In addition, the increased MLBs found in patient skin fibroblasts led us further examined the effect of these variants in lysosomes. In fly adult brains, we found what appeared to be enhanced lysosome-GFP signals associated with Cdk8 depletion as well as expressing variant under the same depleted background. This finding indicates that Cdk8/CDK19 may participate in regulating inter-organelle interactions, as demonstrated in previous chapter that mitochondria and lysosome are tightly associated in the mitophagy pathway. Lastly, we tested the therapeutic potential of the antioxidant drug NACA in Cdk8 RNAi flies. Promising preliminary results show that Cdk8 RNAi flies raised on the NACA food can revert the climbing defects, as well as the mitochondrial morphology that are associated with Cdk8 depletion, while has no effect on the negative control flies that were raised in the same condition. The preliminary results indicates that NACA could be a suitable treatment for patients with CDK19 de novo mutations in the long run.

In summary, we further examined the pathogenic activities of CDK19 de novo mutations Y32H and T196A in fly muscles, and found they act in a dominant negative fashion. The consistent results between patient skin fibroblast and fly muscles allow us to use fruit flies to further examine other features that are associated with CDK19 patients including potential therapeutic treatments.

4.4.1. Tissue specific subcellular localization suggests distinct pathogenic functions of CDK19 variants

We found expression of either variant in the *Cdk8* depleted background in adult IFM led to enhanced extensive mitochondrial morphology alterations along with increased myofibril width. These findings suggest that expressing the two variants results in comparable phenotypes. However, when we examined the localization of these variants in the IFM, the data indicated that the two variants have different localizations. HA detection of $CDK19^{Y32H}$ suggests that it has both nuclear and cytoplasmic localization, which is consistent with $CDK19^{WT}$. It may suggest that the mutation in Y32H still preserves partial function of wildtype CDK19; whereas localization of $CDK19^{T196A}$ is solely cytoplasmic in IFM (Fig. 4.1 d''', e'''). The differences in localization may explain the severity in lethality when these two lines are crossed to *nSybGal4* as shown in Table 4.1. However, we first need to confirm the localization of these variants in our assays before making further conclusion. In addition, we only examined the localization of these variants in adult indirect flight muscle, and they were previously shown in adult brains using neuronal driver *Elav-Gal4*[102]. We have limited information on their localization in different tissue types throughout development. Therefore, it will be crucial to examine their localizations in variety of tissue types including wing disc, salivary glands, larval nerve cord, larval body wall muscle in turn to conclude if these variants have potential tissue specific localization that could give clues as to their functions in causing DEE87.

The difference in the number of eclosed progeny when either $CDK19^{Y32H}$ or $CDK19^{T196A}$ is expressed in an *nSybGal4>Cdk8 RNAi* background suggests there is variation in pathogenic severity associated with these two variants (Table 4.1, Fig. 4.2). It may be associated with the amino acid position where the point mutation has taken place. While Y32H and T196A mutations both occur within the kinase domain of CDK19, the mutations are in different regions of the protein. Y32H is located within the glycine-rich loop, where ATP binding occurs, whereas T196A is found in the activation segment which promotes phosphorylation[101]. In addition, the property of the amino acids may also play a role in contributing pathogenic phenotypes. Tyrosine (Y) is one of the polar amino acids which is converted to a histidine (H), which depending on the environment and pH can also be polar; thus, it may not impact the native protein folding of CDK19 but may result in less affinity in binding of ATP. In the contrast, threonine (T) is mutated to an

alanine (A). Threonine is another polar amino acid, which can form hydrogen bonds because of its hydroxyl group (-OH). However, alanine is a hydrophobic amino acid. Mutating a polar amino acid to a hydrophobic one changes the properties dramatically, such that hydrogen bonding can no longer form. Further analyses on protein structure of these de novo variants are needed to investigate the property of these amino acids in contributing to pathogenic phenotypes.

One drawback from our assays is that we tried to mimic the patient condition where they have one copy of wildtype CDK19 with a copy of the variant. In our assays, we assumed that expressing *Cdk8* RNAi in a tissue specific fashion can provide a similar genetic background as seen in patients. However, we did not validate the percentage of knock down of *Cdk8* RNAi when it is expressed in the muscle. We may knock down more than 50 percent of endogenous Cdk8 under this condition. Thus, the phenotypes that we observed here with variants under *Cdk8* depleted condition may enhance the severity in phenotypes that we observed in patient variants. One way to circumvent this situation is to generate stocks of patient variants in a heterozygous *cdk8*-null allele background. This way, we can truly mimic the patient conditions and prevent potential skewing of data when we analyze the effects of patient variants using Drosophila.

4.4.2. NACA as potential treatment for patient with de novo mutations of CDK19

We showed the CDK19 and Cdk8 are conserved in regulating mitochondrial morphology, and expression of CDK19 wildtype can rescue the defective phenotypes caused by Cdk8 depletion in our assays. Furthermore, we demonstrated that expression of CDK19 variants further enhances the defective phenotypes caused by Cdk8. These data suggest that the variants are behaving as dominant negative. Our preliminary drug testing focused on wildtype flies and Cdk8 depleted flies raised on normal or NACA diet. The rescuing effect from NACA in restoring the climbing ability as well as mitochondrial morphology without affecting the wildtype flies made it a promising candidate for potential therapeutic treatment. However, we cannot imply or correlate what we observed in Cdk8 depleted flies will work the same in CDK19 patients. Thus, further testing is needed to test the ability of NACA on flies expressing CDK19 variants. We will examine the mitochondrial as well as muscle morphology between flies expressing patient variants that are raised on normal and NACA diet. Once, we have data on flies

expressing variants, we may move on with the drug testing using patient skin fibroblasts with our collaborators. We hope our findings in the flies can provide insights to clinicians.

Chapter 5. Role of SREBP-mediated lipogenic pathway in Parkinsonism

The work shown in **Chapter 5** is unpublished

5.1. Contribution to the chapter

The experiments in this chapter were carried out entirely by me.

5.2. Introduction

Cyclin dependent kinase 8 (Cdk8) has a well-known role in regulating transcription, and as a result can influence multiple pathways by upregulating or downregulating transcription factor activity[308].

Sterol-regulatory element binding protein (SREBP) is one of transcription factors that is found to be negatively regulated by Cdk8 in both Drosophila, mammalian hepatocytes, and mouse liver[309]. Depletion of Cdk8 and its partner Cyc C resulted in elevated lipid levels and lipogenic gene expression which is governed by pivotal activators such as SREBP[309,310]. SREBP target genes are responsible for biosynthesis of cholesterol, fatty acids, triglycerides and lipid droplets (LDs)[311–314]. Newly synthesized SREBP is inserted into the endoplasmic reticulum (ER) membrane as an inactive precursor. Reduction of cellular sterol levels or activated insulin signaling can trigger two subsequent proteolytic cleavages at the C-terminus of SREBP, releasing the soluble N-terminal domain of SREBP as nuclear SREBP (nSREBP). This allows nSREBP to translocate to the nucleus where it acts as an active transcription factor[137]. Three isoforms of SREBPs are found in vertebrates[311,312], whereas Drosophila has only one ortholog called SREBP[137]. It has been found that expression of CDK8 negatively regulates the stability of nSREBP-1c, one of the three isoforms found in vertebrates. In vitro kinase assays using extracted endogenous CDK8 from HEK293 cells along with recombinant GST-nSREBP-1c with different truncations identified threonine 402 as a direct target of CDK8[309]. Upon phosphorylation, the nSREBP fragment is subjected to degradation, marked with elevated levels of ubiquitin[309]. This threonine residue is well conserved across species including human, mouse, Drosophila and zebrafish[309]. Mutation of this residue to alanine (T402A) in nSREBP-1c completely abolished the regulative effect of CDK8, as T402A nSREBP-1c is stabilized at the protein level in comparison to gradually reduced protein levels of wildtype nSREBP in the presence of CDK8. This finding indicates that CDK8 and its partner CycC act as suppressors of SREBP-1c mediated de novo lipogenesis by regulating the protein levels of the transcription factor[138,315].

In Drosophila, SREBP plays a critical role in determining the larval-pupal transition based on the abundance of lipid content in larvae[310]. In addition, elevated transcript levels of SREBP are associated with fly model of Alzheimer's Disease, where

dysfunctional mitochondria triggered elevated ROS levels, which subsequently lead to neurodegeneration[305]. Furthermore, the authors found transient accumulation of lipid droplets in the glial cells, which is likely due to the elevated SREBP activity promoting the lipogenesis pathway. Expression of antioxidant genes in the same Alzheimer's model can suppress the accumulation of LD as well as delay neurodegeneration[305].

Interestingly, studies on lipid metabolism have started to garner increasing attention for their role in understanding the underlying pathogenesis of neurodegeneration in the last decade[316–318]. A growing number of causative genes and risk loci for Parkinson's disease have also been implicated in lipid metabolism, including PLA2G6/PARK14, and GBA[253,319,320]. *PLA2G6* encodes calcium-independent phospholipase A2 β (iPLA2β), an enzyme that catalyzes the hydrolysis of glycerophospholipids. This enzyme is particularly abundant in the brain. Mouse and fly models of iPLA2β mutants have shown motor defects, autophagic dysfunction, the degradation of axons and synapses, mitochondrial abnormalities that mimic symptoms from patients with PD[321–323]. *GBA* encodes Glucocerebrosidase (GCase), which forms ceramide through the hydrolysis of glucosylceramide. Mutations in either *PLA2G6* or *GBA* lead to elevated level of ceramide in both patients with neurodegeneration as well as in model organisms[324–326]. Lowering the levels of ceramide or enhancing the recycling of lipids can alleviate defective phenotypes associated with a fly PD model[323].These findings further emphasize the need to understand the role of lipid metabolism in pathogenesis of neurodegeneration.

Given the connection between SREBP and Cdk8, as well as its association with the onset of neurodegeneration, we further wondered about the role of SREBP in the *pink1*^{B9} Parkinsonism model. In this chapter, we investigated whether modulation of the SREBP-mediated lipogenic pathway affects the *pink1*^{B9} mediated PD model, as well as testing its role in regulating mitochondrial morphology.

5.3. Result

5.3.1. *pink1* mutation leads to elevated mRNA levels of SREBP

Oxidative stress has been shown to enhance the transcript level of *SREBP* in human hepatic cell line HepG2[327,328] and animal models[305,329]. We and others have shown that there is significantly elevated ROS production in the *pink1* mutant background in comparison to control, FM7/Y (Chapter 3)[285,330,331]. To test the model that elevated ROS could lead to increased *SREBP* transcription, we performed qRT-PCR to test the mRNA levels of *SREBP* in control and *pink1* mutant tissues using mRNA prepared from three days old adult thoraxes which are enriched in IFM (Fig. 5.1). Our preliminary data found that *pink1* transcription in the mutant background is almost undetectable, which confirmed the null phenotype of our mutant line (Fig. 5.1). Furthermore, we found there is an almost three-fold increase in mRNA levels of *SREBP* in the *pink1* mutant background compared to the *FM7/Y* control flies. These findings indicate that enhanced SREBP mRNA levels leading to its enhanced lipogenic activity are found in the *pink1* mutant background. Two of the key target genes of SREBP are *Fasn1* and *Acc*. These genes encode two enzymes that are involved in fatty acid synthesis. Acc functions in the first committed step of fatty acid synthesis where acetyl-CoA is converted to malonyl-CoA in an ATP dependent fashion[332]. Fasn1 participates in the following step to convert malonyl-CoA to long-chain fatty acid that can serve as the building blocks for cholesterol, fatty acids, triglycerides and lipid droplets (LDs)[333].

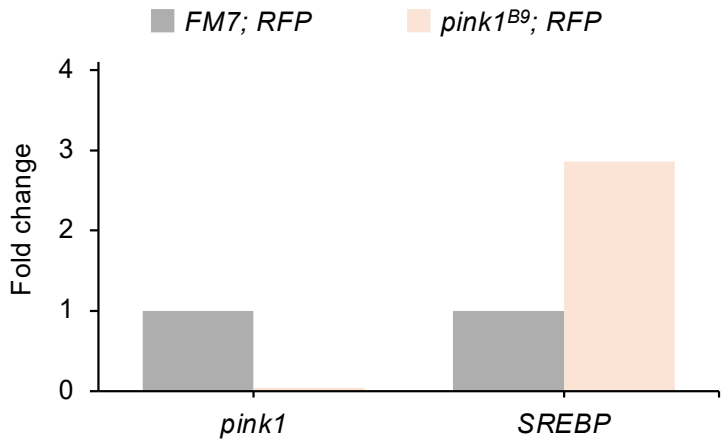

Figure 5.1. Mutation in *pink1* causes elevated mRNA level of SREBP.

qRT-PCR analysis of *pink1* and *SREBP* gene expression in FM7/Y and $pink1^{B9}$ in a *Mef2>mitoGFP* background. Data are mean, n = 2 independent experiments.

5.3.2. Suppressing the lipogenic pathway can rescue phenotypes in a *pink1^{B9}* mediated familial Parkinsonism model

Given that expression of *SREBP* is elevated in a *pink1* mutant background (Fig. 5.1), we wondered whether some of the mutant phenotypes might be caused by elevated lipogenesis resulting from increased SREBP levels. We therefore asked if suppressing the lipogenic pathways have any rescuing effect on the *pink1^{B9}* mutant flies by examining the thorax indentation and climbing abilities (Fig. 5.2a, respectively). To interfere with lipogenesis, we took advantage of a dominant negative transgene of SREBP where the first 75 amino acids of nSREBP are deleted, rendering it unable to enter the nucleus. We also expressed *Fasn1* RNAi to deplete on of the key factors in the lipogenic pathway. Both of these were expressed in the *pink1* mutant background, using two independent transgenes for each. Consistent with our proposed mechanism, we found that expressing either SREBP^{DN} or *Fasn1* RNAi in the *pink1* mutant background could rescue the muscle degeneration, as we observed a significant rescue in thorax indentation (Fig. 5.2a). In addition, we found a significant rescue in climbing ability when the lipogenic pathway was suppressed in a *pink1* mutant background (Fig. 5.2b) These data suggest that suppressing the lipogenic pathway has beneficial effects in rescuing defects in a *pink1* mutant PD model.

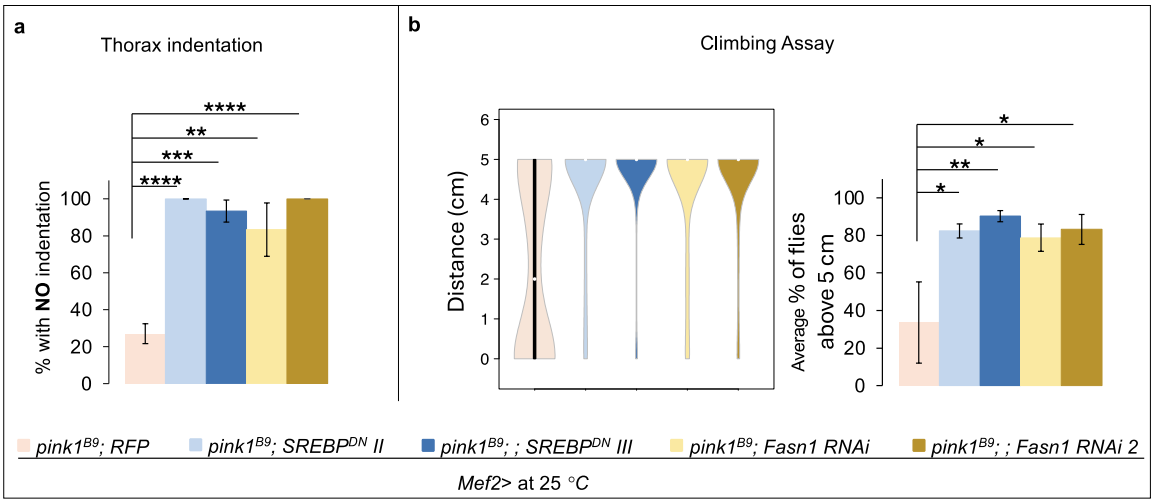

Figure 5.2. Knocking down components of lipogenic pathway can rescue the thorax indentation and climbing ability caused by *pink1^{B9}* mutants.

(a) Quantification of percent with no indentation in 3-day-old flies expressing either RFP, SREBP^{DN} II, SREBP^{DN} III, Fasn RNAi, or Fasn RNAi 2 with Mef2-Gal4 in the *pink1^{B9}* mutant background compared to *pink1* mutant flies. (b) Violin plots showing the distribution of climbing activity of RFP, SREBP^{DN} II, SREBP^{DN} III, Fasn RNAi, or Fasn RNAi 2 with Mef2-Gal4 in the *pink1^{B9}* background. The average percent of flies that reach the target line in indicated genotypes.

Modulating expression of lipogenic pathway components alters mitochondrial morphology under physiological conditions

We found that suppressing the lipogenic pathway can rescue defective phenotypes including thorax indentation and climbing ability in a *pink1*-mediated PD model. Since Pink1 is a well-known regulator in maintaining the homeostasis of mitochondria as I described in previous chapters, we next wondered whether mitochondrial morphology is affected when the lipogenic pathway is modulated. To address this question, we examined the mitochondrial morphology in larval body wall cells when expression of some of the lipogenic pathway components including SREBP, acetyl-CoA carboxylase (Acc) and fatty acid synthase 1 (Fasn1) are modulated. Expression of two different lines of $SREBP^{DN}$ leads to spherical shapes of mitochondria in comparison to control (Fig. 5.3b-b', c-c'). However, the morphology of mitochondria was shifted to hypertubular structures when $SREBP^{CA}$ (constitutively active, expressing only the soluble nSREBP fragment)[334] is expressed (Fig. 5.3d-d'), which indicates that there is a potential role of fatty acid metabolism in shaping mitochondrial morphology. Interestingly, a recent publication looking at larval fat bodies, which is the predominant tissue for regulating lipid homeostasis in Drosophila, found that expressing *Fasn1 RNAi* results in reduced mitochondrial mass along with some blebby mitochondria with highly electron-dense matrix and vacuolar structures[335]. Despite the tissue difference, our quantification data also indicates reduced mitochondrial area with relatively spherical morphologies when *Fasn1 RNAi* is expressed in comparison to control (Fig. 5.3j).

Next, we examined the morphology when Acc, the rate limiting enzyme that participates in fatty acid synthesis is modulated. We found phenotypes in mitochondria consistent with those we saw after modulating SREBP expression (Fig. 5.3e-e', f-f'). We found round-shaped mitochondria associated with depletion of *Acc*, whereas filamentous morphology is found in muscles expressing wildtype Acc. Furthermore, depletion of *Fasn1* RNA results in similar phenotypes as seen with expressing $SREBP^{DN}$ and *Acc* RNAi (Fig. 5.3g-g'). We quantified the mitochondrial morphology using MiNA, as defined previously (Fig. 2.3). We found there is significant reduction in mitochondrial length, branching and mitochondrial area when the lipogenic pathway is suppressed in general (Fig. 5.3h-j). Overexpression of either SREBP or Acc leads to significant increases in branching (Fig. 5.3i). Altogether, we found that modulating the expression of components that participate in the lipogenic pathway can significantly alter the

mitochondrial morphology, where elevated lipogenic pathway promotes elongation of mitochondria, and suppressed lipogenic pathway leads to fragmentation of mitochondria.

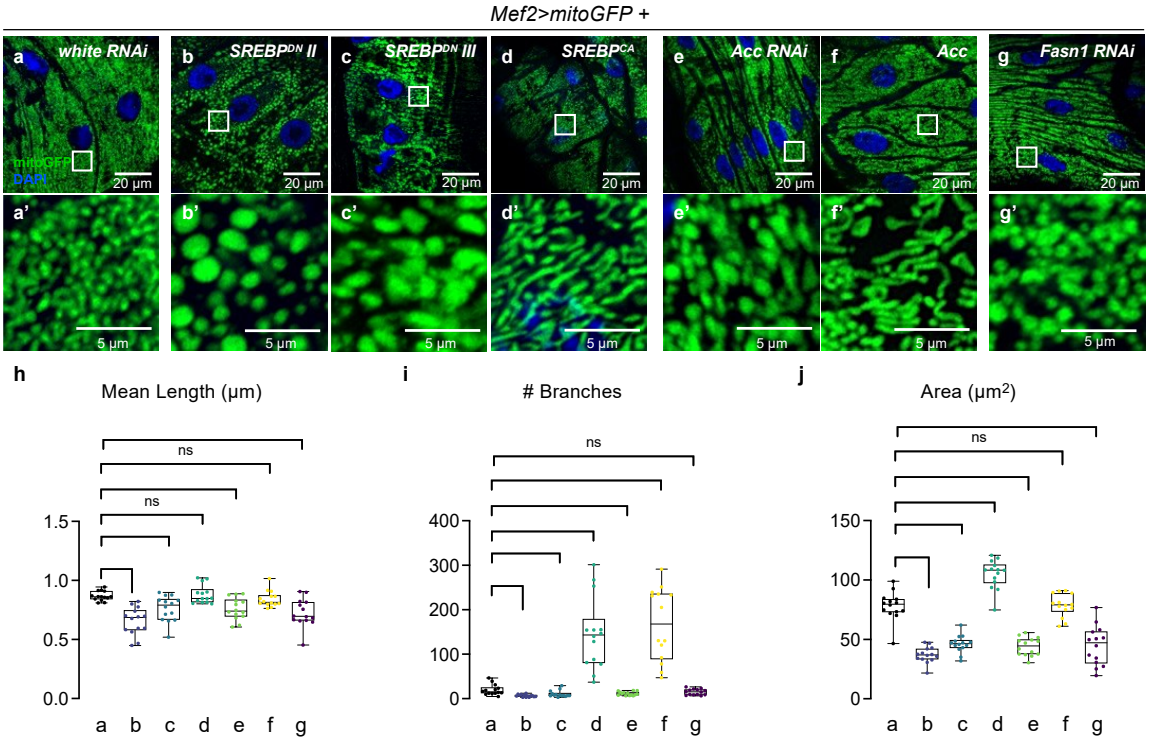

Figure 5.3. Expression of SREBP mediated lipogenic pathway alters mitochondrial morphology under physiological condition

(a–g) Mitochondrial morphology of larval body wall muscles in (a) w^{1118} control or expressing (b) $SREBP^{DN}$ II, (c) $SREBP^{DN}$ III, (d) $SREBP^{CA}$, (e) Acc RNAi, (f) Acc and (g) Fasn RNAi with Mef2-Gal4>mitoGFP, raised at 29 °C. Scale bar: 20 µm. (a'–g') Representative magnified sections from (a–g). Scale bar: 5 µm. (e–g) Quantification of mitochondrial morphology showing the (h) the mean mitochondrial length, (i) the number of branches, and (j) the mitochondrial area in larval body wall muscles of the indicated genotypes. All in comparison to *w1118*. Letters (a–g) refer to the genotypes shown in panels (a–g). Quantifications were calculated by the MiNA toolset. n = 5 per genotype. Data were presented as box plots (center line at the median, upper bound at 75th percentile, lower bound at 25th percentile) with whiskers at minimum and maximum values. An unpaired two-tailed t-test is used to generate the statistics. ∗p < 0.05, ∗∗p < 0.01, ∗∗∗p < 0.001, ∗∗∗∗p < 0.0001, ns no significance.

5.3.3. SREBP-mediated target gene expression is altered in response to change in Cdk8 expression

It has been shown that Cdk8 negatively regulates the SREBP-mediated lipogenic pathway, where Cdk8 phosphorylates the master transcription factor SREBP, in turn to promote degradation of nSREBP and ultimately results in downregulation of the lipogenic pathway. Elevated mRNA levels of *Acc*, *Fasn 1* as well as acetyl-CoA synthetase (*acs*) were observed in both *Cdk8*- and *Cyc c* null mutants[315]. To replicate their findings, we prepared RNA samples from third instar larvae expressing either *RFP* or *Cdk8* RNAi ubiquitously and compared the mRNA levels of *acc* and *Fasn 1* between the two genotypes using qRT-PCR (Fig. 5.4a). We found a significant increase in *Fasn 1* transcripts when *Cdk8* is knocked down ubiquitously using *Act5c-Gal4,* while mRNA levels of *acc* seems unaffected by the knockdown of Cdk8. Since Acc is the rate limiting step in fatty acid biosynthesis pathway, we performed the qRT-PCR again using lines expressing either RFP or wildtype Cdk8 using a slightly weaker Gal4 driver (Arm-Gal4) to avoid protein toxicity, since we had previously found that expression of wildtype Cdk8 with Act5c was lethal (Fig. 5.4b). We found significant reductions in mRNA levels of *acc* and *Fasn 1* when Cdk8 is ectopically expressed. This finding along with previous data on *Cdk8* depletion confirms that Cdk8 normally suppresses SREBP target gene expression.

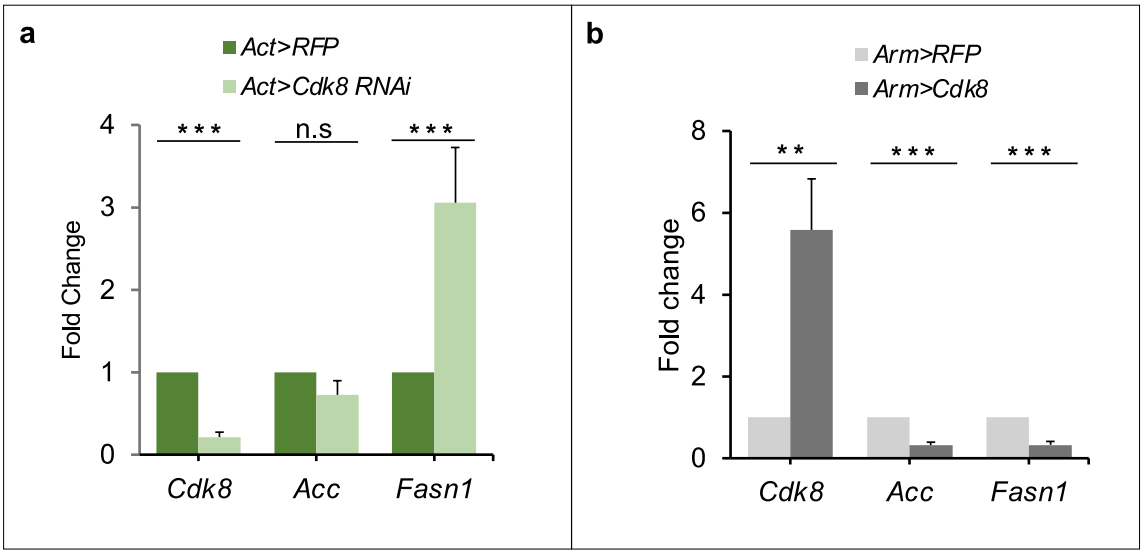

Figure 5.4. Expression of Cdk8 negatively regulates transcription of two components in the lipogenic pathway

(a) qRT-PCR analysis of acetyl-CoA carboxylase (acc) and fatty acid synthase 1 (*Fasn1*) gene expression in Act5c>Cdk8 RNAi relative to control sample (Act5c>RFP). (b) qRT-PCR analysis of acetyl-CoA carboxylase (acc) and fatty acid synthase 1 (*Fasn 1*) gene expression in Arm>Cdk8 relative to control sample (Arm>RFP). Data are mean ± SD. n = 3 independent experiments. Unpaired two-tailed t-test is used to generate the statistics.

5.4. Discussion

In this chapter, we examined the role of the SREBP-mediated lipogenic pathway in both diseased and physiological conditions. We found enhanced SREBP transcription in *pink1* mutant flies. Suppressing the lipogenic pathway by expressing a dominant negative version of SREBP or Fasn 1 RNAi in the *pink1* mutant background can significantly restore both muscle degeneration (as seen by thorax indentation) as well as climbing defects. Furthermore, we examined the mitochondrial morphology when components of the lipogenic pathway were modulated under physiological conditions. In general, we found suppression of the lipogenic pathway leads to fission-like mitochondrial morphology while expression of a constitutively active form of SREBP or wildtype Acc leads to fusion-like mitochondrial morphology. Lastly, it has been previously shown that Cdk8 can negatively regulate the stability of nSREBP-1c, and our qRT-PCR data further validated this finding as expression of *acc* and *Fasn 1* is significantly reduced when Cdk8 is overexpressed. This leads to a complex interplay of SREBP with its transcriptional targets as well as being regulated by Cdk8. Our challenge is to determine if these events can be functionally separated.

5.4.1. SREBP is identified as a risk locus for Sporadic Parkinson's disease

Our findings suggest that elevated SREBP and its downstream targets participate in a *pink1*-mediated Parkinsonism model. Suppressing the lipogenic pathway can restore the defective phenotypes that are caused by the $pink1^{B9}$ mutation. The *SREBP* locus was identified in genome wide associated studies (GWAS) as one of the risk factors for the occurrence of Sporadic Parkinson's disease[336]. Later, a genome wide genetic screen using both Drosophila S2-R+ cells and human HeLa cells identified that SREBP acts as a positive regulator of mitophagy by promoting the translocation of Parkin from the cytoplasm to mitochondria[337]. These findings seem contradictory at first with our data since we find that SREBP expression promotes mitochondrial fusion rather than mitophagy. We found that suppressing SREBP can be beneficial in the PD model, whereas they found expressing SREBP promotes mitophagy. The difference can be context-specific, as we examined the effect of SREBP in a *pink1* mutant background, where they examined the function of SREBP under physiological condition with presence of endogenous PINK1 and Parkin. Furthermore, the authors found that the

ability of SREBP to promote translocation of Parkin requires Pink1 to be stabilized on the outer mitochondrial membrane first. Since they did not examine the effect of SREBP in the absence of *pink1*, it left the question unanswered.

Here, we demonstrated that the SREBP-mediated lipogenic pathway is transcriptionally active in the absence of *pink1*, and suppressing the SREBP-mediated lipogenic pathway can rescue defective phenotypes associated with *pink1* mutant. Our finding is consistent with the model where accumulation of ceramide is found in the *pink1* mutant flies[322,326] as well as in patient derived fibroblast with *PINK1* deficiency[326]. In addition, Vos et al. found accumulated ceramide is accompanied with reduced β-oxidation in *pink1* deficient flies and patient fibroblasts, which is the process in which fatty acids are broken down to generate acetyl-CoA that provides substrates for the cellular energy production in mitochondria and peroxisomes[338]. They found lowering the level of ceramides can revert the defective phenotypes associate with *pink1* mutant including restoring the electron transport chain function as well as stimulating β-oxidation[326]. It would be interesting to test the ceramide level in our model when the SREBP-mediated lipogenic pathway is suppressed in a *pink1* mutant background. Since SREBP controls the biosynthesis of de novo lipogenesis, suppressing SREBP and its downstream target may have a similar effect as reducing the overall ceramide level that can be accumulated in *pink1* mutant.

In addition, it would be interesting to see how translocation of Parkin is affected under such circumstances. Furthermore, it has been previously shown that elevated ROS can lead to elevated SREBP activity[305,327,329]. It would be interesting to see if supplementing antioxidants in the same mutant background can suppress the elevated SREBP levels in a $pink1^{B9}$ background. Altogether, our data suggests that elevated SREBP may be associated with the defective phenotypes in the *pink1* mutant background as suppressing the lipogenic pathway can significantly restore the defects.

5.4.2. Role of fatty acid and lipid in neurodegeneration

Imbalanced homeostasis of lipids has been found to have implications in several neurodegenerative disorders including Amyotrophic lateral sclerosis (ALS)[339], Parkinson's disease (PD)[340], Alzheimer's disease (AD)[341,342], and Huntington's Disease (HD)[343]. One of the lipids that has been identified to play a role in PD pathogenesis is

cardiolipin[344]. Cardiolipin is a mitochondrial specific lipid that functions in the organization of ATP synthase in mitochondria and participates in mitochondrial dynamics[345,346]. Interestingly, it is found that expressing Fasn RNAi in the *pink1* mutant background can restore the lowered enzymatic activity of complex I[182,347]. The rescuing effect is likely due to increased levels of mitochondrial cardiolipin, as supplementing cardiolipin to mutant flies completely restores complex I activty[344]. Synthesis of cardiolipin depends on the abundance of unsaturated phosphatidyl glycerol[348–350]. Increased unsaturated phosphatidyl glycerol is found in *Pink1* mutant MEF sample when Fasn is suppressed. In addition, increased level of mitochondrial cardiolipin is detected when Fasn is depleted under *pink1* mutant background in Drosophila[344]. Findings in both mouse and fly model with Pink1 deficiency suggest loss of Fasn results in increases in mitochondrial cardiolipin. In their findings, pharmacological inhibition of Fasn rescues flight defects and reduced ATP levels in Pink1 deficient flies. Furthermore, Fasn is known have conserved functions in regulating the synthesis of fatty acid palmitate [351]. Indeed, reduced palmitate levels are found when Fasn RNAi is expressed in the *pink1* mutant background. Vos et al.'s findings establish a new pathway where altering fatty acid level can be beneficial to rescue *pink1* mutant mediated PD model. Since we found similar rescuing ability when we knocked down Fasn 1 RNAi or expressed Cdk8 in the PD model, it would be interesting to test the palmitate level as well as the abundance of cardiolipin in mutant flies with Cdk8 overexpression in comparison to negative control and mutant flies alone. It may provide more insight on how Cdk8 regulates mitochondrial morphology.

It has been shown that palmitate can induce ceramide synthesis in monocytes[352], macrophages[353], as well as in porcine oocytes[354]. It would be interesting to test if the rescuing effect that we observed with suppressing SREBP-mediated lipogenic pathway in *pink1* mutant flies is due to reducing overall palmitate level, which in turn could prevent ceramide accumulation in the mutant flies (Fig. 5.5).

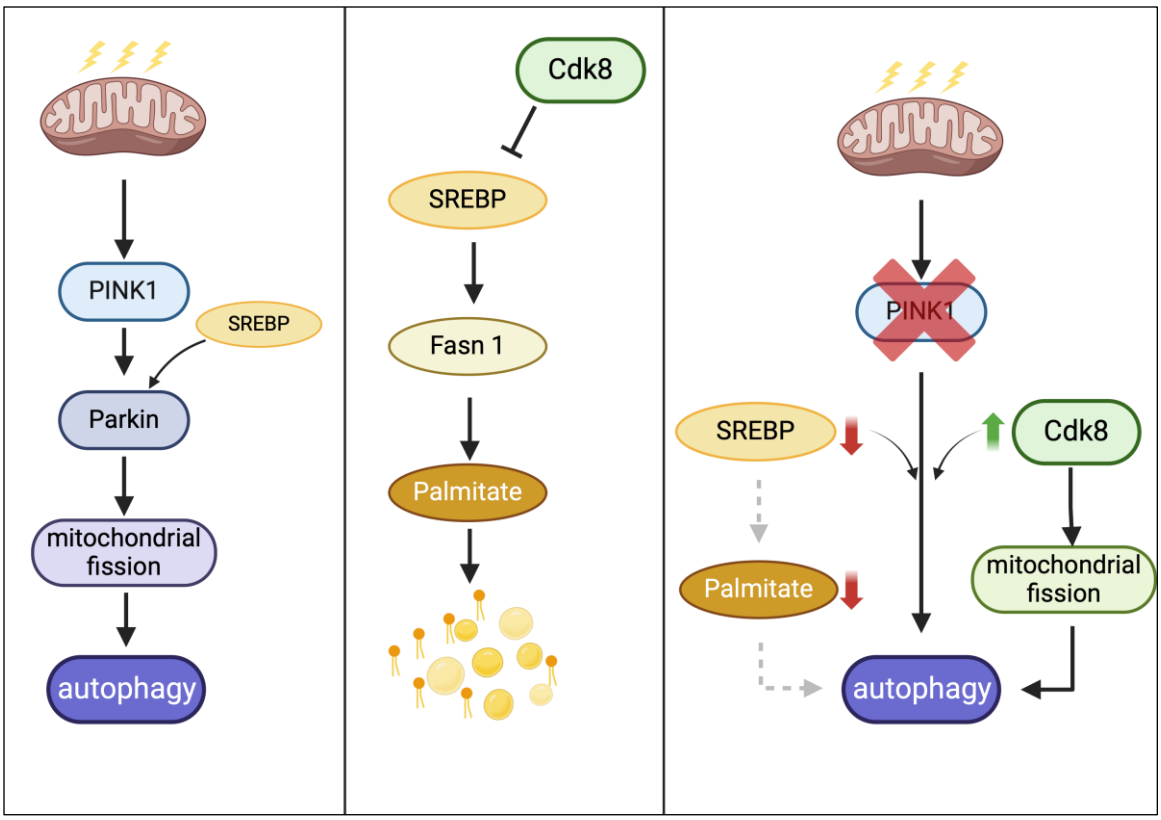

Figure 5.5. Function of SREBP in Pink1/Parkin mediated mitophagy pathway and its role in lipogenic pathway.

SREBP is identified as a risk factor for Parkinson's disease, and is found to participate in the Pink1/Parkin mediated mitophagy pathway by promoting the translocation of Parkin from cytosol to outer membrane of mitochondria in the presence of Pink1 (Left). In addition, SREBP is a known master transcription factor for synthesis of fatty acid and lipid. Enhanced expression of SREBP ultimately results in elevated lipogenic pathway by elevating the expression of *Fasn 1*, which is one of main enzymes for generating palmitate, a saturated long chain fatty acid. Interestingly, Cdk8 is identified as a negative regulator of SREBP; thus, expressing Cdk8 is the same as suppressing SREBP-mediated lipogenic pathway (Middle). We found expressing ectopic Cdk8 in the *pink1* mutant background can restore the mitophagy by enhancing the phospho-status of Drp1, which in turn promoting mitochondrial fission. On the other hand, we found suppressing SREBP-mediated lipogenic pathway can also restore the phenotypic defects under the *pink1* mutant background. The underlying mechanism is still unknown. Since accumulation of ceramides is found in neurodegeneration, as well as in the *pink1* mutant background. Suppressing the SREBP-lipogenic pathway may reduce the overall level of ceramide by reduced palmitate synthesis. Palmitate has been implicated in promoting ceramide production in different cell types. Thus, the rescuing effect that we observed in suppressing SREBP-mediated lipogenic pathway may explain by the overall reduced ceramide (Right). Figure generated by Biorender.

Chapter 6. Conclusion

Cyclin-dependent kinase 8 (CDK8) plays a crucial role throughout development as it was demonstrated that depletion of CDK8 can cause lethality during the embryonic stage in mice, causes larval lethality in fruit flies, and causes lethality in both embryonic and larval stages in *C. elegans*[132]. Furthermore, CDK8 and its paralog CDK19 have been shown to exert specific functions. For instance, the Cdk8 kinase module regulates axon guidance in *C. elegans,* and the kinase activity of both CDK8 and CDK19 are required for proper craniofacial formation in zebrafish[105]. The recent finding of *de novo* mutations in CDK8 and CDK19 in patients with neurological disorders further demonstrated their essential functions in neurogenesis[101–106].

We utilized the power of genetics in Drosophila to further characterize the functions of Cdk8 throughout development and organismal homeostasis. We observed phenotypic differences between Cdk8 depleted flies and control flies including reduced survival rate, pupal lethality, locomotion defect, infertility, and abnormal wing postures (Figs. 2.1, 2.2). These phenotypes were observable because we did not completely deplete Cdk8, which would have led to lethality before adult stages. Mitochondria are known for generating cellular energy in the form of ATP that is required for an organism to survive and thrive. In addition, impaired mitochondria are found to be associated with infertility in both flies and mice[156,157,355]. All the information directed us to further investigate the mitochondria in muscles, a tissue that utilize abundant cellular energy. We found expression of Cdk8 plays a novel function in regulating mitochondrial morphologies by directly interacting with the fission regulator, dynamin-related protein 1 (Drp1) (Figs. 2.13-2.15).

The phenotypes that we observed in Cdk8 depleted flies (Figs. 2.1-2.5, 2.10) resembled defective phenotypes that are found in fly models of Parkinson's disease (PD) [92,157,167,166,100–102], which led us to further characterize the function of Cdk8 in a neurodegenerative disease setting. We found expression of Cdk8 suppresses muscle degeneration, restores mitochondrial integrity without activating expression of the antioxidant genes that are often found to be elevated under disease setting with increased ROS (Figs. 3.2-3.4). We further demonstrated that Cdk8 rescues the impaired mitophagy in the *pink1* mutant background by re-activating Drp1[167,215,216]. In the

collaboration with Dr. Bellen on their CDK19 project, we characterized the function of CDK19, the human ortholog of fly Cdk8 (Figs. 3.9, 3.11-3.13). We found introducing CDK19 in the fly system also rescues defective phenotypes in a PD model to same extent as fly Cdk8. Furthermore, we demonstrated that CDK19 shares conserved function with fly Cdk8 in regulating mitochondrial morphology, and both Cdk8/CDK19 have tissue-specific subcellular localizations, which suggests cytoplasmic functions of Cdk8/CDK19.

The conserved function between Cdk8/CDK19 led us further utilized the power of genetics in flies to characterize two *de novo* mutations in CDK19 that are found to be recurrent among patients with DEE87. Introducing the two variants in a Cdk8 depleted background failed to suppress the increased muscle fibre width and elongated mitochondria in Cdk8 depleted condition (Fig. 4.1). Instead, the expression of the variants further enhanced the phenotypes, suggesting the two variants may behave in a dominant negative fashion (Figs. 4.1, 4.2). Preliminary data from Bellen' group on patient skin fibroblast further validated our findings of hyperfused mitochondrial morphologies. To provide potential therapeutic insight, we performed a drug test using NACA, and preliminary data suggests it can be beneficial in restoring the climbing defects as well as mitochondrial morphology associated with Cdk8 depletion (Figs. 4.4, 4.5).

Lastly, we examined the role of SREBP-mediated lipogenic pathway in mitochondrial morphology as well as in PD setting. Interestingly, SREBP is a GWAS risk locus in PD, and it is found to participate in the Pink1/Parkin mediated mitophagy. On the other hand, SREBP is negatively regulated by Cdk8, where Cdk8 phosphorylates and destabilizes its nuclear localization. We found suppressing the SREBP-mediated lipogenic pathway has the same effect as Cdk8 overexpression in regulating mitochondria morphology as well as in rescuing PD associated defective phenotypes (Fig. 5.2). How Cdk8 and SREBP function in mitochondria in the context of physiological condition or disease setting remained to be discovered.

6.1. Identifying a new role for Cdk8 in the cytoplasm

The subcellular localizations that we detected using Cdk8::GFP indicates that Cdk8 may have cytoplasmic localization in some contexts. For decades, researchers have focused on the nuclear function of CDKs. However, it is known in general that

CDKs with their binding partner Cyclins can shuttle in and out of the nucleus[58]. Among the cell-cycle related CDKs, translocation of CDKs is an approach to distinguish the inactive and active status of CDK complexes[58]. Most of the CDKs involved in the cell cycle rely on their Cyclin partners to activate their activities[27]. Once activated, CDKs exert their kinase activity on their downstream targets in proximity. Changes in subcellular localizations prevent unnecessary phosphorylation from the CDK complexes. For instance, CDK1/Cyclin B and CDK4/Cyclin D are found to have cytoplasmic localizations[60]. CDK1 complexes shuttle between nucleus and cytoplasm, and depending on the condition, CDK1 complexes translocate to mitochondria to promote cellular energy generation that is required for cell cycle progression[56]. Despite the fact that the functions of transcription-related CDKs are mainly inside the nucleus, the subcellular localizations of those CDKs are not solely located in the nucleus. For instance, CDK7 is found to be present in the cytoplasm in A549 human lung carcinoma cells [88,89], and CDK13 is found in the cytosol and Golgi apparatus when expressed in SiHa cells and HeLa cells, respectively. Interestingly, a recent study showed that CDK8 is primarily localized in cytoplasmic in murine pancreatic cells where it regulates insulin secretion[235], which is in line with our observation on Cdk8. While the function associated with their changed subcellular localization is not well defined, it demonstrates that CDKs do change their subcellular localizations in a context-dependent condition. Thus, it has not surprising to detect cytoplasmic localization for Cdk8.

The immunolabelling data along with co-immunoprecipitation data from Cdk8::GFP (Fig.3.10 and Fig.2.15) indicate that Cdk8 interacts with Drp1 in the cytoplasm. Interestingly, it has been shown that Drp1 can be regulated by CDK1 and CDK5 at the same S616 site by phosphorylation[210,213,214]. Thus, it is not surprising to see that Cdk8, another member of CDKs can exert its kinase function on Drp1 at the same residue. Altogether, we demonstrate that Cdk8 has cytoplasmic localization, and is interacting with Drp1 directly in the cytoplasm to exert its kinase activity.

6.2. The challenge to demonstrate non-nuclear functions of CDK19 in a tissue specific fashion

It is difficult to address the cytoplasmic function of CDK19$^{\Delta NLS}$ in a Cdk8 depleted background, as some argued that the remaining nuclear function of Cdk8 in the background may alter the results. A challenge in any overexpression study is to

differentiate between something a protein can do, and something a protein normally does. To prevent confounding factors, one approach we took was to make sure all the crosses have same numbers of UAS transgenes included when we examined the function between $CDK19^{WT}$ and $CDK19^{\Delta NLS}$ in indirect flight muscles, so that we could rule out any titration of Gal4 proteins as causing different effects between wildtype and cytoplasmic CDK19 (Fig. 3.12b-e). The immunolabelling of indirect flight muscles in Fig. 3.9 validated the predicted nuclear localization sequence, as no detectable $CDK19^{\Delta NLS}$ overlapped with nuclei (Fig. 3.9c). In contrast, the immunolabelling of $CDK19^{WT}$ demonstrates it had nuclear and cytoplasmic localization, which further indicates a potential cytoplasmic role of $CDK19^{WT}$. To distinguish between the potential cytoplasmic and nuclear function of CDK19, we relied on the muscle and mitochondrial morphologies in a Cdk8 depleted background (Fig. 3.12b-e). Expression of either $CDK19^{WT}$ or $CDK19^{\Delta NLS}$ alters the mitochondrial morphology from elongated to fragmented in the same Cdk8 depleted background, suggesting the function that regulates mitochondria is likely to be cytoplasmic, as expression of $CDK19^{\Delta NLS}$ resulted in similar mitochondrial morphology and muscle fiber width as expressing $CDK19^{WT}$. The only difference between the two CDK19 lines is the localization. Thus, these findings indicate the cytoplasmic function of Cdk8/CDK19 is regulating the mitochondrial morphology. We further analyzed the effect of expressing the CDK19 lines using a neuronal-specific driver, *ElavGal4* and examined the climbing ability between the lines in a Cdk8 depleted background (Fig. 3.12a). The rescuing effect of $CDK19^{\Delta NLS}$ in climbing ability seems better compared to $CDK19^{WT}$, suggesting the cytoplasmic function of CDK19 is required for proper neuronal development[102].

In all the assays, we cannot completely rule out the nuclear function of Cdk8/CDK19 as depletion of Cdk8 left a small fraction of endogenous Cdk8 present in the flies (Figs. 3.9, 3.11, 3.12). We cannot comment on the nuclear effects of Cdk8 in regulating mitochondrial morphology without generating RNAseq data. We could also perform IP-MS to detect protein interaction partners using Cdk8::GFP to determine which exclusively cytoplasmic proteins interact with endogenously tagged Cdk8. We cannot rule out the potential that Cdk8 may also regulate mitochondrial dynamics at transcriptional level through its effect on SREBP; however, the fact that expressing $CDK19^{\Delta NLS}$ shifts mitochondrial morphology demonstrates its cytoplasmic function in regulating mitochondria at least in the muscle. Dual functions of Cdk8

In previous chapters, we found that expression of Cdk8 promotes fragmentation of mitochondria, whereas depletion of Cdk8 leads to elongation of mitochondria (Figs. 2.3, 2.4). Furthermore, we found ectopic expression of Cdk8 can rescue the defective phenotypes caused by *pink1* mediated Parkinsonism model (Figs. 3.2-3.4). These observations are likely due to the interaction with the fission regulator, Drp1, as we found elevated level of phospho-Drp1 when Cdk8 is overexpressed (Fig. 2.12). Strikingly, we found similar effects on *pink1* when the SREBP-mediated lipogenic pathway is inhibited (Fig. 5.2). We found suppressing the lipogenic pathway in the *pink1* mutant background restored numerous defective phenotypes (Fig. 5.2). In addition, inhibiting the lipogenic pathway leads to round-shaped mitochondria, and enhanced lipogenic pathway function promotes hypertubular structure of mitochondria (Fig. 5.3). Interestingly, both Li's group[138] and our data indicate that Cdk8 can negatively regulate the SREBP-mediated lipogenic pathway at the transcriptional level. These findings led us to question if the rescuing effect of Cdk8 is an additive effect that is achieved by suppressing the SREBP-mediated lipogenic pathway and promoting activity of Drp1 by phosphorylation.

Researchers have linked the change in mitochondrial architecture with nutrient supply and energy demand[190]. They found mitochondrial fission can be induced under nutrient-rich conditions in different cell types [193,356–358]. Furthermore, physiological fragmentation is found to increase the fatty acid utilization through fatty acid oxidation (FAO) in brown adipose tissue. In a recent publication, Ngo et al. found a strong correlation between mitochondria fission and rates of fatty acid oxidation (FAO) in HepG2 hepatocarcinoma cells[359]. The authors measured the oxygen consumption rate (OCR) in respirometry assays to determine the rate of FAO. They found a significant increase in FAO when the fusion regulator MFN is depleted. Supplementing excess nutrients under otherwise physiological conditions elevates the rate of FAO along with fragmentated mitochondrial morphology. However, when they expressed a dominant negative version of DRP1 under the same excess nutrient condition, the rates of FAO stayed at basal level. All these data suggest that the fission morphology of mitochondria drives FAO, potentially as a cause-and-effect relationship. These findings are interesting, because in our *pink1*-mediated Parkinsonism model, we found elevated SREBP transcription. Although we did not determine the level of lipids present in the *pink1* mutant background, it has been showed there is accumulation of lipids in the form of lipid droplets in neurodegenerative models with impaired mitochondria[305].

In the *pink1*-mediated Parkinsonism model, ectopic expression of Cdk8 has dual functions (Fig.6.1). First, expression of Cdk8 suppresses the expression of SREBP target genes involved in the lipogenic pathway. Although we do not have data to show mRNA levels when Cdk8 is expressed in the *pink1* mutant background, we suspect the levels of mRNAs of SREBP or its downstream targets such as *acc* and *Fasn1* will be reduced. Furthermore, Cdk8 can promote mitochondrial fission via phosphorylation of Drp1[167]. Activating Drp1 not only restores the homeostasis of mitochondria in the *pink1* background; furthermore, mitochondrial fission drives FAO, which helps to reduce the amount of lipid that is accumulated in the *pink1* mutant background. These findings indicate that Cdk8 has dual function in both regulating the transcriptional level of SREBP-mediated downstream lipogenic pathway, as well as indirectly enhancing the rate of FAO by promoting mitochondrial fission, and increased FAO under the mutant background can ultimately result in reduced lipid accumulation. (Fig.6.1).

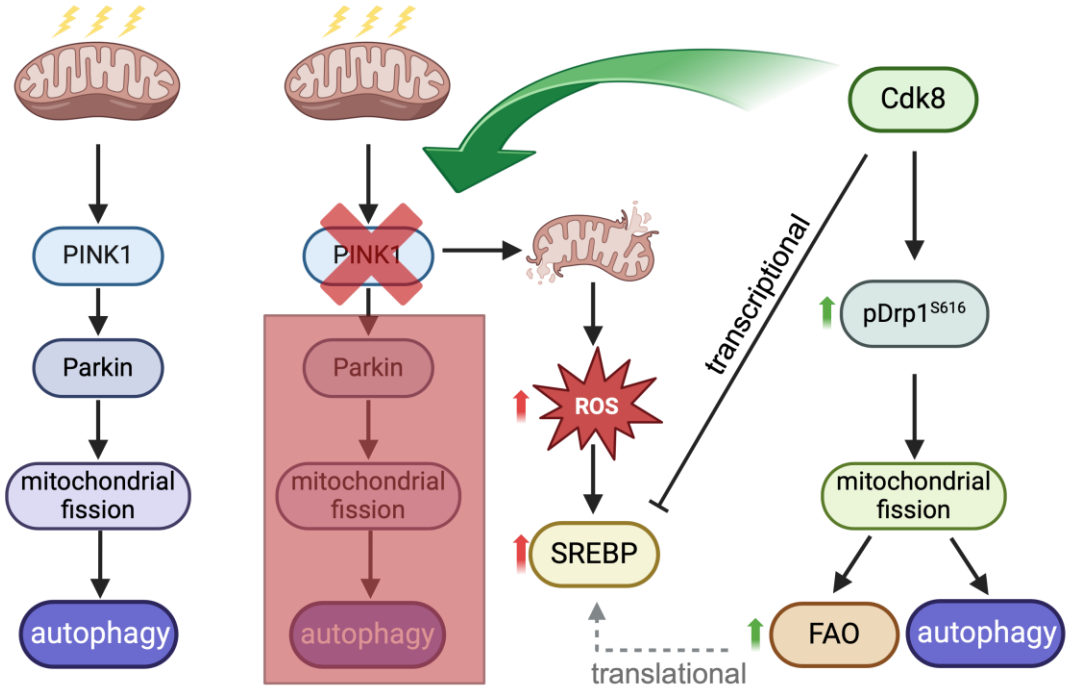

Figure 6.1. Dual functions of Cdk8 in rescuing the *pink1*-mediated Parkinsonism model.

Damaged mitochondria can activate PINK1/Parkin mediated mitophagy by promoting mitochondrial fission in turn to separate the damaged pool of mitochondria from the healthy pool, which subsequently target for degradation by autophagosome. When PINK1 is mutated, the PINK1/Parkin mediated mitophagy is impeded, resulting in accumulation of damaged mitochondrial, elevated ROS level, and subsequently elevated SREBP transcript with lipid accumulation. Supplementing Cdk8 in the pink1 mutant background has dual functions. First, Cdk8 can regulate the stability of SREBP by phosphorylation, which in turn negatively regulates the expression of downstream targets of SREBP at transcriptional level to tune down the biosynthesis of lipids. Secondly, Cdk8 can promote the mitochondrial fission by phosphorylating Drp1S616. Once mitochondrial fission is restored under the *pink1* mutant background, autophagosome can continue to recycle the damaged mitochondria in turn to maintain the mitochondrial homeostasis. Furthermore, elevated mitochondrial fission enhances the rate of fat utilization by fatty acid oxidation (FAO), which ultimately reduces the amount of accumulated lipids in the *pink1* mutant background.

Collectively, our work expands the knowledge about CDK8/19 family proteins and raises interesting questions about applying that knowledge in the treatment of developmental syndromes associated with CDK8 and CDK19 mutations. Further, our work may provide additional avenues of research to understand and treat familial Parkinsonism. This work also demonstrates the power of using Drosophila to dissect conserved molecular mechanisms essential for development and disease.

Chapter 7. Material and Methods

7.1. Drosophila husbandry

Drosophila melanogaster flies were raised on standard cornmeal-molasses food. Stocks were kept at 25ºC. Crosses were carried out at 25ºC and 29ºC as indicated. Since Gal4 activity is elevated at higher temperatures [360,361], we could modulate expression levels using both temperatures. Results found at 29ºC were more penetrant, so the main figures include these data, and supplemental figures show data from 25ºC. The following fly strains were used: *Act5c-Gal4/TM6B* (BL #3954), *Mef2-Gal4* (BL #27390), *Appl-Gal4* (BL #32040), *pink1^{B9}* (BL #34749), *UAS-Cdk8-RNAi* (BL #35324), *UAS-RFP* (BL #7119), *UAS-white-RNAi (BL #33762)*, *UAS-mito-HA-GFP* (abbreviated as *UAS-mitoGFP*; BL #8442), *UAS-hPINK1-FLAG* (BL #52004), *UAS-Cdk8^{ORF}* which expresses a full-length open reading frame (F001348), *UAS-Cdk8-RNAi* (BL #67010), *UAS-Cdk8-3xHA* which expresses a full-length HA-tagged Cdk8 (F001713), *UAS-Cdk8^{KD}* was obtained from Dr. J-Y Ji from Tulane University School of Medicine, *UAS-CycC-RNAi* (BL #33753), *UAS-CycC-3xHA* which expresses a full-length HA-tagged CycC (F003051), *UAS-SREBP^{DN} II* (BL #8245), *UAS-SREBP^{DN} III* (BL #8246), *UAS-SREBP^{CA}* (BL #8244), *UAS-Acc* (BL #63224), *UAS-Acc RNAi (*BL #32885), *UAS-Fasn 1 RNAi* (VDRC #108339), *UAS-Fasn 1 RNAi* (BL #28930; denoted as *UAS-Fasn 1 RNAi 2*), UAS-luciferase RNAi (BL #35788), UAS-CDK19^{WT}, UAS-CDK19^{Y32H} and UAS-CDK19^{T196A} were generated in the previous study (Chung et al., 2020). Strains with BL stock number were obtained from Bloomington Drosophila Stock Center (Bloomington, IN, USA). Strains labeled with an F initial were obtained from FlyORF Drosophila Stock Center (ZurichORFeome Project, Zurich, Switzerland). Strain labeled with VDRC is obtained from Vienna Drosophila Resource Center (Vienna In Europe).

7.2. RT-qPCR

Whole larvae from third instar larval stage or adult thoraxes were briefly washed in PBS and temporarily stored in RNAlater Stabilization solution (Invitrogen AM7020). Total RNA was extracted using RNeasy Mini Kits (Qiagen 74101). First strand cDNA was synthesized using OneScript Plus cDNA Synthesis Kit (Abm G236). qRT-PCR were

performed using SensiFast SYBR Lo-ROX Kit (Bioline 94005) on StepOne Real-time PCR System (Applied Biosystems). Primers used are:

cdk8 F	CATCCGGGTGTTTCTGTCG
cdk8 R	CAGCCCGATGGAACTTAATGAT
cyc C F	AGTTTCCCTACCGCACCAATC
cyc C R	ACAATCAAGCAGCAATCCAGG
pink1 F	AAGCGAGGCTTTCCCCTAC
pink1 R	GCACTACATRGACCACCGATTT
parkin F	GAAGCCTCCAAGCCTCTAAATG
parkin R	ACGGACTCTTTCTTCATCGGT
opa1 F	CAAGCTGCGATACATCGTCC
opa1 R	GCAGTCCATCCTTCCATTCC
marf F	GAGACGACCACCTTTATCAACG
marf R	CCACCTTCATGTGATCCCG
drp1 F	ACAGCCCACTCGATGATCG
drp1 R	AAGCACTTCTTGGTGTGCAG
gstD F	TGGGAACGCTGTACCAGAG
gstD R	AGGTGTTCAGGAACTCGAGG
catalase F	GATGCGGCTTCCAATCAGTTG
catalase R	GCAGCAGGATAGGTCCTCG
sod1 F	GCAATTCAATCCGTATGGCAA

sod1 R	CGAAGAGCGTAATCTTGGAGT
Fasn1 F	GACATGGTCAACGATGATCCC
Fasn1 R	ACCGAAGAACTGTTGGTCAAAG
acc F	CGAGCGGGCCATTAGGTTT
acc R	GCCATCTTGATGTATTCGGCAT
rp49 F	AGCATACAGGCCCAAGATCG
rp49 R	TGTTGTCGATACCCTTGGGC

7.3. Pupal Lethality Assay

The numbers of pupal cases were counted 3 days after most control flies had eclosed. Counting includes the number of pupal cases in total and number of pupal cases with dead pharate adults. The test was repeated three times.

7.4. Survival assay

Adult flies were maintained on standard media at 25ºC and transferred to fresh vials every three days. Mortality was scored daily.

7.5. Fertility assay

Newly eclosed virgin females and males expressing *Act5c>Cdk8 RNAi* are collected in separated vials. Crosses were set up with *w1118* flies to count for number progeny.

7.6. Climbing assay

Flies raised at both 25ºC and 29ºC were subjected to a climbing assay at 3 days, 1 week, 2 weeks, 3 weeks or 4 weeks after eclosion raised at both 25ºC and 29ºC. Adult flies were transferred into an empty polystyrene vial with a label at a height of 5 cm. Prior to the assay, flies were gently tapped down to the bottom of the vial and their climbing in 15 seconds was recorded and quantified. The test was repeated six times for each vial and 3 vials per genotype were tested. When using either muscle or neuronal drivers, defects were only manifested in two-week-old flies, while ubiquitous knockdown caused climbing defects by day 3.

7.7. Quantification of mitochondrial morphology using MiNA in larval body wall muscle

Airyscan-processed images of larval body wall muscles were subjected to binary and skeletonize processes using Image J prior to morphological quantification. Each processed image was randomly assigned into five sections, and each section was subjected to Mitochondrial Network Analysis (MiNA) to quantify the following three parameters: numbers of networks (structure with at least one junction), mean length of network branches (mean branch length), and mitochondrial footprint (area). Data collected from five sections with four biological replicates were pooled together for statistics and generating boxplots. Airyscan-processed images of adult indirect flight muscles were used in Image J for morphological quantification. Length of mitochondria is measured, where number of mitochondria are manually counted. Data collected from two sections with five biological replicated were pooled together for statistics and generating boxplots.

7.8. Quantification of mitochondrial morphology in adult indirect flight muscle

Airyscan-processed images were randomly assigned into five sections, and mitochondrial length within the section were measured using Image J, whereas the

number of mitochondria within the section were manually counted. Data collected from five sections were pooled together for statistics and generating boxplots.

7.9. Quantification of myofibril width

Airyscan-processed images were randomly assigned into five sections, and myofibril within the section were measured using Image J. Data collected from five sections were pooled together for statistics and generating boxplots.

7.10. Immunostainings

Larval body wall muscles and adult thoraxes were dissected in PBS and fixed in 4% paraformaldehyde (PFA) for 15 min at room temperature. Samples were washed with PBS with 0.1% Triton X-100 (PBST). After blocking with 5% BSA in PBST for 1 h at room temperature, samples were incubated with primary antibodies overnight at 4°C. The following primary antibodies were used: rabbit anti-Drp1 (1:500; Cell Signaling D6C7), Rabbit anti-Drp1 S616 (1:500, Cell Signaling D9A1), mouse anti-HA (1:500; Abm G036), rabbit anti-CDK19 (1:200; Sigma-Aldrich SAB4301196), mouse- anti-Lamin C (1:100, DSHB LC28.26), mouse anti-ATP5α (1:500; Abcam ab14748) and rabbit anti-HA (1:500; Abcam ab9110). After washing with PBST, samples were incubated with Cy3- and/or Alexa Fluor 647-conjugated secondary antibodies (1:500; Jackson ImmunoResearch Laboratories), DAPI (final concentration: 0.2 µg per ml; Invitrogen D1306) for 2 h at room temperature. Samples were mounted in 70% glycerol in PBS after washing. Images were taken on a Nikon Air laser-scanning confocal microscope or a Zeiss LSM880 with Airyscan confocal microscope and processed using ImageJ.

7.11. Western blot

Cells or tissues were lysed with 1× Cell Lysis Buffer (Cell Signaling Technology), supplemented with 1× Protease Inhibitors (Roche) and 1 mM phenylmethylsulfonyl fluoride. Protein lysates with 1× SDS sample buffer were resolved on SDS/PAGE and then transferred to nitrocellulose membranes. Membranes were blocked with 5% skimmed milk or 5% bovine serum albumin. The following primary antibodies were used: rabbit anti-Drp1 (1:2500; Cell Signaling D6C7), rabbit anti-pDrp1S616 (1:2500; Cell Signaling 4494), mouse anti-Myc (1:2500; Millipore clone 4A6), rat anti-HA-peroxidase

(1:5000; Sigma Aldrich clone 3F10), mouse anti-Actin (1:5000; Abcam ab3280), rabbit anti-GFP (1:5000, ThermoFisher A11122) and mouse anti-HSP60 (1:1000; ThermoFisher MA3-012). HRP (Jackson ImmunoResearch) conjugated secondary antibodies were used. Images were acquired by Amersham Imager 600.

7.12. ROS detection

ROS assays were performed according to the previously described protocol for *in vivo* detection of ROS [362]. Briefly, adult thoraxes were dissected in PBS and incubated with 30 μM DHE (Cayman 12013) for 7 mins in the dark at room temperature. After rinse with PBS briefly, samples were fixed in 8% PFA and washed with PBS, each for 5 minutes before mounting. Images were taken within two days.

For the detection of ROS in adult brains, a previously described protocol was used with minor modifications [363]. Day 5 fly brains were dissected in Schneider's medium (SDM). After brief washing with SDM, the brains were incubated for 5 min with 150 μL DHE (final concentration 30 μM, Invitrogen, Cat# D11347) to detect ROS. After washing (5 min x 3 times) in SDM, brains were mounted with VECTASHIELD Antifade Mounting Medium and then observed immediately with a Leica SP8X confocal microscope. Images were obtained as Z series with the same interval (4 μm) for the whole brain. Z series images were merged by ImageJ (Image-Stacks-Z projection-SUM slices), and then the fluorescence intensity was measured.

7.13. Spectrophotometry

Thoraxes with corresponded genotypes are collected, and grinded in 100 μL of ice-cold PBS with pestle. Samples were centrifuged 5 min at 4C with maximum rpm. Working solution of DHE is prepped while waiting with 1 to 1000 dilution with PBS. In the reading plate, 90 μL DHE working solution is added to each well, samples were loaded after with increased volume. A blank lane is included by adding water to DHE working solution. Plate is immediately subjected to spectrophotometry for reading. The excitation and emission wavelength is adjusted to 518/606 nm according to manufacture protocol (Cayman 12013).

7.14. Plasmids and cell culture

Entry clones were created by TOPO cloning (pENTR-D-TOPO, ThermoFisher) according to manufacturer's instruction. The ORFs for *Cdk8* [CG10572, FMO10168 (DGRC Stock 1637668; https://dgrc.bio.indiana.edu//stock/1637668 ; RRID:DGRC_1637668)] and *Drp1* [CG3210, FI19305 (DGRC Stock 1647302 ; https://dgrc.bio.indiana.edu//stock/1647302 ; RRID:DGRC_1647302)] were from the DGRC clone collection. All ORFs were amplified by PCR using primers bearing flanking attB1 and attB2 sequences and subjected to BP recombination reactions using the pDONR/Zeo vector (Invitrogen) to generate Entry vectors. Expression vectors were obtained through LR recombination reactions using the pAWM and pAWH vectors from the DGRC Gateway collection.

Drosophila S2R+ cells (DGRC stock 150) were maintained at 25C in Schneider's medium supplemented with 10% heat-inactivated FCS (Thermo Fisher Scientific). Cells were transfected with Effectene (Qiagen) according to manufacturer's recommendation. 24 hours after transfection, cells were lysed for subsequent biochemical analysis.

7.15. Subcellular fractionation

All preparations were performed on ice. Subcellular fractionation was performed as described in[364] with slight modification. S2R+ insect cells co-transfected with Cdk8 and Drp1 plasmids were resuspended and homogenized in 0.1% Triton in 200µL 1x PBS (pH 7.4). 30µL of homogenized solution was collected as whole lysate. Rest of the solution was centrifuged at 10000g for 30s. 30µL of supernatant was collected as cytoplasmic fraction. To clear out the debris in nuclear fraction, five subsequent washings with 0.1% Triton were performed followed by centrifugation at 10000g for 1 min per washing. Whole lysate and cytoplasmic fractions were boiled for 5 mins with 4x Laemmli, whereas the nuclear fractions were boiled for 10 mins with 1x Laemmli, and sonicated with 2 pulse, 5 seconds each.

7.16. Kinase assay

Clean cytoplasmic fractions from S2R+ insect cells containing pAWM-Cdk8 and pAWH-Drp1 from subcellular fractionations were subjected to coimmunoprecipitation

with Myc-agarose beads (Abcam ab1253) overnight at 4C. The beads were washed with lysis buffer, and centrifugated at 3000 g for 2 mins at 4C. Beads were kept to perform subsequent kinase assay following protocol listed in[365,366] with a final concentration of 0.2mM ATP added. The reactions were paused after 30 mins and centrifugated at max speed for 5 mins at 4C and boiled for 10 mins with 4x Laemmli. The level of Cdk8, Drp1 and pDrp1 were detected using mouse anti-Myc (1:2500; Millipore clone 4A6), rabbit anti-Drp1 (1:2500; Cell Signaling D6C7), rabbit anti-pDrp1S616 (1:2500; Cell Signaling 4494) on western blots, respectively.

7.17. Generation of endogenously tagged Cdk8::GFP flies

The Cdk8-superfolder-GFP line (referred to as Cdk8::GFP) was generated as described [223]. Briefly, a fragment with gRNAs targeting 5′UTR (GTTATCGGGAGACAGCTGATTGG) and end of coding region (TTAGAAGGCTAGAAATTAGTAGG) of *cdk8* and 200 bps of homology arms (corresponding to 200 bps upstream of 5' sgRNA cut site and 200 bps downstream 3' sgRNA cut site) were synthesized and cloned in pUC57_Kan_gw_OK2 custom vector backbone, generating a homology donor intermediate vector by Genewiz/Azenta. Fragments for the gene coding region (between 5' sgRNA PAM sequence up to final amino acid before the stop codon), linker-sfGFP-stop codon and Scarless-DsRed were PCR amplified with primers containing overlaps and the fragments were assembled using NEB-HiFi DNA Assembly kit (New England Biolabs #E2621) using manufacturer's instructions, in the homology donor intermediate linearized by BsaI-HF (NEB #R3535) to generate the homology donor vector for injection. Homology donor vector (250 ng/µL) was injected into *y*^{1}*w***; attP40(y+){nos-Cas9(v+)}; iso5* embryos[239]. The resulting G0 males and females were crossed to *y w* flies to screen for the presence of 3XP3-DsRed. Resulting transgenics were PCR verified with primers that amplify tagged gene specific amplicons.

7.18. Coimmunoprecipitation

Protein extracts were incubated with indicated with IgG (Abcam ab104155), HA (Abcam ab214758), or Myc-agarose beads (Abcam ab1253) overnight at 4 °C. The beads were washed with lysis buffer and boiled in 4x Laemmli buffer. The supernatants

were then analyzed by Western blotting. For detecting the endogenous *Cdk8::GFP*, protein extracts prepped from adult thoraxes were pre-cleared with IgG (Santa Cruz, sc-2343) for 1 hour at 4°C, lysates were then incubated with either IgG (Santa Cruz, sc-2343) or anti-HA (Santa Cruz, sc-7392) overnight at 4 °C. The beads were washed with lysis buffer and boiled in 4x Laemmli buffer. The supernatants were then analyzed by Western blotting.

7.19. Acridine orange staining of adult brain

Acridine orange (AO) staining were used to detect dying cells in adult brains. The chemicals were prepared as follows: 1.3 µL of 1 mM AO (Invitrogen, A1301) in 1 mL of 1X PBS. For AO staining, fly brains were dissected in PBS, washed with PBS, and then incubated in 150 µL AO for 10 min. The tissue was washed three times with PBS, mounted in Fluoromount-G, and observed immediately with an Intravital multi-photon confocal laser scanning microscope (IMP-LSM; LSM 780 NLO, Carl Zeiss) (Ye-jin Park et al. 2021 iScience).

7.20. Making NACA food

NACA food is made with 10.9 g agar, 31.9 g yeast, 77.4 g cornmeal, 71.6mL molasses with 1172.4 mL water. Once food is boiled and cooled below 60C, antibiotics were added. Penicillin with 0.2 g/L and streptomycin with 0.5 g/L were used with antifungal agent tegosept with 2.0 g/L (dissolve with ethanol). NACA is measured and added with a final concentration of 80 µg/mL.

7.21. Statistical analyses

We used GraphPad Prism for statistical analysis and generation of figures. Statistical analysis was done with the default settings of the software ($*$ indicates $p<0.05$, $**$ indicates $p<0.01$, $***$ indicates $p<0.001$, $****$ indicates $p<0.0001$). Violin plots were generated using BoxPlotR (Spitzer et al. 2014) to demonstrate the average distribution of climbing assays.

7.22. Web Resources

cNLS Mapper: https://nls-mapper.iab.keio.ac.jp/cgi-bin/NLS_Mapper_form.cgi)

References

1. Morgan, T. H. Sex limited inheritance in drosophila. *Science (80-.).* **32**, 120–122 (1910).

2. Lewis, E. B. A gene complex controlling segmentation in Drosophila. *Nature* **276**, 565–570 (1978).

3. Nüsslein-volhard, C. *et al.* Mutations affecting segment number and polarity in Drosophila. **287**, 795–801 (1980).

4. Ugur, B., Chen, K. & Bellen, H. J. Drosophila tools and assays for the study of human diseases. *DMM Disease Models and Mechanisms* vol. 9 235–244 (2016).

5. Bier, E. Drosophila, the golden bug, emerges as a tool for human genetics. *Nat. Rev. Genet. 2005 61* **6**, 9–23 (2005).

6. Lemke, S. B. & Schnorrer, F. Mechanical forces during muscle development. *Mech. Dev.* **144**, 92–101 (2017).

7. Nikonova, E., Kao, S. Y., Ravichandran, K., Wittner, A. & Spletter, M. L. Conserved functions of RNA-binding proteins in muscle. *Int. J. Biochem. Cell Biol.* **110**, 29–49 (2019).

8. Tanaka, T. & Chung, H.-L. Exploiting fly models to investigate rare human neurological disorders. *Neural Regen. Res.* **20**, 21–28 (2025).

9. Hirth, A., Michelsen, U. & Wöhrle, D. Photodynamische Tumortherapie. *Chemie unserer Zeit* **33**, 84–94 (1999).

10. Pires-daSilva, A. & Sommer, R. J. The evolution of signalling pathways in animal development. *Nat. Rev. Genet. 2003 41* **4**, 39–49 (2003).

11. Bonner, J. M. & Boulianne, G. L. Drosophila as a model to study age-related neurodegenerative disorders: Alzheimer's disease. *Exp. Gerontol.* **46**, 335–339 (2011).

12. Cowan, C. M., Chee, F., Shepherd, D. & Mudher, A. Disruption of neuronal function by soluble hyperphosphorylated tau in a Drosophila model of tauopathy. *Biochem. Soc. Trans.* **38**, 564–570 (2010).

13. Prüßing, K., Voigt, A. & Schulz, J. B. Drosophila melanogaster as a model organism for Alzheimer's disease. *Mol. Neurodegener.* **8**, 35 (2013).

14. Feany, M. B. & Bender, W. W. A Drosophila model of Parkinson's disease. **404**, 394–398 (2000).

15. Pareek, G., Thomas, R. E. & Pallanck, L. J. Loss of the Drosophila m-AAA mitochondrial protease paraplegin results in mitochondrial dysfunction, shortened lifespan, and neuronal and muscular degeneration. *Cell Death Dis. 2018 93* **9**, 1–14 (2018).

16. Greene, J. J. C. *et al.* Mitochondrial pathology and apoptotic muscle degeneration in Drosophila parkin mutants. **100**, 4078–4083 (2003).

17. Dietz, K. N. *et al.* The Drosophila Huntington's disease gene ortholog dhtt influences chromatin regulation during development. *Hum. Mol. Genet.* **24**, 330–345 (2015).

18. Zala, D., Hinckelmann, M. V. & Saudou, F. Huntingtin's Function in Axonal Transport Is Conserved in Drosophila melanogaster. *PLoS One* **8**, e60162 (2013).

19. Rosas-Arellano, A., Estrada-Mondragón, A., Piña, R., Mantellero, C. A. & Castro, M. A. The Tiny Drosophila Melanogaster for the Biggest Answers in Huntington's Disease. *Int. J. Mol. Sci.* **19**, (2018).

20. Jennings, B. H. Drosophila – a versatile model in biology & medicine. *Mater. Today* **14**, 190–195 (2011).

21. Cheng, L., Baonza, A. & Grifoni, D. Drosophila Models of Human Disease. *Biomed Res. Int.* **2018**, (2018).

22. Verheyen, E. M. The power of Drosophila in modeling human disease mechanisms. *Dis. Model. Mech.* **15**, (2022).

23. Brand, A. H. & Perrimon, N. Targeted gene expression as a means of altering cell fates and generating dominant phenotypes. *Development* **118**, 401–415 (1993).

24. McGuire, S. E., Roman, G. & Davis, R. L. Gene expression systems in Drosophila: a synthesis of time and space. *Trends Genet.* **20**, 384–391 (2004).

25. Alpatov, W. W. & Pearl, R. Experimental Studies on the Duration of Life. XII. Influence of Temperature during the Larval Period and Adult Life on the Duration of the Life of the Imago of Drosophila melanogaster. *https://doi.org/10.1086/280236* **63**, 37–67 (1929).

26. Miquel, J., Lundgren, P. R., Bensch, K. G. & Atlan, H. Effects of temperature on the life span, vitality and fine structure of Drosophila melanogaster. *Mech. Ageing Dev.* **5**, 347–370 (1976).

27. Malumbres, M. Cyclin-dependent kinases. *Genome Biol.* **15**, (2014).

28. Colas, P. Cyclin-dependent kinases and rare developmental disorders. *Orphanet J. Rare Dis.* **15**, 1–14 (2020).

29. Arellano, M. & Moreno, S. Regulation of CDK/cyclin complexes during the cell cycle. *Int. J. Biochem. Cell Biol.* **29**, 559–573 (1997).

30. Sherr, C. J. & Roberts, J. M. Living with or without cyclins and cyclin-dependent kinases. **18**, 2699–2711 (2004).

31. Morgan, D. O. Cyclin-dependent kinases: Engines, clocks, and microprocessors. *Annu. Rev. Cell Dev. Biol.* **13**, 261–291 (1997).

32. Fung, T. K. & Poon, R. Y. C. A roller coaster ride with the mitotic cyclins. *Semin. Cell Dev. Biol.* **16**, 335–342 (2005).

33. Edgar, B. A. & Orr-Weaver, T. L. Endoreplication cell cycles: More for less. *Cell* **105**, 297–306 (2001).

34. Sherr, C. J. Cancer Cell Cycles. *Science (80-.).* **274**, 1672–1674 (1996).

35. Harbour, J. W., Luo, R. X., Dei Santi, A., Postigo, A. A. & Dean, D. C. Cdk phosphorylation triggers sequential intramolecular interactions that progressively block Rb functions as cells move through G1. *Cell* **98**, 859–869 (1999).

36. Ewen, M. E. The cell cycle and the retinoblastoma protein family. *Cancer Metastasis Rev.* **13**, 45–66 (1994).

37. Bagchi, S., Weinmann, R. & Raychaudhuri, P. The retinoblastoma protein copurifies with E2F-I, an E1A-regulated inhibitor of the transcription factor E2F. *Cell* **65**, 1063–1072 (1991).

38. Chellappan, S. P., Hiebert, S., Mudryj, M., Horowitz, J. M. & Nevins, J. R. The E2F transcription factor is a cellular target for the RB protein. *Cell* **65**, 1053–1061 (1991).

39. Ohtani, K., Degregori, J. & Nevins, J. R. Regulation of the cyclin E gene by transcription factor E2F1. *Proc. Natl. Acad. Sci. U. S. A.* **92**, 12146 (1995).

40. Koff, A. *et al.* Human cyclin E, a new cyclin that interacts with two members of the CDC2 gene family. *Cell* **66**, 1217–1228 (1991).

41. Koff, A. *et al.* Formation and activation of a cyclin E-cdk2 complex during the G1 phase of the human cell cycle. *Science* **257**, 1689–1694 (1992).

42. Akiyama, T., Ohuchi, T., Sumida, S., Matsumoto, K. & Toyoshima, K. Phosphorylation of the retinoblastoma protein by cdk2. *Proc. Natl. Acad. Sci. U. S. A.* **89**, 7900 (1992).

43. Resnitzky, D., Gossen, M., Bujard, H. & Reed, S. I. Acceleration of the G1/S phase transition by expression of cyclins D1 and E with an inducible system. *Mol. Cell. Biol.* **14**, 1669–1679 (1994).

44. Knoblich, J. A. *et al.* Cyclin E controls S phase progression and its down-regulation during Drosophila embryogenesis is required for the arrest of cell proliferation. *Cell* **77**, 107–120 (1994).

45. Lundberg, A. S. & Weinberg, R. A. Functional inactivation of the retinoblastoma protein requires sequential modification by at least two distinct cyclin-cdk complexes. *Mol. Cell. Biol.* **18**, 753–761 (1998).

46. Petersen, B. O., Lukas, J., Sørensen, C. S., Bartek, J. & Helin, K. Phosphorylation of mammalian CDC6 by cyclin A/CDK2 regulates its subcellular localization. *EMBO J.* **18**, 396–410 (1999).

47. Coverley, D., Pelizon, C., Trewick, S. & Laskey, R. A. Chromatin-bound Cdc6 persists in S and G2 phases in human cells, while soluble Cdc6 is destroyed in a cyclin A-cdk2 dependent process. *J. Cell Sci.* **113 (Pt 11)**, 1929–1938 (2000).

48. Furuno, N., Elzen, N. Den & Pines, J. Human cyclin A is required for mitosis until mid prophase. *J. Cell Biol.* **147**, 295–306 (1999).

49. Hoffmann, I., Clarke1, P. R., Jesu's Marcote, M., Karsenti1, E. & Draetta, G. Phosphorylation and activation of human cdc25-C by cdc2--cyclin B and its involvement in the self-amplification of MPF at mitosis. *EMBO J.* **12**, 53 (1993).

50. Nishi, K., Inoue, H., Schnier, J. B. & Rice, R. H. Cyclin D1 Downregulation is Important for Permanent Cell Cycle Exit and Initiation of Differentiation Induced by Anchorage-Deprivation in Human Keratinocytes. *J. Cell. Biochem.* **106**, 63 (2009).

51. Ezhevsky, S. A. *et al.* Hypo-phosphorylation of the retinoblastoma protein (pRb) by cyclin D:Cdk4/6 complexes results in active pRb. *Proc. Natl. Acad. Sci. U. S. A.* **94**, 10699 (1997).

52. Pines, J. & Hunter, T. Cyclin-dependent kinases: a new cell cycle motif? *Trends Cell Biol.* **1**, 117–121 (1991).

53. Gavet, O. & Pines, J. Progressive activation of CyclinB1-Cdk1 coordinates entry to mitosis. *Dev. Cell* **18**, 533–543 (2010).

54. Schmidt, M. *et al.* Regulation of G2/M Transition by Inhibition of WEE1 and PKMYT1 Kinases. **22**, (2017).

55. Deneke, V. E., Melbinger, A., Vergassola, M. & Di Talia, S. Waves of Cdk1 Activity in S Phase Synchronize the Cell Cycle in Drosophila Embryos. *Dev. Cell* **38**, 399–412 (2016).

56. Wang, Z. *et al.* CyclinB1/Cdk1 Coordinates Mitochondrial Respiration for Cell Cycle G2/M Progression. *Dev. Cell* **29**, 217 (2014).

57. Pahel, G. *et al.* Structural and functional characterization of the HPV16 E7 protein

expressed in bacteria. *J. Biol. Chem.* **268**, 26018–26025 (1993).

58. Jackman, M., Kubota, Y., Den Elzen, N., Hagting, A. & Pines, J. Cyclin A- and Cyclin E-Cdk Complexes Shuttle between the Nucleus and the Cytoplasm. *Mol. Biol. Cell* **13**, 1030 (2002).

59. Narasimha, A. M. *et al.* Cyclin D activates the Rb tumor suppressor by mono-phosphorylation. *Elife* **3**, (2014).

60. Wang, Z. *et al.* Migratory Localization of Cyclin D2-Cdk4 Complex Suggests a Spatial Regulation of the G1-S Transition. *Cell Struct. Funct.* **33**, 171–183 (2008).

61. Lehner, C. F. & O'Farrell, P. H. Expression and Function of Drosophila Cyclin A during Embryonic Cell Cycle Progression. *Cell* **56**, 957 (1989).

62. Follette, P. J. & O'Farrell, P. H. Cdks and the Drosophila cell cycle. *Curr. Opin. Genet. Dev.* **7**, 17 (1997).

63. Pérez de Castro, I., de Cárcer, G. & Malumbres, M. A census of mitotic cancer genes: new insights into tumor cell biology and cancer therapy. *Carcinogenesis* **28**, 899–912 (2007).

64. Yang, L. *et al.* Cyclin-dependent kinase 2 is an ideal target for ovary tumors with elevated cyclin E1 expression. *Oncotarget* **6**, 20801 (2015).

65. Łukasik, P., Załuski, M. & Gutowska, I. Cyclin-Dependent Kinases (CDK) and Their Role in Diseases Development–Review. *Int. J. Mol. Sci.* **22**, 1–33 (2021).

66. Roberts, P. J. & Der, C. J. Targeting the Raf-MEK-ERK mitogen-activated protein kinase cascade for the treatment of cancer. *Oncogene 2007 2622* **26**, 3291–3310 (2007).

67. Puntervoll, H. E. *et al.* Original article: Melanoma prone families with CDK4 germline mutation: phenotypic profile and associations with MC1R variants. *J. Med. Genet.* **50**, 264 (2013).

68. Meyer, C. A. *et al.* Drosophila Cdk4 is required for normal growth and is dispensable for cell cycle progression. *EMBO J.* **19**, (2000).

69. Hussain, M. S. *et al.* CDK6 associates with the centrosome during mitosis and is mutated in a large Pakistani family with primary microcephaly. *Hum. Mol. Genet.* **22**, 5199–5214 (2013).

70. Corden, J. L., Cadena, D. L., Ahearn, J. M. & Dahmus, M. E. A unique structure at the carboxyl terminus of the largest subunit of eukaryotic RNA polymerase II. *Proc. Natl. Acad. Sci. U. S. A.* **82**, 7934–7938 (1985).

71. Parua, P. K. & Fisher, R. P. Dissecting the Pol II transcription cycle and derailing

cancer with CDK inhibitors. *Nat. Chem. Biol.* **16**, 716–724 (2020).

72. Li, Y. C. *et al.* Structure and noncanonical Cdk8 activation mechanism within an Argonaute-containing Mediator kinase module. *Sci. Adv.* **7**, (2021).

73. Li, T., Tang, H. C. & Tsai, K. L. Unveiling the noncanonical activation mechanism of CDKs: insights from recent structural studies. *Front. Mol. Biosci.* **10**, 1290631 (2023).

74. Fant, C. B. & Taatjes, D. J. Regulatory functions of the Mediator kinases CDK8 and CDK19. *Transcription* **10**, 76–90 (2019).

75. Nikolov, D. B. & Burley, S. K. RNA polymerase II transcription initiation: A structural view. *Proc. Natl. Acad. Sci. U. S. A.* **94**, 15 (1997).

76. Donner, A. J., Ebmeier, C. C., Taatjes, D. J. & Espinosa, J. M. CDK8 is a positive regulator of transcriptional elongation within the serum response network. *Nat. Struct. Mol. Biol.* **17**, 194–201 (2010).

77. Galbraith, M. D., Donner, A. J. & Espinosa, J. M. CDK8: A positive regulator of transcription. *Transcription* **1**, 4 (2010).

78. Fisher, R. P., Jin, P., Chamberlin, H. M. & Morgan, D. O. Alternative mechanisms of CAK assembly require an assembly factor or an activating kinase. *Cell* **83**, 47–57 (1995).

79. Harper, J. W. & Elledge, S. J. The role of Cdk7 in CAK function, a retro-retrospective. *Genes Dev.* **12**, 285–289 (1998).

80. Larochelle, S., Pandur, J., Fisher, R. P., Salz, H. K. & Suter, B. Cdk7 is essential for mitosis and for in vivo Cdk-activating kinase activity. *Genes Dev.* **12**, 370 (1998).

81. Larochelle, S. *et al.* T-loop phosphorylation stabilizes the CDK7–cyclin H–MAT1 complex in vivo and regulates its CTD kinase activity. *EMBO J.* **20**, 3749 (2001).

82. Rossignol, M., Kolb-Cheynel, I. & Egly, J. M. Substrate specificity of the cdk-activating kinase (CAK) is altered upon association with TFIIH. *EMBO J.* **16**, 1628 (1997).

83. Akhtar, M. S. *et al.* TFIIH kinase places bivalent marks on the carboxyl-terminal domain of RNA polymerase II. *Mol. Cell* **34**, 387 (2009).

84. Glover-Cutter, K. *et al.* TFIIH-associated Cdk7 kinase functions in phosphorylation of C-terminal domain Ser7 residues, promoter-proximal pausing, and termination by RNA polymerase II. *Mol. Cell. Biol.* **29**, 5455–5464 (2009).

85. Nilson, K. A. *et al.* THZ1 Reveals Roles for Cdk7 in Co-transcriptional Capping

and Pausing. *Mol. Cell* **59**, 576–587 (2015).

86. Viladevall, L. *et al.* TFIIH and P-TEFb Coordinate Transcription with Capping Enzyme Recruitment at Specific Genes in Fission Yeast. *Mol. Cell* **33**, 738 (2009).

87. Core, L. & Adelman, K. Promoter-proximal pausing of RNA polymerase II: a nexus of gene regulation. *Genes Dev.* **33**, 960–982 (2019).

88. Rimel, J. K. & Taatjes, D. J. The essential and multifunctional TFIIH complex. **27**, (2018).

89. Rimel, J. K. *et al.* Selective inhibition of CDK7 reveals high-confidence targets and new models for TFIIH function in transcription. *Genes Dev.* **34**, 1452–1473 (2020).

90. Ding, L. *et al.* The Roles of Cyclin-Dependent Kinases in Cell-Cycle Progression and Therapeutic Strategies in Human Breast Cancer. *Int. J. Mol. Sci.* **21**, (2020).

91. Wang, Y. *et al.* Phosphatase PPM1A Regulates Phosphorylation of Thr-186 in the Cdk9 T-loop. *J. Biol. Chem.* **283**, 33578 (2008).

92. Ramakrishnan, R., Dow, E. C. & Rice, A. P. Characterization of Cdk9 T-loop phosphorylation in resting and activated CD4+ T lymphocytes. *J. Leukoc. Biol.* **86**, 1345 (2009).

93. Kohoutek, J. & Blazek, D. Cyclin K goes with Cdk12 and Cdk13. *Cell Div.* **7**, 12 (2012).

94. Bösken, C. A. *et al.* The structure and substrate specificity of human Cdk12/Cyclin K. *Nat. Commun. 2014 51* **5**, 1–14 (2014).

95. Liang, K. *et al.* Characterization of Human Cyclin-Dependent Kinase 12 (CDK12) and CDK13 Complexes in C-Terminal Domain Phosphorylation, Gene Transcription, and RNA Processing. *Mol. Cell. Biol.* **35**, 928 (2015).

96. Leclerc, V., Tassan, J. P., O'Farrell, P. H., Nigg, E. A. & Leopold, P. Drosophila Cdk8, a kinase partner of cyclin C that interacts with the large subunit of RNA polymerase II. *Mol. Biol. Cell* **7**, 505–513 (1996).

97. Lis, J. T., Mason, P., Peng, J., Price, D. H. & Werner, J. P-TEFb kinase recruitment and function at heat shock loci. *Genes Dev.* **14**, 792–803 (2000).

98. VH, P., RB, O., WH, W. & FT, J. Trichothiodystrophy: sulfur-deficient brittle hair as a marker for a neuroectodermal symptom complex. *Arch. Dermatol.* **116**, 1375–1384 (1980).

99. Stefanini, M. Trichothiodystrophy: A Disorder Highlighting the Crosstalk between DNA Repair and Transcription. (2013).

100. Coin, F., Bergmann, E., Tremeau-Bravard, A. & Egly, J. M. Mutations in XPB and XPD helicases found in xeroderma pigmentosum patients impair the transcription function of TFIIH. *EMBO J.* **18**, 1357 (1999).

101. Zarate, Y. A. *et al.* CDK19-related disorder results from both loss-of-function and gain-of-function de novo missense variants. *Genet. Med.* **23**, 1050–1057 (2021).

102. Chung, H. lok *et al.* De Novo Variants in CDK19 Are Associated with a Syndrome Involving Intellectual Disability and Epileptic Encephalopathy. *Am. J. Hum. Genet.* **106**, 717–725 (2020).

103. Yang, S., Yu, W., Chen, Q. & Wang, X. A novel variant of CDK19 causes a severe neurodevelopmental disorder with infantile spasms. *Cold Spring Harb. Mol. Case Stud.* **7**, (2021).

104. Calpena, E. *et al.* De Novo Missense Substitutions in the Gene Encoding CDK8, a Regulator of the Mediator Complex, Cause a Syndromic Developmental Disorder. (2019) doi:10.1016/j.ajhg.2019.02.006.

105. Uehara, T. *et al.* Pathogenesis of CDK8-associated disorder: two patients with novel CDK8 variants and in vitro and in vivo functional analyses of the variants. *Sci. Rep.* **10**, 17575 (2020).

106. Sugawara, Y. *et al.* Cerebrospinal fluid abnormalities in developmental and epileptic encephalopathy with a de novo CDK19 variant. *Neurol. Genet.* **6**, (2020).

107. Calpena, E. *et al.* De Novo Missense Substitutions in the Gene Encoding CDK8, a Regulator of the Mediator Complex, Cause a Syndromic Developmental Disorder. *Am. J. Hum. Genet.* **104**, 709–720 (2019).

108. Shaheen, R. *et al.* Accelerating matchmaking of novel dysmorphology syndromes through clinical and genomic characterization of a large cohort. (2016) doi:10.1038/gim.2015.147.

109. Maddirevula, S. *et al.* Autozygome and high throughput confirmation of disease genes candidacy. *Genet. Med.* **21**, 736 (2019).

110. Nishina, S. *et al.* Biallelic CDK9 variants as a cause of a new multiple-malformation syndrome with retinal dystrophy mimicking the CHARGE syndrome. *J. Hum. Genet. 2021 6610* **66**, 1021–1027 (2021).

111. Sifrim, A. *et al.* Distinct genetic architectures for syndromic and nonsyndromic congenital heart defects identified by exome sequencing. *Nat. Genet. 2016 489* **48**, 1060–1065 (2016).

112. Uehara, T. *et al.* Redefining the phenotypic spectrum of de novo heterozygous CDK13 variants: Three patients without cardiac defects. *Eur. J. Med. Genet.* **61**, 243–247 (2018).

113. Bostwick, B. L. *et al.* Phenotypic and molecular characterisation of CDK13-related congenital heart defects, dysmorphic facial features and intellectual developmental disorders. **9**, 73 (2017).

114. Hamilton, M. J. *et al.* Original Article: Heterozygous mutations affecting the protein kinase domain of CDK13 cause a syndromic form of developmental delay and intellectual disability. *J. Med. Genet.* **55**, 28 (2018).

115. Shukla, A. K., Spurrier, J., Kuzina, I. & Giniger, E. Erratum: Hyperactive Innate Immunity Causes Degeneration of Dopamine Neurons upon Altering Activity of Cdk5 (Cell Reports (2019) 26(1) (131–144.e4), (S2211124718319557), (10.1016/j.celrep.2018.12.025)). *Cell Rep.* **35**, (2021).

116. Lin, H., Lin, T. Y. & Juang, J. L. Abl deregulates Cdk5 kinase activity and subcellular localization in Drosophila neurodegeneration. *Cell Death Differ. 2007 143* **14**, 607–615 (2006).

117. Ino, H., Ishizuka, T., Chiba, T. & Tatibana, M. Expression of CDK5 (PSSALRE kinase), a neural cdc2-related protein kinase, in the mature and developing mouse central and peripheral nervous systems. *Brain Res.* **661**, 196–206 (1994).

118. Magen, D. *et al.* Autosomal recessive lissencephaly with cerebellar hypoplasia is associated with a loss-of-function mutation in CDK5. **134**, 305–314 (2015).

119. Ao, C., Li, C., Chen, J., Tan, J. & Zeng, L. The role of Cdk5 in neurological disorders. *Front. Cell. Neurosci.* **16**, (2022).

120. Quan, Q., Qian, Y., Li, X. & Li, M. Pioglitazone Reduces β Amyloid Levels via Inhibition of PPARγ Phosphorylation in a Neuronal Model of Alzheimer's Disease. *Front. Aging Neurosci.* **11**, (2019).

121. He, F. *et al.* Quantitative Phosphoproteomic Analysis in Alpha-Synuclein Transgenic Mice Reveals the Involvement of Aberrant p25/Cdk5 Signaling in Early-stage Parkinson's Disease. *Cell. Mol. Neurobiol.* **40**, 897–909 (2020).

122. He, R. *et al.* Cdk5 Inhibitory Peptide Prevents Loss of Dopaminergic Neurons and Alleviates Behavioral Changes in an MPTP Induced Parkinson's Disease Mouse Model. *Front. Aging Neurosci.* **10**, (2018).

123. Poss, Z. C. *et al.* Identification of Mediator Kinase Substrates in Human Cells using Cortistatin A and Quantitative Phosphoproteomics. *Cell Rep.* **15**, 436–50 (2016).

124. Wang, J. *et al.* MARRVEL: Integration of Human and Model Organism Genetic Resources to Facilitate Functional Annotation of the Human Genome. *Am. J. Hum. Genet.* **100**, 843–853 (2017).

125. Firestein, R. *et al.* CDK8 is a colorectal cancer oncogene that regulates β-catenin

activity. *Nature* **455**, 547–551 (2008).

126. Morris, E. J. *et al.* E2F1 represses β-catenin transcription and is antagonized by both pRB and CDK8. *Nature* **455**, (2008).

127. Kapoor, A. *et al.* The histone variant macroH2A suppresses melanoma progression through regulation of CDK8. **468**, (2010).

128. Broude, E. *et al.* Expression of CDK8 and CDK8-interacting Genes as Potential Biomarkers in Breast Cancer. *Curr. Cancer Drug Targets* **15**, 739–749 (2015).

129. Sato, S. *et al.* A set of consensus mammalian mediator subunits identified by multidimensional protein identification technology. *Mol. Cell* **14**, 685–691 (2004).

130. Westerling, T., Kuuluvainen, E. & Mäkelä, T. P. Cdk8 is essential for preimplantation mouse development. *Mol. Cell. Biol.* **27**, 6177–82 (2007).

131. McCleland, M. L. *et al.* Cdk8 deletion in the Apc(Min) murine tumour model represses EZH2 activity and accelerates tumourigenesis. *J. Pathol.* **237**, 508–519 (2015).

132. Steimel, A. *et al.* The C. elegans CDK8 Mediator module regulates axon guidance decisions in the ventral nerve cord and during dorsal axon navigation. *Dev. Biol.* **377**, 385–398 (2013).

133. Loncle, N. *et al.* Distinct roles for Mediator Cdk8 module subunits in Drosophila development. *EMBO J.* **26**, 1045–1054 (2007).

134. Treisman, J. E. Drosophila homologues of the transcriptional coactivation complex subunits TRAP240 and TRAP230 are required for identical processes in eye-antennal disc development. *Development* **128**, 603–615 (2001).

135. Buszczak, M. *et al.* The Carnegie Protein Trap Library: A Versatile Tool for Drosophila Developmental Studies. *Genetics* **175**, 1505–1531 (2007).

136. Li, X. *et al.* The Mediator CDK8-Cyclin C complex modulates Dpp signaling in Drosophila by stimulating Mad-dependent transcription. *PLoS Genet.* **16**, (2020).

137. Shimano, H. & Sato, R. SREBP-regulated lipid metabolism: Convergent physiology-divergent pathophysiology. *Nature Reviews Endocrinology* vol. 13 710–730 (2017).

138. Li, X. *et al.* Cdk8 attenuates lipogenesis by inhibiting SREBP-dependent transcription in Drosophila. **15**, (2022).

139. Cooper, K. F., Khakhina, S., Kim, S. K. & Strich, R. Stress-Induced Nuclear-to-Cytoplasmic Translocation of Cyclin C Promotes Mitochondrial Fission in Yeast. *Dev. Cell* **28**, 161–173 (2014).

140. Wang, K., Yan, R., Cooper, K. F. & Strich, R. Cyclin C mediates stress-induced mitochondrial fission and apoptosis. *Mol. Biol. Cell* **26**, (2015).

141. Ganesan, V. *et al.* Cyclin C directly stimulates Drp1 GTP affinity to mediate stress-induced mitochondrial hyperfission. *Mol. Biol. Cell* **30**, (2019).

142. Jezek, J., Chang, K., Joshi, A. M. & Strich, R. Mitochondrial translocation of cyclin C stimulates intrinsic apoptosis through Bax recruitment. **20**, (2019).

143. Strich, R. & Cooper, K. F. The dual role of cyclin C connects stress regulated gene expression to mitochondrial dynamics. *Microbial Cell* vol. 1 318–324 (2014).

144. Bruter, A. V. *et al.* Knockout of cyclin dependent kinases 8 and 19 leads to depletion of cyclin C and suppresses spermatogenesis and male fertility in mice. *Elife* **13**, (2024).

145. Zhang, Z. *et al.* CDK19 regulates the proliferation of hematopoietic stem cells and acute myeloid leukemia cells by suppressing p53-mediated transcription of p21. *Leuk. 2022 364* **36**, 956–969 (2022).

146. Mukhopadhyay, A. *et al.* CDK19 is disrupted in a female patient with bilateral congenital retinal folds, microcephaly and mild mental retardation. *Hum. Genet.* **128**, 281 (2010).

147. Lin, C. H., Chou, I. C. & Hong, S. Y. Genetic factors and the risk of drug-resistant epilepsy in young children with epilepsy and neurodevelopment disability: A prospective study and updated meta-analysis. *Medicine (Baltimore).* **100**, E25277 (2021).

148. Bancerek, J. *et al.* CDK8 kinase phosphorylates transcription factor STAT1 to selectively regulate the interferon response. *Immunity* **38**, 250–62 (2013).

149. Clarke, P. A. *et al.* Assessing the mechanism and therapeutic potential of modulators of the human Mediator complex-associated protein kinases. *Elife* **5**, (2016).

150. Putz, E. M. *et al.* CDK8-mediated STAT1-S727 phosphorylation restrains NK cell cytotoxicity and tumor surveillance. *Cell Rep.* **4**, 437–444 (2013).

151. Lee, A. *et al.* Control of dendritic development by the Drosophila fragile X-related gene involves the small GTPase Rac1. *Development* **130**, 5543–5552 (2003).

152. Lu, Y. *et al.* The Drosophila homologue of the Angelman syndrome ubiquitin ligase regulates the formation of terminal dendritic branches. *Hum. Mol. Genet.* **18**, 454 (2009).

153. Fergestad, T., Bostwick, B. & Ganetzky, B. Metabolic Disruption in Drosophila Bang-Sensitive Seizure Mutants. *Genetics* **173**, 1357 (2006).

154. Valente, E. M. *et al.* Hereditary early-onset Parkinson's disease caused by mutations in PINK1. *Science* **304**, 1158–60 (2004).

155. Kitada, T. *et al.* Mutations in the parkin gene cause autosomal recessive juvenile parkinsonism. *Nature* **392**, 605–8 (1998).

156. Clark, I. E. *et al.* Drosophila pink1 is required for mitochondrial function and interacts genetically with parkin. *Nature* (2006) doi:10.1038/nature04779.

157. Park, J. *et al.* Mitochondrial dysfunction in Drosophila PINK1 mutants is complemented by parkin. *Nature* (2006) doi:10.1038/nature04788.

158. Narendra, D. P. *et al.* PINK1 Is Selectively Stabilized on Impaired Mitochondria to Activate Parkin. *PLoS Biol.* **8**, e1000298 (2010).

159. Kane, L. A. *et al.* PINK1 phosphorylates ubiquitin to activate parkin E3 ubiquitin ligase activity. *J. Cell Biol.* **205**, 143–153 (2014).

160. Palikaras, K., Lionaki, E. & Tavernarakis, N. Mechanisms of mitophagy in cellular homeostasis, physiology and pathology. *Nat. Cell Biol. 2018 209* **20**, 1013–1022 (2018).

161. Wade Harper, J., Ordureau, A. & Heo, J. M. Building and decoding ubiquitin hains for mitophagy. *Nature Reviews Molecular Cell Biology* vol. 19 93–108 (2018).

162. Riley, B. E. *et al.* Structure and function of Parkin E3 ubiquitin ligase reveals aspects of RING and HECT ligases. *Nat. Commun. 2013 41* **4**, 1–9 (2013).

163. Yamano, K., Matsuda, N. & Tanaka, K. The ubiquitin signal and autophagy: an orchestrated dance leading to mitochondrial degradation. *EMBO Rep.* **17**, 300–316 (2016).

164. Mhyre, T. R., Boyd, J. T., Hamill, R. W. & Maguire-Zeiss, K. A. Parkinson's Disease. *Subcell. Biochem.* **65**, 389 (2012).

165. Dong-Chen, X., Yong, C., Yang, X., Chen-Yu, S. T. & Li-Hua, P. Signaling pathways in Parkinson's disease: molecular mechanisms and therapeutic interventions. *Signal Transduct. Target. Ther. 2023 81* **8**, 1–18 (2023).

166. Yang, Y. *et al.* Mitochondrial pathology and muscle and dopaminergic neuron degeneration caused by inactivation of Drosophila Pink1 is rescued by Parkin. *Proc. Natl. Acad. Sci. U. S. A.* **103**, 10793–10798 (2006).

167. Liao, J. Z. *et al.* Cdk8/CDK19 promotes mitochondrial fission through Drp1 phosphorylation and can phenotypically suppress pink1 deficiency in Drosophila. *Nat. Commun. 2024 151* **15**, 1–19 (2024).

168. Greene, J., Whitworth, A., Kuo, I., Andrews, L. & Feany, M. Mitochondrial

pathology and apoptotic muscle degeneration in Drosophila parkin mutants. *Proc Natl Acad Sci U S A* **100**, (2003).

169. Deng, H., Dodson, M. W., Huang, H. & Guo, M. The Parkinson's disease genes pink1 and parkin promote mitochondrial fission and/or inhibit fusion in Drosophila. *Proc. Natl. Acad. Sci. U. S. A.* **105**, 14503–14508 (2008).

170. Poole, A. C. *et al.* The PINK1/Parkin pathway regulates mitochondrial morphology. *Proc. Natl. Acad. Sci. U. S. A.* **105**, 1638–43 (2008).

171. Kühlbrandt, W. Structure and function of mitochondrial membrane protein complexes. *BMC Biol.* **13**, 1–11 (2015).

172. Zhao, R. Z., Jiang, S., Zhang, L. & Yu, Z. Bin. Mitochondrial electron transport chain, ROS generation and uncoupling (Review). *Int. J. Mol. Med.* **44**, 3 (2019).

173. Tan, P., Feng, Z., Zhang, L., Hou, T. & Li, Y. The mechanism of proton translocation in respiratory complex I from molecular dynamics. *J. Recept. Signal Transduct. Res.* **35**, 170–179 (2015).

174. Wikström, M. & Hummer, G. Stoichiometry of proton translocation by respiratory complex I and its mechanistic implications. *Proc. Natl. Acad. Sci. U. S. A.* **109**, 4431–4436 (2012).

175. Sun, F. *et al.* Crystal structure of mitochondrial respiratory membrane protein complex II. *Cell* **121**, 1043–1057 (2005).

176. Wikstrom, M. K. F. Proton pump coupled to cytochrome c oxidase in mitochondria. *Nat. 1977 2665599* **266**, 271–273 (1977).

177. Varanasi, L. & Hosler, J. P. Subunit III-depleted cytochrome c oxidase provides insight into the process of proton uptake by proteins. *Biochim. Biophys. Acta* **1817**, 545–551 (2012).

178. Jonckheere, A. I., Smeitink, J. A. M. & Rodenburg, R. J. T. Mitochondrial ATP synthase: architecture, function and pathology. *J. Inherit. Metab. Dis.* **35**, 211–225 (2012).

179. Su, L. J. *et al.* Reactive Oxygen Species-Induced Lipid Peroxidation in Apoptosis, Autophagy, and Ferroptosis. *Oxid. Med. Cell. Longev.* **2019**, (2019).

180. Renault, T. T. & Chipuk, J. E. Death upon a kiss: mitochondrial outer membrane composition and organelle communication govern sensitivity to BAK/BAX-dependent apoptosis. *Chem. Biol.* **21**, 114–123 (2014).

181. Mann, V. M. *et al.* Complex I, Iron, and ferritin in Parkinson's disease substantia nigra. *Ann. Neurol.* **36**, 876–881 (1994).

182. Morais, V. A. *et al.* Parkinson's disease mutations in PINK1 result in decreased Complex I activity and deficient synaptic function. *EMBO Mol. Med.* **1**, 99–111 (2009).

183. Holper, L., Ben-Shachar, D. & Mann, J. Multivariate meta-analyses of mitochondrial complex I and IV in major depressive disorder, bipolar disorder, schizophrenia, Alzheimer disease, and Parkinson disease. *Neuropsychopharmacology* **44**, 837–849 (2019).

184. Reddy, P. H. & Beal, M. F. Amyloid beta, mitochondrial dysfunction and synaptic damage: implications for cognitive decline in aging and Alzheimer's disease. *Trends Mol. Med.* **14**, 45 (2008).

185. Manoharan, S. *et al.* The Role of Reactive Oxygen Species in the Pathogenesis of Alzheimer's Disease, Parkinson's Disease, and Huntington's Disease: A Mini Review. *Oxid. Med. Cell. Longev.* **2016**, (2016).

186. Rehman, J. *et al.* Inhibition of mitochondrial fission prevents cell cycle progression in lung cancer. *FASEB J.* **26**, 2175–2186 (2012).

187. Chen, W., Zhao, H. & Li, Y. Mitochondrial dynamics in health and disease: mechanisms and potential targets. *Signal Transduct. Target. Ther. 2023 81* **8**, 1–25 (2023).

188. Chen, Y., Liu, Y. & Dorn, G. W. Mitochondrial fusion is essential for organelle function and cardiac homeostasis. *Circ. Res.* **109**, 1327–1331 (2011).

189. Dorn, G. W. Mitochondrial Dynamics in Heart Disease. *Biochim. Biophys. Acta* **1833**, 233 (2013).

190. Liesa, M. & Shirihai, O. S. *Mitochondrial dynamics in the regulation of nutrient utilization and energy expenditure*. vol. 17 491–506 (2013).

191. Picard, M., Shirihai, O. S., Gentil, B. J. & Burelle, Y. Mitochondrial morphology transitions and functions: Implications for retrograde signaling? *American Journal of Physiology - Regulatory Integrative and Comparative Physiology* vol. 304 R393 (2013).

192. Rambold, A. S., Kostelecky, B., Elia, N. & Lippincott-Schwartz, J. Tubular network formation protects mitochondria from autophagosomal degradation during nutrient starvation. *Proc. Natl. Acad. Sci. U. S. A.* **108**, 10190–10195 (2011).

193. Molina, A. J. A. *et al.* Mitochondrial networking protects β-cells from nutrient-induced apoptosis. *Diabetes* **58**, 2303–2315 (2009).

194. Youle, R. J. & van der Bliek, A. M. Mitochondrial fission, fusion, and stress. *Science* **337**, 1062–5 (2012).

195. Yu, R., Lendahl, U., Nistér, M. & Zhao, J. Regulation of Mammalian Mitochondrial Dynamics: Opportunities and Challenges. *Front. Endocrinol. (Lausanne).* **11**, 534124 (2020).

196. Katti, P., Rai, M., Srivastava, S., Silva, P. D. & Nongthomba, U. Marf-mediated mitochondrial fusion is imperative for the development and functioning of indirect flight muscles (IFMs) in drosophila. *Exp. Cell Res.* **399**, (2021).

197. Kalia, R. *et al.* Structural basis of mitochondrial receptor binding and constriction by DRP1. *Nat. 2018 5587710* **558**, 401–405 (2018).

198. Mears, J. A. *et al.* Conformational changes in Dnm1 support a contractile mechanism for mitochondrial fission. *Nat. Struct. Mol. Biol.* **18**, 20 (2011).

199. Otera, H., Ishihara, N. & Mihara, K. New insights into the function and regulation of mitochondrial fission. *Biochim. Biophys. Acta* **1833**, 1256–1268 (2013).

200. Fonseca, T. B., Sánchez-Guerrero, Á., Milosevic, I. & Raimundo, N. Mitochondrial fission requires DRP1 but not dynamins. *Nature* **570**, E34–E42 (2019).

201. Ponte, S. *et al.* Drp1-mediated mitochondrial fission regulates calcium and F-actin dynamics during wound healing. *Biol. Open* **9**, (2020).

202. Lee, T. T. *et al.* Loss of Fis1 impairs proteostasis during skeletal muscle aging in Drosophila. *Aging Cell* **20**, e13379 (2021).

203. Yang, Y. *et al.* Pink1 regulates mitochondrial dynamics through interaction with the fission/fusion machinery. *Proc. Natl. Acad. Sci. U. S. A.* **105**, 7070–7075 (2008).

204. Samant, S. A. *et al.* SIRT3 deacetylates and activates OPA1 to regulate mitochondrial dynamics during stress. *Mol. Cell. Biol.* **34**, 807–819 (2014).

205. Frank, S. *et al.* The Role of Dynamin-Related Protein 1, a Mediator of Mitochondrial Fission, in Apoptosis. *Dev. Cell* **1**, 515–525 (2001).

206. Parra, V. *et al.* Insulin stimulates mitochondrial fusion and function in cardiomyocytes via the AktmTOR-NFkB-Opa-1 signaling pathway. *Diabetes* **63**, 75–88 (2014).

207. Twig, G. *et al.* Fission and selective fusion govern mitochondrial segregation and elimination by autophagy. **27**, (2008).

208. Tondera, D. *et al.* SLP-2 is required for stress-induced mitochondrial hyperfusion. *EMBO J.* **28**, 1589–1600 (2009).

209. Shutt, T., Geoffrion, M., Milne, R. & McBride, H. M. The intracellular redox state is a core determinant of mitochondrial fusion. **13**, 909–915 (2012).

210. Chang, C. R. & Blackstone, C. Dynamic regulation of mitochondrial fission through modification of the dynamin-related protein Drp1. *Ann. N. Y. Acad. Sci.* **1201**, 34–39 (2010).

211. Adaniya, S. M., O-Uchi, J., Cypress, M. W., Kusakari, Y. & Jhun, B. S. Posttranslational modifications of mitochondrial fission and fusion proteins in cardiac physiology and pathophysiology. *Am. J. Physiol. Cell Physiol.* **316**, C583–C604 (2019).

212. Sabouny, R. & Shutt, T. E. Reciprocal Regulation of Mitochondrial Fission and Fusion. *Trends in Biochemical Sciences* vol. 45 564–577 (2020).

213. Zaja, I. *et al.* Cdk1, PKCδ and calcineurin-mediated Drp1 pathway contributes to mitochondrial fission-induced cardiomyocyte death. *Biochem Biophys Res Commun* **453**, 710–721 (2014).

214. Liu, D. *et al.* Cdk5 Promotes Mitochondrial Fission via Drp1 Phosphorylation at S616 in Chronic Ethanol Exposure-Induced Cognitive Impairment. *Mol. Neurobiol.* **59**, 7075–7094 (2022).

215. Han, H. *et al.* PINK 1 phosphorylates Drp1 S616 to regulate mitophagy-independent mitochondrial dynamics . *EMBO Rep.* **21**, 1–17 (2020).

216. Gao, Q. *et al.* PINK1-mediated Drp1 S616 phosphorylation modulates synaptic development and plasticity via promoting mitochondrial fission. *Signal Transduct. Target. Ther.* **7**, (2022).

217. Wasiak, S., Zunino, R. & McBride, H. M. Bax/Bak promote sumoylation of DRP1 and its stable association with mitochondria during apoptotic cell death. *J. Cell Biol.* **177**, 439–450 (2007).

218. Lee, W., Andrews, B. C., Faust, M., Walldorf, U. & Verheyen, E. M. Hipk is an essential protein that promotes Notch signal transduction in the Drosophila eye by inhibition of the global co-repressor Groucho. *Dev. Biol.* **325**, 263–272 (2009).

219. Verheyen, E. M., Swarup, S. & Lee, W. Hipk proteins dually regulate Wnt/Wingless signal transduction. (2012) doi:10.4161/fly.20143.

220. Tettweiler, G., Blaquiere, J. A., Wray, N. B. & Verheyen, E. M. Hipk is required for JAK/STAT activity during development and tumorigenesis. *PLoS One* **14**, (2019).

221. Wang, S. J. H. *et al.* Homeodomain-interacting protein kinase (Hipk) plays roles in nervous system and muscle structure and function. *PLoS One* **15**, e0221006 (2020).

222. Blaquiere, J. A., Lam Wong, K. K., Kinsey, S. D., Wu, J. & Verheyen, E. M. Homeodomain-interacting protein kinase promotes tumorigenesis and metastatic cell behavior. *Dis. Model. Mech.* **11**, (2018).

223. Swarup, S., Pradhan-Sundd, T. & Verheyen, E. M. Genome-wide identification of phospho-regulators of Wnt signaling in Drosophila. **142**, 1502–1515 (2015).

224. Deora, T., Gundiah, N. & Sane, S. P. Mechanics of the thorax in flies. *J. Exp. Biol.* **220**, 1382–1395 (2017).

225. Madabattula, S. T. *et al.* Quantitative Analysis of Climbing Defects in a Drosophila Model of Neurodegenerative Disorders. *J. Vis. Exp.* **2015**, 52741 (2015).

226. Eslamieh, M., Mirsalehi, A., Markova, D. N. & Betrán, E. COX4-like, a Nuclear-Encoded Mitochondrial Gene Duplicate, Is Essential for Male Fertility in Drosophila melanogaster. *Genes (Basel).* **13**, 424 (2022).

227. Anderson, L., Camus, M. F., Monteith, K. M., Salminen, T. S. & Vale, P. F. Variation in mitochondrial DNA affects locomotor activity and sleep in Drosophila melanogaster. *Heredity (Edinb).* **129**, 225–232 (2022).

228. Valente, A. J., Maddalena, L. A., Robb, E. L., Moradi, F. & Stuart, J. A. A simple ImageJ macro tool for analyzing mitochondrial network morphology in mammalian cell culture. *Acta Histochem.* **119**, 315–326 (2017).

229. Wong, K. K. L., Liao, J. Z., Shih, C. R. Y., Harden, N. & Verheyen, E. M. Hyperpolarized mitochondria accumulate in Drosophila Hipk-overexpressing cells to drive tumor-like growth. *J. Cell Sci.* **133**, (2020).

230. Robinson, S. W., Herzyk, P., Dow, J. A. T. & Leader, D. P. FlyAtlas: database of gene expression in the tissues of Drosophila melanogaster. *Nucleic Acids Res.* **41**, D744 (2013).

231. Verstreken, P. *et al.* Synaptic mitochondria are critical for mobilization of reserve pool vesicles at Drosophila neuromuscular junctions. *Neuron* **47**, 365–78 (2005).

232. Vos, M., Lauwers, E. & Verstreken, P. Synaptic mitochondria in synaptic transmission and organization of vesicle pools in health and disease. *Front. Synaptic Neurosci.* **2**, 139 (2010).

233. Songyang, Z. *et al.* Use of an oriented peptide library to determine the optimal substrates of protein kinases. *Curr. Biol.* **4**, 973–982 (1994).

234. Moses, A. M., Hériché, J. K. & Durbin, R. Clustering of phosphorylation site recognition motifs can be exploited to predict the targets of cyclin-dependent kinase. *Genome Biol.* **8**, R23 (2007).

235. Xue, J., Scotti, E. & Stoffel, M. CDK8 Regulates Insulin Secretion and Mediates Postnatal and Stress-Induced Expression of Neuropeptides in Pancreatic β Cells. *Cell Reports* vol. 28 2892-2904.e7 (2019).

236. Taguchi, N., Ishihara, N., Jofuku, A., Oka, T. & Mihara, K. Mitotic Phosphorylation

of Dynamin-related GTPase Drp1 Participates in Mitochondrial Fission. **282**, 11521–11529 (2007).

237. Han, X. J. *et al.* CaM kinase Iα–induced phosphorylation of Drp1 regulates mitochondrial morphology. *J. Cell Biol.* **182**, 573 (2008).

238. Wang, W. *et al.* Mitochondrial fission triggered by hyperglycemia is mediated by ROCK1 activation in podocytes and endothelial cells. *Cell Metab.* **15**, 186–200 (2012).

239. Kanca, O. *et al.* An expanded toolkit for Drosophila gene tagging using synthesized homology donor constructs for CRISPR-mediated homologous recombination. *Elife* **11**, (2022).

240. Ma, R. *et al.* DUSP6 SUMOylation protects cells from oxidative damage via direct regulation of Drp1 dephosphorylation. *Sci. Adv.* **6**, eaaz0361 (2020).

241. Rai, M. & Nongthomba, U. Effect of myonuclear number and mitochondrial fusion on Drosophila indirect flight muscle organization and size. *Exp. Cell Res.* **319**, 2566–2577 (2013).

242. Avellaneda, J. *et al.* Myofibril and mitochondria morphogenesis are coordinated by a mechanical feedback mechanism in muscle. **12**, 1–18 (2021).

243. Redpath, C. J., Bou Khalil, M., Drozdzal, G., Radisic, M. & McBride, H. M. Mitochondrial Hyperfusion during Oxidative Stress Is Coupled to a Dysregulation in Calcium Handling within a C2C12 Cell Model. *PLoS One* **8**, e69165 (2013).

244. Crowley, L. C., Christensen, M. E. & Waterhouse, N. J. Measuring Mitochondrial Transmembrane Potential by TMRE Staining. *Cold Spring Harb. Protoc.* **2016**, 1092–1096 (2016).

245. Bourbon, H. M. Comparative genomics supports a deep evolutionary origin for the large, four-module transcriptional mediator complex. *Nucleic Acids Res.* **36**, 3993–4008 (2008).

246. Léopold, P. & O'Farrell, P. H. An evolutionarily conserved cyclin homolog from Drosophila rescues yeast deficient in G1 cyclins. *Cell* **66**, 1207–16 (1991).

247. Lew, D. J., Dulić, V. & Reed, S. I. Isolation of three novel human cyclins by rescue of G1 cyclin (Cln) function in yeast. *Cell* **66**, 1197–206 (1991).

248. Cooper, K. F., Mallory, M. J., Smith, J. B. & Strich, R. Stress and developmental regulation of the yeast C-type cyclin Ume3p (Srb11p/Ssn8p). *EMBO J.* **16**, 4665–75 (1997).

249. Hattori, N. *et al.* Point mutations (Thr240Arg and Gln311Stop) [correction of Thr240Arg and Ala311Stop] in the Parkin gene. *Biochem. Biophys. Res.*

Commun. **249**, 754–8 (1998).

250. Lücking, C. B. *et al.* Homozygous deletions in parkin gene in European and North African families with autosomal recessive juvenile parkinsonism. The European Consortium on Genetic Susceptibility in Parkinson's Disease and the French Parkinson's Disease Genetics Study Group. *Lancet (London, England)* **352**, 1355–6 (1998).

251. Poewe, W. *et al.* Parkinson disease. *Nat. Rev. Dis. Prim.* **3**, 1–21 (2017).

252. Vekrellis, K., Xilouri, M., Emmanouilidou, E., Rideout, H. J. & Stefanis, L. Pathological roles of α-synuclein in neurological disorders. *The Lancet Neurology* vol. 10 1015–1025 (2011).

253. Nalls, M. A. *et al.* Large-scale meta-analysis of genome-wide association data identifies six new risk loci for Parkinson's disease. *Nat. Genet.* **46**, 989–993 (2014).

254. Soldner, F. *et al.* Parkinson-associated risk variant in distal enhancer of α-synuclein modulates target gene expression. *Nature* **533**, 95–99 (2016).

255. Beilina, A. *et al.* Mutations in PTEN-induced putative kinase 1 associated with recessive parkinsonism have differential effects on protein stability. *Proc. Natl. Acad. Sci. U. S. A.* **102**, 5703 (2005).

256. Pesah, Y., Pham, T., Burgess, H., Middlebrooks, B. & Verstreken, P. Drosophila parkin mutants have decreased mass and cell size and increased sensitivity to oxygen radical stress. *Development* **131**, (2004).

257. Fernandes, C. & Rao, Y. Genome-wide screen for modifiers of Parkinson's disease genes in Drosophila. *Mol. Brain* **4**, (2011).

258. Sen, A., Kalvakuri, S., Bodmer, R. & Cox, R. T. Clueless, a protein required for mitochondrial function, interacts with the PINK1-Parkin complex in Drosophila. *DMM Dis. Model. Mech.* **8**, 577–589 (2015).

259. Pickrell, A. M. & Youle, R. J. *The roles of PINK1, Parkin, and mitochondrial fidelity in parkinson's disease*. *Neuron* vol. 85 (Cell Press, 2015).

260. Silvestri, L. *et al.* Mitochondrial import and enzymatic activity of PINK1 mutants associated to recessive parkinsonism. *Hum. Mol. Genet.* **14**, 3477–3492 (2005).

261. Pogson, J. H. *et al.* The Complex I Subunit NDUFA10 Selectively Rescues Drosophila pink1 Mutants through a Mechanism Independent of Mitophagy. *PLoS Genet.* **10**, e1004815 (2014).

262. Lee, J. J., Andreazza, S. & Whitworth, A. J. The STING pathway does not contribute to behavioural or mitochondrial phenotypes in Drosophila Pink1/parkin

or mtDNA mutator models. *Sci. Reports 2020 101* **10**, 1–10 (2020).

263. Shiba-Fukushima, K., Inoshita, T., Hattori, N. & Imai, Y. PINK1-Mediated Phosphorylation of Parkin Boosts Parkin Activity in Drosophila. *PLoS Genet.* **10**, e1004391 (2014).

264. Zhang, T., Mishra, P., Hay, B. A., Chan, D. & Guo, M. Valosin-containing protein (VCP/p97) inhibitors relieve mitofusin-dependent mitochondrial defects due to VCP disease mutants. *Elife* **6**, (2017).

265. Abramov, A. Y. *et al.* Bioenergetic consequences of PINK1 mutations in Parkinson disease. *PLoS One* **6**, e25622 (2011).

266. Uttara, B., Singh, A., Zamboni, P. & Mahajan, R. Oxidative Stress and Neurodegenerative Diseases: A Review of Upstream and Downstream Antioxidant Therapeutic Options. *Curr. Neuropharmacol.* **7**, 65–74 (2009).

267. Schulz, J. B., Lindenau, J., Seyfried, J. & Dichgans, J. Glutathione, oxidative stress and neurodegeneration. *Eur. J. Biochem.* **267**, 4904–4911 (2000).

268. Koehler, C. L., Perkins, G. A., Ellisman, M. H. & Jones, D. L. Pink1 and Parkin regulate Drosophila intestinal stem cell proliferation during stress and aging. *J. Cell Biol.* **216**, 2315–2327 (2017).

269. Tang, C. *et al.* PINK1-PRKN/PARK2 pathway of mitophagy is activated to protect against renal ischemia-reperfusion injury. *Autophagy* **14**, 880–897 (2018).

270. Bradley, K. J. *et al.* Parafibromin is a nuclear protein with a functional monopartite nuclear localization signal. *Oncogene* **26**, 1213–1221 (2007).

271. Lu, J. *et al.* Types of nuclear localization signals and mechanisms of protein import into the nucleus. *Cell Commun. Signal.* **19**, 1–10 (2021).

272. Nguyen Ba, A. N., Pogoutse, A., Provart, N. & Moses, A. M. NLStradamus: A simple Hidden Markov Model for nuclear localization signal prediction. *BMC Bioinformatics* **10**, 1–11 (2009).

273. Ogawa, O., Zhu, X., Perry, G. & Smith, M. A. Mitochondrial abnormalities and oxidative imbalance in neurodegenerative disease. *Sci. Aging Knowledge Environ.* **2002**, (2002).

274. Zhu, X. *et al.* Oxidative imbalance in Alzheimer's disease. *Mol. Neurobiol.* **31**, 205–217 (2005).

275. Jankovic, M. *et al.* Current Concepts on Genetic Aspects of Mitochondrial Dysfunction in Amyotrophic Lateral Sclerosis. *Int. J. Mol. Sci.* **22**, (2021).

276. Zhao, J. *et al.* The Impact of Mitochondrial Dysfunction in Amyotrophic Lateral

Sclerosis. *Cells 2022, Vol. 11, Page 2049* **11**, 2049 (2022).

277. Zong, Y. *et al.* Mitochondrial dysfunction: mechanisms and advances in therapy. *Signal Transduct. Target. Ther. 2024 91* **9**, 1–29 (2024).

278. Chan, D. C. Mitochondria: dynamic organelles in disease, aging, and development. *Cell* **125**, 1241–52 (2006).

279. Hoppins, S. The regulation of mitochondrial dynamics. *Curr. Opin. Cell Biol.* **29**, 46–52 (2014).

280. Song, Z., Ghochani, M., McCaffery, J. M., Frey, T. G. & Chan, D. C. Mitofusins and OPA1 mediate sequential steps in mitochondrial membrane fusion. *Mol. Biol. Cell* **20**, 3525–32 (2009).

281. Bleazard, W. *et al.* The dynamin-related GTPase Dnm1 regulates mitochondrial fission in yeast. *Nat. Cell Biol.* **1**, 298–304 (1999).

282. Perdiz, D., Lorin, S., Leroy-Gori, I. & Poüs, C. Stress-induced hyperacetylation of microtubule enhances mitochondrial fission and modulates the phosphorylation of Drp1 at 616Ser. *Cell. Signal.* **39**, 32–43 (2017).

283. Kashatus, J. A. *et al.* Erk2 phosphorylation of Drp1 promotes mitochondrial fission and MAPK-driven tumor growth. *Mol. Cell* **57**, 537–51 (2015).

284. Xu, S. *et al.* CaMKII induces permeability transition through Drp1 phosphorylation during chronic β-AR stimulation. *Nat. Commun.* **7**, 13189 (2016).

285. Esposito, G. *et al.* Aconitase Causes Iron Toxicity in Drosophila pink1 Mutants. *PLoS Genet.* **9**, e1003478 (2013).

286. Yang, H. *et al.* Clueless/CLUH regulates mitochondrial fission by promoting recruitment of Drp1 to mitochondria. *Nat. Commun. 2022 131* **13**, 1–19 (2022).

287. Takahashi, M. *et al.* Cloning and expression of the ret proto-oncogene encoding a tyrosine kinase with two potential transmembrane domains. *Oncogene* **3**, 571–578 (1988).

288. Von Stockum, S. *et al.* Inhibition of the deubiquitinase USP8 corrects a Drosophila PINK1 model of mitochondria dysfunction. *Life Sci. Alliance* **2**, (2019).

289. Klein, P. *et al.* Ret rescues mitochondrial morphology and muscle degeneration of Drosophila Pink1 mutants. **33**, (2014).

290. Ham, S. J. *et al.* Loss of UCHL1 rescues the defects related to Parkinson's disease by suppressing glycolysis. *Sci. Adv.* **7**, (2021).

291. Terriente-Felix, A., Wilson, E. L. & Whitworth, A. J. Drosophila

phosphatidylinositol-4 kinase fwd promotes mitochondrial fission and can suppress Pink1/parkin phenotypes. *PLOS Genet.* **16**, e1008844 (2020).

292. Quinsay, M. N., Thomas, R. L., Lee, Y. & Gustafsson, Å. B. Bnip3-mediated mitochondrial autophagy is independent of the mitochondrial permeability transition pore. *Autophagy* **6**, 855 (2010).

293. Sandoval, H. *et al.* Essential role for Nix in autophagic maturation of erythroid cells. *Nature* **454**, 232–235 (2008).

294. Schwarten, M. *et al.* Nix directly binds to GABARAP: A possible crosstalk between apoptosis and autophagy. *Autophagy* **5**, 690–698 (2009).

295. Murakawa, T. *et al.* Bcl-2-like protein 13 is a mammalian Atg32 homologue that mediates mitophagy and mitochondrial fragmentation. *Nat. Commun. 2015 61* **6**, 1–14 (2015).

296. Liu, L. *et al.* Mitochondrial outer-membrane protein FUNDC1 mediates hypoxia-induced mitophagy in mammalian cells. *Nat. Cell Biol.* **14**, 177–185 (2012).

297. Chen, M. *et al.* Mitophagy receptor FUNDC1 regulates mitochondrial dynamics and mitophagy. *Autophagy* **12**, 689–702 (2016).

298. Waterham, H. R. *et al.* A lethal defect of mitochondrial and peroxisomal fission. *N. Engl. J. Med.* **356**, 1736–41 (2007).

299. Chao, Y.-H. *et al.* Missense variants in the middle domain of DNM1L in cases of infantile encephalopathy alter peroxisomes and mitochondria when assayed in Drosophila. *Hum. Mol. Genet.* **25**, 1846–56 (2016).

300. Li, C. *et al.* The Role of Mitochondrial Dynamin in Stroke. *Oxid. Med. Cell. Longev.* **2022**, (2022).

301. Ishihara, N. *et al.* Mitochondrial fission factor Drp1 is essential for embryonic development and synapse formation in mice. *Nat. Cell Biol.* **11**, 958–66 (2009).

302. Raga, S., Specchio, N., Rheims, S. & Wilmshurst, J. M. Developmental and epileptic encephalopathies: recognition and approaches to care. *Epileptic Disord.* **23**, 40–52 (2021).

303. Imler, E. *et al.* A Drosophila model of neuronal ceroid lipofuscinosis CLN4 reveals a hypermorphic gain of function mechanism. *Elife* **8**, (2019).

304. Schimel, A. M. *et al.* N-Acetylcysteine Amide (NACA) Prevents Retinal Degeneration by Up-Regulating Reduced Glutathione Production and Reversing Lipid Peroxidation A S I P 2 0 1 1. *Am. J. Pathol.* **178**, 2032–2043 (2011).

305. Liu, L. *et al.* Glial lipid droplets and ROS induced by mitochondrial defects

promote neurodegeneration. *Cell* **160**, 177–190 (2015).

306. Paquet, V. E. *et al.* Lipid composition of multilamellar bodies secreted by Dictyostelium discoideum reveals their amoebal origin. *Eukaryot. Cell* **12**, 1326–1334 (2013).

307. Chung, H.-L. *et al.* Loss- or Gain-of-Function Mutations in ACOX1 Cause Axonal Loss via Different Mechanisms. *Neuron* **106**, 589-606.e6 (2020).

308. Nemet, J., Jelicic, B., Rubelj, I. & Sopta, M. The two faces of Cdk8, a positive/negative regulator of transcription. *Biochimie* **97**, 22–27 (2014).

309. Zhao, X. *et al.* Regulation of lipogenesis by cyclin-dependent kinase 8–mediated control of SREBP-1. *J. Clin. Invest.* **122**, 2417–2427 (2012).

310. Xie, X. J. *et al.* CDK8-cyclin C mediates nutritional regulation of developmental transitions through the ecdysone receptor in Drosophila. *PLoS Biol.* **13**, (2015).

311. Horton, J. D., Goldstein, J. L. & Brown, M. S. SREBPs: activators of the complete program of cholesterol and fatty acid synthesis in the liver. *J. Clin. Invest.* **109**, 1125–1131 (2002).

312. Shao, W. & Espenshade, P. J. Expanding roles for SREBP in metabolism. *Cell Metabolism* vol. 16 414–419 (2012).

313. Liang, K. X. *et al.* N-acetylcysteine amide ameliorates mitochondrial dysfunction and reduces oxidative stress in hiPSC-derived dopaminergic neurons with POLG mutation. *Exp. Neurol.* **337**, 113536 (2021).

314. Chung, H. lok *et al.* Loss- or Gain-of-Function Mutations in ACOX1 Cause Axonal Loss via Different Mechanisms. *Neuron* **106**, 589-606.e6 (2020).

315. Zhao, X. *et al.* Regulation of lipogenesis by cyclin-dependent kinase 8 - Mediated control of SREBP-1. *J. Clin. Invest.* **122**, 2417–2427 (2012).

316. Mandik, F. & Vos, M. Neurodegenerative Disorders: Spotlight on Sphingolipids. *Int. J. Mol. Sci. 2021, Vol. 22, Page 11998* **22**, 11998 (2021).

317. Estes, R. E., Lin, B., Khera, A. & Davis, M. Y. Lipid Metabolism Influence on Neurodegenerative Disease Progression: Is the Vehicle as Important as the Cargo? *Front. Mol. Neurosci.* **14**, 788695 (2021).

318. Chiurchiù, V. Lipids in Neurodegenerative Diseases. *Int. J. Mol. Sci.* **24**, 11523 (2023).

319. Paisan-Ruiz, C. *et al.* Characterization of PLA2G6 as a locus for dystonia-parkinsonism. *Ann. Neurol.* **65**, 19–23 (2009).

320. Sidransky, E. & Lopez, G. The link between the GBA gene and parkinsonism. *Lancet. Neurol.* **11**, 986–998 (2012).

321. Malik, I. *et al.* Disrupted Membrane Homeostasis and Accumulation of Ubiquitinated Proteins in a Mouse Model of Infantile Neuroaxonal Dystrophy Caused by PLA2G6 Mutations. *Am. J. Pathol.* **172**, 406 (2008).

322. Kinghorn, K. J. *et al.* Loss of PLA2G6 leads to elevated mitochondrial lipid peroxidation and mitochondrial dysfunction. *Brain* **138**, 1801–1816 (2015).

323. Lin, G. *et al.* Phospholipase PLA2G6, a Parkinsonism-Associated Gene, Affects Vps26 and Vps35, Retromer Function, and Ceramide Levels, Similar to α-Synuclein Gain. *Cell Metab.* **28**, 605-618.e6 (2018).

324. Ferrazza, R. *et al.* LRRK2 deficiency impacts ceramide metabolism in brain. *Biochem. Biophys. Res. Commun.* **478**, 1141–1146 (2016).

325. Abbott, S. K. *et al.* Altered ceramide acyl chain length and ceramide synthase gene expression in Parkinson's disease. *Mov. Disord.* **29**, 518–526 (2014).

326. Vos, M. *et al.* Ceramide accumulation induces mitophagy and impairs β-oxidation in PINK1 deficiency. *Proc. Natl. Acad. Sci. U. S. A.* **118**, e2025347118 (2021).

327. Sekiya, M., Hiraishi, A., Touyama, M. & Sakamoto, K. Oxidative stress induced lipid accumulation via SREBP1c activation in HepG2 cells. **375**, 602–607 (2008).

328. Varghese, J. F., Patel, R. & Yadav, U. C. S. Sterol regulatory element binding protein (SREBP) -1 mediates oxidized low-density lipoprotein (oxLDL) induced macrophage foam cell formation through NLRP3 inflammasome activation. *Cell. Signal.* **53**, 316–326 (2019).

329. Zhang, Z. H. *et al.* Tlr4-mutant mice are resistant to acute alcohol-induced sterol-regulatory element binding protein activation and hepatic lipid accumulation. *Sci. Reports 2016 61* **6**, 1–12 (2016).

330. He, Y. *et al.* Mitochondrial complex I defect induces ROS release and degeneration in trabecular meshwork cells of POAG patients: protection by antioxidants. *Invest. Ophthalmol. Vis. Sci.* **49**, 1447–1458 (2008).

331. Xiao, B. *et al.* Reactive oxygen species trigger Parkin/PINK1 pathway-dependent mitophagy by inducing mitochondrial recruitment of Parkin. *J. Biol. Chem.* **292**, 16697–16708 (2017).

332. Wang, Y. *et al.* Acetyl-CoA Carboxylases and Diseases. *Front. Oncol.* **12**, (2022).

333. Lee, K. Z., Kniazeva, M., Han, M., Pujol, N. & Ewbank, J. J. The fatty acid synthase fasn-1 acts upstream of WNK and Ste20/GCK-VI kinases to modulate antimicrobial peptide expression in C. elegans epidermis. *Virulence* **1**, 113 (2010).

334. Mariano, V. *et al.* SREBP modulates the NADP+/NADPH cycle to control night sleep in Drosophila. *Nat. Commun. 2023 141* **14**, 1–15 (2023).

335. Xu, M. *et al.* NAD kinase sustains lipogenesis and mitochondrial metabolismthrough fatty acid synthesis. *Cell Rep.* **37**, (2021).

336. Do, C. B. *et al.* Web-Based Genome-Wide Association Study Identifies Two Novel Loci and a Substantial Genetic Component for Parkinson's Disease. *PLOS Genet.* **7**, e1002141 (2011).

337. Ivatt, R. M. *et al.* Genome-wide RNAi screen identifies the Parkinson disease GWAS risk locus SREBF1 as a regulator of mitophagy. *Proc. Natl. Acad. Sci. U. S. A.* **111**, 8494–8499 (2014).

338. Houten, S. M. & Wanders, R. J. A. A general introduction to the biochemistry of mitochondrial fatty acid β-oxidation. *J. Inherit. Metab. Dis.* **33**, 469–477 (2010).

339. Theopoldt, U., Ekengren, S., Hultmark, D. & Goldstein, J. L. *HLH106, a Drosophila transcription factor with similarity to the vertebrate sterol responsive element binding protein Communicated by*. *Cell Biology* vol. 93 (1996).

340. Pennetta, G. & Welte, M. A. Emerging Links between Lipid Droplets and Motor Neuron Diseases. *Developmental Cell* vol. 45 427–432 (2018).

341. Colebc, N. B. *et al.* Lipid droplet binding and oligomerization properties of the Parkinson's disease protein α-synuclein. *J. Biol. Chem.* **277**, 6344–6352 (2002).

342. Fanning, S., Selkoe, D. & Dettmer, U. Parkinson's disease: proteinopathy or lipidopathy? *npj Parkinson's Disease* vol. 6 1–9 (2020).

343. Hamilton, L. K. *et al.* Aberrant Lipid Metabolism in the Forebrain Niche Suppresses Adult Neural Stem Cell Proliferation in an Animal Model of Alzheimer's Disease. *Cell Stem Cell* **17**, 397–411 (2015).

344. Vos, M. *et al.* Cardiolipin promotes electron transport between ubiquinone and complex I to rescue PINK1 deficiency. *J. Cell Biol.* **216**, 695 (2017).

345. Acehan, D. *et al.* Cardiolipin Affects the Supramolecular Organization of ATP Synthase in Mitochondria. *Biophys. J.* **100**, 2184 (2011).

346. Paradies, G., Paradies, V., Ruggiero, F. M. & Petrosillo, G. Role of Cardiolipin in Mitochondrial Function and Dynamics in Health and Disease: Molecular and Pharmacological Aspects. *Cells 2019, Vol. 8, Page 728* **8**, 728 (2019).

347. Gautier, C., Kitada, T. & Shen, J. Loss of PINK1 causes mitochondrial functional defects and increased sensitivity to oxidative stress. *Proc Natl Acad Sci U S A* **105**, (2008).

348. Hoch, F. L. Cardiolipins and biomembrane function. *Biochim. Biophys. Acta - Rev. Biomembr.* **1113**, 71–133 (1992).

349. Rytömaa, M. & Kinnunen, P. K. J. Evidence for two distinct acidic phospholipid-binding sites in cytochrome c. *J. Biol. Chem.* **269**, 1770–1774 (1994).

350. Bobyleva, V., Bellei, M., Pazienza, T. L. & Muscatello, U. Effect of cardiolipin on functional properties of isolated rat liver mitochondria. *Biochem. Mol. Biol. Int.* **41**, 469–480 (1997).

351. Chirala, S. S. & Wakil, S. J. Structure and function of animal fatty acid synthase. *Lipids* **39**, 1045–1053 (2004).

352. Gao, D., Pararasa, C., Dunston, C. R., Bailey, C. J. & Griffiths, H. R. Palmitate promotes monocyte atherogenicity via de novo ceramide synthesis. *Free Radic. Biol. Med.* **53**, 796–806 (2012).

353. Schilling, J. D. *et al.* Palmitate and lipopolysaccharide trigger synergistic ceramide production in primary macrophages. *J. Biol. Chem.* **288**, 2923–2932 (2013).

354. Itami, N., Shirasuna, K., Kuwayama, T. & Iwata, H. Palmitic acid induces ceramide accumulation, mitochondrial protein hyperacetylation, and mitochondrial dysfunction in porcine oocytes. *Biol. Reprod.* **98**, 644–653 (2018).

355. Kujoth, C. C. *et al.* Medicine: Mitochondrial DNA mutations, oxidative stress, and apoptosis in mammalian aging. *Science (80-.).* **309**, 481–484 (2005).

356. Shenouda, S. M. *et al.* Altered mitochondrial dynamics contributes to endothelial dysfunction in diabetes mellitus. *Circulation* **124**, 444–453 (2011).

357. Gao, A. W., Cantó, C. & Houtkooper, R. H. Mitochondrial response to nutrient availability and its role in metabolic disease. *EMBO Mol. Med.* **6**, 580–589 (2014).

358. Gasier, H. G., Dohl, J., Suliman, H. B., Piantadosi, C. A. & Yu, T. Skeletal muscle mitochondrial fragmentation and impaired bioenergetics from nutrient overload are prevented by carbon monoxide. *Am. J. Physiol. - Cell Physiol.* **319**, C746–C756 (2020).

359. Ngo, J. *et al.* Mitochondrial morphology controls fatty acid utilization by changing CPT1 sensitivity to malonyl-CoA . *EMBO J.* **42**, (2023).

360. Martinez-Vicente, M. *et al.* Cargo recognition failure is responsible for inefficient autophagy in Huntington's disease. *Nat. Neurosci.* **13**, 567–576 (2010).

361. Aditi, K., Shakarad, M. N. & Agrawal, N. Altered lipid metabolism in Drosophila model of Huntington's disease. *Sci. Rep.* **6**, 1–12 (2016).

362. Duffy, J. B. GAL4 system in Drosophila: A fly geneticist's Swiss army knife.

Genesis vol. 34 1–15 (2002).

363. Owusu-Ansah, E., Yavari, A. & Banerjee, U. A protocol for in vivo detection of reactive oxygen species. *Protoc. Exch.* **doi:10.103**, 1–12 (2008).

364. Park, Y.-J. *et al.* Phosphatidylserine synthase plays an essential role in glia and affects development, as well as the maintenance of neuronal function. *iScience* **24**, 102899 (2021).

365. Nabbi, A. & Riabowol, K. Rapid Isolation of Nuclei from Cells In Vitro. *Cold Spring Harb. Protoc.* **2015**, 769–772 (2015).

366. Suzuki, K., Bose, P., Leong-Quong, R. Y., Fujita, D. J. & Riabowol, K. REAP: A two minute cell fractionation method. *BMC Res. Notes* **3**, 1–6 (2010).